

**Structure and Reactivity Studies of
Bis(pyridylimino)isoindolate Transition Metal Complexes**

**by
Kuei-Nin T. Tseng**

A dissertation submitted in partial fulfillment
of the requirements for the degree of
Doctor of Philosophy
(Chemistry)
in the University of Michigan
2016

Doctoral Committee:

Assistant Professor Nathaniel K. Szymczak, Chair
Professor Vincent L. Pecoraro
Professor Melanie S. Sanford
Professor Levi T. Thompson, Jr.

© Kuei-Nin T. Tseng 2016

DEDICATION

For my family, especially my grandmother

ACKNOWLEDGMENTS

First, I want to thank Prof. Nathaniel (Nate) Szymczak for inviting me to join his lab and mentoring my development as a scientist and teacher over the past five years. I feel very fortunate to have been one of his first students and help build up a new research program using bis(pyridylimino)isoindoline transition-metal complexes. Since I joined the lab, Nate has always pushed me to my fullest potential. I can't count the number of times I've sat down in his office to chat about chemistry or the amount of wisdom he has passed onto me. Because of his guidance, I've learned how to write stories, think critically, present with confidence, and, most importantly, perform world-class science. I am and will always be grateful to him.

Next, I want to thank the members of my dissertation committee: Prof. Melanie Sanford, Prof Vincent Pecoraro, and Prof. Levi Thompson. In particular, I would not be an organometallic chemist if it was not for Prof. Sanford and Prof. Pecoraro. I can still remember the times I fell in love with chemistry. In the winter semester of 2005, I was an undergraduate student taking Prof. Sanford's double honors organic chemistry II class. The lecture on Grubb's catalyst and olefin metathesis blew my mind and I knew at that moment I wanted to study organometallic chemistry. Two years later, I took Prof. Pecoraro's class on advanced inorganic chemistry. The wide variety of topics covered in that class made me further pursue the fundamentals of inorganic chemistry and also made me realize that I would happily be a student of chemistry forever.

The chemistry presented in this thesis would not have been possible without the aid of Dr. Jeff Kampf and Roy Wentz. Jeff has taught me tremendous amount about crystallography. We have published more than 16 new crystal structures and acquired crystallographic data on more than 40 new crystal structures. I would not have been prolific in my research without his assistance. Roy is the wise old man in the department for advice on any number of topics. I thank him for being always helpful and providing glassware whenever I needed.

The Szymczak lab has been a great place to practice chemistry and to earn my degree. I like to thank all members of the group, past and present, for always being there for discussions and fun times. Specifically, I want to thank Dr. Cameron Moore and Dr. Oscar Tutusaus-Santandreu for helping me become a better chemist and their friendship. I also want to thank the following mentees for helping me become a better teacher and person: Andrew Rizzi, Nomaan Rezayee, Alex Nett, Andrew Vitek, Ben Johnson, Ruxi Dai, Steve Lin, and Lily Hale. Of particular note, I like to thank Andrew Rizzi, Steve Lin, and Lily Hale for being such great students and I wish you the best in your future endeavors.

I want to thank the Donors of the American Chemical Society Petroleum Research Fund, National Science Foundation CAREER grant, Rackham Graduate School, and the University of Michigan Department of Chemistry for support of this research. I am also grateful to Prof. John Montgomery for helpful discussions.

Finally, I want like to thank my family for all of their love. I want to thank my Mom and Grandma for supporting me through everything in my life. They have always encouraged me to perform my best and reach for the stars. I also want to thank my dad, Aunt Weiwei, Uncle Dennis, and my brother Tony for all their support and whatever else I required in my life. Last but not least, thank you, Betsy, for every moment of laughter, encouragement through graduate school, and the love you have given me over the past three years. I am very excited to start my life together with you and I cannot wait to see where life takes us next.

TABLE OF CONTENTS

DEDICATION	ii
ACKNOWLEDGMENTS	iii
LIST OF FIGURES	x
LIST OF TABLES	xiv
ABSTRACT	xv
CHAPTER	
1. Introduction	1
1.1 Homogeneous Transition Metal Catalyzed Dehydrogenative Reactions	1
1.1.1 Dehydrogenative Activation of Organic Substrates	1
1.1.2 Hydrogen Borrowing Chemistry	2
1.2 Bis(pyridylimino)isoindolate Transition Metal Complexes	13
1.2.1 Introduction	13
1.2.2 Synthesis and Characterization of Bis(pyridylimino)isoindoline Compounds	14
1.2.3 Oxidation Reactions Catalyzed by Bis(pyridylimino)isoindoline Complexes	16
1.2.4 Reduction Reactions Catalyzed by Bis(pyridylimino)isoindoline Complexes	19
1.2.5 Outlook for Catalytic Applications Using Bis(pyridylimino)isoindoline Ligands	21
1.3 Dissertation Outline and Scope	21
1.4 References	22
2. Dehydrogenative Activation of Alcohol Substrates	28
2.1 Promoterless and Chemoselective Alcohol Dehydrogenation	28
2.1.1 Introduction	28
2.1.2 Synthesis and Characterization of Ru(bMepi)(PPh ₃)Cl and HRu(bMepi)(PPh ₃) ₂	29
2.1.3 Transfer Hydrogenation of Ketones Catalyzed by HRu(bMepi)(PPh ₃) ₂	30
2.1.4 Base-Free and Acceptorless Alcohol Dehydrogenation	31

2.1.5 Poisoning Experiments for Acceptorless Alcohol Dehydrogenation	31
2.1.6 Base Dependence	33
2.1.7 Initial H ₂ Pressure Dependence	34
2.1.8 Acceptorless Dehydrogenative Coupling Catalyzed by HRu(bMepi)(PPh ₃) ₂	35
2.1.9 Chemoselective Dehydrogenation of Secondary Alcohols in the Presence of Primary Alcohols	36
2.1.10 Summary	37
2.2 Upgrading Ethanol to 1-Butanol	37
2.2.1 Introduction	37
2.2.2 Upgrading EtOH to 1-BuOH Catalyzed by Ru(bpi)(PPh ₃) ₂ Cl	39
2.2.3 Reaction Profile of Upgrading EtOH Catalyzed by Ru(bpi)(PPh ₃) ₂ Cl	43
2.2.4 Catalyst Deactivation <i>via</i> Decarbonylation Pathway	44
2.2.5 Poisoning Experiments for Upgrading EtOH	45
2.2.6 Summary	46
2.3 Experimental Section	46
2.3.1 General Considerations	46
2.3.2 Preparation of Ru(bMepi)(PPh ₃)Cl, Ru(bMepi)(PMe ₃) ₂ [Cl], HRu(bMepi)(PR ₃) ₂ (R = Ph, Me), Ru(b4Mepi)Py ₂ Cl, and Carbonyl Complexes	47
2.3.3 General Procedure for the Dehydrogenation of ⁱ PrOH Catalyzed by HRu(bMepi)(PPh ₃) ₂	51
2.3.4 General Procedure for the Dehydrogenation of 1PhEtOH Catalyzed by HRu(bMepi)(PPh ₃) ₂	51
2.3.5 General Procedure for 1,10-Phenanthroline Poisoning Experiments	52
2.3.6 General Procedure for the Initial H ₂ Pressure Dependence Experiments	52
2.3.7 General Procedure for the Dehydrogenation of Primary Alcohols and Diols and Chemoselective Dehydrogenation of Secondary Alcohols	52
2.3.8 General Procedure for Upgrading EtOH under N ₂	53
2.3.9 General Procedure for Upgrading EtOH under Air	53
2.3.10 General Procedure for Poisoning Experiments of EtOH Upgrading	53
2.4 References	53
3. On the Mechanism of <i>N,N,N</i> -Amide Ruthenium(II) Hydride Mediated Acceptorless Alcohol Dehydrogenation	58
3.1 Introduction	58
3.2 Results and Discussion	61
3.2.1 Limiting Mechanistic Scenarios for Acceptorless Alcohol Dehydrogenation Catalyzed by HRu(bMepi)(PPh ₃) ₂	61

3.2.2 Standard Conditions for Kinetic Studies	62
3.2.3 Triphenylphosphine Dependence	63
3.2.4 1-Phenylethanol Dependence	64
3.2.5 Temperature Dependence	65
3.2.6 Isotopic Labeling Studies	67
3.2.7 Synthesis and Reactivity of Ru(bMepi ^{Me})(PPh ₃)(OTf) ₂	69
3.2.8 Hammett Studies	73
3.2.9 Isolation of a Ruthenium(II)-Alkoxide Complex	75
3.2.10 Catalyst Resting State and Mechanistic Discussion	76
3.2.11 Proposed Mechanism	78
3.2.12 Primary versus Secondary Alcohol Dehydrogenation	79
3.2.13 Steric and Electronic Effects of the bMepi Ligand on Dehydrogenation Activity	82
3.2.14 Base-Promoted Acceptorless Alcohol Dehydrogenation Catalysis	85
3.2.15 Isolation of an Alternative Promoterless Alcohol Dehydrogenation Catalyst	87
3.2.16 Reversible Catalytic Hydrogenation–Dehydrogenation Reactions	89
3.2.17 Summary	90
3.3 Experimental Section	91
3.3.1 General Considerations	91
3.3.2 General Procedure for 1PhEtOH Dehydrogenation Catalyzed by HRu(bMepi)(PPh ₃) ₂	92
3.3.3 General Procedure for Base-Promoted 1PhEtOH Dehydrogenation	93
3.3.4 Preparation and Characterization of Ruthenium HbMepi, bMepi, bpi, b4Rpi, and bMepi ^{Me} Complexes.	93
3.4 References	100
4. Oxidant-Free Conversion of Primary Amines to Nitriles	103
4.1 Introduction	103
4.2 Results and Discussion	104
4.2.1 Dehydrogenation of <i>n</i> -Octylamine to <i>n</i> -Octanenitrile	104
4.2.2 Dependence of <i>n</i> -Octylamine Dehydrogenation on H ₂ pressure	105
4.2.2 Scope of Amine Dehydrogenation	106
4.2.3 Comparison of Common Transfer Hydrogenation Catalysts for <i>n</i> -Octylamine Dehydrogenation	108
4.2.4 Chemoselective Oxidation of Primary Amines	108
4.2.5 Preliminary Results for the Mechanism of Amine Dehydrogenation	109
4.2.5 Summary	110
4.3 Experimental Section	111

4.3.1 General Considerations	111
4.3.2 General Procedure for Amine Dehydrogenation Catalyzed by HRu(bMepi)(PPh ₃) ₂	111
4.3.3 Procedure for <i>n</i> -Octylamine Dehydrogenation Catalyzed by Ru(bMepi)(PPh ₃)Cl	112
4.3.4 General Procedure for the H ₂ Pressure Dependence Experiments	112
4.3.5 General Procedure for Poisoning Experiments	112
4.3.6 Procedure for Mercury Poisoning Experiment	112
4.4 References	113
5. Iron-Catalyzed Hydrofunctionalization Reactions	117
5.1 Introduction	117
5.2 Results and Discussion	118
5.2.1 Syntheses and Characterization of Iron–bMepi Complexes	118
5.2.2 Hydroboration of 1-Octene Catalyzed by Fe(bMepi)Br	122
5.2.3 Olefin and Alkyne Hydroboration Catalyzed by Electronically Distinct Iron Complexes	122
5.2.4 The Effect of the Metal Environment on Rate of Hydroboration	124
5.2.5 Distinct Selectivity for Internal Alkene Hydroboration	125
5.2.6 Poisoning Experiments for Iron-Catalyzed Alkene Hydroboration	126
5.2.7 Iron-Catalyzed Hydrosilylation of Ketones	127
5.2.8 Summary	128
5.3 Experimental Section	128
5.3.1 General Considerations	128
5.3.2 Preparation of Iron–bMepi Complexes	129
5.3.3 General Procedure for Catalytic Hydroboration	131
5.3.4 General Procedure for Hydroboration–Oxidation	132
5.3.5 General Procedure for Kinetic Experiments	132
5.3.6 General Procedure for Poisoning Experiments	132
5.4 References	132
6. Modular Attachment of Appended Boron Lewis Acids to a Ruthenium Pincer Catalyst: Metal–Ligand Cooperativity Enables Selective Alkyne Hydrogenation	136
6.1 Introduction	136
6.2 Results and Discussion	138
6.2.1 Synthesis and Characterization of Bifunctional Ruthenium Complexes with Appended Boron Lewis Acids	138
6.2.2 Reactivity of Bifunctional Ruthenium Complexes Toward H ₂ and Chlorinated Hydrocarbons	142

6.2.3 Hydrogenation Catalysis Mediated by Bifunctional Ruthenium Complexes	144
6.2.4 Origin of Selective Alkyne Reduction	146
6.2.5 Proposed Mechanism for Alkyne Hydrogenation Mediated by Bifunctional Ruthenium Complexes	147
6.2.6 Summary	148
6.3 Experimental Section	148
6.3.1 General Considerations	148
6.3.2 General Procedure for Hydrogenation Reactions Catalyzed by Ru(CH9BBNMepi)PPh3	149
6.3.3 Preparation of Bifunctional Ruthenium Complexes with Appended Boron Lewis Acids	149
6.4 References	151
7. Outlook	154
7.1 Publications from This Doctoral Research	154
7.2 Outlook	155
7.2.1 Development of Next Generation Catalysts for Sustainable Energy Applications Derived from Biomass Feedstocks	155
7.2.2 Hydrogen Storage Based on Primary Amine–Nitrile Couples	156
7.2.3 Late-State Functionalization Strategy Opens up New Possibilities in Small Molecule Transformations	157
APPENDIX	159

LIST OF FIGURES

Figure 1-1 General schemes for hydrogen borrowing chemistry and acceptorless dehydrogenative coupling reactions.	2
Figure 1-2 The three-step reaction sequence for the Guerbet process.	2
Figure 1-3 Hydrogen-transfer reactions using an alcohol as a H ₂ surrogate.	3
Figure 1-4 Bifunctional catalysts that operate through metal–ligand cooperative pathways for alcohol dehydrogenation.	4
Figure 1-5 Selective lactonization or esterification catalyzed by Ru(H) ₂ (PPh ₃) ₄ .	7
Figure 1-6 Generalized examples of ADC of alcohols with amines to form amides.	8
Figure 1-7 Oxidation of primary amines to nitriles using transition-metal catalysts under aerobic and dehydrogenative conditions.	10
Figure 1-8 Primary amine dehydrogenative pathways.	11
Figure 1-9 Primary amine dehydrogenation studies by Brookhart and Jensen.	12
Figure 1-10 Coordination modes of bis(pyridylimino)isoindoline ligand.	13
Figure 1-11 Synthesis of bis(pyridylimino)isoindoline compounds.	14
Figure 1-12 General ¹ H NMR and IR characterization trends for bis(pyridylimino)isoindolines.	15
Figure 1-13 Aerobic alcohol oxidation catalyzed by Ru(Hb4Mepi)Cl ₃ .	16
Figure 1-14 Hydroxylation of alkanes and peroxylation of alkenes catalyzed by first row metal–bpi complexes.	17
Figure 1-15 Epoxidation of alkenes catalyzed by Ir–b4'Bupi complexes.	18
Figure 1-16 Thioanisole and benzyl alcohol oxidation catalyzed by Fe–Hbpi complex.	19
Figure 1-17 Alkene hydrogenation catalyzed by Pd–b5Mepi complex.	20
Figure 1-18 Asymmetric hydrosilylation of ketones catalyzed by Fe and Co complexes with chiral bpi ligands.	20
Figure 2-1 Synthesis and crystal structure (thermal ellipsoids depicted at 50% probability) of HRu(bMepi)(PPh ₃) ₂ .	30
Figure 2-2 Reaction profiles of ⁱ PrOH dehydrogenation with low catalyst loading.	31
Figure 2-3 Reaction profiles of 1PhEtOH dehydrogenation with and without added catalyst poisons.	32
Figure 2-4 The initial 10 min of 1PhEtOH dehydrogenation catalyzed by HRu(bMepi)(PPh ₃) ₂ .	33

Figure 2-5 Reaction profiles of base dependence experiments.	33
Figure 2-6 Dependence of 1PhEtOH dehydrogenation catalyzed by HRu(bMepi)(PPh ₃) ₂ on the initial H ₂ pressure.	34
Figure 2-7 Chemoselective dehydrogenation of secondary alcohols in the presence of primary alcohols.	36
Figure 2-8 Previous work demonstrated reversible transformations between ketones and alcohols <i>via</i> sequential hydrogenation–dehydrogenation reactions mediated by HRu(bMepi)(PPh ₃) ₂ . This work presents the catalytic conversion of EtOH to 1-BuOH.	38
Figure 2-9 Reaction profile of conversion of EtOH to 1-BuOH catalyzed by Ru(bpi)(PPh ₃) ₂ Cl.	43
Figure 2-10 Crystal structures (thermal ellipsoids depicted at 50% probability) of Ru(bMepi)(PPh ₃)(Cl)CO, Ru(b4OMepi)(PPh ₃)(Cl)CO, and Ru(bpi)(CO) ₂ Cl.	44
Figure 2-11 Synthesis and crystal structure (thermal ellipsoids depicted at 50% probability) of HRu(bMepi)(PMe ₃) ₂ .	49
Figure 3-1 Generalized catalytic cycles for the inner-sphere and outer-sphere dehydrogenation pathways.	58
Figure 3-2 Proposed AAD reaction pathway mediated by bifunctional catalysts developed by Milstein and Yamaguchi.	59
Figure 3-3 1PhEtOH dehydrogenation rate dependence on the concentration of HRu(bMepi)(PPh ₃) ₂ .	61
Figure 3-4 Proposed inner-sphere and outer-sphere dehydrogenation pathways.	62
Figure 3-5 Standard reaction conditions for AAD of 1PhEtOH catalyzed by HRu(bMepi)(PPh ₃) ₂ .	62
Figure 3-6 Complete reaction profile of 1PhEtOH dehydrogenation.	63
Figure 3-7 Influence of [PPh ₃] on the reaction rates for 1PhEtOH dehydrogenation catalyzed by HRu(bMepi)(PPh ₃) ₂ .	64
Figure 3-8 Influence of [1PhEtOH] on the reaction rates for 1PhEtOH dehydrogenation catalyzed by HRu(bMepi)(PPh ₃) ₂ .	65
Figure 3-9 Eyring plots for 1PhEtOH dehydrogenation catalyzed by HRu(bMepi)(PPh ₃) ₂ . Left panel [1PhEtOH] ₀ = 7.5 M. Right panel [1PhEtOH] ₀ = 8.2 M.	66
Figure 3-10 Proposed 1-PhEtOH deprotonation with 1PhEtOH as a proton-transfer shuttle in the inner-sphere and outer-sphere pathways.	67
Figure 3-11 Isotopic labeling experiments for the dehydrogenation of 1PhEtOH.	68
Figure 3-12 Synthesis and crystal structure (thermal ellipsoids depicted at 50% probability) of Ru(bMepi ^{Me})(PPh ₃)OTf ₂ .	70
Figure 3-13 Synthesis and crystal structure (thermal ellipsoids depicted at 50% probability) of Ru(HbMepi)(PPh ₃)Cl[PF ₆].	71
Figure 3-14 Proposed proton transfer <i>via</i> stepwise metal–ligand cooperativity.	72
Figure 3-15 Reaction rate comparison between the bMepi and bMepi ^{Me} ligated Ru complexes.	73

Figure 3-16 Hammett plot for 1PhEtOH dehydrogenation catalyzed by HRu(bMepi)(PPh ₃) ₂ .	73
Figure 3-17 Comparison of Hammett parameters derived from Ru-catalyzed alcohol oxidation.	74
Figure 3-18 Synthesis and crystal structure (thermal ellipsoids depicted at 50% probability) of Ru(bMepi)(PPh ₃)(OCH ₂ CF ₃).	75
Figure 3-19 Proposed mechanism for AAD catalyzed by HRu(bMepi)(PPh ₃) ₂ .	79
Figure 3-20 Competition experiments between BnOH and 1PhEtOH.	80
Figure 3-21 Catalyst resting state and activity for competitive experiment between BnOH and 1PhEtOH.	81
Figure 3-22 Synthesis and crystal structures (thermal ellipsoids depicted at 50% probability) of Ru(b4Rpi)(PPh ₃) ₂ Cl.	82
Figure 3-23 Synthesis and crystal structure (thermal ellipsoids depicted at 50% probability) of Ru(b4OHpi)(PPh ₃) ₂ Cl.	83
Figure 3-24 Base-promoted AAD catalysis.	86
Figure 3-25 Synthesis and crystal structure (thermal ellipsoids depicted at 50% probability) of Ru(HbMepi)(PPh ₃) ₂ Cl ₂ .	87
Figure 3-26 Synthesis and crystal structure (thermal ellipsoids depicted at 50% probability) of [Ru(CH ₂ Mepi)(PPh ₃)] ₂ .	88
Figure 3-27 [Ru(CH ₂ Mepi)(PPh ₃)] ₂ promoted AAD catalysis.	88
Figure 3-28 Reversible hydrogenation–dehydrogenation reactions catalyzed by HRu(bMepi)(PPh ₃) ₂ .	89
Figure 3-29 Proposed cycle for catalytic acceptorless alcohol dehydrogenation and isolation of precursors.	90
Figure 3-30 Atom numbering of the bpi ligand for NMR characterizations.	92
Figure 4-1. Transfer and acceptorless dehydrogenation of <i>n</i> -octylamine.	105
Figure 4-2 Dependence of <i>n</i> -octylamine dehydrogenation catalyzed by HRu(bMepi)(PPh ₃) ₂ .	105
Figure 4-3 Dehydrogenation of amines catalyzed by HRu(bMepi)(PPh ₃) ₂ .	106
Figure 4-4 Chemoselective oxidation of 3-aminobenzylamine.	108
Figure 4-5 Ru(bMepi)(PPh ₃)Cl mediated <i>n</i> -octylamine dehydrogenation in the presence of base.	109
Figure 4-6 Reaction profile of <i>n</i> -octylamine dehydrogenation catalyzed by HRu(bMepi)(PPh ₃) ₂ .	110
Figure 5-1 Electronic tunability of a pincer ligand <i>via</i> backbone alkylation.	117
Figure 5-2 Synthesis of Fe(bMepi)(THF)OTf (left) and Fe(bMepi ^{Me})OTf ₂ (right) with thermal ellipsoids depicted at 50% probability.	119
Figure 5-3 Synthesis and crystal structure (thermal ellipsoids depicted at 30% probability) of Fe ₂ (bMepi) ₂ Br[BF ₄].	120
Figure 5-4 DPV of Fe(bMepi)Br and Fe(bMepi)(THF)OTf.	121

Figure 5-5 DPV of Fe(bMepi)(THF)OTf and Fe(bMepi ^{Me})OTf ₂ .	121
Figure 5-6 Hydroboration of 1-octene catalyzed by Fe(bMepi)Br.	122
Figure 5-7 Hydroboration of unsaturated hydrocarbons catalyzed by Fe(bMepi)(THF)OTf or Fe(bMepi ^{Me})OTf ₂ .	123
Figure 5-8 Initial rate of 1-octene hydroboration for Fe(bMepi)Br.	124
Figure 5-9 Initial rate of 1-octene hydroboration for Fe(bMepi)(THF)OTf.	125
Figure 5-10 Initial rate of 1-octene hydroboration for Fe(bMepi ^{Me})OTf ₂ .	125
Figure 5-11 Selectivity of internal alkene hydroboration.	126
Figure 5-12 Reaction profiles of 1-octene hydroboration with and without added PMe ₃ .	127
Figure 5-13 Hydrosilylation of acetophenone catalyzed by Fe(bMepi)(CH ₂ SiMe ₃).	128
Figure 6-1 Conceptual development of late-stage catalyst redesign to introduce Lewis acidic sites for metal–ligand cooperativity.	137
Figure 6-2 Synthesis and crystal structures (thermal ellipsoids depicted at 50% probability) of HRu(CH ₂ BCatMepi)PPh ₃ and Ru(CBPIn ₂ Mepi)PPh ₃ . The hydrogen atoms, except the hydride, and PPh ₃ phenyl groups are omitted for clarity.	139
Figure 6-3 Synthesis and crystal structures (thermal ellipsoids depicted at 50% probability) of Ru(CH ₉ BBNMepi)PPh ₃ and HRu(CH ₂ ₉ BBNMepi)(PPh ₃)CO. The hydrogen atoms, except the hydride, and PPh ₃ phenyl groups are omitted for clarity.	141
Figure 6-4 Limiting resonance description and solution equilibrium process for Ru(CH ₉ BBNMepi)PPh ₃ .	142
Figure 6-5 Influence of appended Lewis acids on the reactivity of Ruthenium hydride toward dihydrogen and dichloromethane.	143
Figure 6-6 Proposed pathway for B–H bond activation <i>via</i> H ₂ elimination .	144
Figure 6-7 Proposed mechanism for stereoselective alkyne hydrogenation catalyzed by bifunctional complexes.	147

LIST OF TABLES

Table 1-1 ADC of Primary Alcohols to Esters	7
Table 2-1 Dehydrogenation of Primary Alcohols to Esters and Diols to Lactones Catalyzed by $\text{HRu}(\text{bMepi})(\text{PPh}_3)_2$	35
Table 2-2 Catalytic Conversion of EtOH to 1-BuOH	39
Table 3-1 Reaction Rates of 1PhEtOH Dehydrogenation	84
Table 6-1 Alkyne Semi-Hydrogenation Catalyzed by Bifunctional Ruthenium Complexes	145
Table 6-2 Catalytic Hydrogenations Promoted by $\text{Ru}(\text{CH}_9\text{BBNMepi})\text{PPh}_3$ with H_2	145

ABSTRACT

Hydrogenation and dehydrogenation transformations are fundamental in chemical synthesis and are used in a wide variety of industrial processes for manufacturing pharmaceutical drugs, agrochemicals, and liquid fuels. Over the past decade, homogeneous transition-metal catalyst mediated dehydrogenation reactions have emerged as an atom-economical and selective methodology to either promote H₂ release from suitable biomass feedstocks for chemical energy storage applications or reveal a reactive unsaturated synthon that can undergo tandem functionalization reactivity to construct new C–C, C–O, or C–N bonds. In this dissertation, transition metal complexes supported by bpi-type (bpi = 1,3-bis(2'-pyridylimino)isoindolate) ligands were designed and synthesized to study their activity, selectivity, and stability in hydrogenation and dehydrogenation reactions and to determine the role of the bpi ligand in these transformations. A new family of Ru–bpi complexes capable of catalyzing promoterless and chemoselective dehydrogenation of alcohols and amines with liberation of H₂ were developed. In particular, the HRu(bMepi)(PPh₃)₂ (bMepi = 1,3-bis(6'-methyl-2'-pyridylimino)isoindolate) system mediates dehydrogenation of secondary alcohols to ketones, dehydrogenative coupling of primary alcohols to esters, and double dehydrogenation of primary amines to nitriles with high conversion efficiencies. An unusual feature of this catalyst system is the high selectivity for secondary alcohol dehydrogenation in the presence of primary alcohols and the chemoselective dehydrogenation of primary amines with –CH₂NH₂ functionality in the presence of primary amines without α hydrogens. By avoiding the use of hazardous reagents and harsh oxidants, these dehydrogenative transformations provide environmentally benign methodologies for fine and commodity chemical synthesis with high atom economy. Furthermore, to understand the relationship between catalyst structure and reactivity, the catalytic mechanism of acceptorless alcohol dehydrogenation was elucidated by a series of kinetic and isotopic labeling studies, isolation of intermediates, and evaluation of new ligand variants. The new chemical knowledge acquired in the mechanistic investigation was applied to conceptualize and develop three new

projects: (1) Fe–bMepi systems that feature control over catalytic alkene hydroboration activity and regioselectivity by remote site modifications, (2) Ru–bpi complexes capable of upgrading ethanol to 1-butanol with state-of-the-art activity (53% conversion and 265 turnovers per hour), and (3) a new series of multifunctional Ru complexes with appended Lewis acidic BR₂ sites *via* B–H bond activation for studying how Lewis acidity influences the reactivity of the Ru hydride moiety and biases the system for *cis*-selective semi-hydrogenation of alkynes. Collectively, the studies presented in this dissertation demonstrate the new development of highly active and chemoselective catalysts capable of promoting challenging dehydrogenation reactions and showcase how precise structural, electronic, and cooperative interactions in the secondary coordination environment can be used to regulate metal-based catalysis.

CHAPTER 1

Introduction

Portions of this chapter have been published:

Tseng, K.-N. T.; Szymczak, N. K. *Synlett* **2014**, *25*, 2385. Reprinted with permission; Copyright (2014) Georg Thieme Verlag Stuttgart.

1.1 Homogeneous Transition Metal Catalyzed Dehydrogenative Reactions

1.1.1 Dehydrogenative Activation of Organic Substrates

Hydrogenation and dehydrogenation reactions are fundamental in synthetic organic chemistry and are used in a variety of industrial- and small- processes for manufacturing fine and commodity chemicals.¹ Homogeneous transition-metal catalyst mediated dehydrogenative reactions have evolved as an atom-economical and selective methodology for upgrading small molecules into higher order products.² In general, the initial dehydrogenation reaction reveals a more reactive organic synthon that can undergo tandem functionalization reactivity to construct new C–C and/or C–E (E = O, N) bonds. The H₂ that is released as a byproduct can be used in a hydrogenation reaction to reduce the functionalized intermediate or a sacrificial hydrogen acceptor. This reaction class is termed “hydrogen borrowing” chemistry and is commonly used in hydrogen-transfer catalysis and processes such as alkane metathesis and amine alkylation (Figure 1-1, left panel).³ Alternatively when H₂ is liberated, this class of reactions is termed acceptorless dehydrogenative coupling (ADC), which has led to coupling reactions of alcohol–alcohol to form esters and lactones and alcohol–amine to generate amides, imines, and heterocyclic amines (Figure 1-1, right panel).⁴

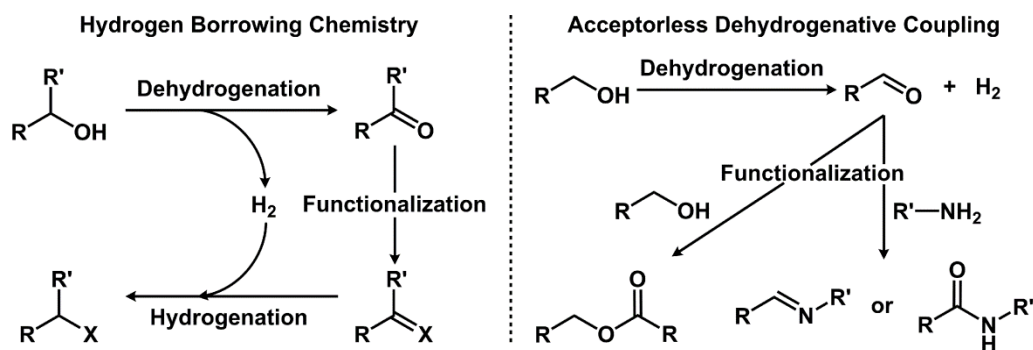


Figure 1-1 General schemes for hydrogen borrowing chemistry and acceptorless dehydrogenative coupling reactions.

1.1.2 Hydrogen Borrowing Chemistry

Over a hundred years ago, the Guerbet reaction was the earliest reported example related to hydrogen borrowing chemistry.⁵ The Guerbet sequence applies a series of reactions for the coupling of linear primary alcohols into β -branched primary alcohols (Figure 1-2).⁶ The mechanism initiates with the dehydrogenation of the alcohol to generate the corresponding aldehyde, which undergoes nucleophilic attack by the aldehyde enolate in an aldol condensation. Loss of H_2O affords an α,β -unsaturated aldehyde that is hydrogenated by hydrogen transfer from the starting alcohols. The final hydrogenation step provides high atom economy by borrowing hydrogens from the initial alcohol dehydrogenation reaction. Thermodynamically, the process of H_2 formation from alcohols is generally unfavorable. For instance, the dehydrogenation of isopropanol ($iPrOH$) to acetone and H_2 is endothermic by 16.5 kcal/mol.⁷ Because the final hydrogenation is exothermic to approximately the same magnitude as the initial dehydrogenation, the hydrogenation reaction helps drive the dehydrogenation step by establishing thermodynamic neutrality for the sum for the first and last steps.

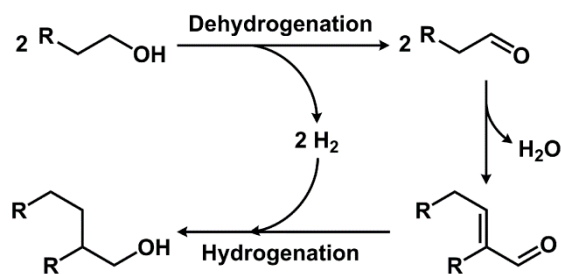


Figure 1-2 The three-step reaction sequence for the Guerbet process.

Recent developments in hydrogen-transfer catalysis have stemmed from studies in the area of alcohol oxidation since 1925.⁸ The oxidation of a C–O bond to a carbonyl unit is thermodynamically unfavorable; hence the reduction of a sacrificial reagent has accompanied the traditional alcohol oxidation methods to drive the reaction toward full conversion. Meerwein–Ponndorf–Verley (MPV) reductions use aluminum alkoxides to mediate the hydrogenation of aldehydes and ketones by formally transferring hydrogen atoms borrowed from alcohols (Figure 1-3).⁹ Secondary alcohols (e.g., *i*PrOH) are commonly used as H₂ surrogates because of greater reducing potential than primary alcohols¹⁰ and the corresponding ketone products are unlikely to deactivate the metal center *via* a decarbonylation pathway, which is commonly observed for aldehydes.¹¹ In particular, the MVP method chemoselectively reduces aldehydes before ketones. The reverse reaction of MVP reduction is the Oppenauer oxidation (Figure 1-3), which dehydrogenates alcohols to aldehydes or ketones with the requirement of added hydrogen acceptors (e.g., acetone).¹² In addition to aluminum-based alkoxides, alkali metal¹³ and lanthanide¹⁴ alkoxides are capable bases in this transformation. Oppenauer oxidation uses less toxic reagents and milder reaction conditions than the typical oxidation routes (e.g., Dess–Martin periodiane,¹⁵ Jones’s oxidant,¹⁶ and Swern’s methodology¹⁷) and chemoselectively oxidizes secondary alcohols faster than primary alcohols. However, MPV reduction and Oppenauer oxidation often require stoichiometric amounts of metal alkoxides, which decrease the atom economy by contributing to unwanted waste products. Thus, catalytically active systems that operate under base-free and acceptorless conditions are highly appealing.

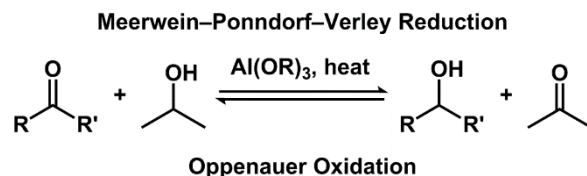


Figure 1-3 Hydrogen-transfer reactions using an alcohol as a H₂ surrogate.

1.1.3 Base-Free and Acceptorless Alcohol Dehydrogenation Catalyzed by Bifunctional Systems

In the 1970s, several reports demonstrated that transition-metal complexes incorporating Rh,¹⁸ Ru,¹⁹ or Ir²⁰ centers catalyzed Oppenauer-type alcohol oxidation reactions. These early examples required the addition of super-stoichiometric quantities of an acidic²¹ or basic²² reagent

with respect to the metal complex or high temperatures (195 °C)^{19b} for efficient catalysis. In contrast, recent reports have shown that bifunctional systems can catalyze acceptorless alcohol dehydrogenation (AAD) reactions under neutral conditions at lower temperatures (90–110 °C).^{4a,8a,23} This class of catalysts operates *via* a metal–ligand cooperative pathway that differs from the classical inner-sphere mechanism by not requiring coordination of the substrate, thus enabling outer-sphere proton transfer to a ligand-based basic site with concurrent hydride transfer to the metal center.^{4b,8g,24}

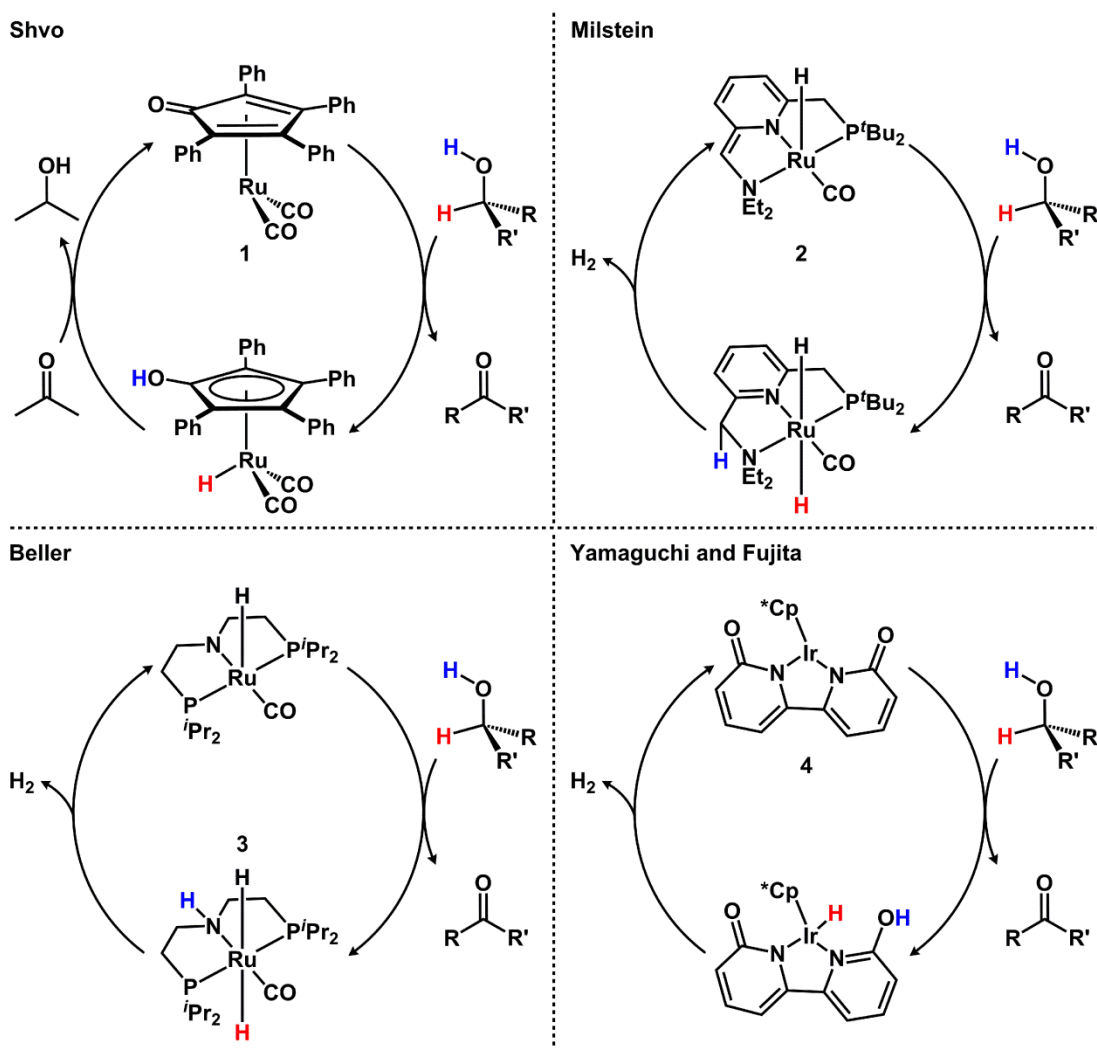


Figure 1-4 Bifunctional catalysts that operate through metal–ligand cooperative pathways for alcohol dehydrogenation.

In 1986, Shvo introduced a Ru dimer system for dehydrogenation and hydrogenation reactions that uses cyclopentadienone ligands to assist in outer-sphere proton transfer (Figure 1-4,

top left panel).^{8b,25} Shvo's bifunctional catalyst (0.5 mol%) promoted dehydrogenation of primary and secondary alcohols to the corresponding aldehydes and ketones under neutral condition in refluxing (56 °C) acetone, which functioned as a hydrogen acceptor.²⁶ Detailed kinetic and isotopic labeling experiments, trapping of intermediates and catalyst modifications have supported an outer-sphere, concerted pathway in which a proton is transferred to the enone ligand and a hydride transfers to the metal center.^{8b,27} In 2010, Guan and co-workers showed that analogous Fe catalysts (Knölker complex) were also efficient for the Oppenauer-type oxidation of primary and secondary alcohols using 3 mol% catalyst loading in acetone at 60 °C.²⁸

A year later, Milstein's group developed a series of PNE (E = NEt₂ or P^tBu₂) Ru complexes (**2**, HRu(^tBuPNN^{Et})CO) capable of catalyzing alcohol dehydrogenation reactions without the requirements of added hydrogen acceptor or base.^{4,24,29} Although Milstein's systems operated at a higher temperature (110 °C) than Shvo's catalyst, the reaction conditions used a lower catalyst loading (0.1 mol%) without any hydrogen acceptors. Computational studies revealed that **2** favors an outer-sphere bifunctional hydrogen transfer pathway that employ cooperation of the metal center with the ligand *via* aromatization–dearomatization sequences of the central pyridinyl group concomitant with protonation–deprotonation of the adjacent methylene arm (Figure 1-4, top right panel).^{23b,30}

Also in 2011, Beller and co-workers demonstrated unprecedented activity for the promoterless dehydrogenation of ethanol (EtOH) and ⁱPrOH catalyzed by Ru(H)₂(PNP^{iPr})CO (**3**),^{23a,31} which features a Ru–amine/amide motif that bears a high resemblance to Noyori's asymmetric hydrogenation catalysts.^{1a,8h,32} For instance, **3** exhibited a turnover number (TON) of more than 40,000 after 12 h for the catalytic conversion of ⁱPrOH to acetone using 4.0 ppm catalyst loading at 90 °C. The operating alcohol dehydrogenation mechanism for **3** was postulated to proceed *via* an outer-sphere pathway involving metal–ligand cooperativity that requires proton transfer to the central amide nitrogen of the pincer ligand and hydride transfer to the metal center (Figure 1-4, bottom left panel).³³

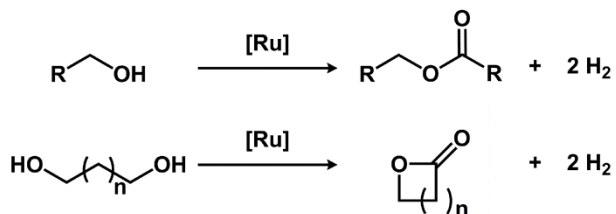
Later that year, Yamaguchi, Fujita, and Kawahara reported a new water-soluble Cp*Ir(bpyO) (**4**, α,α' -bipyridonate) catalyst for the dehydrogenation of primary and secondary alcohols which can be performed in water with no additives.³⁴ The advantage of using **4** (1 mol%) in aqueous media was demonstrated by easily recovering the catalyst in the aqueous

phase to allow for eight consecutive dehydrogenation of 1-(4-methoxyphenyl)ethanol with minimal loss in catalytic activity (94–98% yield). Computation studies showed that **4** also operates *via* an outer-sphere pathway, where the metal center and the bipyridonate motif work synergistically to oxidize the alcohol en route to H₂ elimination with the aid of an alcohol bridge (Figure 1-4, bottom right panel).³⁵

In summary, collectively, these and related studies establish the importance of a cooperative mechanism to achieve efficient alcohol dehydrogenation activity with high atom economy. The field of alcohol oxidation using homogeneous catalysis has transitioned from performing the reaction using hazardous/energy-intensive oxidants under harsh reaction conditions to promoter- and activator-less conditions at 90–110 °C. TONs have significantly improved from less than 100 to more than 40,000 for dehydrogenation of model substrates, hereof especially ⁱPrOH and 1-phenylethanol (1PhEtOH) derivatives. However, most of these catalytic systems required precious metals such as Ru and Ir. The development of new efficient systems containing non-toxic, abundant, and inexpensive metals for catalytic dehydrogenation of alcohols is highly desirable.

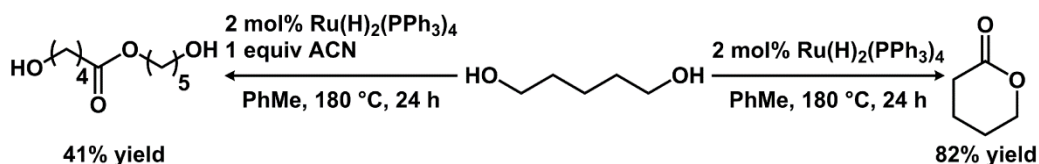
1.1.4 Acceptorless Dehydrogenative Coupling

Because C–E (E = O, N) bonds are ubiquitous in natural products, pharmaceutical drugs, and many other commodity chemicals, ADC reactions have emerged as an environmentally benign and atom-economical synthetic strategy for the preparation of a diverse collection of useful products.^{4a} In this context, dehydrogenated products from AAD reactions can undergo follow up reactivity to form new C–E bonds without the requirement of stoichiometric amounts of activating reagents or pre-functionalization of substrates. For example, AAD of primary alcohols exposes an electrophilic aldehyde group that can undergo nucleophilic attack by alcohols or amines to generate ester or amide products with concomitant release of H₂. Thermodynamically analogous to alcohol dehydrogenation (*vide supra*), the formation of these coupling products and H₂ from alcohols/amines is generally unfavorable. For instance, the homocoupling of EtOH to generate ethyl acetate and 2 equiv of H₂ is endothermic by 17.4 kcal/mol. Thus, ADC reactions are only possible at elevated temperatures or if the hydrogen gas produced are expelled from the system.

Table 1-1 ADC of Primary Alcohols to Esters

entry	alcohol or diol	catalyst (mol%)	T (°C)	solvent	time (h)	TON
1	1-butanol	2 mol% Ru(H) ₂ (PPh ₃) ₄	180	PhMe	24	40
2 ^a	1,4-butanediol	2 mol% Ru(H) ₂ (PPh ₃) ₄	180	PhMe	3	50
3	1-butanol	0.1 mol% 2	117	neat	5	900
4	1-butanol	0.1 mol% Ru(H) ₂ (PPh ₃) ₄	117	neat	72	0
5	benzyl alcohol	0.1 mol% Shvo's Ru dimer	115	neat	24	0
6	1-butanol	0.1 mol% 2-BH₄	110	PhMe	24	960
7	1,4-butanediol	0.3 mol% 2-BH₄	115	PhMe	48	258

^aAdded 1 equiv of acetone.

**Figure 1-5** Selective lactonization or esterification catalyzed by Ru(H)₂(PPh₃)₄.

In 1981, Murahashi's group demonstrated the first example of ADC reactivity with primary alcohols. Aliphatic and aromatic primary alcohols and diols were converted to ester and lactone products in 52–88% yield using 2 mol% Ru(H)₂(PPh₃)₄ (**5**) in PhMe heated to 180 °C in a sealed vessel (Table 1-1, entries 1 and 2).³⁶ The conversion of diols to lactones required exogenous 1–3 equiv of acetone as a hydrogen acceptor. In the absence of acetone, the conversion was limited to 40–50% (TON of 20–25). Four years later, Shvo and Blum described a single example of ADC of benzyl alcohol to benzoate catalyzed by Shvo's Ru dimer with a TON of 225 at 145 °C in a closed system.³⁷ Unfortunately, no further experimental details or substrate scope has since been reported using Shvo's catalyst. In 1987, Murahashi and co-workers followed up on the 1981 Letter and showed that perfume esters such as 2-methylpentyl 2-methylpentanoate (60% yield) were obtained using a similar protocol.³⁸ In addition, selective lactonization or esterification was achieved using 1,5-pentanediol and 2 mol% **5** in PhMe heated

to 180 °C for 24 h (Figure 1-5). With no additives, intramolecular ADC coupling of 1,5-pentanediol generated δ -valerolactone in 82% yield. However, addition of 1 equiv of ACN to the reaction mixture inhibited lactonization and exclusively synthesized 5-hydroxypentyl 5-hydroxypentanoate in 41% yield.

The field of ADC remained stagnant until 2005 when Milstein and co-workers reported **2** for efficient catalytic dehydrogenation of primary alcohols to esters with liberation of H₂ under mild conditions.³⁹ A TON of 900 was measured for the conversion of 1-butanol (1-BuOH) to butyl butyrate in the presence of 0.1 mol% **2** in neat alcohol heated to 117 °C for 5 h (Table 1, entry 3). Under the same reaction conditions, Milstein illustrated that no ester product and 2% aldehyde products were observed when **5** or Shvo's catalyst was used instead of **2** (Table 1-1, entries 4 and 5). In addition, Milstein's group developed a borohydride variant (**2-BH₄**, HRu(HRu(^tBuPNN^{Et}))BH₄) of **2** by substituting the carbonyl ligand for a η^2 -BH₄ ligand on the Ru center.²⁹ **2-BH₄** was found to catalyze ADC reactivity of primary alcohols and diols (Table 1-1, entries 6 and 7). For instance, 72–90% yields of lactones were obtained from acceptorless dehydrogenative cyclization of diols mediated by **2-BH₄** under base-free conditions in refluxing PhMe.

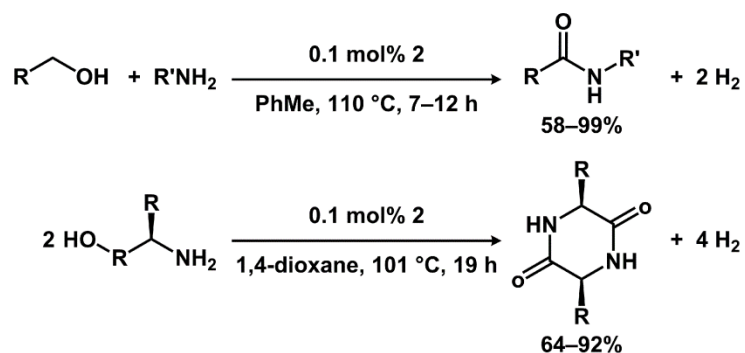


Figure 1-6 Generalized examples of ADC of alcohols with amines to form amides.

Since 2005, Milstein's group has been investigating ADC reactions for a variety of synthetic applications by expanding the scope of the coupling partners to include amines.^{4a} In 2007, Gunanathan, Ben-David, and Milstein introduced the first example of amide synthesis using ADC of primary alcohols with amines catalyzed by **2** (Figure 1-6, top equation).⁴⁰ The substrate scope included coupling of aliphatic alcohols with alkyl and aryl amines and diamines to produce the corresponding amides and diamides in 58–99% yield with release of 2 equiv of H₂

under 0.1 mol% **2** in refluxing PhMe for 7–12 h. ADC reactions of alcohols with activated amines generally resulted in lower yields due to the decrease in nucleophilicity of aryl amines. Following this report, a number of Ru systems incorporating carbene and/or phosphine ligands were found to catalyze this transformation with higher catalyst loading (5 mol%) and the requirement of added base (10–35 mol%).⁴¹ In 2011, Milstein and co-workers examined intramolecular ADC reactions of alkanolamines.⁴² For instance, complex **2** catalyzed the conversion of various alkanolamines with substituents larger than methyl α to the amine group to the corresponding cyclic dipeptides (diketopiperazines) as the sole products in 64–92% yields (Figure 1-6, bottom equation).^{42b}

In summary, the synthetic applications of ADC have broadened considerably since the seminal work from Murahashi and co-workers in 1981. An assortment of useful products, which include esters, lactones, acetals, amides, lactams, peptides, polyamides, imides, imines, indoles, pyrroles, and pyrazines, can be synthesized using ADC methodologies. These examples demonstrate the versatility of dehydrogenation as an activation strategy to generate a more reactive unsaturated intermediate that can undergo tandem functionalization under mild conditions with no waste products. Future goals would target catalyst systems with enhanced activity and stability to deploy these reactions on an industrial scale.

1.1.5 Dehydrogenative Oxidation of Amines to Nitriles

Amine oxidation is a widely used synthetic strategy to generate key building blocks and synthons for further elaboration.⁴³ Metal-based oxidants incorporating mid–high valent metals (Cr, Mn, Pb) and/or metal oxides (MnO₂, Ag₂O) are typically used as the hydrogen and/or electron acceptor.⁴⁴ In some cases, these routes exhibit moderate to low selectivity and/or functional group tolerance, which may be overcome with milder oxidative protocols such as organic hydroperoxides, Dess-Martin periodinane, and Swern oxidation.⁴⁵ However, all of these methods require stoichiometric or greater quantities, which necessarily are followed by the co-production of waste byproducts that may be environmentally deleterious. These constraints have guided the development of transition-metal catalysts that mediate aerobic and dehydrogenative oxidation of polar N–H bonds (Figure 1-7).^{2,46}

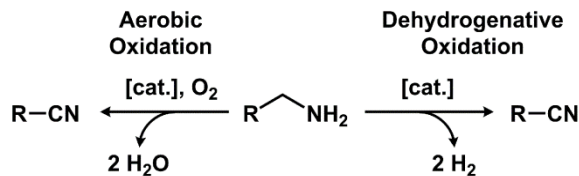


Figure 1-7 Oxidation of primary amines to nitriles using transition-metal catalysts under aerobic and dehydrogenative conditions.

Transition-metal catalyzed amine oxidation has recently emerged as a complementary route that can achieve high selectivity and produce minimal waste.^{46a,46b} The conversion of amines to nitriles can be promoted in either an oxidative^{46c-e} or reductive^{46f-i} environment. Using an oxidative catalyst protocol (exogenous *O*-atom donors and/or O₂), water is formed as a byproduct.^{46c} An alternative strategy is to use transition metal catalyzed dehydrogenative oxidation, wherein the release of H₂ (a reductant) accompanies substrate oxidation.

Although amine oxidation using dehydrogenative protocols may be conceptually analogous to alcohol oxidation,^{2,31c,47} few examples of transition-metal catalyzed amine dehydrogenation have been reported.^{34b,46f-i,48} The distinct reactivity likely stems from differences in nucleophilicity (required to coordinate to a transition metal and to initiate oxidation) and electrophilicity of the intermediate oxidation products having carbonyl and imine units. For instance, the imine intermediate that is generated following dehydrogenative activation of amines is more electrophilic than the corresponding carbonyl; thus, the imine unit is more likely to undergo nucleophilic attack by amines or alcohols/alkoxides under basic conditions. This unproductive pathway results in a decreased selectivity for the targeted oxidized product. Furthermore, ligand exchange and β -hydride elimination reactions from amino and/or amido complexes are generally slow, which presents a challenging scenario for catalysis.

Most reported systems that catalyze amine dehydrogenation are limited to secondary amine substrates, where the corresponding secondary aldimine is less susceptible to nucleophilic attack.⁴⁹ In contrast to secondary amines, when primary amines containing α -CH₂ groups are subjected to dehydrogenative conditions, alkylation often ensues. Instead of double dehydrogenation to afford the nitrile, a secondary aldimine and/or secondary amine is formed in a reaction known as transamination (Figure 1-8),² which is a type of hydrogen borrowing chemistry. Analogous to ADC of primary alcohols, the amine–amine coupling (transamination)

reaction operates *via* a similar pathway: dehydrogenation of a primary amine affords an imine intermediate that is susceptible to nucleophilic attack by an amine. Following elimination of ammonia, the corresponding secondary aldimine can be isolated, or more typically, is further hydrogenated to afford a secondary amine. This strategy can be used to synthesize tertiary amines when secondary amines are used as the nucleophilic partner. Following the initial report of transamination by Murahashi using Pd black,⁵⁰ various late metal complexes containing Ru, Os, Ir, Pd, and Pt were also found to be active.⁵¹ In transamination reactions, nucleophilic attack of an amine on the transiently formed imine intermediate diverts the imine from a second dehydrogenation event. This competitive side reaction has so far limited the double dehydrogenation of primary amines to nitriles. Thus, a current challenge in dehydrogenative oxidation is the double dehydrogenation of primary amines to nitriles.

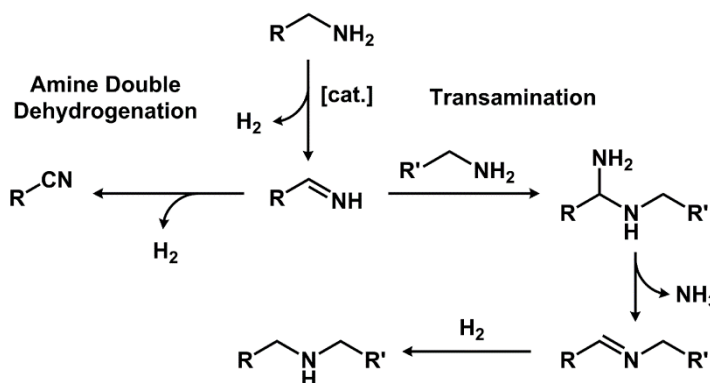


Figure 1-8 Primary amine dehydrogenative pathways.

In contrast to the myriad reports detailing transition metal catalyzed dehydrogenation of alcohols, analogous reports for amine dehydrogenation are scarce and even fewer are reported for the double dehydrogenation of primary amines.^{46f-i} In 1979, the first example of amine double dehydrogenation catalyzed by $\text{HRh}(\text{P}^i\text{Pr}_3)_3$ was reported by Yoshida and co-workers.^{46f} Their report described a single example of the dehydrogenation of benzyl amine to benzonitrile in 27% yield after 24 h at 110 °C using 1 mol% catalyst loading. Unfortunately, no further experimental details or substrate scope has since been reported that uses this intriguing system.

Almost 30 years later, Brookhart and Bernskoetter reported that an Ir-dihydride pincer complex (**6**) promoted the dehydrogenation of isobutylamine to form isobutyronitrile in the presence of excess hydrogen acceptor (*tert*-butylethylene) at 200 °C after 24 h (Figure 1-9).^{46g}

The proposed catalytic cycle, supported by a series of kinetic rate data and isotopic labeling experiments, is consistent with a reversible N–H oxidative addition reaction followed by rate-determining β -hydride elimination to generate an Ir-dihydride imine intermediate. Subsequent steps to afford an Ir-nitrile complex, which is the resting state of the catalyst, proceed rapidly with no dependence on the hydrogen acceptor.

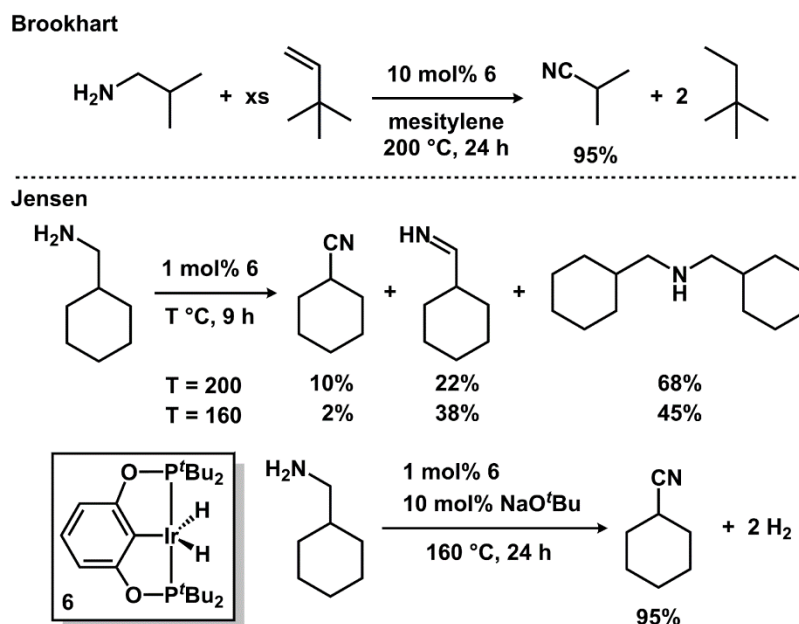


Figure 1-9 Primary amine dehydrogenation studies by Brookhart and Jensen.

Later work by Jensen and co-workers showed that a hydrogen acceptor was not required for dehydrogenative reactivity by **6**, and was reported for cyclohexanemethylamine (Figure 1-9).^{46h} In the absence of additives, they noted that nitrile, imine, and transamination products were formed. The product selectivity was not significantly affected by changing the reaction temperature (postulated to inhibit transamination). However, the selectivity for nitrile formation was improved in the presence of NaO^tBu. When 10 mol% of NaO^tBu was added, complex **6** catalyzed the double dehydrogenation of cyclohexanemethylamine to cyclohexanecarbonitrile in 95% yield, with trace amounts of the dialkylamine and imine products. Although these studies demonstrated the viability of amine dehydrogenation using **6** and either a hydrogen acceptor or an added base, a catalyst system that can accomplish this transformation without any additives and in good conversions remains highly attractive.

1.2 Bis(pyridylimino)isoindolate Transition Metal Complexes

1.2.1 Introduction

The coordination chemistry of transition-metal complexes is dictated by the ancillary ligands, which also define their physical and chemical properties.^{23b,52} Since the late 1970s, pincer-type ligands have been extensively studied in organometallic chemistry and homogeneous catalysis.⁵³ The term “pincer” is commonly used for all meridionally coordinating tridentate chelate ligands. The use of pincer frameworks in metal complexes has led to remarkable achievements in the field of small-molecule bond activation, which is relevant for catalytic applications.^{53a-c}

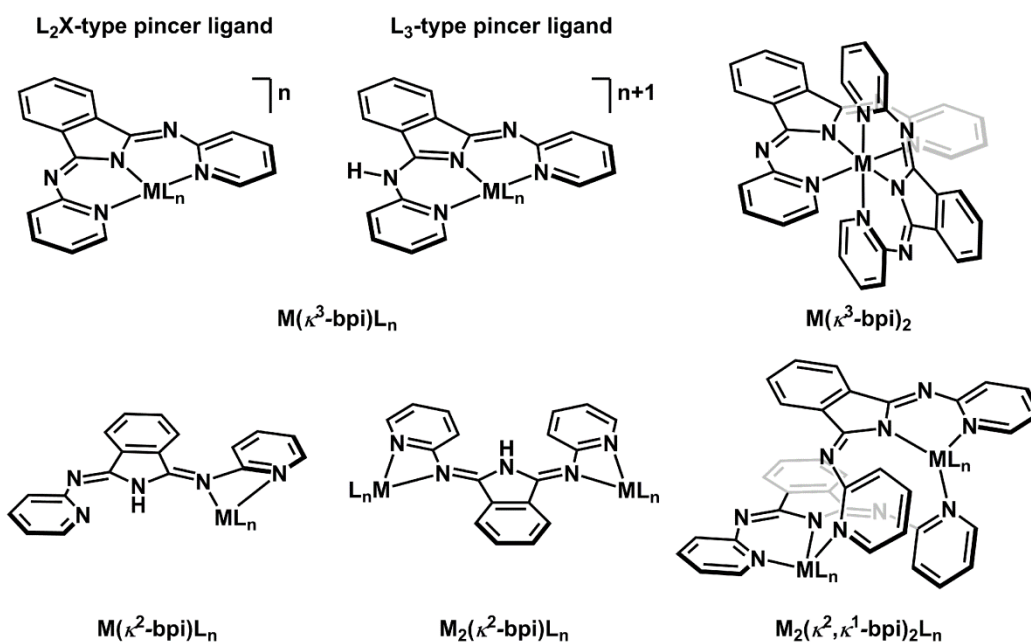


Figure 1-10 Coordination modes of bis(pyridylimino)isoindoline ligand.

In 1952, Elvidge and Linstead introduced the first 1,3-bis(2'-pyridylimino)isoindoline (bpi) ligand as a byproduct of research into phthalocyanine derivatives, which are used as organic dyes/pigments.⁵⁴ The bpi framework contains a central isoindoline group that is linked to two pyridyl rings with imine moieties.⁵⁵ Investigation into the coordination chemistry of metal–bpi complexes started in the 1970s,⁵⁶ and bpi-type ligands typically coordinate in a meridional tridentate (*N,N,N*) fashion to the metal center as a L₂X- or L₃-type donor.⁵⁷ Other denticities, such as κ^2 -(*N,N*), and coordination modes have also been characterized to afford homoleptic or

binuclear complexes (Figure 1-10).^{57c,57h,58} To date, bpi scaffolds have been employed as pincer ligands with almost the full range of transition metals, including Mn,^{58a,58d,59} Fe,^{57d,57e,57g,57m,58a,58e,58h} Co,^{57d,57f,57g,57i,57m,58a} Ni,^{58a,60} Cu,^{57l,58a,61} Zn,^{58a,60,61c,62} Mo,^{58i,63} Ru,⁶⁴ Pd,^{57k,62a} Cd,^{62,65} Rh,⁶⁶ Os,^{57b} Ir,^{57c,57h,66} Pt,⁶⁷ and Hg⁶⁸. Recent developments demonstrated bpi metal complexes as tunable and versatile structural building blocks for appealing applications ranging from material science (e.g., ion sensors,^{67b} photoactive materials,⁶⁹ and molecular electronics⁷⁰) to enzyme modeling (e.g., phenoxazinone synthase,^{59,71} catalase,^{58d,72} catechol oxidase,^{58c,59,73} catechol dioxygenase,^{57n,61a,74} and superoxide dismutase⁷⁵). In some cases, these transition-metal complexes have emerged as molecular catalysts in oxidation,^{57h,57k,57m,57n,58h,76} hydrogenation,^{57k} and asymmetric hydrosilylation^{57f,57j} reactions.

1.2.2 Synthesis and Characterization of Bis(pyridylimino)isoindoline Compounds

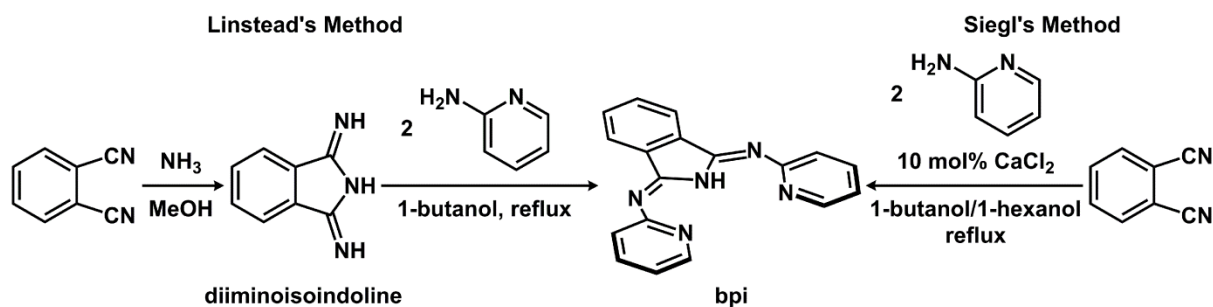


Figure 1-11 Synthesis of bis(pyridylimino)isoindoline compounds.

The synthesis of bpi derivatives is highly modular and readily achieved from cheap, commercially available starting materials to easily access a large variety of compounds. The original synthetic route was a two-step process that initiated with the condensation of phthalonitrile with ammonia in dry methanol to generate diiminoisoindoline, which undergoes condensation with 2 equiv of 2-aminopyridine in refluxing 1-BuOH (117 °C) to afford bpi (Linstead's method, Figure 1-11).⁵⁴ However, in 1974, Siegl found that bpi compounds could be synthesized directly from the condensation of phthalonitrile with 2 equiv of 2-aminopyridine in the presence of Lewis acidic CaCl₂ (10 mol%) to activate the nitrile groups and to template the condensation reaction (Siegl's method, Figure 1-11).^{60,77} To obtain higher yields, particularly for sterically crowded ligand environments, the condensation reaction could be performed in 1-hexanol instead of 1-butanol, which allows for higher reaction temperatures (boiling point of 1-hexanol is 155–159 °C).^{57l} Because of the modular assembly of bpi compounds, functional

groups on both the isoindolato backbone and the pyridyl rings are easily installed by modifications of the starting materials.^{57j}

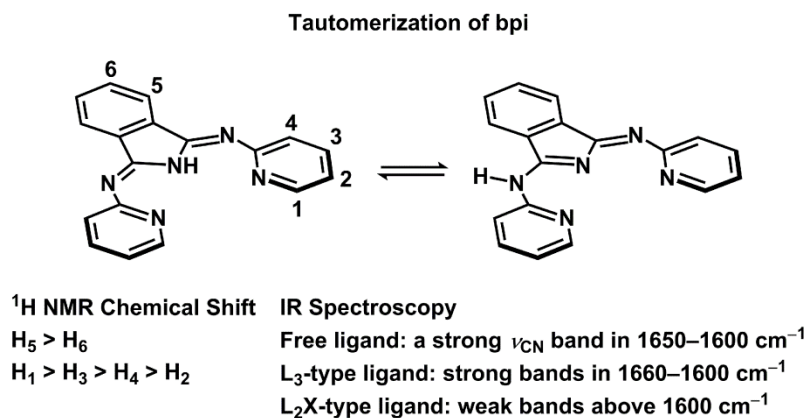


Figure 1-12 General ¹H NMR and IR characterization trends for bis(pyridylimino)isoindolines.

The imine motifs on the bpi framework strongly influence the structural and electronic properties of the free ligand and the coordinated complexes.⁵⁵ The double bond of the imine linkers extends the π system throughout the bpi scaffold, which forces a planar structure and enhances the rigidity and robustness of the system.⁷⁸ Depending on the substitution pattern in the pyridyl rings (e.g., sterically encumbered groups *ortho* to the pyridyl nitrogens), this planar conformation may be disrupted by the twisting of the pyridyl groups out of the molecular plane. In addition, the N–H proton lies in the plane of the molecule and exhibits hydrogen bonding to the pyridyl nitrogen atoms, which is revealed by a downfield chemical shift of the N–H hydrogens (12–14 ppm) in the ¹H NMR spectrum. The N–H functionality coupled with imine groups, whose lone electron pair can be engaged upon protonation, enable proton-responsive activity in bpi compounds depending on the pH environment.⁷⁹ In coordination chemistry, the bpi ligand can function as a monoanionic L₂X donor when the N–H proton is deprotonated or a neutral L₃-type donor when the N–H proton is shifted onto one of the imine arms (Figure 1-10). In general, the IR spectra of bpi compounds exhibit a very strong ν_{CN} band in the 1650–1600 cm⁻¹ region and four moderate–strong bands in the 1600–1400 cm⁻¹, which are assigned to pyridyl skeletal vibrations.⁷⁷ The donor properties of the bpi ligand can be easily distinguished using IR spectroscopy. For instance, strong bands are detected in the 1660–1600 cm⁻¹ region when the bpi ligand act as a L₃-type ligand and weak bands above 1600 cm⁻¹ for a L₂X bpi ligand. In most cases, the aromatic hydrogens on bpi compounds are well separated in the ¹H

NMR spectra and assignments can be made. On the isoindolato ring, H₅ appear more downfield than H₆ due to deshielding by the imino π -electron cloud. The hydrogens on the pyridyl ring typically shift more downfield in the following order: H₁ > H₃ > H₄ > H₂ (Figure 1-12).⁷⁷

1.2.3 Oxidation Reactions Catalyzed by Bis(pyridylimino)isoindoline Complexes

Following the investigation of the coordination chemistry of transition-metal bpi complexes, several groups reported on the catalytic capabilities of these complexes in oxidative catalysis. In 1984, Gagné and Marks demonstrated aerobic oxidation of primary and secondary alcohols catalyzed by Ru(Hb4Mepi)Cl₃ (Hb4Mepi = 1,3-bis(4'-methyl-2'-pyridylimino)isoindoline) at room temperature to 90 °C.^{76a} Catalytic aerobic oxidation of aliphatic primary and secondary alcohols was general to afford the corresponding aldehydes and acetals and ketones, respectively (Figure 1-13). For example, **7** demonstrated 100 turnovers in 24 h for the conversion of 1-BuOH to a mixture of butyraldehyde and 1,1-dibutoxybutane, and the oxidation of 2-butanol to 2-butanone. Unfortunately, the product distribution or selectivity for primary alcohol oxidation was not reported. Under the same reaction conditions, no reactivity was observed when Co(Hb4Mepi)Br₂ or Fe(b4Mepi)Cl₂ was used instead of Ru(Hb4Mepi)Cl₃.

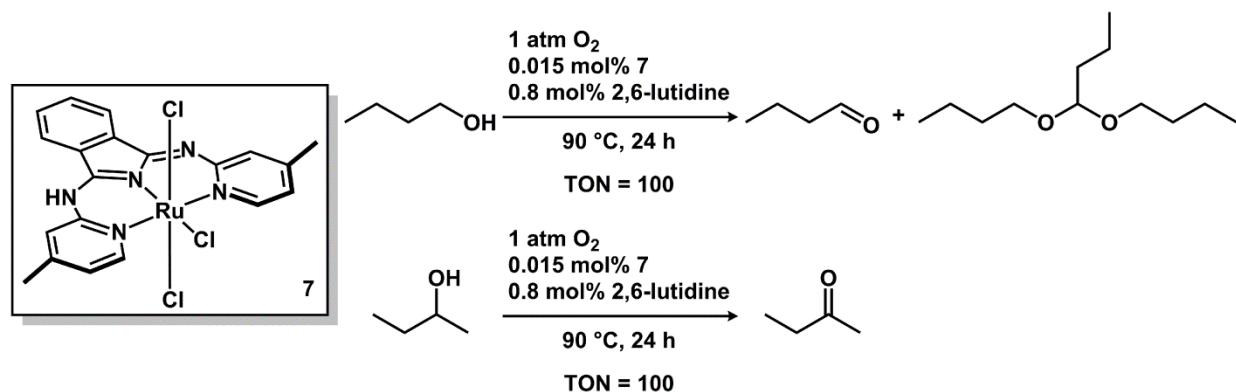


Figure 1-13 Aerobic alcohol oxidation catalyzed by Ru(Hb4Mepi)Cl₃.

A year later, Mimoun and co-workers described a detailed study of hydroxylation of alkanes and peroxylation alkenes using Co(bpi)(OAc) precursors, which included structural characterization of Co alkylperoxy complexes (**8**) as the catalytically-active species (Figure 1-14).^{76b} Unfortunately, oxidation of hydrocarbons formed a mixture of *t*-butyl peroxide, alcohol, and carbonyl compounds with no selectivity using 97% pure ^tBuOOH as the oxidant in the presence of **8** at 20–80 °C. In the case of alkane substrates, complex **8** catalyzed the oxidation of

cyclohexane to a mixture of cyclohexanol (33%), cyclohexanone (20%), and *t*-butylperoxycyclohexane (6%) at 80 °C for 1.5 h. In 2003, this transformation was mediated by a less active binuclear Fe–bpi catalyst (**9**) that showed 15% yields of cyclohexanol and cyclohexanone using 1 mol% catalyst loading and H₂O₂ in ACN at room temperature for 10 h (Figure 1-14).^{58h}

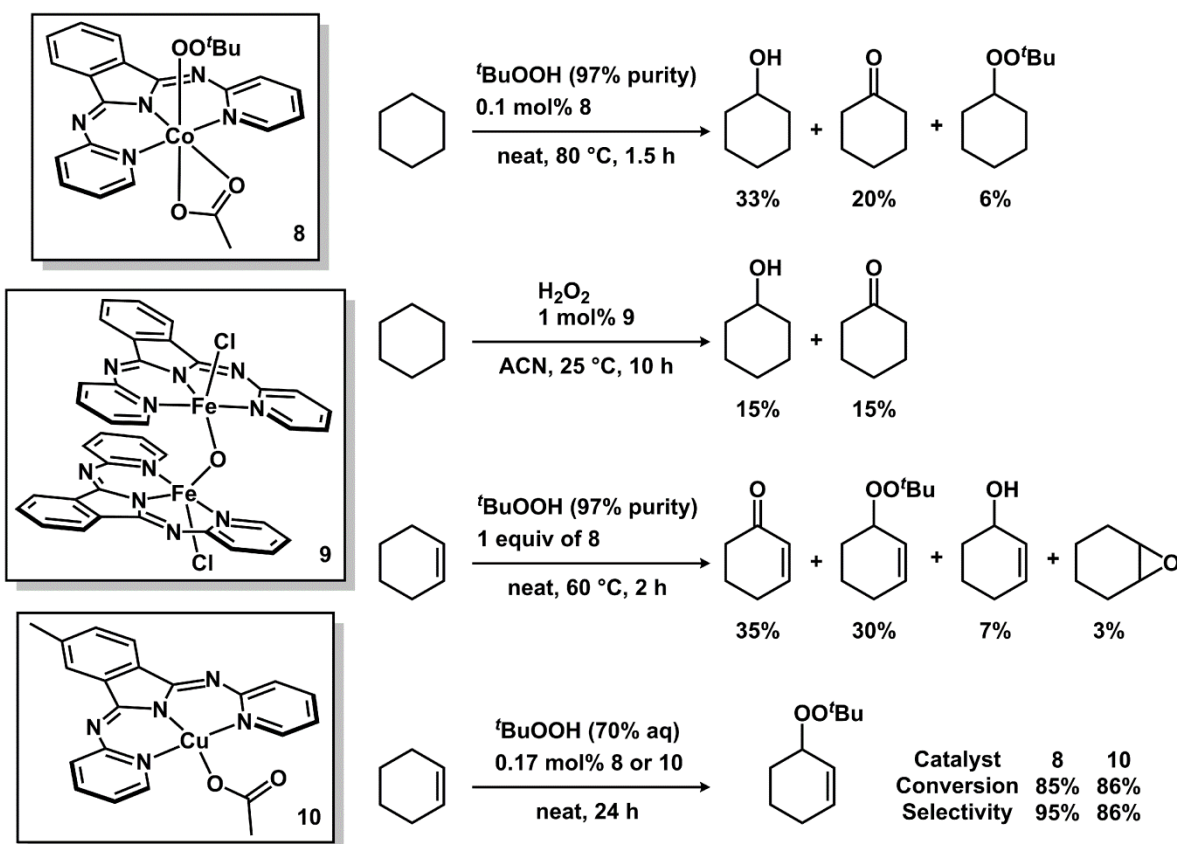


Figure 1-14 Hydroxylation of alkanes and peroxylation of alkenes catalyzed by first row metal–bpi complexes.

For alkene substrates, only stoichiometric oxidation reactions were performed using **8** and *t*BuOOH. For instance, cyclohexene was converted to a mixture of cyclohex-2-en-1-one (35%), cyclohex-2-ene-1-*t*-butylperoxide (30%), cyclohex-2-en-1-ol (7%), and epoxy-cyclohexane (3%) at 60 °C.^{76b} Subsequently, Gade and co-workers optimized the reaction conditions to using 0.17 mol% **8** and 70% aqueous solution of *t*BuOOH at room temperature to catalytically oxidize cyclohexene to cyclohex-2-ene-1-*t*-butylperoxide with 85% conversion and 95% selectivity.^{57m} In addition, the activity and selectivity of the Co catalysts were not influenced by electron-donating and -withdrawing groups *para* and/or *meta* to the pyridyl

nitrogen atoms on the bpi ligand. Furthermore, under identical reaction conditions, an analogous Cu complex (**10**, Figure 1-14) exhibited similar oxidation activity as **8** with lower selectivity.⁵⁷ⁱ The decrease in selectivity was attributed to a slower secondary reaction which oxidized the dialkyl peroxide product to cyclohex-2-en-1-one.

In addition to peroxylation of unsaturated hydrocarbons, Gade's group also reported on epoxidation of alkenes using Ir complexes with bpi-type ligands (Figure 1-15).^{57h} Complex **11** featured κ^2 -(*N,N*) coordination mode of the bpi ligand where one of the pyridine units is twisted away from the Ir center. In contrast, the synthesis of **12** using sterically less demanding ethylene ligands than 1,5-cyclooctadiene ligand led to the anticipated meridional coordination of the bpi ligand, which resulted in trigonal bipyramidal geometry about Ir. The two Ir–bpi complexes displayed similar activities for the catalytic epoxidation of alkenes using PPO, which is a highly reactive oxaziridine-type oxidizing reagent. Screening of other oxygen-transfer agents such as H₂O₂ and iodosobenzene showed either rapid catalyst deactivation or incomplete conversion. Epoxidation of a wide range of aliphatic cyclic and acyclic alkenes (18 examples) was general to afford the corresponding epoxides in 24–96% yields using 1 mol% catalyst loading and 1.5 equiv of PPO in DCM for 7–48 h (Figure 1-15). For example, *trans*-stilbene was converted to the corresponding epoxide in 91% isolated yield after 24 h.

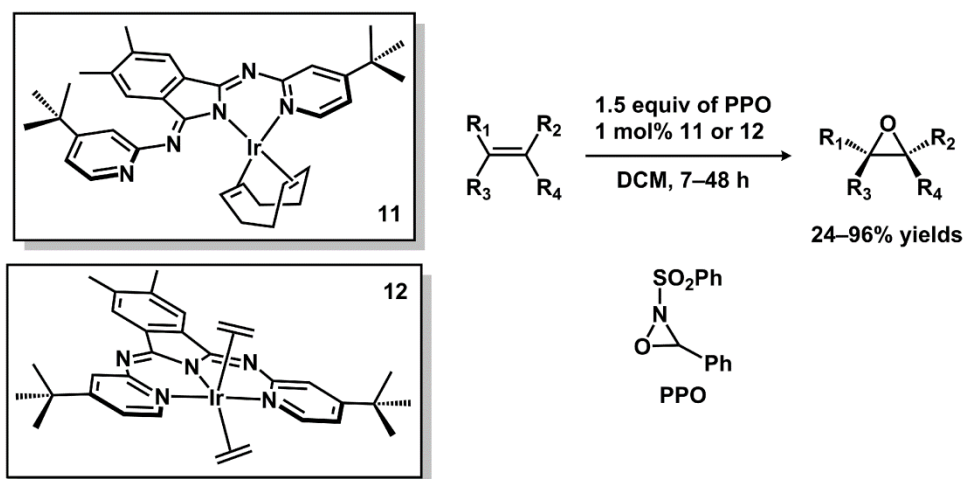


Figure 1-15 Epoxidation of alkenes catalyzed by Ir–b^{4'}Bupi complexes.

More recently in 2013, Que, Kaizer, Speier, and co-workers developed a Fe(Hbpi)(ACN)₃[ClO₄]₂ (**13**) system capable of catalytic oxidation of thioanisoles and benzyl

alcohols using H₂O₂.⁵⁷ⁿ Complex **13** was isolated by allowing Hbpi to react with Fe(ClO₄)₂ in ACN, and the X-ray structure revealed an octahedral geometry around the Fe center with an asymmetric neutral bpi ligand meridionally coordinated and three ACN ligands. Investigation of **13** as a catalyst for the oxidation of thioanisoles and benzyl alcohols demonstrated that **13** is capable of catalyzing both oxygen-atom transfer and hydrogen-atom abstraction. For instance, oxidation of thioanisole to the corresponding sulfoxide and sulfone required 1 mol% **13** and 2.5 equiv of H₂O₂ in ACN at 25 °C for 1 h (Figure 1-16). Analysis of isotopic labeling and Hammett studies suggested that **13** operates *via* a direct oxygen-atom transfer pathway with an electrophilic metal-centered oxidant as an intermediate in the mechanism.

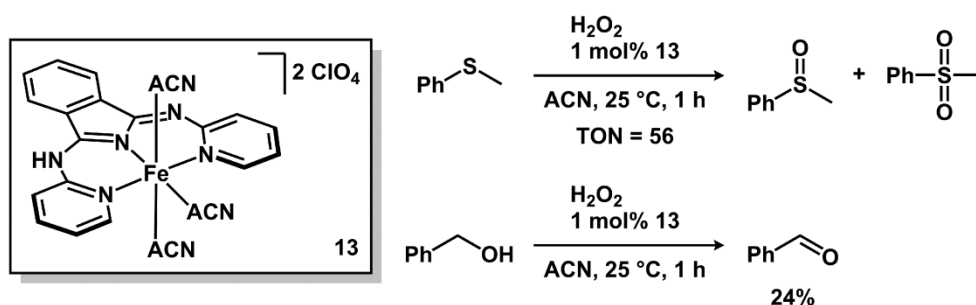


Figure 1-16 Thioanisole and benzyl alcohol oxidation catalyzed by Fe–Hbpi complex.

1.2.4 Reduction Reactions Catalyzed by Bis(pyridylimino)isoindoline Complexes

Although oxidation catalysis has been widely studied using first, second, and third row metal–bpi complexes, few examples of reductive catalysis with bpi ligand have been reported.^{57f,57j,57k} In 2004, Gade’s group developed a series of Pd complexes with *meta*-substituted bpi pincer ligands, including Me, Br, and alkyne functional groups.^{57k} In particular, Pd(b5Mepi)Cl (**14**, b5Mepi = 1,3-bis(5’methyl-2’-pyridylimino)isoindolate) was examined as an alkene hydrogenation catalyst using H₂ at room temperature (Figure 1-17). Hydrogenation of styrene under 1 atm of H₂ and 2 mol% **14** in THF at 25 °C for 9 h afford ethylbenzene in 80% conversion. The stability of this system was demonstrated by recycling the catalyst in multiple hydrogenation cycles with minimal loss of catalytic activity. The mechanism of hydrogenation was proposed to operate through bifunctional metal–ligand catalysis, in which H₂ heterolysis is cleaved across the backbone imine group on the bpi ligand and the metal center. Unfortunately, the proposed metal–ligand cooperative pathway was not supported by any experimental or computational evidence.

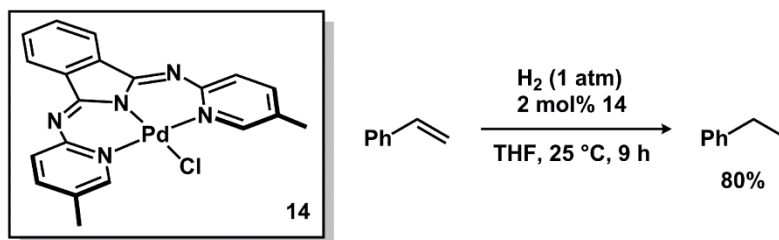


Figure 1-17 Alkene hydrogenation catalyzed by Pd–b5Mepi complex.

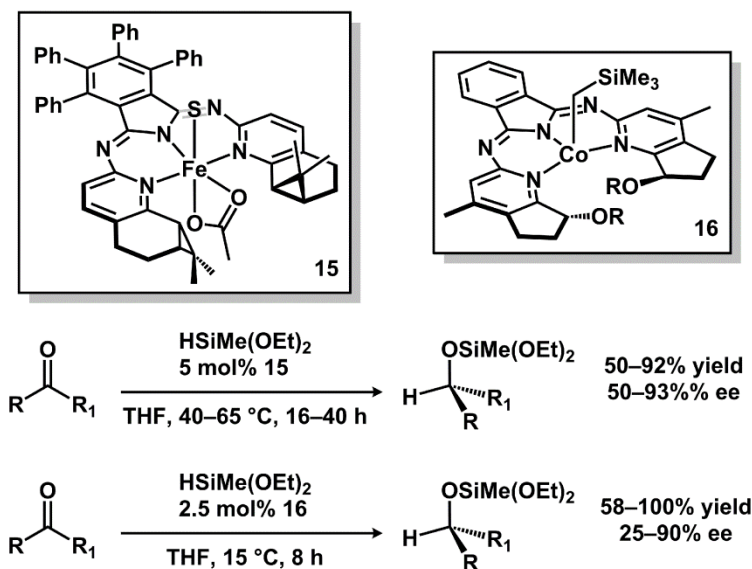


Figure 1-18 Asymmetric hydrosilylation of ketones catalyzed by Fe and Co complexes with chiral bpi ligands.

Recent developments in the use of bpi ligands have targeted chiral derivatives for enantioselective hydrosilylation catalysis. Chiral bpi variants can be prepared by installing the chiral information onto the pyridyl rings that are in close proximity to the metal center. In 2008, Langoltaz, Wadepohl, and Gade reported the synthesis of chiral bpi ligands from chiral aminopyridines derived from commercially available terpenes.^{57j} This new family of chiral bpi ligands was metalated with $\text{Fe}(\text{OAc})_2$ and $\text{Co}(\text{OAc})_2$ to generate distorted octahedral $\text{M}(\text{bpi})(\text{OAc})\text{L}$ type complexes ($\text{L} = \text{MeOH}$ or THF). Of particular note, complex **15** demonstrated the highest enantiomeric excess (50–93%) for the asymmetric hydrosilylation of ketones with yields of 50–92% using 5 mol% **15** in THF at 40–65 °C for 16–40 h (Figure 1-18). In general, higher yields and enantioselectivities were achieved when aryl alkyl ketones were used instead of dialkyl ketone substrates. In addition, this transformation was also promoted by $\text{Co}-\text{CH}_2\text{SiMe}_3$ systems with a different family of chiral bpi ligands (**16**) using lower catalyst

loading (2.5 mol%) and temperature (15 °C) for a shorter amount of time (8 h).^{57f} For example, aryl alkyl ketones were reduced to the corresponding chiral hydrosilylated products in 58–100% yields with 25–90% enantioselectivities (Figure 1-18).

1.2.5 Outlook for Catalytic Applications Using Bis(pyridylimino)isoindoline Ligands

Pincer scaffolds provide a versatile framework to control the steric and electronic properties of transition metal complexes as well as enhance the stability in part due to the rigid and robust nature of most pincer ligands. The bpi pincer ligand incorporates amine/amide and imine functionalities, which were demonstrated to participate in bifunctional metal–ligand catalysis on other pincer scaffolds. In addition, the lone electron pair on the imine linkers can be engaged upon protonation, thus enabling ligand tautomerization to use the bpi pincer ligands as monoanionic L₂X or neutral L₃ donors. Although prior reports developed metal–bpi complexes for oxidative and reductive catalysis, the activity and selectivity in these transformations were often unremarkable and mirrored the behavior of previously established metal-based systems. Furthermore, the relationship between catalyst structure and reactivity remains ambiguous and underdeveloped, specifically the role of the bpi pincer ligand during catalysis. Because of the potential participation of the backbone amine and imines on the bpi ligand in bifunctional metal–ligand catalysis, the use of bpi-type ligands in dehydrogenative transformations might uncover new reactivity profiles. Moreover, the prior use of bpi ligands often contain no functional groups *ortho* to the pyridyl nitrogen atoms, therefore appending functionalities at that position, which is in close proximity to the metal center, might enable new synergistic interactions for small molecule activation.

1.3 Dissertation Outline and Scope

This dissertation is framed around the synthesis, structure, and reactivity of transition-metal complexes supported by bMepi-derived (1,3-bis(6'-methyl-2'-pyridylimino)isoindolate) architectures. In Chapter 2, the development of dehydrogenative transformations of alcohols catalyzed by Ru–bpi complexes is described. The hydride variant of Ru–bMepi complex (HRu(bMepi)(PPh₃)₂) is capable of catalyzing dehydrogenation and dehydrogenative coupling reactions of secondary and primary alcohols/diols, respectively, without requirements of exogenous base or acceptor additives. Additionally, unprecedented catalytic activity for

upgrading EtOH to 1-BuOH *via* the Guerbet sequence using Ru(bpi)(PPh₃)₂Cl precursors is highlighted. Chapter 3 discloses a detailed mechanistic analysis of AAD mediated by HRu(bMepi)(PPh₃)₂ using a series of kinetic and isotopic labeling studies, isolation of intermediates, and catalytic modifications. Chapter 4 accounts the development of HRu(bMepi)(PPh₃)₂ as a catalyst for oxidant-free, acceptorless, and chemoselective dehydrogenation of primary and secondary amines to the corresponding nitriles and imines with liberation of H₂. The amine dehydrogenation methodology is noteworthy because this system catalyzes the chemoselective oxidation of primary amines with –CH₂NH₂ functionality in the presence of primary amines without α hydrogens. In Chapter 5, the principles of dehydrogenation and hydrogenation are extended to functionalization reactions such as hydroboration and hydrosilylation promoted by Fe–bMepi complexes. Alkylation of the imine backbone of the bMepi framework is used to as a late-stage modification to confer a more electrophilic complex. The alkylated Fe system, compared to the parent complex, catalyzes olefin hydroboration with an increased reaction rate and exhibits distinct regioselectivity for internal alkene hydroboration. Chapter 6 details the development of a new series of multifunctional Ru complexes with appended BR₂ groups *via* B–H bond activation and demonstrate by variation of the borane moiety how Lewis acidity influences the reactivity of the Ru hydride and biases the system for *Z*-selective semi-hydrogenation of alkynes. Lastly, perspective and prospects on new applications using bpi-based transition metal systems are discussed in Chapter 7.

1.4 References

- (1) (a) Kitamura, M.; Noyori, R. In *Ruthenium in Organic Synthesis*; Wiley-VCH: Weinheim, Germany, 2005. (b) Zhou, C.-H.; Beltramini, J. N.; Fan, Y.-X.; Lu, G. Q. *Chem. Soc. Rev.* **2008**, *37*, 527.
- (2) Dobereiner, G. E.; Crabtree, R. H. *Chem. Rev.* **2010**, *110*, 681.
- (3) Hamid, M. H. S. A.; Slatford, P. A.; Williams, J. M. J. *Adv. Synth. Catal.* **2007**, *349*, 1555.
- (4) (a) Gunanathan, C.; Milstein, D. *Science* **2013**, *341*. (b) Gunanathan, C.; Milstein, D. *Acc. Chem. Res.* **2011**, *44*, 588.
- (5) Guerbet, M. *Compt. rend.* **1909**, *149*, 129.

- (6) Gabriels, D.; Hernandez, W. Y.; Sels, B.; Van Der Voort, P.; Verberckmoes, A. *Catal. Sci. Technol.* **2015**, *5*, 3876.
- (7) Wiberg, K. B.; Crocker, L. S.; Morgan, K. M. *J. Am. Chem. Soc.* **1991**, *113*, 3447.
- (8) (a) Nielsen, M. In *Hydrogen Production and Remediation of Carbon and Pollutants*; Lichtfouse, E., Schwarzbauer, J., Robert, D., Eds.; Springer International Publishing: Cham, Switzerland, 2015. (b) Conley, B. L.; Pennington-Boggio, M. K.; Boz, E.; Williams, T. J. *Chem. Rev.* **2010**, *110*, 2294. (c) Samec, J. S. M.; Baeckvall, J.-E.; Andersson, P. G.; Brandt, P. *Chem. Soc. Rev.* **2006**, *35*, 237. (d) Wang, D.; Astruc, D. *Chem. Rev.* **2015**, *115*, 6621. (e) Chelucci, G.; Baldino, S.; Baratta, W. *Acc. Chem. Res.* **2015**, *48*, 363. (f) Ikariya, T.; Blacker, A. J. *Acc. Chem. Res.* **2007**, *40*, 1300. (g) Clapham, S. E.; Hadzovic, A.; Morris, R. H. *Coord. Chem. Rev.* **2004**, *248*, 2201. (h) Noyori, R.; Hashiguchi, S. *Acc. Chem. Res.* **1997**, *30*, 97.
- (9) (a) de, G. C. F.; Peters, J. A.; van, B. H.; Huskens, J. *Synthesis* **1994**, 1007. (b) Cohen, R.; Graves, C. R.; Nguyen, S. T.; Martin, J. M. L.; Ratner, M. A. *J. Am. Chem. Soc.* **2004**, *126*, 14796.
- (10) Adkins, H.; Eloffson, R. M.; Rossow, A. G.; Robinson, C. C. *J. Am. Chem. Soc.* **1949**, *71*, 3622.
- (11) (a) Ho, H.-A.; Manna, K.; Sadow, A. D. *Angew. Chem., Int. Ed.* **2012**, *51*, 8607. (b) Melnick, J. G.; Radosevich, A. T.; Villagran, D.; Nocera, D. G. *Chem. Commun.* **2010**, *46*, 79. (c) Crabtree, R. H.; Pearman, A. J. *J. Organomet. Chem.* **1978**, *157*, 335. (d) Sieffert, N.; Reocreux, R.; Lorusso, P.; Cole-Hamilton, D. J.; Buehl, M. *Chem. - Eur. J.* **2014**, *20*, 4141.
- (12) Oppenauer, R. V. *Recl. Trav. Chim. Pays-Bas Belg.* **1937**, *56*, 137.
- (13) Woodward, R. B.; Wendler, N. L.; Brutschy, F. J. *J. Am. Chem. Soc.* **1945**, *67*, 1425.
- (14) Namy, J. L.; Soupe, J.; Collin, J.; Kagan, H. B. *J. Org. Chem.* **1984**, *49*, 2045.
- (15) Dess, D. B.; Martin, J. C. *J. Org. Chem.* **1983**, *48*, 4155.
- (16) Bowden, K.; Heilbron, I. M.; Jones, E. R. H.; Weedon, B. C. L. *J. Chem. Soc.* **1946**, 39.
- (17) (a) Omura, K.; Swern, D. *Tetrahedron* **1978**, *34*, 1651. (b) Harris, J. M.; Liu, Y.; Chai, S.; Andrews, M. D.; Vederas, J. C. *J. Org. Chem.* **1998**, *63*, 2407.
- (18) Svoboda, P.; Hetflejš, J. *Collect. Czech. Chem. Commun.* **1977**, *42*, 2177.
- (19) (a) Sasson, Y.; Blum, J. *J. Org. Chem.* **1975**, *40*, 1887. (b) Regen, S. L.; Whitesides, G. M. *J. Org. Chem.* **1972**, *37*, 1832. (c) Imai, H.; Nishiguchi, T.; Fukuzumi, K. *J. Org. Chem.* **1976**, *41*, 2688.
- (20) Haddad, Y. M. Y.; Henbest, H. B.; Husbands, J.; Mitchell, T. R. B. *Proc. Chem. Soc.* **1964**, 361.
- (21) (a) Charman, H. B. *J. Chem. Soc. B* **1970**, *4*, 584. (b) Morton, D.; Cole-Hamilton, D. J. *J. Chem. Soc., Chem. Commun.* **1987**, 248. (c) Lighthart, G. B. W. L.; Meijer, R. H.; Donners, M. P. J.; Meuldijk, J.; Vekemans, J. A. J. M.; Hulshof, L. A. *Tetrahedron Lett.* **2003**, *44*, 1507.

- (22) Grigg, R.; Mitchell, T. R. B.; Sutthivaiyakit, S. *Tetrahedron* **1981**, *37*, 4313.
- (23) (a) Werkmeister, S.; Neumann, J.; Junge, K.; Beller, M. *Chem. - Eur. J.* **2015**, *21*, 12226. (b) Li, H.; Zheng, B.; Huang, K.-W. *Coord. Chem. Rev.* **2015**, *293-294*, 116.
- (24) Khusnutdinova, J. R.; Milstein, D. *Angew. Chem., Int. Ed.* **2015**, *54*, 12236.
- (25) (a) Shvo, Y.; Czarkie, D.; Rahamim, Y.; Chodosh, D. F. *J. Am. Chem. Soc.* **1986**, *108*, 7400. (b) Karvembu, R.; Prabhakaran, R.; Natarajan, K. *Coord. Chem. Rev.* **2005**, *249*, 911.
- (26) Almeida, M. L. S.; Kocovsky, P.; Baeckvall, J.-E. *J. Org. Chem.* **1996**, *61*, 6587.
- (27) (a) Johnson, J. B.; Baeckvall, J.-E. *J. Org. Chem.* **2003**, *68*, 7681. (b) Thorson, M. K.; Klinkel, K. L.; Wang, J.; Williams, T. J. *Eur. J. Inorg. Chem.* **2009**, 295.
- (28) Coleman, M. G.; Brown, A. N.; Bolton, B. A.; Guan, H. *Adv. Synth. Catal.* **2010**, *352*, 967.
- (29) Zhang, J.; Balaraman, E.; Leitus, G.; Milstein, D. *Organometallics* **2011**, *30*, 5716.
- (30) Li, H.; Wang, X.; Huang, F.; Lu, G.; Jiang, J.; Wang, Z.-X. *Organometallics* **2011**, *30*, 5233.
- (31) (a) Nielsen, M.; Kammer, A.; Cozzula, D.; Junge, H.; Gladiali, S.; Beller, M. *Angew. Chem., Int. Ed.* **2011**, *50*, 9593. (b) Nielsen, M.; Junge, H.; Kammer, A.; Beller, M. *Angew. Chem., Int. Ed.* **2012**, *51*, 5711. (c) Nielsen, M.; Alberico, E.; Baumann, W.; Drexler, H.-J.; Junge, H.; Gladiali, S.; Beller, M. *Nature* **2013**, *495*, 85.
- (32) (a) Abdur-Rashid, K.; Clapham, S. E.; Hadzovic, A.; Harvey, J. N.; Lough, A. J.; Morris, R. H. *J. Am. Chem. Soc.* **2002**, *124*, 15104. (b) Sandoval, C. A.; Ohkuma, T.; Muniz, K.; Noyori, R. *J. Am. Chem. Soc.* **2003**, *125*, 13490.
- (33) Zhang, G.; Vasudevan, K. V.; Scott, B. L.; Hanson, S. K. *J. Am. Chem. Soc.* **2013**, *135*, 8668.
- (34) (a) Kawahara, R.; Fujita, K.-i.; Yamaguchi, R. *J. Am. Chem. Soc.* **2012**, *134*, 3643. (b) Fujita, K.-i.; Tanaka, Y.; Kobayashi, M.; Yamaguchi, R. *J. Am. Chem. Soc.* **2014**, *136*, 4829. (c) Yamaguchi, R.; Ikeda, C.; Takahashi, Y.; Fujita, K.-i. *J. Am. Chem. Soc.* **2009**, *131*, 8410.
- (35) Zeng, G.; Sakaki, S.; Fujita, K.-i.; Sano, H.; Yamaguchi, R. *ACS Catal.* **2014**, *4*, 1010.
- (36) Murahashi, S.; Ito, K.; Naota, T.; Maeda, Y. *Tetrahedron Lett.* **1981**, *22*, 5327.
- (37) Blum, Y.; Shvo, Y. *J. Organomet. Chem.* **1985**, *282*, C7.
- (38) Murahashi, S.; Naota, T.; Ito, K.; Maeda, Y.; Taki, H. *J. Org. Chem.* **1987**, *52*, 4319.
- (39) Zhang, J.; Leitus, G.; Ben-David, Y.; Milstein, D. *J. Am. Chem. Soc.* **2005**, *127*, 10840.
- (40) (a) Gunanathan, C.; Ben-David, Y.; Milstein, D. *Science* **2007**, *317*, 790. (b) Gnanaprakasam, B.; Milstein, D. *J. Am. Chem. Soc.* **2011**, *133*, 1682.
- (41) (a) Nordstrom, L. U.; Vogt, H.; Madsen, R. *J. Am. Chem. Soc.* **2008**, *130*, 17672. (b) Schley, N. D.; Dobereiner, G. E.; Crabtree, R. H. *Organometallics* **2011**, *30*, 4174.

- (42) (a) Zeng, H.; Guan, Z. *J. Am. Chem. Soc.* **2011**, *133*, 1159. (b) Gnanaprakasam, B.; Balaraman, E.; Ben-David, Y.; Milstein, D. *Angew. Chem., Int. Ed.* **2011**, *50*, 12240.
- (43) (a) Fleming, F. F.; Yao, L.; Ravikumar, P. C.; Funk, L.; Shook, B. C. *J. Med. Chem.* **2010**, *53*, 7902. (b) Fleming, F. F. *Nat. Prod. Rep.* **1999**, *16*, 597.
- (44) Sheldon, R. A.; Kochi, J. K. In *Metal-catalyzed Oxidations of Organic Compounds*; Academic Press: 1981.
- (45) Nicolaou, K. C.; Mathison, C. J. N. *Angew. Chem., Int. Ed.* **2005**, *44*, 5992.
- (46) (a) Schumperli, M. T.; Hammond, C.; Hermans, I. *ACS Catal.* **2012**, *2*, 1108. (b) Murahashi, S.-I.; Imada, Y. In *Transition Metals for Organic Synthesis*; Wiley-VCH: Weinheim, Germany, 2008; pp 497. (c) Yamaguchi, K.; Mizuno, N. *Angew. Chem., Int. Ed.* **2003**, *42*, 1480. (d) Kim, J.; Stahl, S. S. *ACS Catal.* **2013**, *3*, 1652. (e) Cristian, L.; Nica, S.; Pavel, O. D.; Mihailciuc, C.; Almasan, V.; Coman, S. M.; Hardacre, C.; Parvulescu, V. I. *Catal. Sci. Technol.* **2013**, *3*, 2646. (f) Yoshida, T.; Okano, T.; Otsuka, S. *J. Chem. Soc., Chem. Commun.* **1979**, 870. (g) Bernskoetter, W. H.; Brookhart, M. *Organometallics* **2008**, *27*, 2036. (h) Wang, Z.; Belli, J.; Jensen, C. M. *Faraday Discuss.* **2011**, *151*, 297. (i) Okano, K.; Saito, Y.; Ogino, Y. *Bull. Chem. Soc. Jap.* **1972**, *45*, 69.
- (47) (a) Rodríguez-Lugo, R. E.; Trincado, M.; Vogt, M.; Tewes, F.; Santiso-Quinones, G.; Grützmacher, H. *Nat Chem* **2013**, *5*, 342. (b) Spasyuk, D.; Smith, S.; Gusev, D. G. *Angew. Chem., Int. Ed.* **2012**, *51*, 2772.
- (48) Wu, J.; Talwar, D.; Johnston, S.; Yan, M.; Xiao, J. *Angew. Chem., Int. Ed.* **2013**, *52*, 6983.
- (49) (a) Prades, A.; Peris, E.; Albrecht, M. *Organometallics* **2011**, *30*, 1162. (b) Yi, C. S.; Lee, D. W. *Organometallics* **2009**, *28*, 947.
- (50) Yoshimura, N.; Moritani, I.; Shimamura, T.; Murahashi, S. *J. Am. Chem. Soc.* **1973**, *95*, 3038.
- (51) (a) Shvo, Y.; Laine, R. M. *J. Chem. Soc., Chem. Commun.* **1980**, 753. (b) Bui The, K.; Concilio, C.; Porzi, G. *J. Organomet. Chem.* **1981**, *208*, 249. (c) Anguille, S.; Brunet, J.-J.; Chu, N. C.; Diallo, O.; Pages, C.; Vincendeau, S. *Organometallics* **2006**, *25*, 2943.
- (52) (a) Younus, H. A.; Ahmad, N.; Su, W.; Verpoort, F. *Coord. Chem. Rev.* **2014**, *276*, 112. (b) Leis, W.; Mayer, H. A.; Kaska, W. C. *Coord. Chem. Rev.* **2008**, *252*, 1787. (c) Pugh, D.; Danopoulos, A. A. *Coord. Chem. Rev.* **2007**, *251*, 610. (d) Dupont, J.; Consorti, C. S.; Spencer, J. *Chem. Rev.* **2005**, *105*, 2527.
- (53) (a) van Koten, G.; Milstein, D.; Editors *Organometallic Pincer Chemistry*; Springer International Publishing, Cham, Switzerland, 2013. (b) Gunanathan, C.; Milstein, D. *Chem. Rev.* **2014**, *114*, 12024. (c) Morales-Morales, D.; Jensen, C. M. In *The Chemistry of Pincer Compounds*; Elsevier Science B.V.: Amsterdam, 2007. (d) Nishiyama, H. *Chem. Soc. Rev.* **2007**, *36*, 1133.
- (54) Elvidge, J. A.; Linstead, R. P. *J. Chem. Soc.* **1952**, 5000.

(55) (a) Csonka, R.; Speier, G.; Kaizer, J. *RSC Adv.* **2015**, *5*, 18401. (b) Sauer, D. C.; Melen, R. L.; Kruck, M.; Gade, L. H. *Eur. J. Inorg. Chem.* **2014**, *2014*, 4715.

(56) (a) Siegl, W. O. *Inorg. Chim. Acta* **1977**, *25*, L65. (b) Gagne, R. R.; Gall, R. S.; Lisensky, G. C.; Marsh, R. E.; Speltz, L. M. *Inorg. Chem.* **1979**, *18*, 771.

(57) (a) Varadi, T.; Pap, J. S.; Giorgi, M.; Parkanyi, L.; Csay, T.; Speier, G.; Kaizer, J. *Inorg. Chem.* **2013**, *52*, 1559. (b) Mueller, A. L.; Wadepohl, H.; Gade, L. H. *Organometallics* **2015**, *34*, 2810. (c) Mueller, A. L.; Bleith, T.; Roth, T.; Wadepohl, H.; Gade, L. H. *Organometallics* **2015**, *34*, 2326. (d) Sauer, D. C.; Kruck, M.; Wadepohl, H.; Enders, M.; Gade, L. H. *Organometallics* **2013**, *32*, 885. (e) Kruck, M.; Wadepohl, H.; Enders, M.; Gade, L. H. *Chem. - Eur. J.* **2013**, *19*, 1599. (f) Sauer, D. C.; Wadepohl, H.; Gade, L. H. *Inorg. Chem.* **2012**, *51*, 12948. (g) Kruck, M.; Sauer, D. C.; Enders, M.; Wadepohl, H.; Gade, L. H. *Dalton Trans.* **2011**, *40*, 10406. (h) Camerano, J. A.; Saemann, C.; Wadepohl, H.; Gade, L. H. *Organometallics* **2011**, *30*, 379. (i) Langlotz, B. K.; Fillol, J. L.; Gross, J. H.; Wadepohl, H.; Gade, L. H. *Chem. - Eur. J.* **2008**, *14*, 10267. (j) Langlotz, B. K.; Wadepohl, H.; Gade, L. H. *Angew. Chem., Int. Ed.* **2008**, *47*, 4670. (k) Siggelkow, B.; Meder, M. B.; Galka, C. H.; Gade, L. H. *Eur. J. Inorg. Chem.* **2004**, 3424. (l) Meder, M. B.; Gade, L. H. *Eur. J. Inorg. Chem.* **2004**, 2716. (m) Meder, M. B.; Siggelkow, B. A.; Gade, L. H. *Z. Anorg. Allg. Chem.* **2004**, *630*, 1962. (n) Pap, J. S.; Cranswick, M. A.; Balogh-Hergovich, E.; Barath, G.; Giorgi, M.; Rohde, G. T.; Kaizer, J.; Speier, G.; Que, L., Jr. *Eur. J. Inorg. Chem.* **2013**, *2013*, 3858.

(58) (a) Gagne, R. R.; Marritt, W. A.; Marks, D. N.; Siegl, W. O. *Inorg. Chem.* **1981**, *20*, 3260. (b) Pap, J. S.; Kaizer, J.; Giorgi, M.; Speier, G. *Inorg. Chem. Commun.* **2010**, *13*, 1069. (c) Csay, T.; Kripli, B.; Giorgi, M.; Kaizer, J.; Speier, G. *Inorg. Chem. Commun.* **2010**, *13*, 227. (d) Kaizer, J.; Barath, G.; Speier, G.; Reglier, M.; Giorgi, M. *Inorg. Chem. Commun.* **2007**, *10*, 292. (e) Balogh-Hergovich, E.; Speier, G.; Reglier, M.; Giorgi, M.; Kuzmann, E.; Vertes, A. *Inorg. Chem. Commun.* **2005**, *8*, 457. (f) Balogh-Hergovich, E.; Speier, G. *J. Mol. Catal. A: Chem.* **2005**, *230*, 79. (g) Balogh-Hergovich, E.; Speier, G.; Reglier, M.; Giorgi, M.; Kuzmann, E.; Vertes, A. *Inorg. Chim. Acta* **2004**, *357*, 3689. (h) Balogh-Hergovich, E.; Speier, G.; Reglier, M.; Giorgi, M.; Kuzmann, E.; Vertes, A. *Eur. J. Inorg. Chem.* **2003**, 1735. (i) Baird, D. M.; Shih, K. Y. *Polyhedron* **1991**, *10*, 229.

(59) Kaizer, J.; Barath, G.; Csonka, R.; Speier, G.; Korecz, L.; Rockenbauer, A.; Parkanyi, L. *J. Inorg. Biochem.* **2008**, *102*, 773.

(60) Siegl, W. O. *Inorg. Nucl. Chem. Lett.* **1974**, *10*, 825.

(61) (a) Balogh-Hergovich, E.; Kaizer, J.; Speier, G.; Huttner, G.; Jacobi, A. *Inorg. Chem.* **2000**, *39*, 4224. (b) Kaizer, J.; Pap, J.; Speier, G.; Parkanyi, L. *Z. Kristallogr. - New Cryst. Struct.* **2004**, *219*, 141. (c) Anderson, O. P.; la Cour, A.; Dodd, A.; Garrett, A. D.; Wicholas, M. *Inorg. Chem.* **2003**, *42*, 122.

(62) (a) Dietrich, B. L.; Egbert, J.; Morris, A. M.; Wicholas, M.; Anderson, O. P.; Miller, S. M. *Inorg. Chem.* **2005**, *44*, 6476. (b) Wicholas, M.; Garrett, A. D.; Gleaves, M.; Morris, A. M.; Rehm, M.; Anderson, O. P.; la Cour, A. *Inorg. Chem.* **2006**, *45*, 5804.

(63) (a) Baird, D. M.; Hassan, R.; Kim, W. K. *Inorg. Chim. Acta* **1987**, *130*, 39. (b) Baird, D. M.; Shih, K. Y.; Welch, J. H.; Bereman, R. D. *Polyhedron* **1989**, *8*, 2359.

- (64) (a) Camerano, J. A.; Rodrigues, A.-S.; Rominger, F.; Wadepohl, H.; Gade, L. H. *J. Organomet. Chem.* **2011**, *696*, 1425. (b) Marks, D. N.; Siegl, W. O.; Gagne, R. R. *Inorg. Chem.* **1982**, *21*, 3140.
- (65) Anderson, O. P.; la Cour, A.; Berg, A.; Garrett, A. D.; Wicholas, M. *Inorg. Chem.* **2003**, *42*, 4513.
- (66) Siegl, W. O. *J. Organomet. Chem.* **1976**, *107*, C27.
- (67) (a) Hanson, K.; Roskop, L.; Patel, N.; Griffe, L.; Djurovich, P. I.; Gordon, M. S.; Thompson, M. E. *Dalton Trans.* **2012**, *41*, 8648. (b) Meder, M.; Galka, C. H.; Gade, L. H. *Monatsh. Chem.* **2005**, *136*, 1693.
- (68) Wicholas, M.; Dietrich, B. L.; Anderson, O. P.; la Cour, A. *Acta Crystallogr., Sect. E: Struct. Rep. Online* **2006**, *62*, m1689.
- (69) Wen, H.-M.; Wu, Y.-H.; Fan, Y.; Zhang, L.-Y.; Chen, C.-N.; Chen, Z.-N. *Inorg. Chem.* **2010**, *49*, 2210.
- (70) Zhang, D.-B.; Wang, J.-Y.; Wen, H.-M.; Chen, Z.-N. *Organometallics* **2014**, *33*, 4738.
- (71) Szavuly, M.; Csonka, R.; Speier, G.; Barabas, R.; Giorgi, M.; Kaizer, J. *J. Mol. Catal. A: Chem.* **2014**, *392*, 120.
- (72) Kaizer, J.; Csay, T.; Kovari, P.; Speier, G.; Parkanyi, L. *J. Mol. Catal. A: Chem.* **2008**, *280*, 203.
- (73) Kaizer, J.; Csay, T.; Speier, G.; Giorgi, M. *J. Mol. Catal. A: Chem.* **2010**, *329*, 71.
- (74) Szavuly, M.; Szilvasi, S. D.; Csonka, R.; Klesitz, D.; Speier, G.; Giorgi, M.; Kaizer, J. *J. Mol. Catal. A: Chem.* **2014**, *393*, 317.
- (75) (a) Kripli, B.; Barath, G.; Balogh-Hergovich, E.; Giorgi, M.; Simaan, A. J.; Parkanyi, L.; Pap, J. S.; Kaizer, J.; Speier, G. *Inorg. Chem. Commun.* **2011**, *14*, 205. (b) Pap, J. S.; Kripli, B.; Banyai, V.; Giorgi, M.; Korecz, L.; Gajda, T.; Arus, D.; Kaizer, J.; Speier, G. *Inorg. Chim. Acta* **2011**, *376*, 158. (c) Pap, J. S.; Kripli, B.; Varadi, T.; Giorgi, M.; Kaizer, J.; Speier, G. *J. Inorg. Biochem.* **2011**, *105*, 911.
- (76) (a) Gagne, R. R.; Marks, D. N. *Inorg. Chem.* **1984**, *23*, 65. (b) Saussine, L.; Brazi, E.; Robine, A.; Mimoun, H.; Fischer, J.; Weiss, R. *J. Am. Chem. Soc.* **1985**, *107*, 3534.
- (77) Siegl, W. O. *J. Org. Chem.* **1977**, *42*, 1872.
- (78) Tamgho, I.-S.; Engle, J. T.; Ziegler, C. J. *Tetrahedron Lett.* **2013**, *54*, 6114.
- (79) Kim, B.; Yalaz, C.; Pan, D. *Tetrahedron Lett.* **2012**, *53*, 4134.

CHAPTER 2

Dehydrogenative Activation of Alcohol Substrates

Portions of this chapter have been published:

Tseng, K.-N. T.; Kampf, J. W.; Szymczak, N. K. *Organometallics* **2013**, *32*, 2046. Reprinted with permission; Copyright (2013) American Chemical Society.

Tseng, K.-N. T.; Lin, S.; Kampf, J. W.; Szymczak, N. K. *Chem. Commun.* **2016**, *52*, 2901. Reprinted with permission; Copyright (2016) The Royal Society of Chemistry.

2.1 Promoterless and Chemoselective Alcohol Dehydrogenation

2.1.1 Introduction

In the past decade, catalytic alcohol dehydrogenation reactions have evolved as an atom-economical methodology to generate H₂ from biologically relevant alcohols¹ and/or to reveal a reactive organic fragment that can undergo follow up reactivity to form higher order liquid products.² In the absence of an added H₂ acceptor, primary alcohols can couple to form esters, with concomitant release of H₂, which is a variant of acceptorless dehydrogenative coupling (ADC) reactivity. Recently, this reaction class has seen substantial growth, typified by catalytic systems incorporating bifunctional metal–ligand scaffolds capable of promoting ADC.³ To achieve high atom economy, reactions that function in the absence of exogenous additives are particularly desirable, when this trait is coupled with mild reaction conditions. However, many alcohol dehydrogenation catalysts require the addition of superstoichiometric quantities (with respect to Ru catalyst) of a basic reagent for efficient catalysis.⁴ The bases (e.g., KO^tBu) are highly caustic, require specialized equipment, and also contribute to unwanted waste products; thus, systems that operate under base-free conditions are highly desirable.

Most known catalysts that effect alcohol dehydrogenation and/or ADC reactivity incorporate pincer-type ligand frameworks that can operate by a metal–ligand cooperative mechanism. Often containing a central pyridine ring, the pincer framework can exhibit multifunctionality by dearomatization–aromatization of the pyridinyl group, which ensues from the deprotonation–protonation of a methylene spacer.^{3,5} We targeted an alternative anionic *N,N,N* pincer framework that substitutes the methylene spacer groups with an imine linker whose orbitals preclude concerted hydrogen transfer to an adjacent acceptor, in order to probe whether a cooperative mechanism is required for efficient dehydrogenation.⁶ Herein, we report the synthesis and characterization of new pincer-ligated Ru complexes, which efficiently catalyze the dehydrogenation of primary and secondary alcohols without the requirement of added hydrogen acceptor or base.

2.1.2 Synthesis and Characterization of Ru(bMepi)(PPh₃)Cl and HRu(bMepi)(PPh₃)₂

To promote rapid dehydrogenation reactivity, we targeted amide-derived *N,N,N* pincer Ru complexes that incorporate the bMepi (1,3-bis(6'-methyl-2'-pyridylimino)isoindolate) ligand.^{6,7} Metalation was achieved by addition of the deprotonated bMepi ligand to Ru(PPh₃)₃Cl₂ over 21 h in THF solvent, which afforded Ru(bMepi)(PPh₃)Cl (**1**)⁸ in 92% yield (Figure 2-1). The ³¹P{¹H} NMR spectrum of **1** exhibits a singlet at 43.5 ppm, while the ¹H NMR spectrum features a single set of ligand based resonances, including a singlet at 1.71 ppm, consistent with symmetric binding of the bMepi ligand. This molecule represents the first reported Ru complex with a bpi (1,3-bis(2'-pyridylimino)isoindolate) ligand having substituents *ortho* to the pyridyl nitrogens.^{7b,9}

Ru–H complexes are implicated as catalytic intermediates in alcohol dehydrogenation with pincer-type ligands^{3b–d,5,10} thus, we targeted hydride variants of Ru–bMepi complexes. The complex HRu(bMepi)(PPh₃)₂ (**2**) was isolated in 89% yield by allowing **1** to react with 1.05 equiv of NaHBET₃ and 1.2 equiv of PPh₃ in THF solution at room temperature for 2 h (Figure 2-1). The ³¹P{¹H} NMR spectrum of **2** exhibits a singlet at 50.9 ppm, and the ¹H NMR spectrum revealed a solution structure consistent with *C*₂ symmetry. A single peak for the *ortho*-substituted CH₃ units was visualized at 3.12 ppm, in addition to a high-field triplet resonance at –9.58 ppm (*J*_{PH} = 20.0 Hz); the latter resonance is consistent with a hydride ligand *trans* to an amido nitrogen.¹¹ Crystals suitable for single-crystal X-ray diffraction were obtained from vapor

diffusion of pentane into a THF solution of **2**, and the solid-state structure of **2** (Figure 2-1) confirmed the proposed geometry, exposing a distorted-octahedral geometry around the Ru(II) center with a hydride ligand (located from the difference map) trans to the pyrrolidine nitrogen atom.

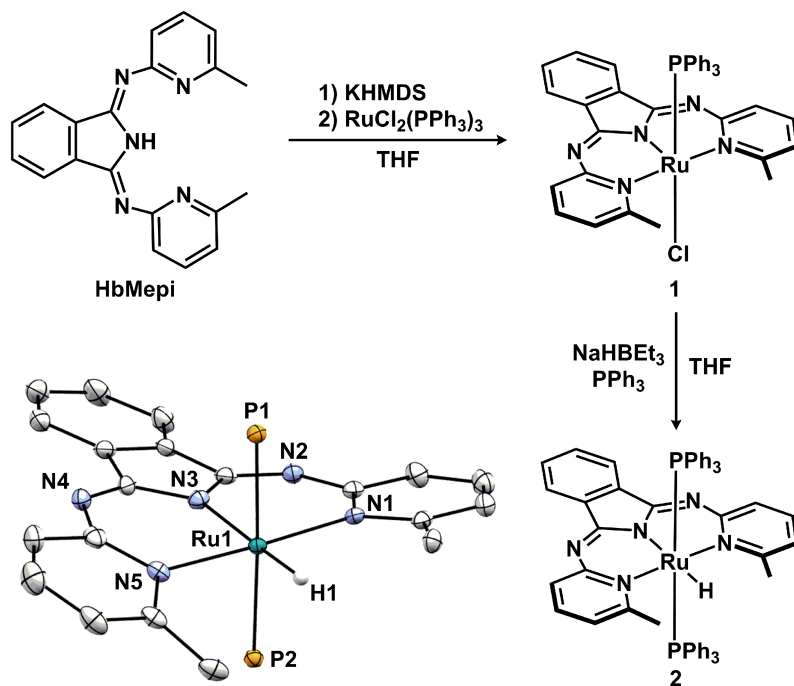


Figure 2-1 Synthesis and crystal structure (thermal ellipsoids depicted at 50% probability) of $\text{HRu}(\text{bMepi})(\text{PPh}_3)_2$.

2.1.3 Transfer Hydrogenation of Ketones Catalyzed by $\text{HRu}(\text{bMepi})(\text{PPh}_3)_2$

The ability of **1** and **2** to effect catalytic transfer hydrogenation with $i\text{PrOH}$ was evaluated using acetophenone as the substrate. Heating a 0.1 M acetophenone $i\text{PrOH}$ solution containing 0.5 mol% of **1** and 1.0 mol% of KO^tBu to 80 °C for 1 h resulted in quantitative conversion (>99%) of acetophenone to 1-phenylethanol (1PhEtOH). No reaction took place in the absence of a base. Complex **2** effected similar hydrogenative transformations with fewer required reagents. For example, without added base, under the reaction conditions listed above, complex **2** catalytically reduced acetophenone to 1PhEtOH in >99% conversion within 1 h.

2.1.4 Base-Free and Acceptorless Alcohol Dehydrogenation

In addition to transfer hydrogenation reactivity by **2**, we hypothesized that dehydrogenation of *i*PrOH should also be possible without an added hydrogen acceptor. Indeed, in the absence of an exogenous ketone, such as acetophenone, *i*PrOH was consumed within 2 h at 80 °C using 10 mol% of **2** in C₆D₆. H₂ and acetone were confirmed as the sole reaction products by *in situ* examination of the reaction mixture in a sealed NMR tube.¹² ¹H NMR spectroscopic analyses revealed the formation of acetone and H₂ in equimolar quantities after 1 h at 80 °C, observed as singlets at 1.55 and 4.47 ppm, respectively.¹³ This catalyst system was found to be remarkably active, and when using 20 ppm of **2** (Figure 2-2), a turnover number (TON) of 314 and turnover frequency (TOF) of 51 h⁻¹ were obtained, on heating to reflux for 6 h.¹⁴ *In situ* analysis of the dehydrogenation reaction revealed the release of free PPh₃ during catalysis, as visualized by ³¹P NMR spectroscopy. Phosphine dissociation from **2** under catalytic conditions is consistent with an inner-sphere type pathway, which requires an open coordination site for substrate binding.

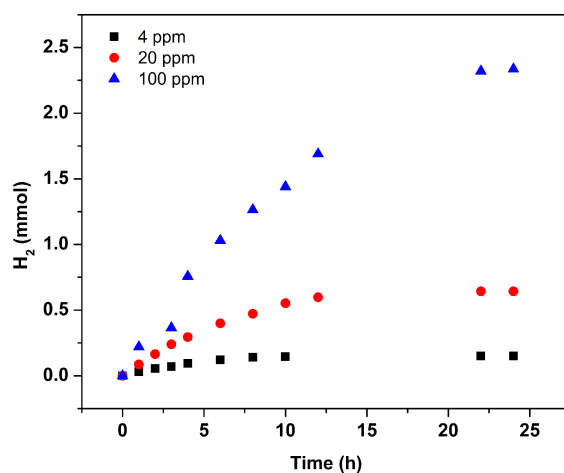


Figure 2-2 Reaction profiles of *i*PrOH dehydrogenation with low catalyst loading.

2.1.5 Poisoning Experiments for Acceptorless Alcohol Dehydrogenation

In order to investigate contributors to the overall reaction efficiency, 1PhEtOH was chosen as a model secondary alcohol substrate (Figure 2-3). This substrate exhibits a dehydrogenation reaction profile similar to that of *i*PrOH and, due to its low volatility, is amenable to reaction sampling by GC-MS and/or ¹H NMR spectroscopy. When the

dehydrogenation reaction was monitored over 24 h in an open system inside an inert atmosphere glovebox, the reaction profile displayed two regions: a linear region (where the maximum rate was measured) and culmination. The reaction profile was linear after 4 min (Figure 2-4)¹⁵ and reached culmination after approximately 12 h.

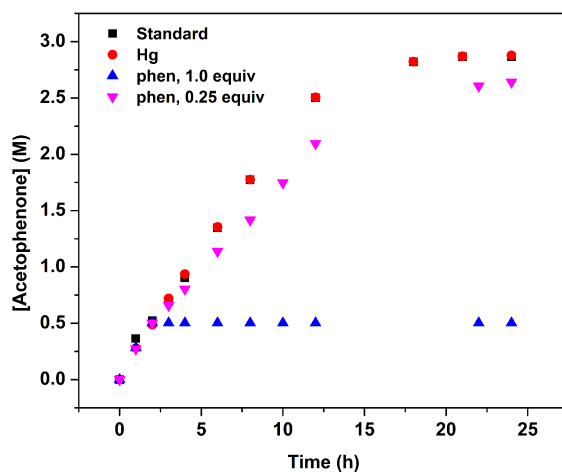
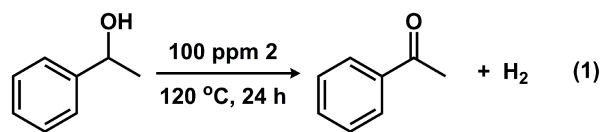


Figure 2-3 Reaction profiles of 1PhEtOH dehydrogenation with and without added catalyst poisons.

The catalyst identity of Ru-catalyzed transfer hydrogenation reactions with alcohols was recently reported to be distinct from that of a presumed homogeneous precursor, which formed catalytically active heterogeneous Ru nano-sized clusters.¹⁶ Accordingly, we undertook initial experiments to probe whether complex **2** participates as a homogeneous catalyst or as a precursor to a heterogeneous species. Among the myriad techniques that collectively can be used to establish the catalyst identity, reproducible kinetic data and poisoning experiments are regarded as highly supportive evidence for homogeneous catalysis.¹⁷ Consistent with an operative homogeneous system, the catalytic activity was unaffected by Hg(0) (~800 equiv) addition (Figure 2-3, Hg), when added during catalysis. Additionally, a substoichiometric ligand poisoning experiment was conducted.¹⁸ Complete poisoning with 1,10-phenanthroline (phen) required 1 equiv (~25% decrease in the rate was observed with 0.25 equiv), inconsistent with a heterogeneous system, where low surface area aggregates are typically poisoned by <<1 equiv of

added ligand poison.¹⁸ Finally, in the absence of any poisoning reagent, highly reproducible and nonsigmoidal reaction kinetic profiles were observed. The combined results of these tests suggest that the active catalytic species is indeed a homogeneous Ru complex.

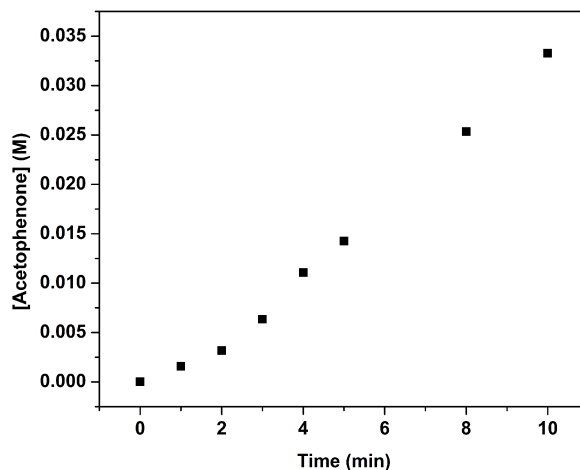


Figure 2-4 The initial 10 min of 1PhEtOH dehydrogenation catalyzed by HRu(bMepi)(PPh₃)₂.

2.1.6 Base Dependence

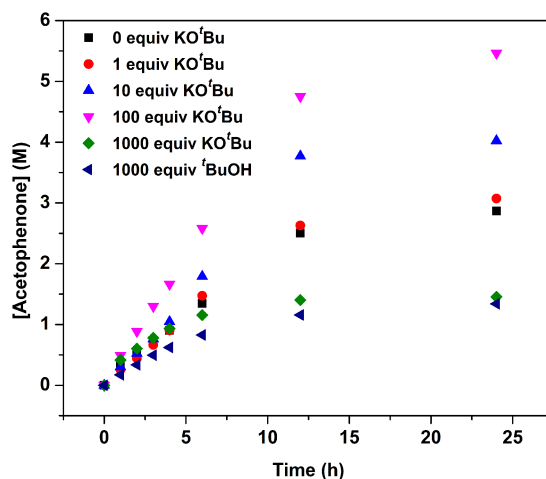


Figure 2-5 Reaction profiles of base dependence experiments.

The rates of alcohol dehydrogenation by structurally related Ru–PNP complexes are often dramatically increased by base additives,⁴ and thus we examined whether complex **2** exhibited similar reactivity toward bases. Addition of 1–1000 equiv of KO^tBu to the dehydrogenation reaction noted above (Figure 2-5) modified the reaction rate in a manner dependent on the quantity of base additive. Increasing the amount of base up to 100 equiv nearly

doubled the reaction rate; however, at 1000 equiv, the reaction rate was suppressed. We hypothesized that, in the presence of excess base, KO^tBu or ^tBuOH could compete with 1PhEtOH coordination, thus impeding catalytic activity by diverting a competitive β -hydride elimination pathway. In support, a control experiment using 1000 equiv of ^tBuOH also exhibited a decreased reaction rate (Figure 2-5), consistent with rate suppression by ^tBuOH.

2.1.7 Initial H₂ Pressure Dependence

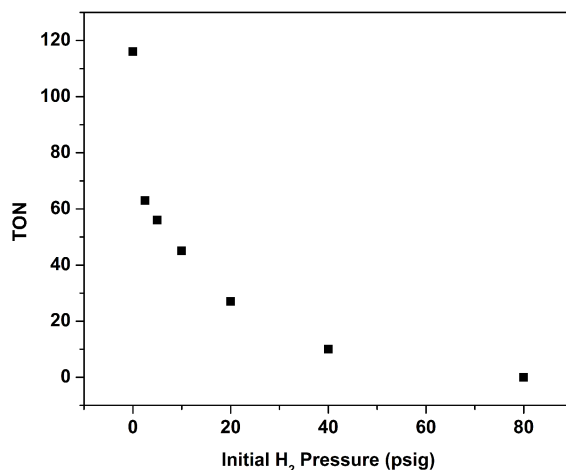


Figure 2-6 Dependence of 1PhEtOH dehydrogenation catalyzed by HRu(bMepi)(PPh₃)₂ on the initial H₂ pressure.

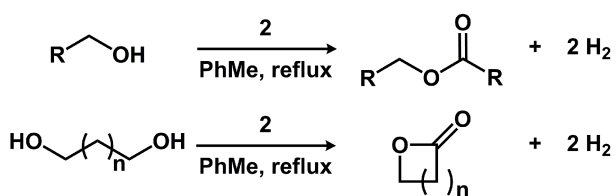
The release of H₂ provides a large entropic contribution to the overall thermodynamic profile of acceptorless alcohol dehydrogenation at a given temperature.¹⁹ Thus, we probed H₂ pressure effects on 1-phenylethanol dehydrogenations (Figure 2-6) to examine how the overall conversion efficiency would be attenuated by elevated pressure. As expected, the reaction was found to be highly sensitive to pressure, and the dehydrogenation reaction was significantly inhibited (66% decrease in TON) when it was performed in a sealed vessel (80 mL headspace). Under as little as 2.5 psig of H₂ initial pressure, we observed a further, sharp decrease in TON (81%), which continued to decrease with increased pressure up to 80 psig (0% conversion). Note that complete product inhibition was not observed at moderate pressures (40 psig of H₂; 10 turnovers for dehydrogenation in 24 h). To determine whether the H₂ pressure effect was the result of rapid equilibration or a kinetic effect (inhibiting H₂ release), a dehydrogenation experiment was performed in a sealed NMR tube using 0.15 mol% of **2** in 2-propanol-*d*₈. HD was not observed in the ¹H NMR spectrum after the reaction mixture was heated to 90 °C for 24

h, suggesting that equilibration of H₂/D₂ is not an operative pathway under the operating conditions and instead inhibition is likely due to a kinetic effect that inhibits H₂ release with increasing pressure. Furthermore, although dehydrogenations are inhibited by product release, pressures of at least 8 psig could be obtained from vessels (5 mL of alcohol; 80 mL of headspace) sealed at room pressure. This observation is noteworthy if considering dehydrogenation of bio-renewable alcohols as a means to release H₂ for use as an energy carrier, where elevated pressures are required for H₂ transport.²⁰

2.1.8 Acceptorless Dehydrogenative Coupling Catalyzed by HRu(bMepi)(PPh₃)₂

We next sought to explore the ADC reactivity of primary alcohols and diols, whose dehydrogenation products contain highly reactive aldehyde fragments. Consistent with our results for the dehydrogenation of secondary alcohols, primary alcohols were similarly dehydrogenated to afford esters with no required additives under moderate reaction conditions. For instance, when 1-butanol was used as a substrate, butyl butyrate was generated in 99% yield after 7 h at 111 °C (Table 2-1, entry 2). High yields of ester products were not general, and when benzyl alcohol was used as a substrate, 50% conversion to benzyl benzoate and 8% conversion to the aldehyde were noted. Furthermore, the conversion of ethanol, a biorelevant alcohol, to ethyl acetate proceeded with low conversion (Table 2-1, entry 1).²¹

Table 2-1 Dehydrogenation of Primary Alcohols to Esters and Diols to Lactones Catalyzed by HRu(bMepi)(PPh₃)₂



entry	alcohol or diol	2 (mol%)	time (h)	conversion (%)	yield (%)
1	ethanol	1	24	9	9
2	1-butanol	1	7	99	99
3	benzyl alcohol	5	24	58	50
4	1,4-butanediol	1	24	88	88
5	1,5-pentanediol	5	24	99	99

Intramolecular reactivity was explored with aliphatic diol substrates, which were converted in high yields to the corresponding lactones. For instance, yields of 88% and 99% were obtained for γ -butyrolactone and δ -valerolactone (Table 2-1, entries 4 and 5), respectively, from 1,4-butanediol and 1,5-pentanediol. Several groups have previously reported homogeneous base-free catalytic oxidation of diols to lactones using a hydrogen acceptor (e.g., acetone) as the solvent.²² However, to the best of our knowledge, only three accounts^{3c,10a,23} of acceptorless and base-free catalytic oxidation of diols to lactones have been reported, and two^{3c,10a} of these reports require significantly high temperatures (>200 °C). Thus, complex **2** is only the second reported example of catalytic ADC reactivity of diols to lactones that does not require an added hydrogen acceptor and base and occurs under moderate (<120 °C) conditions.

2.1.9 Chemoselective Dehydrogenation of Secondary Alcohols in the Presence of Primary Alcohols

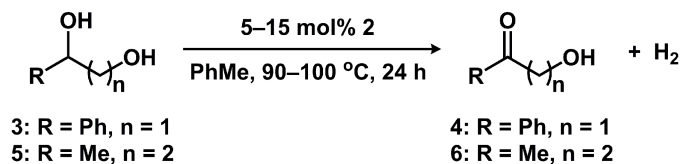


Figure 2-7 Chemoselective dehydrogenation of secondary alcohols in the presence of primary alcohols.

Guided by our results that demonstrated distinct conditions were required for the oxidation of primary and secondary alcohols, we reasoned that **2** should be capable of chemoselective oxidations of secondary alcohols in the presence of primary alcohols. Indeed, using temperatures lower than those required for ADC reactivity (90 °C), **2** chemoselectively oxidized the secondary alcohol moiety in 1-phenyl-1,2-ethanediol (**3**) in the absence of exogenous base or hydrogen acceptor additives and **4** was obtained as the only product in 70% yield, which demonstrates the high chemoselectivity of **2** for alcohol dehydrogenation (Figure 2-7). Because the methine C–H bond of **3** is weakened with respect to the primary alcohol due to the adjacent phenyl group, we investigated whether alkanediols of less disparate bond strengths can be similarly oxidized chemoselectively. Gratifyingly, when 1,3-butanediol (**5**) was subjected to modified dehydrogenation conditions (15 mol% of **2**, 100 °C) selective oxidation of the secondary alcohol was achieved (Figure 2-7) as the sole reaction product in 52% yield. To the

best of our knowledge, such chemoselective oxidations of secondary alcohols in the presence of primary alcohols by homogeneous catalysis are exceptionally rare.²⁴

2.1.10 Summary

In conclusion, we have developed an amide-derived Ru(II) hydride complex capable of catalyzing acceptorless dehydrogenation and dehydrogenative couplings of secondary and primary alcohols/diols, respectively, without requirements of added exogenous base or acceptor additives. Although prior reports demonstrated ADC reactivity of primary alcohols to esters and H₂, few catalysts accomplish this without base or acceptor additives.^{3a,d,5,22a,25} Thus, when base-free, acceptorless alcohol oxidation catalysts under moderate (<120 °C) conditions are compared, the activity of **2** ranks among the best known ADC catalysts. In addition, **2** is particularly noteworthy because it mediates the chemoselective oxidation of secondary alcohols in the presence of primary alcohols without exogenous base or hydrogen acceptor additives, a difficult selective transformation.^{24b}

2.2 Upgrading Ethanol to 1-Butanol

2.2.1 Introduction

Interest in alternative energy solutions for the transportation sector is driven largely by the finite supply of fossil fuels.²⁶ One potentially interim approach is to replace or blend gasoline with sustainable biofuels, such as alcohols.²⁷ Ethanol (EtOH), which is a direct product of biomass fermentation, has been widely used as a blend additive with gasoline.²⁸ However, several of the inherent properties of EtOH have limited broad implementation in the global transportation sector. Key roadblocks are that EtOH: (1) has ~70% energy density of gasoline, (2) is corrosive to engine technology and fuel pipelines, and (3) forms an azeotrope with H₂O, and over extended timeframes, separates from gasoline blends; both leading to storage problems.²⁹ These disadvantages are generally mitigated for higher order alcohols, including 1-butanol (1-BuOH), whose fuel properties more closely resemble those of gasoline (~90% energy density of gasoline). Furthermore 1-BuOH can be blended in higher 1-BuOH:gasoline ratios, and is immiscible with water.³⁰ Although 1-BuOH is a highly desirable biofuel, the large-scale

synthesis (fermentative production) from bio-feedstocks has been fraught with low conversion and poor selectivity.³¹

As an alternative to fermentation, an atom-economical approach for the bulk synthesis of 1-BuOH is the Guerbet reaction.³² This route applies a series of reactions related to “borrowed hydrogen” chemistry for the conversion of primary alcohols into higher order alcohol products.³³ For upgrading EtOH to 1-BuOH, EtOH dehydrogenation affords acetaldehyde, which undergoes aldol coupling to generate crotonaldehyde. Hydrogenation of crotonaldehyde produces 1-BuOH. Key parameters used to evaluate this reaction are the TON, TOF, and selectivity (yield of 1-BuOH divided by the total yield of Guerbet products). A few recent reports have demonstrated this reaction with heterogeneous^{34,35} and homogeneous³⁶ catalysts. To date, the best TONs reported with >30% conversion are 458,^{36d} 314,^{36b} 340,^{36a} and 304,^{36c} while the highest TOF reported was 79 h⁻¹ (314 TONs), using a Ru(II) complex with a bidentate P–N ligand.^{36b} A recent report demonstrated extremely high selectivity at the sacrifice of activity using a two-component Ir catalyst (TON = 185, TOF = 8 h⁻¹).^{36a} However, for large-scale applications required for the transportation sector, higher conversion and turnover are required.

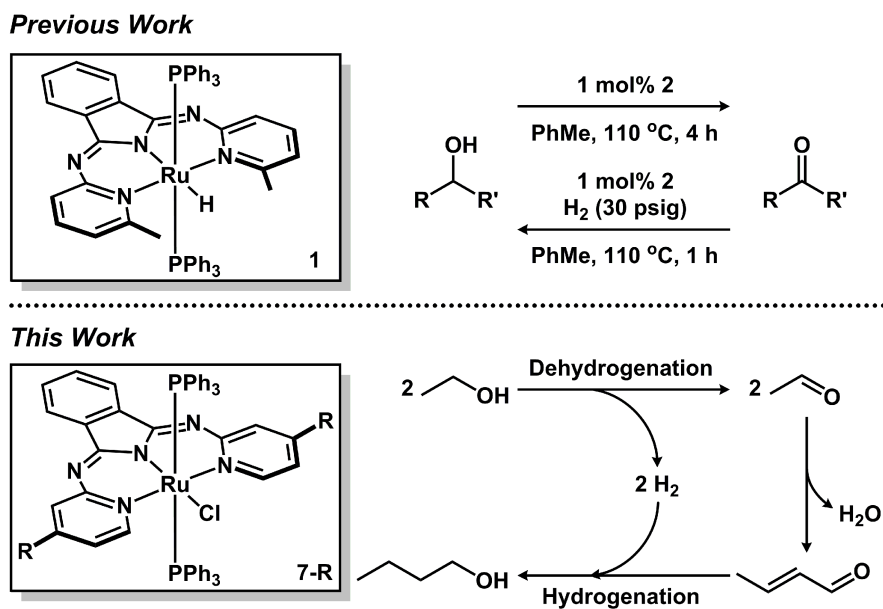


Figure 2-8 Previous work demonstrated reversible transformations between ketones and alcohols *via* sequential hydrogenation–dehydrogenation reactions mediated by HRu(bMepi)(PPh₃)₂. This work presents the catalytic conversion of EtOH to 1-BuOH.

We recently reported an *N,N,N*-bMepi Ru(II) hydride complex (**2**, HRu(bMepi)(PPh₃)₂) capable of mediating reversible transformations between ketones and alcohols *via* sequential hydrogenation-acceptorless dehydrogenation reactions (Figure 2-8).³⁷ Mechanistic analysis of the acceptorless alcohol dehydrogenation (AAD)³⁸ revealed that **2** operated *via* an inner-sphere β -H elimination pathway where β -H elimination is the turnover-limiting step at high alcohol concentration. Because of the steric hindrance of the methyl groups on the β -H elimination process, higher catalytic AAD activity was observed when Ru–b4Rpi complexes (**7-R**) were used. As a result of the ability of **2** to promote successive hydrogenation–dehydrogenation reactions, we hypothesized that, if using our family of Ru(II)–bpi complexes,^{37a} similar “borrowed hydrogen” chemistry might be adapted for alcohol upgrading reactions. Herein, we report the application of **7-R** as homogeneous catalysts that promote the conversion of EtOH to 1-BuOH with unprecedented activity and high selectivity.

2.2.2 Upgrading EtOH to 1-BuOH Catalyzed by Ru(bpi)(PPh₃)₂Cl

Table 2-2 Catalytic Conversion of EtOH to 1-BuOH

entry	catalyst	modifications	1-butanol (%)	2-ethyl-1-butanol (%)	1-hexanol (%)	2-ethyl-1-hexanol (%)	1-octanol (%)	conversion (%)	selectivity (%)	TON	TOF (h ⁻¹)
1	Ru(bMepi)(PPh ₃)Cl	-	10	0	1	0	0	11	91	118	59
2	HRu(bMepi)(PPh ₃) ₂	-	10	0	0	0	0	10	100	101	51
3	Ru(bpi)(PPh ₃) ₂ Cl	-	25	1	3	0	0	30	91	296	148
4	Ru(b4OMepi)(PPh ₃) ₂ Cl	-	24	1	3	0	0	28	89	284	142
5	Ru(b4Clpi)(PPh ₃) ₂ Cl	-	21	1	3	0	0	25	89	251	126
6	Ru(bpi)(PPh ₃) ₂ Cl	5 mol% LiOEt	4	0	0	0	0	4	100	39	20
7	Ru(bpi)(PPh ₃) ₂ Cl	5 mol% KOEt	19	1	2	0	0	23	89	226	113
8	Ru(bpi)(PPh ₃) ₂ Cl	5 mol% NaOH	26	1	3	0	0	30	90	300	150
9	Ru(bpi)(PPh ₃) ₂ Cl	10 mol% NaOEt	31	2	6	1	1	42	82	422	211
10	Ru(bpi)(PPh ₃) ₂ Cl	180 °C	28	4	6	2	1	41	78	410	205
11	Ru(bpi)(PPh ₃) ₂ Cl	0.3 mol % Ru	23	1	3	0	0	27	89	92	46
12	Ru(bpi)(PPh ₃) ₂ Cl	0.05 mol% Ru	20	2	3	0	0	25	81	501	250
13	Ru(bpi)(PPh ₃) ₂ Cl	0.01 mol% Ru	5	0	1	0	0	6	86	625	313
14	Ru(bpi)(PPh ₃) ₂ Cl	0.001 mol% Ru	1	0	0	0	0	1	100	1423	711
15	Ru(bpi)(PPh ₃) ₂ Cl	Set up under air	27	2	5	0	0	34	83	342	171

16	Ru(bpi)(PPh ₃) ₂ Cl	10 mol% NaOEt under air	29	3	6	0	0	38	80	385	192
17	Ru(bpi)(PPh ₃) ₂ Cl	0.5 h	3	0	0	0	0	3	100	31	62
18	Ru(bpi)(PPh ₃) ₂ Cl	1 h	11	0	1	0	0	12	96	116	116
19	Ru(bpi)(PPh ₃) ₂ Cl	4 h	31	3	6	1	1	45	81	448	112
20	Ru(bpi)(PPh ₃) ₂ Cl	6 h	32	4	7	2	1	46	80	457	76
21	Ru(bpi)(PPh ₃) ₂ Cl	24 h	33	4	7	1	1	46	80	460	19
22	Ru(bpi)(PPh ₃) ₂ Cl	20% v/v 1- BuOH	23	3	7	1	1	35	85	348	174
23	Ru(bpi)(PPh ₃) ₂ Cl	0.1 mol% PPh ₃	38	3	8	0	0	49	84	489	245
24	Ru(bpi)(PPh ₃) ₂ Cl	0.2 mol% PPh ₃	36	3	8	1	1	49	81	489	245
25	Ru(bpi)(PPh ₃) ₂ Cl	0.4 mol% PPh ₃	37	3	10	1	2	53	78	529	265
26	Ru(bpi)(PPh ₃) ₂ Cl	10 mol% NaOEt 0.4 mol% PPh ₃	35	3	12	0	0	50	73	505	253
27	Ru(bpi)(PPh ₃) ₂ Cl	0.4 mol% AsPh ₃	30	3	6	0	0	39	82	391	195
28	Ru(bpi)(PPh ₃) ₂ Cl	0.4 mol% AsPh ₃ 24 h	34	4	7	0	0	45	81	455	19
29	Ru(bpi)(PPh ₃) ₂ Cl	0.025 mol% PBU ₃	25	1	3	0	0	30	88	299	150
30	Ru(bpi)(PPh ₃) ₂ Cl	0.1 mol% PBU ₃	25	2	4	0	0	30	86	298	149
31	Ru(bpi)(PPh ₃) ₂ Cl	0.2 mol% PBU ₃	3	0	0	0	0	3	100	31	16
32	Ru(bpi)(PPh ₃) ₂ Cl	~20 mol% Hg(0)	26	2	4	0	0	31	87	312	156
33	Ru(bpi)(PPh ₃) ₂ Cl	5% v/v Water	24	1	2	0	0	28	90	279	140
34	Ru(bpi)(PPh ₃) ₂ Cl	10% v/v Water	4	0	0	0	0	4	100	40	20
35	Ru(bpi)(PPh ₃) ₂ Cl	20% v/v Water	8	0	0	0	0	8	100	81	41
36	Ru(bpi)(PPh ₃) ₂ Cl	No base	0	0	0	0	0	0	0	0	0
37	No catalyst	-	0	0	0	0	0	0	0	0	0
38	Ru(bpi)(PPh ₃) ₂ Cl	5 mol% NaOEt 5 mol% Ti(OEt) ₄	28	2	4	0	0	34	87	335	168
39	Ru(bpi)(PPh ₃) ₂ Cl	10 mol % Ti(OEt) ₄	1	0	0	0	0	1	100	7	4
40	Ru(bpi)(PPh ₃) ₂ Cl	5 mol% NaOEt 5 mol% TIOEt	15	0	1	0	0	16	96	157	79
41	Ru(bpi)(PPh ₃) ₂ Cl	10 mol % TIOEt	3	0	0	0	0	3	100	27	13
42	Ru(bpi)(PPh ₃) ₂ Cl	0 psig H ₂	7	0	1	0	0	8	90	78	39
43	Ru(bpi)(PPh ₃) ₂ Cl	45 psig H ₂	28	4	7	2	1	42	76	421	211
44	Ru(bpi)(PPh ₃) ₂ Cl	90 psig H ₂	23	4	5	3	1	36	73	365	182
45	Ru(bpi)(PPh ₃) ₂ Cl	No Stirring	29	2	4	0	0	35	88	347	174
46	Ru(bpi)(PPh ₃) ₂ Cl	Teflon vessel in Parr bomb	30	3	6	1	1	40	82	397	199
47	Ru(bMepi)(PPh ₃)(Cl)CO	-	16	0	1	0	0	17	95	168	84
48	Ru(bpi)(CO) ₂ Cl	-	3	0	0	0	0	3	100	31	16
49	Ru(bMepi ^{Me})(PPh ₃)(OTf) ₂	-	6	0	0	0	0	6	100	60	30
50	Ru(bMepi)(PMe ₃) ₂ Cl	-	3	1	1	1	0	6	70	55	28
51	Os(bMepi)(Cl)(PPh ₃)	-	4	0	0	0	0	4	100	38	19
52	Ir ₂ (H) ₄ (bMepi)(PPh ₃) ₄ [PF ₆]	-	1	0	0	0	0	1	100	5	3
53	Co(bMepi)(CH ₂ SiMe ₃)	-	1	0	0	0	0	1	100	5	3
54	Ru(bpi)(PPh ₃) ₂ Cl	1 mol% Sc(OTf) ₃	10	0	0	0	0	10	100	107	53
55	Ru(bpi)(PPh ₃) ₂ Cl	2 mol% Sc(OTf) ₃	1	0	0	0	0	1	100	10	5
56	Ru(bpi)(PPh ₃) ₂ Cl	0.1 mol% ZnCl ₂	5	0	0	0	0	5	100	53	27
57	Ru(bpi)(PPh ₃) ₂ Cl	0.1 mol% Sc(OTf) ₃	29	2	4	0	0	35	87	351	176
58	Ru(bpi)(PPh ₃) ₂ Cl	0.5 mol% LiBAR ₄ ^F	29	2	4	0	0	35	88	353	176

59	Ru(bpi)(PPh ₃) ₂ Cl	0.5 mol% LiBF ₄	29	1	3	0	0	33	89	340	170
60	Ru(bpi)(PPh ₃) ₂ Cl	0.5 mol% LiPF ₆	31	3	5	1	1	41	83	404	202
61	Ru(bpi)(PPh ₃) ₂ Cl	0.2 mol% Yb(OTf) ₃	21	1	2	0	0	24	93	234	117
62	Ru(bpi)(PPh ₃) ₂ Cl	0.4 mol% PPh ₃ 0.1 mol% CrCl ₂	23	1	4	0	1	29	86	279	139
63	Ru(bpi)(PPh ₃) ₂ Cl	0.4 mol% PPh ₃ 0.1 mol% MnBr ₂	36	3	9	0	0	48	80	477	239
64	Ru(bpi)(PPh ₃) ₂ Cl	0.4 mol% PPh ₃ 0.1 mol% FeBr ₂	7	0	1	0	0	8	88	79	40
65	Ru(bpi)(PPh ₃) ₂ Cl	0.4 mol% PPh ₃ 0.1 mol% CoBr ₂	24	1	6	1	1	33	81	322	161
66	Ru(bpi)(PPh ₃) ₂ Cl	0.4 mol% PPh ₃ 0.1 mol% NiBr ₂	19	1	4	1	1	26	83	246	123
67	Ru(bpi)(PPh ₃) ₂ Cl	0.4 mol% PPh ₃ 0.1 mol% CuBr ₂	2	0	0	0	0	2	100	18	9
68	Ru(bpi)(PPh ₃) ₂ Cl	0.4 mol% PPh ₃ 0.1 mol% FeCl ₃	29	1	5	0	0	35	87	348	174
69	Ru(bpi)(PPh ₃) ₂ Cl	0.1 mol% Co(TPP)	30	3	6	0	0	39	81	393	197
70	Ru(bpi)(PPh ₃) ₂ Cl	0.1 mol% Co(TPP) 4 h	31	2	3	0	0	36	89	361	90
71	Ru(bpi)(PPh ₃) ₂ Cl	0.3 mol% Co(TPP) 4 h	31	2	5	0	0	38	85	380	95
72	Ru(b4Mepi)Py ₂ Cl	-	12	0	1	0	0	13	94	133	67
73	Ru(b4Mepi)Py ₂ Cl	0.1 mol% PPh ₃	15	1	2	0	0	18	87	177	88
74	Ru(b4Mepi)Py ₂ Cl	0.2 mol% PPh ₃	21	1	2	0	0	24	91	240	120
75	Ru(b4Mepi)Py ₂ Cl	0.3 mol% PPh ₃	3	0	0	0	0	3	100	32	16
76	Ru(b4Mepi)Py ₂ Cl	0.1 mol% IMes	23	1	2	0	0	26	89	266	133
77	Ru(b4Mepi)Py ₂ Cl	0.2 mol% IMes	18	1	1	0	0	20	93	194	97
78	Ru(b4Mepi)Py ₂ Cl	0.1 mol% IPr	14	0	1	0	0	15	96	148	74
79	Ru(b4Mepi)Py ₂ Cl	0.2 mol% IPr	14	0	1	0	0	15	95	147	74
80	Ru(b4Mepi)Py ₂ Cl	0.1 mol% ICy	5	0	0	0	0	5	100	52	26
81	Ru(b4Mepi)Py ₂ Cl	0.1 mol% IAd	13	0	0	0	0	13	100	134	67
82	Ru(b4Mepi)Py ₂ Cl	0.1 mol% ITol	13	0	1	0	0	14	96	135	68
83	Ru(b4Mepi)Py ₂ Cl	0.1 mol% SIMes	13	0	0	0	0	13	100	132	66
84	Ru(b4Mepi)Py ₂ Cl	0.1 mol% SIPr	12	0	0	0	0	12	100	122	61
85	Ru(b4Mepi)Py ₂ Cl	0.1 mol% NHC (3,4- Me, R=	6	0	0	0	0	6	100	64	32
86	Ru(b4Mepi)Py ₂ Cl	Me) 0.1 mol% NHC (3,4- Me, R= ⁱ Pr)	12	0	1	0	0	13	93	131	66
87	Ru(bpi)(PPh ₃) ₂ Cl	1 mL Heptane	20	1	2	0	0	23	91	235	117
88	Ru(bpi)(PPh ₃) ₂ Cl	1 mL HDMSO	17	1	2	0	0	20	85	210	105
89	Ru(bpi)(PPh ₃) ₂ Cl	1 mL Perfluorodecalin	23	1	0	0	0	24	93	245	122

We initiated studies on Guerbet catalysis with EtOH using our previously reported Ru–bpi complexes (**2** and **7-R**). Standard reaction conditions employed a 10 mL vial containing 17.1 mmol of EtOH, 5 mol% NaOEt base, and 0.1 mol% Ru(II) precatalyst.³⁹ After the reaction mixture was heated to 150 °C for 2 h, the product distribution was determined by GC-FID using

naphthalene as an internal standard. Higher activity ($>3\times$) was found when **7-H** (Table 2-2, entry 3) was used instead of Ru(bMepi)(PPh₃)Cl or HRu(bMepi)(PPh₃)₂ (Table 2-2, entries 1 and 2). Analysis of the reaction products (Table 2-2, entry 3) showed high selectivity (91%) for the production of 1-BuOH and 4% yield of C₆ alcohols (2-ethylbutanol and 1-hexanol, Table 2-2) as side products, consistent with Guerbet coupling of 1-BuOH with EtOH. Control experiments showed that **7-H** and NaOEt were both required for catalysis (Table 2-2, entries 36 and 37). In addition, electronic modifications of the pincer scaffold had no effect on the activity and selectivity. For instance, the conversion and selectivity were within the experimental error ($\pm 3\%$)⁴⁰ when **7-OMe** (Table 2-2, entry 4) or **7-Cl** (Table 2-2, entry 5) was used instead of **7-H**. However, modifications to the bMepi backbone (Table 2-2, entry 50) and changing the identity of the auxiliary ligand (PMe₃; Table 2-2, entry 51) or transition metal (Os, Ir, or Co; Table 2-2, entries 52-54) decreased the conversion of upgrading EtOH.

Guided by the high selectivity for 1-BuOH exhibited by **7-H**, we investigated conditions to improve the activity. The identity of the alkali metal had a significant effect. For example, lower activities were observed when LiOEt (Table 2-2, entry 6) or KOEt (Table 2-2, entry 7) was used instead of NaOEt, while NaOH (Table 2-2, entry 8) produced the same results as NaOEt (consistent with solvent leveling effects). Although a higher catalyst loading (0.3 mol%; Table 2-2, entry 11) did not improve activity and selectivity, higher TONs and TOFs (1400 turnovers at 10 ppm; Table 2-2, entries 12–14) were achieved at low catalyst loadings. Furthermore, at high temperature (180 °C; Table 2-2, entry 10) or higher NaOEt base loading (10 mol%; Table 2-2, entry 9), the conversion increased, with concomitant decrease in selectivity for 1-BuOH. For instance, when 10 mol% NaOEt was used, 42% conversion of EtOH to Guerbet alcohols was noted with 82% selectivity for 1-BuOH. Analysis of the reaction products showed higher yield of side products, which included C₆ alcohols (10%) and C₈ alcohols (2% yield of 2-ethylhexanol and 1-octanol, Table 2-2). Note that further attempts to enhance the process of EtOH upgrading catalyzed by Ru(bpi)(PPh₃)₂Cl *via* increasing the base concentration by adding liquid bases (TiOEt or TlOEt; Table 2-2, entries 38–41), performing the reaction under excess initial H₂ pressure (45 and 90 psig, Table 2-2, entries 42–44), adding exogenous Lewis acids or metal salts (Table 2-2, entries 54–71), and diluting the reaction mixture with nonpolar solvents (Table 2-2, entries 87–89) were unsuccessful.

Air-stable catalysts provide significant practical advantages, and are more easily deployed on an industrial-scale. We found that the activity of **7-H** was retained when set up under room conditions. For example, when weighing all reagents in the air and adding air saturated solvents followed by heating the sealed vessel containing 17.1 mmol EtOH, 0.1 mol% **7-H**, and 5 or 10 mol% NaOEt to 150 °C for 2 h (Table 2-2, entries 15 and 16), we obtained 34% and 39% conversion (30% under N₂) respectively. These results demonstrate that catalytic performance is unaffected in the presence of O₂, which suggests that the active species is neither decomposed nor oxidized to a higher-valent Ru complex. Based on known reports of upgrading EtOH to 1-BuOH, **2-H** is the first Ru catalyst to mediate this reaction under air.

2.2.3 Reaction Profile of Upgrading EtOH Catalyzed by Ru(bpi)(PPh₃)₂Cl

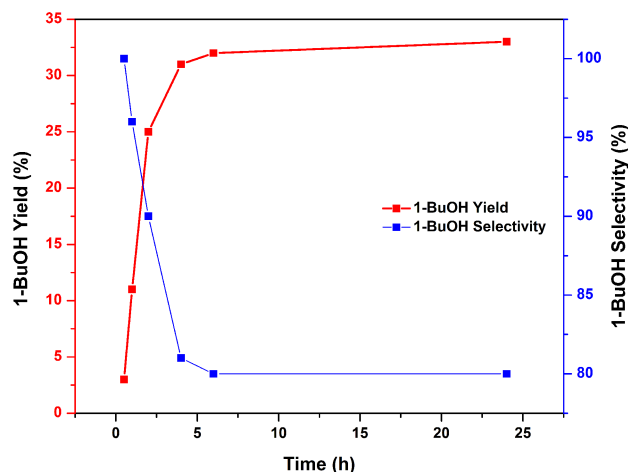


Figure 2-9 Reaction profile of conversion of EtOH to 1-BuOH catalyzed by Ru(bpi)(PPh₃)₂Cl.

To assess the overall reaction efficiency, a time dependence study was conducted by varying the reaction time at 150 °C (Figure 2-9 and Table 2-2, entries 17–21). When evaluated over 24 h, the reaction profile displayed a linear region and reached culmination after approximately 4 h. Analysis of the reaction profile and the reaction products revealed an increase in production of higher order alcohols (10% to 14% C₆ and C₈ Guerbet products from 4 to 6 h) while the yield of 1-BuOH remained constant. We hypothesized that high concentration (ca. 2.1 M or 25% yield) of 1-BuOH could compete with EtOH as a substrate, and thus impede production of 1-BuOH by competitive Guerbet pathways to generate longer chain alcohols. In support, a control experiment using 20% of 1-BuOH by volume (Table 2-2, entry 22) afforded similar conversion and yield. Furthermore, the yield of longer chain alcohols increased from 4%

to 12% and the yield of 1-BuOH remained 23% (25% without the addition of 1-BuOH), which is consistent with competitive 1-BuOH binding/reactivity at high concentration.

2.2.4 Catalyst Deactivation *via* Decarbonylation Pathway

To complement the time dependence study that demonstrated minimal catalyst activity after 6 h, we targeted Ru–bpi compounds with CO ligands that likely bear similarity to the catalyst deactivation product (ν_{CO} band at 1923 cm^{-1} observed by IR spectroscopy).^{41–43} Three different types of CO complexes were prepared from bpi variants to aid in the assignment of the decomposition products. The addition of CO (30 psig) to a solution of Ru(bMepi)(PPh₃)Cl resulted in the clean conversion to Ru(bMepi)(PPh₃)(Cl)CO (**8**). The ³¹P{¹H} NMR spectrum exhibited a singlet at 43.5 ppm, and the IR spectrum displayed a ν_{CO} band at 1929 cm^{-1} . The solid-state structure revealed CO ligand *trans* to the isoindolate nitrogen atom (Figure 2-10).

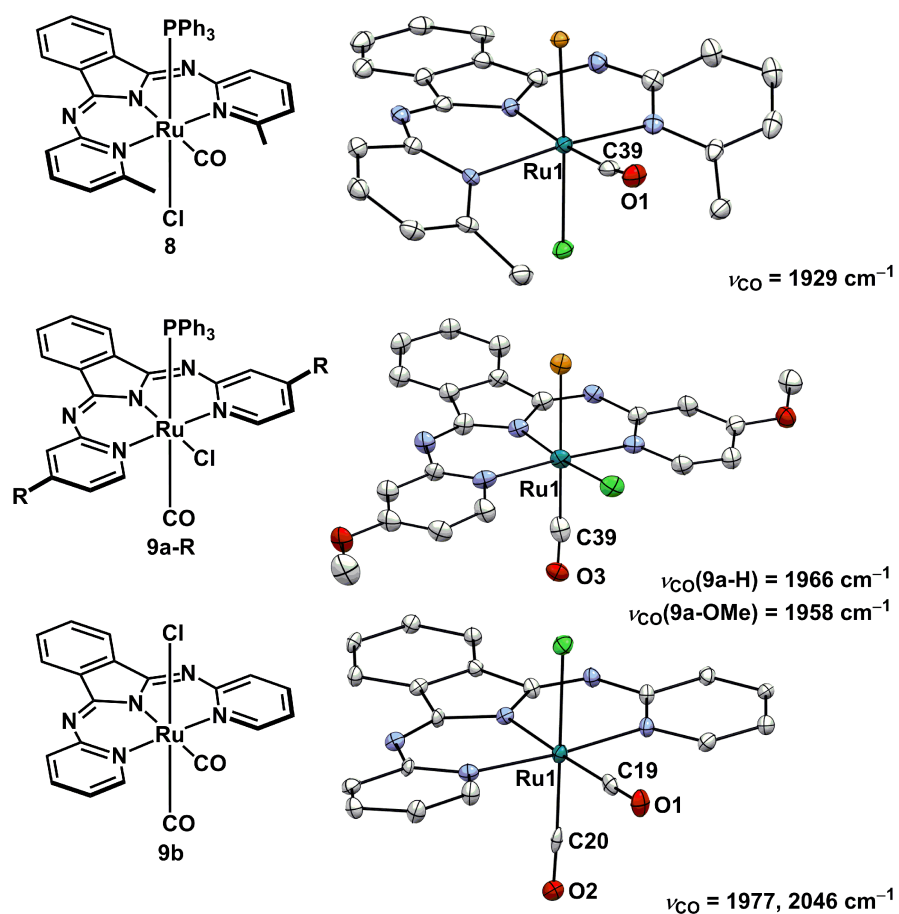


Figure 2-10 Crystal structures (thermal ellipsoids depicted at 50% probability) of Ru(bMepi)(PPh₃)(Cl)CO, Ru(b4OMepi)(PPh₃)(Cl)CO, and Ru(bpi)(CO)₂Cl.

Carbonyl complexes with the **bpi** ligand were prepared using a similar method. The addition of 30 psig CO to a solution of **7-H** resulted in a mixture of **9a-H** and **9b** in a 37:1 ratio. The $^{31}\text{P}\{^1\text{H}\}$ NMR spectrum displayed one major resonance at 10.7 ppm with concomitant formation of free PPh_3 , and the IR spectrum showed one major ν_{CO} band at 1966 cm^{-1} . After 24 h, the mixture fully converted to the bis-CO complex (**9b**), and the IR spectrum exhibited new ν_{CO} bands at 2046 and 1977 cm^{-1} , while the solid state structure revealed a Ru(II) center coordinated to two *cis* CO ligands and a chloride (Figure 2-10). Although a crystal structure of **9a** could not be obtained, a substituted variant (**9a-OMe**)⁴⁴ that featured a very similar ν_{CO} band (1958 cm^{-1}) was structurally characterized by X-ray (Figure 2-10). Because of the close proximity of the ν_{CO} bands between **8** and the decomposition product from Guerbet reactions (1929 versus 1923 cm^{-1}), we propose that the deactivated catalyst contains a CO ligand (resulting from decarbonylation) *trans* to the isoindolate nitrogen atom.

To optimize activity by preventing a competitive EtOH decarbonylation pathway, excess PPh_3 was added to suppress phosphine dissociation. Addition of 1 equiv of PPh_3 (with respect to catalyst) to the standard reaction conditions (0.1 mol% **2-H**, 5 mol% NaOEt, $150\text{ }^\circ\text{C}$; Table 2-2, entry 23) enhanced the catalyst activity to 49% conversion (an increase of 76% based on conversion and 72% based on TOF). Increasing the PPh_3 loading to 4 equiv had a minimal increase on the catalyst activity (53%; Table 2-2, entry 25). When the reaction was performed using excess base (10 mol%; Table 2-2, entry 26) in the presence of excess PPh_3 or AsPh_3 instead of PPh_3 (Table 2-2, entries 27 and 28), no further enhancement of the catalyst activity was observed. Prior state-of-the-art catalysts afforded a TON of 458 (46% conversion; TOF = 19 h^{-1})^{36d} or 314 (31% conversion; TOF = 79 h^{-1}).^{36b} Thus, our system surpasses the activity of the previous premier systems by exhibiting a higher TON of 530, with a TOF of 265 h^{-1} at 53% conversion for catalytically upgrading EtOH.

2.2.5 Poisoning Experiments for Upgrading EtOH

The Guerbet reactions can be catalyzed by both heterogeneous or homogeneous species, and the active species of precursor **7-H** was probed using catalyst-poisoning studies.¹⁶⁻¹⁸ When $\text{Hg}(0)$ was added to the reaction mixture 30 min after the reaction was initiated, the catalytic activity was unaffected, which is consistent with an operative homogeneous system (Table 2-2, entry 32). To further interrogate the active catalytic species, substoichiometric ligand poisoning

experiments were performed. In the presence of 0.25 or 1 equiv of PBU_3 , the catalyst activity remained unchanged (Table 2-2, entries 29 and 30). In contrast, complete poisoning was achieved using 2 equiv of PBU_3 (Table 2-2, entry 31). These results are inconsistent with a heterogeneous system, where low surface area aggregates are typically poisoned by $\ll 1$ equiv of ligand poison, and suggest that the active catalyst for upgrading ethanol in this system is a homogeneous catalyst. Note that excess water also acts as a catalyst poison. The standard reaction (Table 2-2, entry 3) generated ~ 150 equiv H_2O with respect to catalyst. In a control experiment, the activity of **7-H** was not diminished in the presence of 5% H_2O by volume (~ 160 equiv; Table 2-2, entry 33). However, trace yields of 1-BuOH were observed in the presence of 10% or 20 % H_2O by volume (Table 2-2, entries 34 and 35). In addition, the activity of **7-H** was not improved in the presence of exogenous molecular sieves.

2.2.6 Summary

In conclusion, we have developed Ru–bpi complexes (**7-R**) capable of converting EtOH to 1-BuOH with up to 91% selectivity. Higher activity ($>50\%$ conversion) was obtained at the sacrifice of selectivity ($\sim 80\%$) when using 1–4 additional equiv of PPh_3 . Note that currently used liquid fuels such as gasoline, are blends of hydrocarbons rather than single components. Thus, mixtures of higher order alcohols can likely serve a similar role as drop-in gasoline additives. Although prior studies have demonstrated homogeneous catalysts for EtOH upgrading, to our knowledge, our system is the most active, with a TOF of 265 h^{-1} at over 50% conversion. Of particular note, complex **7-H** upgrades EtOH to 1-BuOH when set up in air with minimal loss of catalytic activity.

2.3 Experimental Section

2.3.1 General Considerations

All manipulations were conducted under a nitrogen atmosphere on a Schlenk manifold or in a glovebox using standard Schlenk techniques, unless otherwise stated. All reagents were purchased from commercial vendors. 1-Phenylethanol (1PhEtOH) and phenyltrimethylsilane (PhTMS) were distilled from CaH_2 under a nitrogen atmosphere, and then stored over 3\AA molecular sieves for at least 24 h. The 3\AA Molecular sieves were dried at $250\text{ }^\circ\text{C}$ under dynamic

vacuum for 24 h. Dichloromethane (DCM), diethyl ether (Et₂O), pentane, benzene (C₆H₆), and tetrahydrofuran (THF) were purified using a Glass Contour solvent purification system consisting of a copper catalyst, neutral alumina, and activated molecular sieves, then passed through an in-line, 2 μm filter immediately before being dispensed.

NMR spectra were recorded on Varian Inova 500, Varian MR400, Varian vnmrs 500, and Varian vnmrs 700 spectrometers at room temperature. ¹H and ¹³C shifts are reported in parts per million (ppm) relative to TMS, with the residual solvent peak used as an internal reference. ³¹P NMR spectra were referenced on a unified scale to their respective ¹H NMR spectra. The following abbreviations are reported as follows: broad (br) singlet (s), doublet (d), doublet of doublets (dd), triplet (t), quartet (q), and multiplet (m). ¹³C NMR resonances were observed as singlets unless otherwise stated.

Solid-state IR spectra were collected using a Nicolet iS10 spectrometer equipped with a diamond attenuated total reflectance (ATR) accessory. Elemental analyses were performed by Midwest Microlab, LLC. GC-MS analyses were performed using a Shimadzu QP-2010 GC/MS; the GC contains a 30 m long DB-5 column with a 0.25 mm I.D.

GC-FID analyses were performed using a Shimadzu GC-2014 GC/FID; the GC contains a 15 m long SH-Rxi-5ms column with a 0.25 mm I.D. and utilized H₂ as the carrier gas. GC measurements were conducted using the following method: 50 °C hold for the first 2 min, ramp to 250 °C at 35 °C/min and hold for 2 min. A calibration curve for the Guerbet products was obtained by GC analysis by plotting the ratios of the areas, A_{sample}/A_{standard}, against the known the concentrations.

2.3.2 Preparation of Ru(bMepi)(PPh₃)Cl, Ru(bMepi)(PMe₃)₂[Cl], HRu(bMepi)(PR₃)₂ (R = Ph, Me), Ru(b⁴Mepi)Py₂Cl, and Carbonyl Complexes

KbMepi. THF (15 mL) was added to a 20 mL vial charged with KHMDS (439 mg, 2.21 mmol), HbMepi (756 mg, 2.31 mmol), and a stir bar at room temperature. The resulting solution was stirred at room temperature for 4.5 h. After 1 h, the product started to precipitate from solution. The precipitates were filtered and washed with Et₂O (4 × 5 mL) and pentane (4 × 5 mL). Yield: 799 mg (99%) of yellow powder. The product was used without further purification. ¹H

NMR (400 MHz, THF): δ 7.76 (br s, 2H), 7.41 (br s, 2H), 7.30 (t, $J_{\text{HH}} = 7.6$ Hz, 2H), 6.85 (br s, 2H), 6.52 (d, $J_{\text{HH}} = 7.2$ Hz, 2H), 2.32 (s, 6H).

Ru(bMepi)(PPh₃)Cl. THF (15 mL) was added to a 20 mL vial charged with KbMepi (309 mg, 0.847 mmol), RuCl₂(PPh₃)₃ (773 mg, 0.807 mmol), and a stir bar at room temperature. The resulting solution was stirred at room temperature for 21 h. THF was removed under vacuum. The crude product was washed with Et₂O (4 × 5 mL) and extracted with DCM (4 × 5 mL). DCM was removed under vacuum affording the product as a lavender powder. Yield: 527 mg (90%). Crystals were obtained by allowing pentane to diffuse into a C₆H₆ solution. ¹H NMR (400 MHz, CDCl₃): δ 7.81-7.76 (m, 4H), 7.59 (d, $J_{\text{HH}} = 8.0$ Hz, 2H), 7.35 (dd, $J_{\text{HH}} = 5.6, 3.2$ Hz, 2H), 7.12 (t, $J_{\text{HH}} = 7.6$ Hz, 2H) 6.92 (t, $J_{\text{HH}} = 8.0$ Hz, 9H), 6.64 (t, $J_{\text{HH}} = 8.0$ Hz, 6H), 1.72 (s, 6H). ¹³C{¹H} NMR (176 MHz, CDCl₃): δ 158.8, 155.0, 153.0, 141.1, 135.2, 133.5, 132.6, 129.2, 128.5, 127.9, 125.4, 119.9, 119.2, 23.0. ³¹P{¹H} NMR (162 MHz, CDCl₃): δ 43.50. IR (ATR, cm⁻¹): 3047, 2160, 1979, 1573, 1515, 1435, 1186, 1111, 795, 741, 693. LCT-MS: $m/z = 726.0$ (100%, MH⁺).

HRu(bMepi)(PPh₃)₂. Ru(bMepi)(PPh₃)Cl (445 mg, 0.614 mmol) was dissolved in THF (100 mL) at room temperature in a 125 mL round bottom flask charged with a stir bar. The solution was filtered to insure all of Ru(bMepi)(PPh₃)Cl was dissolved. Then PPh₃ (193 mg, 0.737 mmol) was added to the solution. The mixture was stirred for 10 min before adding NaHBEt₃ (0.645 mL, 0.645 mmol). The reaction solution color changed from blue to green immediately. The reaction solution was allowed to stir for 2 h before removing THF under vacuum. The crude product was washed with pentane (4 × 15 mL), and then extracted with C₆H₆ (4 × 20 mL). C₆H₆ was removed under vacuum affording the product as a green powder. Yield: 524 mg (89%). Crystals were obtained by allowing pentane to diffuse into a THF solution. ¹H NMR (400 MHz, C₆D₆): δ 8.27 (dd, $J_{\text{HH}} = 5.6, 3.2$ Hz, 2H), 7.30 (16H), 6.88 (t, $J_{\text{HH}} = 6.8$ Hz, 6H), 6.81 (t, $J_{\text{HH}} = 7.6$ Hz, 12H), 6.67 (t, $J_{\text{HH}} = 7.6$ Hz, 2H), 5.91 (d, $J_{\text{HH}} = 7.2$ Hz, 2H), 3.12 (s, 6H), -9.58 (t, $J_{\text{PH}} = 20.2$ Hz, 1H). ¹³C{¹H} NMR (176 MHz, CDCl₃): δ 164.1, 161.2, 152.3, 142.7, 133.7, 131.3, 128.1, 127.9, 127.0, 126.9, 120.6, 116.7, 34.3. ³¹P{¹H} NMR (162 MHz, C₆D₆): δ 50.97. IR (ATR, cm⁻¹): 3047, 2170, 2043, 1575, 1508, 1429, 1188, 1110, 789, 742, 695. Anal. Calculated (found): C, 70.58 (70.39); H, 4.97 (4.77); N, 7.35 (7.27).

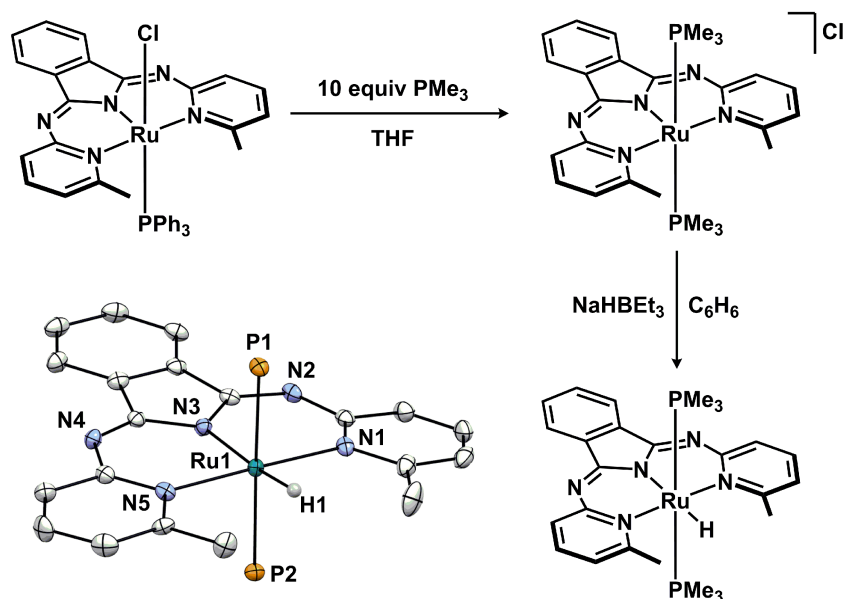


Figure 2-11 Synthesis and crystal structure (thermal ellipsoids depicted at 50% probability) of $\text{HRu}(\text{bMepi})(\text{PMe}_3)_2$.

$\text{Ru}(\text{bMepi})(\text{PMe}_3)_2[\text{Cl}]$. THF (10 mL) was added to a 20 mL vial charged with $\text{Ru}(\text{bMepi})(\text{PPh}_3)\text{Cl}$ (230 mg, 0.317 mmol) and a stir bar. Then PMe_3 (0.330 mL, 3.17 mmol) was added to the solution. After 20 h at room temperature, the precipitates were collected and washed with THF (4×5 mL) and Et_2O (4×5 mL). Evaporation of the volatiles under vacuum afforded the product as a purple powder. Crystals were obtained by allowing Et_2O to diffuse into a DCM solution. Yield: 171 mg (88%). ^1H NMR (400 MHz, CDCl_3): δ 8.03 (dd, $J_{\text{HH}} = 5.6, 3.2$ Hz, 2H), 7.89 (t, $J_{\text{HH}} = 7.6$ Hz, 2H), 7.66 (d, $J_{\text{HH}} = 7.6$ Hz, 2H), 7.56 (dd, $J_{\text{HH}} = 5.6, 3.2$ Hz, 2H), 7.23 (d, $J_{\text{HH}} = 7.2$ Hz, 2H), 1.84 (s, 6H), 0.71 (t, $J_{\text{PH}} = 3.0$ Hz, 18H). $^{31}\text{P}\{^1\text{H}\}$ NMR (162 MHz, CDCl_3): δ -3.17.

$\text{HRu}(\text{bMepi})(\text{PMe}_3)_2$. C_6H_6 (5 mL) was added to a 20 mL vial charged with $\text{Ru}(\text{bMepi})(\text{PMe}_3)_2[\text{Cl}]$ (28 mg, 0.045 mmol) and a stir bar. Then NaHEt_3B (0.047 mL, 0.047 mmol) was added to the solution. The reaction solution color changed from purple to green immediately. The reaction solution was allowed to stir for 3 h. The C_6H_6 solvent was removed under vacuum, and the crude product was extracted with pentane (4×5 mL). Evaporation of the volatiles under vacuum afforded the product as a green powder. Crystals were obtained by cooling a pentane solution to -35 °C. ^1H NMR (400 MHz, C_6D_6): δ 8.48 (dd, $J_{\text{HH}} = 5.6, 3.2$ Hz, 2H), 7.78 (dd, $J_{\text{HH}} = 8.0, 1.2$ Hz, 2H), 7.35 (dd, $J_{\text{HH}} = 5.6, 3.2$ Hz, 2H), 7.11 (t, $J_{\text{HH}} = 7.6$ Hz, 2H),

6.63 (dd, $J_{\text{HH}} = 7.2, 1.6$ Hz, 2H), 3.17 (s, 6H), 0.27 (t, $J_{\text{HH}} = 2.4$ Hz, 18H), -10.77 (t, $J_{\text{PH}} = 23.0$ Hz, 1H). ^{31}P NMR (162 MHz, CDCl_3): δ 2.14 (d, $J_{\text{PH}} = 22.7$ Hz). IR (ATR, cm^{-1}): 3066, 2962, 2918, 2885, 2796, 2105, 1969, 1605, 1569, 1505, 1418, 1374, 1197, 1123, 772, 713, 683, 658.

Ru(bMepi)(PPh₃)(Cl)CO. DCM (5 mL) was added to a Fischer–Porter tube containing Ru(bMepi)(PPh₃)Cl (101.1 mg, 0.139 mmol) and a stir bar. The reaction vessel was charged with CO (30 psig) and allowed to stir at room temperature for 15 h. The DCM solution was layered with pentane (15 mL). After 24 h at room temperature, the precipitates were collected and washed with pentane (4×10 mL). Evaporation of the volatiles under vacuum afforded the product as a dark orange solid. Crystals were obtained from vapor diffusion of pentane into a C_6H_6 solution at room temperature. Yield: 79 mg (75%). ^1H NMR (400 MHz, CD_2Cl_2): δ 7.76 (dd, $J_{\text{HH}} = 5.6, 2.4$ Hz, 2H), 7.52 (dd, $J_{\text{HH}} = 5.6, 2.4$ Hz, 2H), 7.49 (t, $J_{\text{HH}} = 7.8$ Hz, 2H), 7.16 (t, $J_{\text{HH}} = 7.6$ Hz, 3H), 7.09 (d, $J_{\text{HH}} = 7.2$ Hz, 2H), 7.03 (d, $J_{\text{HH}} = 7.8$ Hz, 2H), 6.93–6.89 (m, 6H), 6.55–6.50 (m, 6H). $^{13}\text{C}\{^1\text{H}\}$ (126 MHz, CD_2Cl_2): δ 206.03 (d, $J_{\text{CP}} = 19.2$ Hz), 165.45, 160.55, 155.63, 141.08, 136.91, 133.24 (d, $J_{\text{CP}} = 9.6$ Hz), 130.78, 130.41, 130.27 (t, $J_{\text{CP}} = 3.3$ Hz), 128.28 (d, $J_{\text{CP}} = 9.6$ Hz), 125.92, 121.72 (d, $J_{\text{CP}} = 8.6$ Hz), 31.71. $^{31}\text{P}\{^1\text{H}\}$ (162 MHz, CD_2Cl_2): δ 43.48 (s). IR (ATR, cm^{-1}): 3066, 3015, 1929, 1639, 1604, 1577, 1545, 1519, 1474, 1432, 1393, 1371, 1318, 1286, 1236, 1187, 1156, 1117, 1094, 992, 903, 882, 800, 782, 750, 735, 714, 688. Anal. Calculated (found): C, 62.19 (62.15); H, 4.15 (4.14); N, 9.30 (9.12).

Ru(bpi)(CO)₂Cl. C_6H_6 (8 mL) was added to a Fischer–Porter tube containing Ru(bpi)(CO)₂Cl (81.5 mg, 0.0849 mmol) and a stir bar. The reaction vessel was charged with CO (30 psig) and allowed to stir at room temperature for 24 h. The precipitates were collected on a frit and washed with Et_2O (5 mL) and pentane (4×10 mL). The product was dried under vacuum to afford a yellow solid. Crystals were obtained from vapor diffusion of Et_2O into a DCM solution at 5 °C. Yield: 33 mg (79%). ^1H NMR (500 MHz, CD_2Cl_2): δ 8.76 (d, $J_{\text{HH}} = 6.0$ Hz, 2H), 8.07 (dd, $J_{\text{HH}} = 5.2, 3.2$ Hz, 2H), 7.86 (t, $J_{\text{HH}} = 7.6$ Hz, 2H), 7.69–7.65 (m, 4H), 7.04 (t, $J_{\text{HH}} = 6.0$ Hz, 2H). $^{13}\text{C}\{^1\text{H}\}$ (126 MHz, CD_2Cl_2): δ 196.27, 192.31, 157.49, 156.84, 156.78, 138.94, 138.89, 131.19, 128.75, 122.00, 120.07. IR (ATR, cm^{-1}): 3091, 3069, 2046, 1977, 1647, 1603, 1577, 1528, 1459, 1428, 1381, 1321, 1307, 1287, 1201, 1184, 1150, 1121, 1101, 1011, 910, 875, 869, 846, 771, 745, 702. Anal. Calculated (found): C, 48.94 (48.73); H, 2.46 (2.45); N, 14.27 (13.71).

Ru(b4Mepi)Py₂Cl. Pyridine (10 mL) was added to a 20 mL vial charged with [Ru(COD)Cl₂]_x (183 mg, 0.654 mmol), Hb4Mepi (204 mg, 0.623), NaO^tBu (59.9 mg, 0.623 mmol), and a stir bar. The reaction solution was allowed to stir at 80 °C for 16 h. After the solution cooled to room temperature, NaCl was filtered using a fine frit and the crude product left on the frit was extracted with excess pyridine (50 mL). The pyridine solvent was removed under vacuum and the crude product was washed with Et₂O (4 × 20 mL) and pentane (4 × 20 mL). The product was recrystallized at -35 °C from a DCM solution layered with pentane. After 2 days, the precipitates were collected and washed with pentane (4 × 10 mL). Evaporation of the volatiles under vacuum afforded the product as a green powder. Yield: 273 mg (71%). ¹H NMR (400 MHz, CD₂Cl₂): δ 10.56 (d, *J*_{HH} = 6.4 Hz, 2H), 8.00 (dd, *J*_{HH} = 5.2, 3.2 Hz, 2H), 7.79 (d, *J*_{HH} = 5.2 Hz, 4H, Py), 7.52 (dd, *J*_{HH} = 5.2, 3.2 Hz, 2H), 7.41 (s, 2H), 7.29 (t, *J*_{HH} = 7.4 Hz, 2H, Py), 6.75-6.69 (m, 6H, Py), 2.37 (s, 6H).

2.3.3 General Procedure for the Dehydrogenation of ⁱPrOH Catalyzed by HRu(bMepi)(PPh₃)₂

ⁱPrOH (5 mL) was added to a 10 mL Schlenk flask charged with **2** (dependent on the catalyst loading; the appropriate amount was transferred from a 2.7 mM PhMe stock solution), PhMe (varying amount depending on the catalyst loading; all ⁱPrOH dehydrogenation reactions had a total volume of 0.5 mL PhMe), and a stir bar. The Schlenk flask was fitted with a reflux condenser capped with a septum that was connected to a line of Tygon tubing that connected to an inverted burette filled with H₂O. The entire reaction setup was purged with N₂ for 5 min before heating the Schlenk flask to 90 °C. After heating the Schlenk flask for 20 min to equilibrate the gas temperature, the burette level at 0 h was measured. At pre-determined time intervals, the gas volume was measured during the reaction course. To confirm reproducibility and to determine the rate, all reactions were performed in triplicate.

2.3.4 General Procedure for the Dehydrogenation of 1PhEtOH Catalyzed by HRu(bMepi)(PPh₃)₂

1PhEtOH (5 mL, 41.4 mmol) was added to a 20 mL vial charged with **2** (3.9 mg, 0.00409 mmol), PhTMS (0.5 mL, 2.9 mmol), and a stir bar. The vial was capped with a septum pierced with a needle to vent the evolved gas. The vial was heated to the desired temperature (90, 100,

110, 120, or 130 °C) using an aluminum heating block inside an inert-atmosphere glovebox. The formation of acetophenone was monitored by sampling 0.5 mL aliquots, and then analyzed by ¹H NMR spectroscopy against PhTMS as an internal standard. To confirm reproducibility and to determine the rates, all reactions were performed in triplicate.

2.3.5 General Procedure for 1,10-Phenanthroline Poisoning Experiments

Following the procedure for the dehydrogenation of 1PhEtOH, the 1,10-phenanthroline poisoning experiment was conducted by first allowing the reaction solution to proceed for 2 h. Then 1,10-phenanthroline was added to the reaction solution while stirring at 120 °C.

2.3.6 General Procedure for the Initial H₂ Pressure Dependence Experiments

A Fischer–Porter tube was first rinsed with 1PhEtOH (3 × 1 mL). 1PhEtOH (5 mL, 41.4 mmol) was added to the tube charged followed by **2** (3.9 mg, 0.00409 mmol), PhTMS (0.5 mL, 2.9 mmol), and a stir bar. The tube was charged with H₂ (2.5, 5, 10, 20, 40, or 80 psig), and heated to 120 °C in an oil bath stirring at 1500 RPM. The reaction was allowed to stir for 24 h. To determine the acetophenone concentration, 0.5 mL aliquot of the reaction solution was analyzed by ¹H NMR spectroscopy against PhTMS as an internal standard.

2.3.7 General Procedure for the Dehydrogenation of Primary Alcohols and Diols and Chemoselective Dehydrogenation of Secondary Alcohols

PhMe (2 mL) was added to a 10 mL Schlenk flask charged with **2** (1 mol%, 4.8 mg, 0.005 mmol; 5 mol%, 23.8 mg, 0.025 mmol; 10 mol%, 47.6 mg, 0.05 mmol; dependent on the catalyst loading), *n*-docosane (31.1 mg, 0.1 mmol), and a stir bar. The alcohol substrate (0.046 mL *n*-butanol, 0.052 mL benzyl alcohol, 0.029 mL EtOH, 0.044 mL 1,4-butanediol, 0.055 mL 1,5-pentanediol, 69.1 mg 1-phenyl-1,2-ethanediol, 0.045 mL 1,3-butanediol; 0.5 mmol) was added to the mixture. A reflux condenser (cooling finger was used for EtOH) was connected to the Schlenk flask, and the reaction solution was heated to the desired temperature using an aluminum heating block and stirred at 1500 RPM. After the reaction was complete, a 0.020 mL aliquot was diluted with 1 mL DCM, and the product(s) and yield were determined by GC-MS using the following method: 30 °C hold for the first 5 min, ramp to 270 °C at 20 °C/min and hold for 15 min, solvent cut was set at 2.5 min and data was collected starting at 2.6 min. For the

EtOH and 1,3-butanediol experiments, the product(s) and yield were determined using ^1H NMR spectroscopy with 0.005 mL PhTMS added to the NMR tube for internal referencing.

2.3.8 General Procedure for Upgrading EtOH under N_2

Inside an inert-atmosphere glovebox, ethanol (1 mL, 17.1 mmol) was added to a 10 mL Biotage microwave vial (Product No. 351521) containing catalyst (0.1 mol%, 0.0172 mmol), base (5 mol%, 0.858 mmol), and a stir bar. Unless otherwise stated, $\text{Ru}(\text{bpi})(\text{PPh}_3)_2\text{Cl}$ (16.4 mg, 0.0172 mmol) and NaOEt (58.3 mg, 0.858 mmol) were used. The vial was crimped with a septum, heated to 150 °C using an aluminum-heating block, and stirred at 1500 RPM. After 2 h, the vial was removed from the aluminum-heating block and cooled to room temperature. The solution was diluted with CHCl_3 to 25 mL and filtered through celite. The products and yields were analyzed using GC-FID against naphthalene as an internal standard.

2.3.9 General Procedure for Upgrading EtOH under Air

On the benchtop, ethanol (1 mL, 17.1 mmol) was added to a 10 mL Biotage microwave vial (Product No. 351521) containing $\text{Ru}(\text{bpi})(\text{PPh}_3)_2\text{Cl}$ (0.1 mol%, 0.0172 mmol, 16.4 mg), NaOEt (5 mol%, 0.858 mmol, 58.3 mg), and a stir bar. The vial was crimped with a septum, heated to 150 °C using an aluminum-heating block, and stirred at 1500 RPM. After 2 h, the vial was removed from the aluminum-heating block and cooled to room temperature. The solution was diluted with CHCl_3 to 25 mL and filtered through celite. The products and yields were analyzed using GC-FID against naphthalene as an internal standard.

2.3.10 General Procedure for Poisoning Experiments of EtOH Upgrading

Following the general procedure for upgrading EtOH under N_2 , the experiment was conducted by allowing the reaction to proceed for 30 min. The reaction was removed from the aluminum-heating block and cooled for 15 min at room temperature. Then PBU_3 or $\text{Hg}(0)$ was added to the reaction. The reaction was crimped and reheated to 150 °C for 1.5 h.

2.4 References

(1) Johnson, T. C.; Morris, D. J.; Wills, M. *Chem. Soc. Rev.* **2010**, *39*, 81.

- (2) Dobereiner, G. E.; Crabtree, R. H. *Chem. Rev.* **2010**, *110*, 681.
- (3) (a) Zhang, J.; Leitus, G.; Ben-David, Y.; Milstein, D. *J. Am. Chem. Soc.* **2005**, *127*, 10840. (b) Nielsen, M.; Kammer, A.; Cozzula, D.; Junge, H.; Gladiali, S.; Beller, M. *Angew. Chem., Int. Ed.* **2011**, *50*, 9593. (c) Zhang, J.; Balaraman, E.; Leitus, G.; Milstein, D. *Organometallics* **2011**, *30*, 5716. (d) He, L.-P.; Chen, T.; Gong, D.; Lai, Z.; Huang, K. -W. *Organometallics* **2012**, *31*, 5208.
- (4) (a) Zhang, J.; Gandelman, M.; Shimon, L. J. W.; Rozenberg, H.; Milstein, D. *Organometallics* **2004**, *23*, 4026. (b) Junge, H.; Beller, M. *Tetrahedron Lett.* **2005**, *46*, 1031.
- (5) Spasyuk, D.; Smith, S.; Gusev, D. G. *Angew. Chem., Int. Ed.* **2012**, *51*, 2772.
- (6) Siggelkow, B.; Meder, M. B.; Galka, C. H.; Gade, L. H. *Eur. J. Inorg. Chem.* **2004**, 3424.
- (7) (a) The methyl groups were also incorporated to prevent the formation of homoleptic Ru complexes. (b) Camerano, J. A.; Rodrigues, A.-S.; Rominger, F.; Wadepohl, H.; Gade, L. H. *J. Organomet. Chem.* **2011**, *696*, 1425.
- (8) The connectivity of **1** was confirmed by single-crystal X-ray diffraction analysis.
- (9) (a) Gagne, R. R.; Marritt, W. A.; Marks, D. N.; Siegl, W. O. *Inorg. Chem.* **1981**, *20*, 3260. (b) Marks, D. N.; Siegl, W. O.; Gagne, R. R. *Inorg. Chem.* **1982**, *21*, 3140. (c) Gagne, R. R.; Marks, D. N. *Inorg. Chem.* **1984**, *23*, 65.
- (10) (a) Zhao, J.; Hartwig, J. F. *Organometallics* **2005**, *24*, 2441. (b) Montag, M.; Zhang, J.; Milstein, D. *J. Am. Chem. Soc.* **2012**, *134*, 10325.
- (11) (a) Jazzar, R. F. R.; Varrone, M.; Burrows, A. D.; Macgregor, S. A.; Mahon, M. F.; Whittlesey, M. K. *Inorg. Chim. Acta* **2006**, *359*, 815. (b) Nag, S.; Butcher, R. J.; Bhattacharya, S. *Eur. J. Inorg. Chem.* **2007**, 1251.
- (12) Different conditions were used: 15 mol% of **2** in 0.7 mL of ⁱPrOH using phenyltrimethylsilane as an internal standard.
- (13) The yield of H₂ gas was determined using phenyltrimethylsilane as an internal standard and corrected for dissolved and free H₂, using Henry's Law, with a constant of 0.01907.
- (14) HRu(bMepi)(PPh₃)₂ is air-sensitive; thus catalytic dehydrogenation is not tolerated in air.
- (15) Monitoring the internal reaction temperature as a function of time required 3.85 min for the reaction solution to reach 120 °C, consistent with temperature equilibration as the primary contributor to the induction period.
- (16) Toubiana, J.; Sasson, Y. *Catal. Sci. Technol.* **2012**, *2*, 1644.
- (17) (a) Widegren, J. A.; Finke, R. G. *J. Mol. Catal. A: Chem.* **2003**, *198*, 317. (b) Crabtree, R. H. *Chem. Rev.* **2012**, *112*, 1536. (c) This test works best with Pt, Pd, and Ni metals, but there has been evidence of Hg(0) affecting Ru heterogeneous catalysts.¹⁶
- (18) Bayram, E.; Finke, R. G. *ACS Catal.* **2012**, *2*, 1967–1975.

- (19) (a) For example, the dehydrogenation of ⁱPrOH to acetone and H₂ is endothermic by 16.5 kcal/mol, and the entropic contribution for a reaction with H₂ release at room temperature is 8 kcal/mol. (b) Wiberg, K. B.; Crocker, L. S.; Morgan, K. M. *J. Am. Chem. Soc.* **1991**, *113*, 3447. (c) Watson, L. A.; Eisenstein, O. *J. Chem. Educ.* **2002**, *79*, 1269.
- (20) Hydrogen as a Future Energy Carrier; Zuttel, A., Borgschulte, A., Schlapbach, L., Eds.; Wiley-VCH: Weinheim, Germany, 2008.
- (21) Thermodynamically, the process of H₂ formation from alcohols is generally unfavorable. For example, the ΔG° value for formation of H₂ plus acetal from ethanol is 9.8 kcal/mol.
- (22) (a) Murahashi, S.; Naota, T.; Ito, K.; Maeda, Y.; Taki, H. *J. Org. Chem.* **1987**, *52*, 4319. (b) Lin, Y.; Zhu, X.; Zhou, Y. *J. Organomet. Chem.* **1992**, *429*, 269. (c) Endo, Y.; Baeckvall, J.-E. *Chem. Eur. J.* **2011**, *17*, 12596. (d) Buntara, T.; Noel, S.; Phua, P. H.; Melian-Cabrera, I.; de Vries, J. G.; Heeres, H. J. *Angew. Chem., Int. Ed.* **2011**, *50*, 7083.
- (23) Muniz, K. *Angew. Chem., Int. Ed.* **2005**, *44*, 6622.
- (24) (a) Manzini, S.; Urbina-Blanco, C. A.; Nolan, S. P. *Organometallics* **2013**, *32*, 660. (b) de, G. C. F.; Peters, J. A.; van, B. H.; Huskens, J. *Synthesis* **1994**, 1007.
- (25) Blum, Y.; Shvo, Y. *J. Organomet. Chem.* **1985**, *282*, C7.
- (26) For reviews on fossil fuel and alternative energy see: (a) Höök, M.; Tang, X. *Energy Policy* **2013**, *52*, 797. (b) Lewis, N. S.; Nocera, D. G. *Proc. Natl. Acad. Sci.* **2006**, *103*, 15729.
- (27) For reviews on biofuels see: (a) Guo, M.; Song, W.; Buhain, J. *Renewable Sustainable Energy Rev.* **2015**, *42*, 712. (b) Ragauskas, A. J.; Williams, C. K.; Davison, B. H.; Britovsek, G.; Cairney, J.; Eckert, C. A.; Frederick, W. J.; Hallett, J. P.; Leak, D. J.; Liotta, C. L.; Mielenz, J. R.; Murphy, R.; Templer, R.; Tschaplinski, T. *Science* **2006**, *311*, 484.
- (28) For a report on the use of EtOH in the global energy economy, see: Group, U. N. E. P. B. W.; Management, U. N. E. P. I. P. f. S. R. *Towards sustainable production and use of resources: assessing biofuels*; UNEP/Earthprint, 2009.
- (29) For a review on bioethanol see: Balat, M. *Energy Convers. Manage.* **2011**, *52*, 858.
- (30) For reviews on 1-BuOH as a biofuel see: (a) Xue, C.; Zhao, X.-Q.; Liu, C.-G.; Chen, L.-J.; Bai, F.-W. *Biotechnol. Adv.* **2013**, *31*, 1575. (b) Jin, C.; Yao, M.; Liu, H.; Lee, C. E.; Ji, J. *Renewable Sustainable Energy Rev.* **2011**, *15*, 4080. (c) Harvey, B. G.; Meylemans, H. A. J. *Chem. Technol. Biotechnol.* **2011**, *86*, 2.
- (31) For a review on the fermentative production of 1-BuOH see: Green, E. M. *Curr. Opin. Biotechnol.* **2011**, *22*, 337.
- (32) For a review on the Guerbet reaction catalyzed by transition-metal complexes see: Gabriels, D.; Hernandez, W. Y.; Sels, B.; Van Der Voort, P.; Verberckmoes, A. *Catal. Sci. Technol.* **2015**, *5*, 3876.

- (33) For reviews on hydrogen borrowing chemistry see reference 2 and Hamid, M. H. S. A.; Slatford, P. A.; Williams, J. M. J. *Adv. Synth. Catal.* **2007**, *349*, 1555.
- (34) For a review on heterogeneous catalysts for the Guerbet reaction, see: Galadima, A.; Muraza, O. *Ind. Eng. Chem. Res.* **2015**, *54*, 7181.
- (35) Riittonen, T.; Toukoniitty, E.; Madnani, D. K.; Leino, A.-R.; Kordas, K.; Szabo, M.; Sapi, A.; Arve, K.; Warna, J.; Mikkola, J.-P. *Catalysts* **2012**, *2*, 68.
- (36) (a) Chakraborty, S.; Piszal, P. E.; Hayes, C. E.; Baker, R. T.; Jones, W. D. *J. Am. Chem. Soc.* **2015**, *137*, 14264. (b) Wingad, R. L.; Gates, P. J.; Street, S. T. G.; Wass, D. F. *ACS Catal.* **2015**, *5*, 5822. (c) Xu, G.; Lammens, T.; Liu, Q.; Wang, X.; Dong, L.; Caiazzo, A.; Ashraf, N.; Guan, J.; Mu, X. *Green Chem.* **2014**, *16*, 3971. (d) Dowson, G. R. M.; Haddow, M. F.; Lee, J.; Wingad, R. L.; Wass, D. F. *Angew. Chem., Int. Ed.* **2013**, *52*, 9005. (e) Koda, K.; Matsu-ura, T.; Obora, Y.; Ishii, Y. *Chem. Lett.* **2009**, *38*, 838.
- (37) (a) Tseng, K.-N. T.; Kampf, J. W.; Szymczak, N. K. *ACS Catal.* **2015**, *5*, 5468. (b) Tseng, K.-N. T.; Kampf, J. W.; Szymczak, N. K. *Organometallics* **2013**, *32*, 2046.
- (38) For recent examples of AAD of primary alcohols see reference 5 and (a) Nielsen, M.; Junge, H.; Kammer, A.; Beller, M. *Angew. Chem., Int. Ed.* **2012**, *51*, 5711. (b) Nielsen, M.; Alberico, E.; Baumann, W.; Drexler, H.-J.; Junge, H.; Gladiali, S.; Beller, M. *Nature* **2013**, *495*, 85. (c) Rodríguez-Lugo, R. E.; Trincado, M.; Vogt, M.; Tewes, F.; Santiso-Quinones, G.; Grützmacher, H. *Nat Chem* **2013**, *5*, 342.
- (39) Note that the reaction glass vessel was etched after the reaction was completed. This can be avoided by performing the reaction in a Parr bomb or a Teflon vessel, which afforded the same conversion and selectivity (Table 2-2, entry 47).
- (40) The experimental error was determined by >3 runs of the standard reaction (Table 2-2, entry 3).
- (41) Decarbonylation is a common deactivation pathway observed in EtOH dehydrogenation, see: (a) Delgado-Lieta, E.; Luke, M. A.; Jones, R. F.; Cole-Hamilton, D. J. *Polyhedron* **1982**, *1*, 836. (b) Sieffert, N.; Réocreux, R.; Lorusso, P.; Cole-Hamilton, D. J.; Bühl, M. *Chem. Eur. J.* **2014**, *20*, 4141.
- (42) Aldehyde decarbonylation has been reported for many late transition-metal complexes. For recent examples see: (a) Ho, H.-A.; Manna, K.; Sadow, A. D. *Angew. Chem., Int. Ed.* **2012**, *51*, 8607. (b) Melnick, J. G.; Radosevich, A. T.; Villagran, D.; Nocera, D. G. *Chem. Commun.* **2010**, *46*, 79.
- (43) Unfortunately, *ex situ* NMR and stoichiometric experiments provided minimal further support of the catalyst identity. For example, the stoichiometric reaction between **7-H** and NaOEt resulted in multiple species (65.9, 55.1, and free PPh₃) as observed by ³¹P NMR spectroscopy.

(44) Single crystals of **9a-OMe** were obtained from vapor diffusion of pentane into a C₆H₆ solution, which confirmed the structure of **9a**. Complex **9a-OMe** shared similar ¹H and ³¹P NMR features, which included a ³¹P NMR resonance at 10.8 ppm (10.7 ppm for **9a-H**).

CHAPTER 3

On the Mechanism of *N,N,N*-Amide Ruthenium(II) Hydride Mediated Acceptorless Alcohol Dehydrogenation

Portions of this chapter have been published:

Tseng, K.-N. T.; Kampf, J. W.; Szymczak, N. K. *ACS Catal.* **2015**, *5*, 5468. Reprinted with permission; Copyright (2015) American Chemical Society.

3.1 Introduction

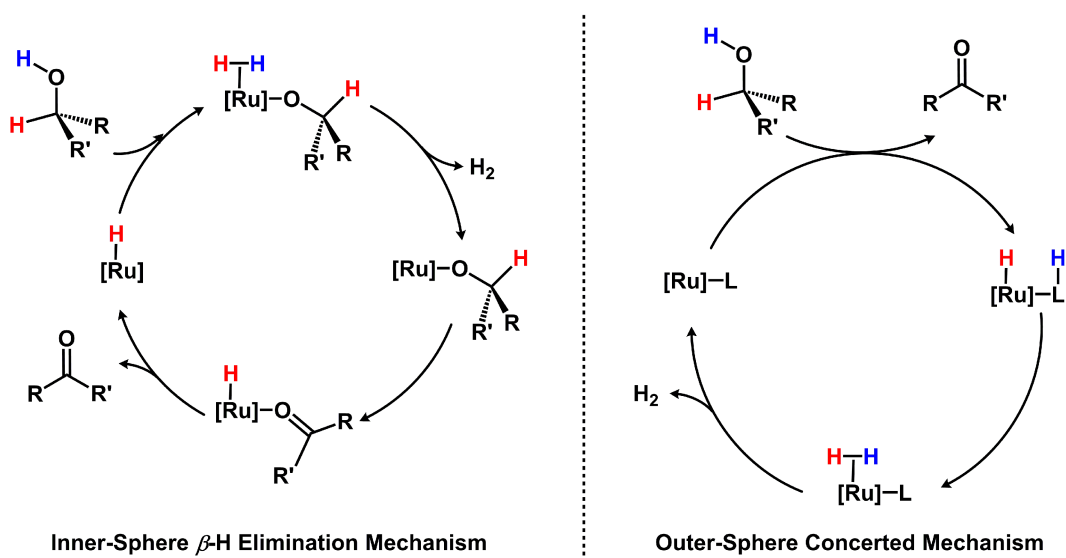


Figure 3-1 Generalized catalytic cycles for the inner-sphere and outer-sphere dehydrogenation pathways.

Transition-metal catalyzed acceptorless alcohol dehydrogenation (AAD) with the liberation of H_2 is an atom-economical and selective route to generate a variety of organic carbonyl synthons.¹ In the context of the “hydrogen energy economy”, AAD also provides a highly desirable strategy

for promoting H₂ release from suitable biomass feedstocks for chemical energy storage applications.²

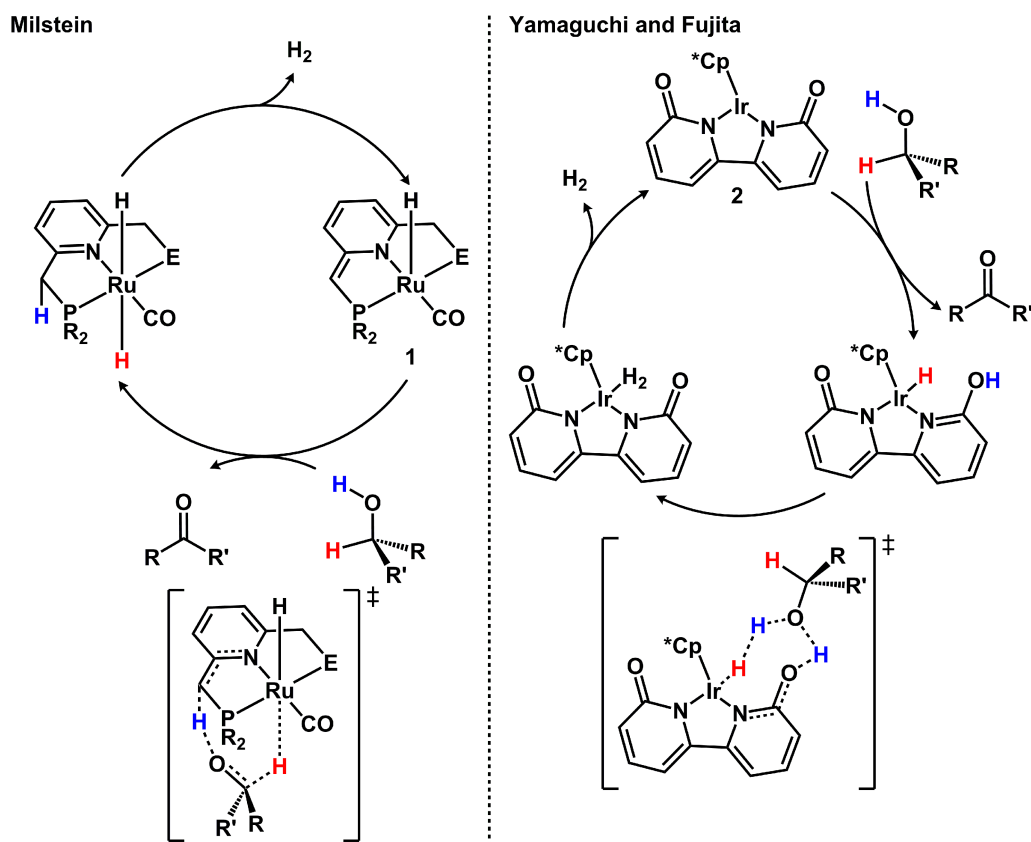


Figure 3-2 Proposed AAD reaction pathway mediated by bifunctional catalysts developed by Milstein and Yamaguchi.

To achieve high atom economy (no exogenous additives), promoterless AAD reactions are most often mediated by bifunctional catalysts that operate *via* a metal–ligand cooperative mechanism. This ligand-assisted, transition-metal catalyzed process differs from the classical inner-sphere mechanism by not requiring coordination of the substrate, thus enabling outer-sphere proton transfer to a ligand-based basic site with concurrent hydride transfer to the metal center (Figure 3-1).³ For example, Milstein's group developed a series of pyridyl PNE (E = PR₂ or NR₂) Ru pincer complexes (**1**, HRu(PNE)(CO)) that employ cooperation of the metal center with the ligand *via* aromatization–dearomatization of the central pyridinyl group concomitant with protonation–deprotonation of the methylene arm (Figure 3-2, left panel).^{1a,4} Computational studies revealed that **1** favors an outer-sphere bifunctional double hydrogen transfer pathway rather than an inner-sphere β -H elimination process.⁵ More recently, a computational study by

Yamaguchi, Fujita, and co-workers demonstrated that the AAD reaction of benzyl alcohol catalyzed by Cp*Ir(bpyO) (**2**, bpyO = α,α' -bipyridonate) also operates *via* an outer-sphere pathway, where the metal center and the bipyridonate motif work synergistically to oxidize benzyl alcohol en route to H₂ elimination with the aid of an alcohol bridge (Figure 3-2, right panel).⁶ Collectively, these and related studies establish the importance of a cooperative mechanism to achieve efficient dehydrogenation activity. However, in systems that contain bifunctional groups, it may be ambiguous whether a cooperative pathway is actually required for efficient dehydrogenation.⁷

We recently reported an *N,N,N*-bMepi (bMepi = 1,3-bis(6'-methyl-2'-pyridylimino)isoindolate) Ru(II) hydride complex (**3**, HRu(bMepi)(PPh₃)₂) capable of catalyzing promoterless and chemoselective AAD reactions.^{8,9} Of particular note, precatalyst **3** promotes acceptorless dehydrogenation of secondary alcohols to ketones, acceptorless dehydrogenative coupling of primary alcohols to esters, and diols to lactone products with high conversion efficiencies. Importantly, neither of these reactions requires exogenous base or hydrogen acceptor additives, and the catalyst system is unusually selective for the dehydrogenation of secondary alcohols in the presence of primary alcohols. Preliminary analysis of the alcohol dehydrogenation reaction revealed two key findings: 1) a homogeneous active catalyst, as assessed by mercury and substoichiometric ligand poisoning experiments, and 2) the release of PPh₃ under catalytic conditions. In this article, we use these observations as an entry point to disclose a detailed mechanistic analysis of a series of kinetic rate data including isotopic labeling studies, stoichiometric reactions to probe catalytic intermediate species, and new ligand variants to understand the steric and electronic effects of the bMepi pincer ligand on the activity of the Ru complex. We aim to answer the following key questions: 1) Does precatalyst **3** participate in an inner- or outer-sphere dehydrogenation pathway? 2) What are the details of the intermediates in the dehydrogenation catalytic cycle? 3) What impact do the steric (*ortho*-substituted methyl groups) and electronic (electron donating and -withdrawing groups in the secondary coordination sphere) profiles of the bMepi pincer ligand have on alcohol dehydrogenation?

3.2 Results and Discussion

3.2.1 Limiting Mechanistic Scenarios for Acceptorless Alcohol Dehydrogenation Catalyzed by HRu(bMepi)(PPh₃)₂

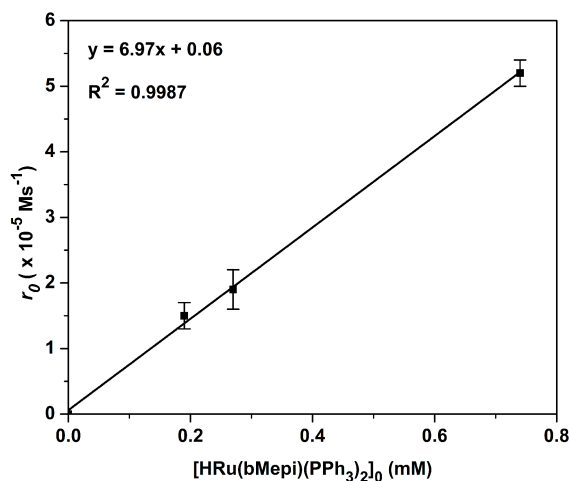


Figure 3-3 1PhEtOH dehydrogenation rate dependence on the concentration of HRu(bMepi)(PPh₃)₂.

Based on prior PPh₃ studies⁸ and the observation of a first-order dependence of the rate of 1-phenylethanol (1PhEtOH) dehydrogenation on **[3]** (Figure 3-3),¹⁰ two limiting monometallic alcohol dehydrogenation pathways mediated by **3** are proposed in Figure 3-4. For either pathway, phosphine dissociation from **3** generates a coordinately unsaturated Ru species that is able to participate in either an inner-sphere β -H elimination pathway (Figure 3-4, top panel) or an outer-sphere concerted pathway (Figure 3-4, bottom panel). In the inner-sphere cycle, proton transfer from the alcohol to the Ru hydride affords a Ru-alkoxide species (likely *via* a transient Ru-H₂ intermediate), which undergoes β -H elimination to complete the cycle. An alternative pathway to the inner-sphere β -H elimination mechanism is the outer-sphere pathway, where both proton and hydride transfer occur without requiring coordination to Ru. Complex **3** operating *via* this pathway may involve proton transfer to the imine (or isoindolate) group on the bMepi-ligand backbone with concurrent hydride transfer to the Ru-metal center. Both of these AAD mechanistic scenarios are evaluated by a series of kinetic experiments, catalyst modifications, as well as isolation of proposed intermediates.

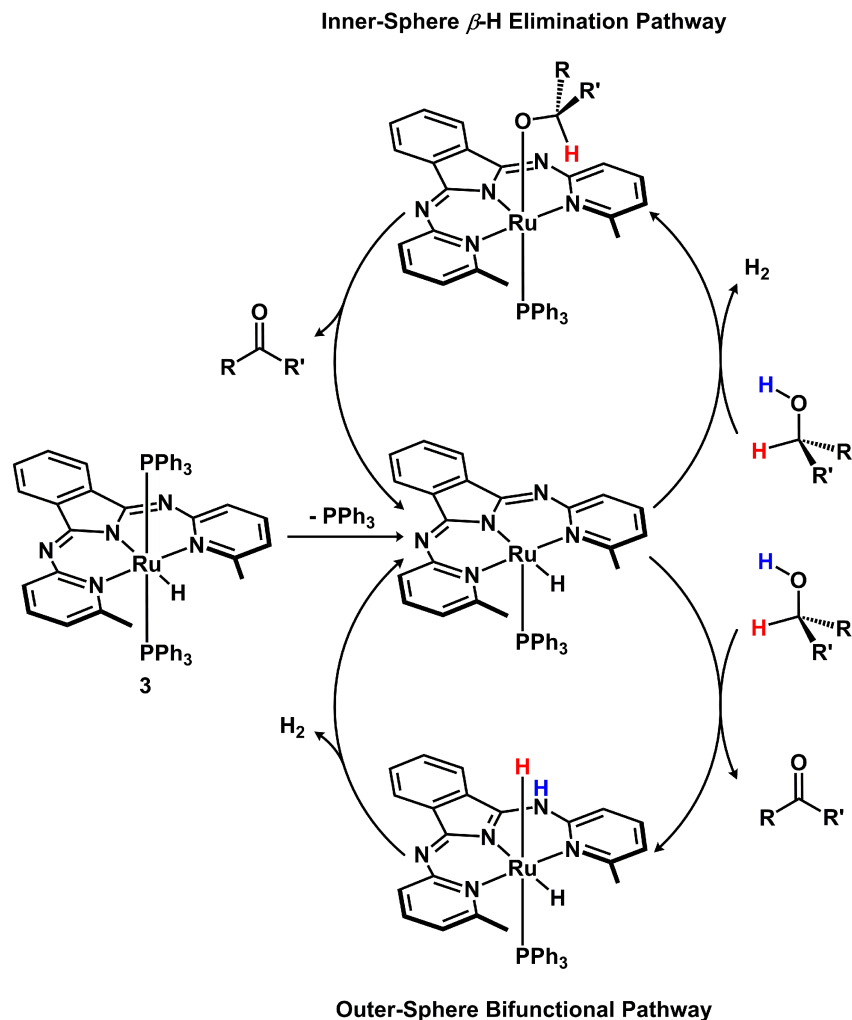
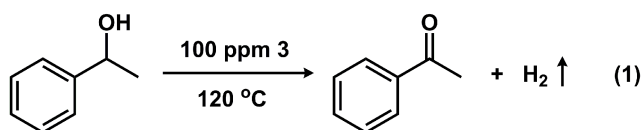


Figure 3-4 Proposed inner-sphere and outer-sphere dehydrogenation pathways.

3.2.2 Standard Conditions for Kinetic Studies



Standard Conditions:
 $[\mathbf{3}] = 7.4 \times 10^{-4}\text{ M}$
 $[\text{PhEtOH}] = 7.5\text{ M}$
 $[\text{PhTMS}] = 0.53\text{ M}$

Figure 3-5 Standard reaction conditions for AAD of 1PhEtOH catalyzed by HRu(bMepi)(PPh₃)₂.

In order to examine the operative pathway for catalysis by **3**, 1PhEtOH was selected as a standard substrate because its low volatility permits heating in an open system. Additionally, the

reverse reaction, reduction of acetophenone to 1PhEtOH, is generally accepted as a standard test for (transfer) hydrogenation catalysis.^{3,11} The dehydrogenation reaction was performed in an open system inside an inert-atmosphere glovebox and the conversion of 1PhEtOH to acetophenone was monitored by ¹H NMR spectroscopy using phenyltrimethylsilane (PhTMS) as an internal standard (Figure 3-5). The observed reaction rates were obtained using the method of initial rates. All kinetic experiments were simultaneously performed in triplicate. Standard reaction conditions for kinetic studies employed a vial containing 7.5 M 1PhEtOH and 0.01 mol% **3**. After the reaction mixture was heated to 120 °C for 4 h, acetophenone was observed in 11.6% conversion, which corresponds to an initial rate of $5.2(2) \times 10^{-5} \text{ M}\cdot\text{s}^{-1}$, a turnover number (TON) of 1213, and a turnover frequency (TOF) of 303 h^{-1} . To establish confidence in the method of initial rates in this system, a reaction rate of $5.8 \times 10^{-5} \text{ M}\cdot\text{s}^{-1}$ (within 10% error of the initial rate) at 4 h was obtained from the first derivative of an exponential fit of the complete dehydrogenation reaction profile (Figure 3-6).

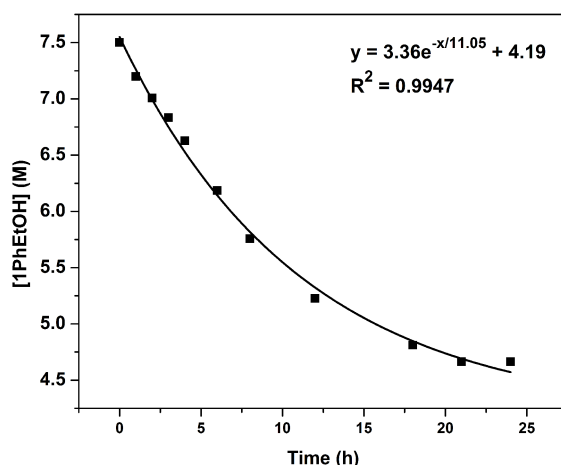


Figure 3-6 Complete reaction profile of 1PhEtOH dehydrogenation.

3.2.3 Triphenylphosphine Dependence

Based on our prior studies that showed free PPh₃ during catalysis, the dependence on PPh₃ concentration was examined to determine whether PPh₃ dissociation contributed to a turnover-limiting step in either of the proposed alcohol dehydrogenation cycles. The order in [PPh₃] was determined by measuring the observed rates for 1PhEtOH dehydrogenation over several PPh₃ concentrations under the reaction conditions listed in Figure 3-5. No dependence on

the rate of 1PhEtOH dehydrogenation was observed up to 20 equiv of PPh₃ (14.5 mM) relative to **3** (Figure 3-7).

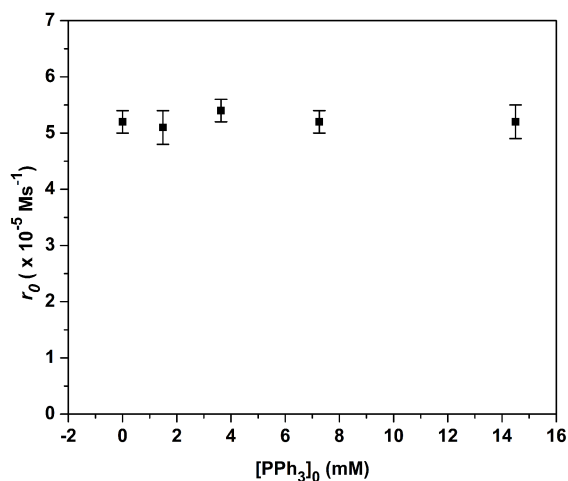


Figure 3-7 Influence of [PPh₃] on the reaction rates for 1PhEtOH dehydrogenation catalyzed by HRu(bMepi)(PPh₃)₂.

The zero-order [PPh₃] dependence (up to 20 equiv) suggests that PPh₃ dissociation from **3** is not included in the turnover-limiting step and furthermore that phosphine binding/release is not in equilibrium with the turnover-limiting step under these conditions. Therefore, the turnover-limiting step must be either β -H elimination (inner-sphere) or H₂ formation reaction (outer-sphere). Alternatively, for this to be true for a proton/hydrogen transfer turnover-limiting step, the alcohol binding would have to be irreversible, which is highly improbable.¹²

3.2.4 1-Phenylethanol Dependence

In both the inner- and outer-sphere dehydrogenation scenarios (Figure 3-4), the next step following PPh₃ dissociation involves the alcohol substrate. A rate dependence on [1PhEtOH] would be anticipated if the turnover-limiting step was alcohol binding followed by deprotonation (inner-sphere) or proton and hydride transfer from the alcohol (outer-sphere). The influence of 1PhEtOH concentration on the catalytic rate was examined by changing the [1PhEtOH] while holding the initial concentration of **3** constant. Over the range of 6.5–8 M 1PhEtOH, the observed reaction rate profile displayed a linear dependence on [1PhEtOH] from 6.5 to 7.5 M 1PhEtOH, then the rate reached culmination after 7.5 M 1PhEtOH with an averaged catalytic rate of $5.2(2) \times 10^{-5} \text{ M}\cdot\text{s}^{-1}$ (Figure 3-8).¹³ The reaction rate dependence on [1PhEtOH] suggests a

pre-equilibrium model in which at high [1PhEtOH] the equilibrium is driven to the right, and the dependence on [1PhEtOH] drops from the rate law. This model could fit either the inner- or outer-sphere pathways, where a pre-equilibrium alcohol binding and proton/hydrogen transfer is followed by a slow metal-based reaction (e.g., β -H elimination or H₂ formation). Given that two different mechanistic regimes exist at high and low [1PhEtOH], it is important to note that the kinetic experiments were performed at an initial [1PhEtOH] of 7.5 M (Figure 3-5, unless otherwise stated) and under these conditions, the catalyst operated in the linear regime when the reaction proceeded 10–15%.

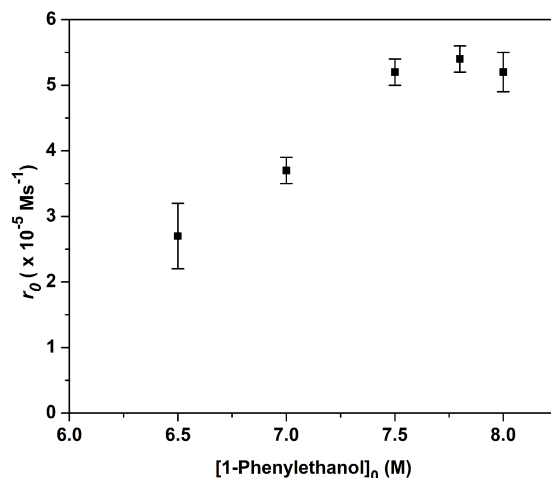


Figure 3-8 Influence of [1PhEtOH] on the reaction rates for 1PhEtOH dehydrogenation catalyzed by HRu(bMepi)(PPh₃)₂.

3.2.5 Temperature Dependence

The activation parameters for 1PhEtOH dehydrogenation mediated by **3** at low and high [1PhEtOH] were analyzed to interrogate the transition-state structures. The reaction rates were measured over a 40 °C temperature range and plotted according to an Eyring analysis (Figure 3-9). In the low [1PhEtOH] regime, analysis of the Eyring plot revealed a free energy activation barrier (ΔG^\ddagger) of 31(3) kcal/mol at 120 °C, an activation enthalpy (ΔH^\ddagger) of 18(1) kcal/mol, and an activation entropy (ΔS^\ddagger) of -32(3) eu.¹⁴ In the high [1PhEtOH] regime, analysis of the Eyring plot revealed a ΔG^\ddagger of 31(3) kcal/mol at 120 °C, an ΔH^\ddagger of 15(1) kcal/mol, and an ΔS^\ddagger of -41(3) eu. An activation enthalpy of this magnitude is consistent with bond-breaking character in the turnover-limiting transition structure.¹⁵ In addition, the relatively large negative entropy of activation suggests not only an associative process but also a higher degree of organization in the

transition state than in the ground state. Analysis of the activation parameters at low and high [1PhEtOH] revealed equivalent ΔG^\ddagger values. However, between the low and high [1PhEtOH] regimes, the magnitude of ΔH^\ddagger decreases, whereas that of ΔS^\ddagger increases. This implies that at high [1PhEtOH] the AAD catalysis is entropically controlled. Unfortunately, these Eyring data could not be used to unambiguously differentiate between the two proposed mechanisms. For example, a highly ordered transition structure could be expected for an alcohol-assisted proton/hydrogen transfer turnover-limiting step in the two pathways as proposed in Figure 3-10.¹⁶ Furthermore, a range of ΔS^\ddagger values (+12 to -30 eu) have been reported for a β -H elimination turnover-limiting step from metal-alkoxide species.¹⁷

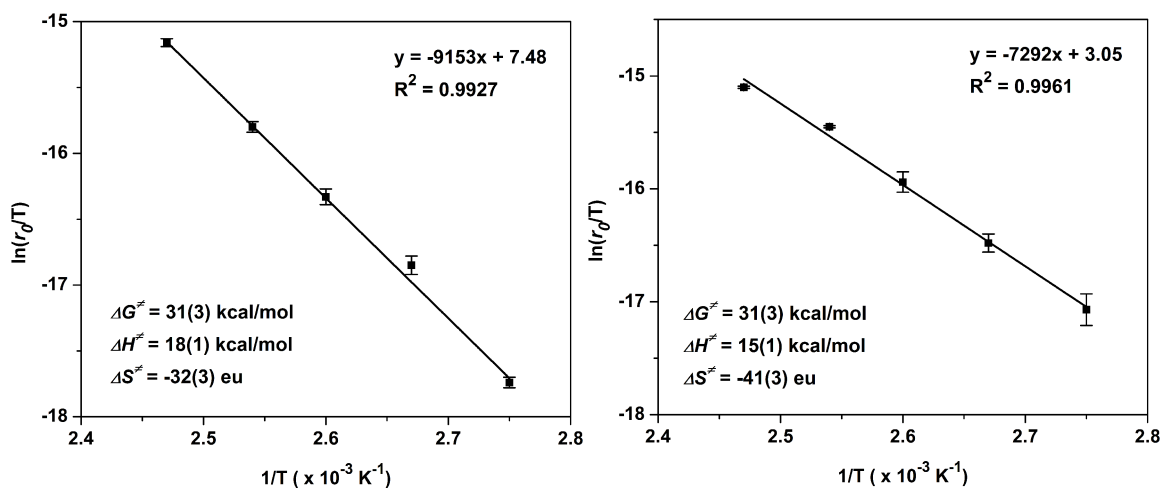


Figure 3-9 Eyring plots for 1PhEtOH dehydrogenation catalyzed by HRu(bMepi)(PPh₃)₂. Left panel $[1\text{PhEtOH}]_0 = 7.5 \text{ M}$. Right panel $[1\text{PhEtOH}]_0 = 8.2 \text{ M}$.

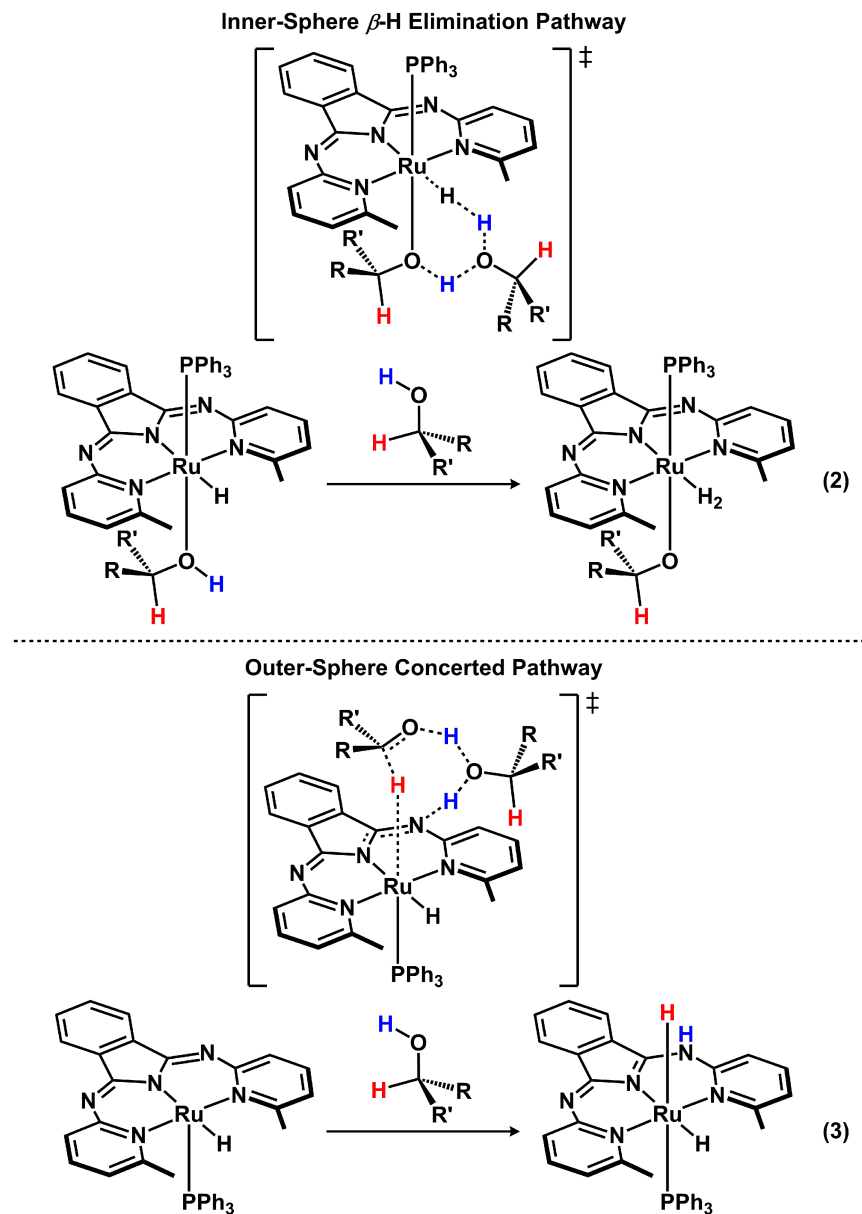


Figure 3-10 Proposed 1-PhEtOH deprotonation with 1PhEtOH as a proton-transfer shuttle in the inner-sphere and outer-sphere pathways.

3.2.6 Isotopic Labeling Studies

A series of deuterium isotopic substitutions of 1PhEtOH were used to interrogate proton and hydride transfer and inner- versus outer-sphere pathways. The scenario of 1PhEtOH deprotonation as the turnover-limiting step was examined by monitoring the dehydrogenation of the 1PhEtOH isotopologue, 1PhEtOD, catalyzed by **3**. A normal primary kinetic isotope effect (KIE) would be anticipated if the O–H bond cleavage is involved in the turnover-limiting step or

precedes it. Dehydrogenation of 1PhEtOD at 120 °C in the presence of 0.01 mol% **3** yielded an observed rate of $2.7(1) \times 10^{-5} \text{ M}\cdot\text{s}^{-1}$ (Figure 3-11, eq 4). This reduced reaction rate, compared to the rate for the perprotio isotopologue, afforded a KIE ($r_{\text{OHCH}}/r_{\text{ODCH}}$) of 1.9(2), thus supporting either O–H bond cleavage in the turnover-limiting step (inner- or outer-sphere) or a β -H elimination turnover-limiting step with a proton-transfer pre-equilibrium (inner-sphere). Hence, it should be noted that the observed isotope effect is likely a composite of both equilibrium and kinetic isotope effects.¹⁸

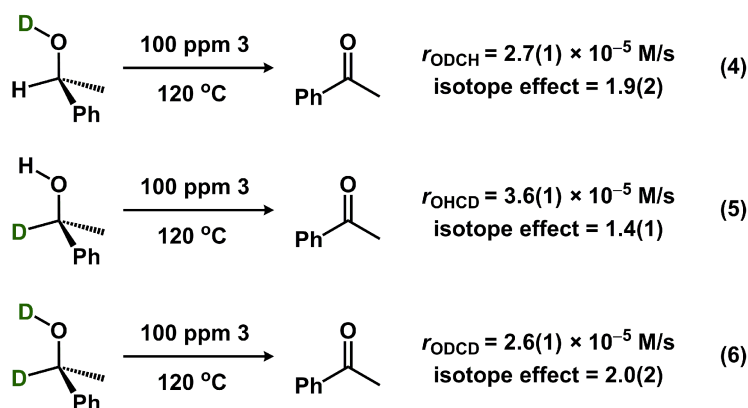


Figure 3-11 Isotopic labeling experiments for the dehydrogenation of 1PhEtOH.

Another set of isotopic labeling experiments were performed with a second isotopologue of 1PhEtOH, 1PhCH₃CDOH. An observed reaction rate of $3.6(1) \times 10^{-5} \text{ M}\cdot\text{s}^{-1}$ was obtained for the dehydrogenation of 1PhCH₃CDOH at 120 °C resulting in a KIE ($r_{\text{OHCH}}/r_{\text{OHCD}}$) of 1.4(1) (Figure 3-11, eq 5). This observed KIE is consistent with the cleavage of the C–H bond in the turnover-limiting step (β -H elimination or outer-sphere pathway) and is too large for a secondary isotope effect. Depending on the nature of the transition state, varying magnitudes of KIE (>1.3) have been measured for β -H elimination from metal-alkoxides.^{18c} However, a KIE with a larger magnitude (2.6) was observed for an outer-sphere concerted pathway.¹⁹ In addition, the measured KIE is also consistent with a proton-transfer turnover-limiting step where a Ru–H(D) species could participate in deprotonation of the alcohol after the first turnover in an inner-sphere pathway.

The outer-sphere concerted pathway can be evaluated using a series of isotopic labeling experiments. For example, Bäckvall and Johnson demonstrated that Shvo's catalyst operated *via* an outer-sphere concerted mechanism by analyzing the KIE for the doubly deuterium labeled

isotopologue of 1PhEtOH, 1PhCH₃CDOD.¹⁹ For a concerted pathway, the observed isotope effect for 1PhCH₃CDOD should be the product of the two individual isotope effects ($r_{\text{OHCH}}/r_{\text{ODCH}} \times r_{\text{OHCH}}/r_{\text{OHCD}}$). When 1PhCH₃CDOD was subjected to the standard dehydrogenation conditions, a reaction rate of $2.6(1) \times 10^{-5} \text{ M}\cdot\text{s}^{-1}$ was observed, providing a kinetic isotope effect ($r_{\text{OHCH}}/r_{\text{ODCD}}$) of 2.0(2) (Figure3-11, eq 6). In contrast, the product of the individual isotope effects is 2.7 (1.9×1.4) and thus inconsistent with the measured combined KIE. Furthermore, to normalize for any secondary isotope effects on the C–H KIE, we averaged the $r_{\text{OHCH}}/r_{\text{OHCD}}$ (1.44) and $r_{\text{ODCH}}/r_{\text{ODCD}}$ (1.04) values to provide a C–H KIE of 1.24. The product of the O–H and averaged C–H KIE is 2.4(1), which also does not match the observed $r_{\text{OHCH}}/r_{\text{ODCD}}$. These analyses provide strong evidence *against* pathways in which both proton and hydride transfer in a concerted manner and are in support of an inner-sphere, stepwise pathway.

3.2.7 Synthesis and Reactivity of Ru(bMepi^{Me})(PPh₃)(OTf)₂

To complement the kinetic isotope studies that discounted an outer-sphere concerted pathway, we targeted Ru(II) compounds with the ligand bMepi^{Me}, in which one of the imine groups is methylated. Prior studies from our laboratory found that a late stage modification can be used to alkylate the imine backbone, thus providing complementary complexes that feature similar primary coordination environments yet differ in charge of the pincer ligand.²⁰ Furthermore, the site of protonation or alkylation in these and related complexes²¹ is the imine nitrogen, rather than the amido nitrogen, which indicates the former as the favored kinetic site for protonation. Hence, metal–ligand cooperative pathways involving proton transfer to the central isoindoline nitrogen are unlikely AAD mechanisms for the bis(pyridylimino)isoindolate framework.

Ru(bMepi^{Me})(PPh₃)OTf₂ (**5**) was prepared by treating a DCM solution of Ru(bMepi)(PPh₃)Cl (**4**) with 10 equiv of MeOTf at room temperature for 18 h. Complex **5** was isolated in 62% yield and characterized by ¹H and ³¹P NMR spectroscopy, elemental analysis, and X-ray crystallography. The ³¹P{¹H} spectrum displays a singlet at 47.8 ppm, and the ¹H NMR spectrum is consistent with the asymmetry of the bMepi^{Me} ligand. In particular, two distinct resonances for the *ortho*-CH₃ groups were located at 1.57 and 1.78 ppm and a singlet was detected at 3.71 ppm and assigned as the methyl group on the ligand backbone. Complex **5**

has a slightly distorted square-based pyramid ($\tau = 0.10$)²² structure, which contains a triflate anion *trans* to the PPh₃ ligand (Figure 3-12).

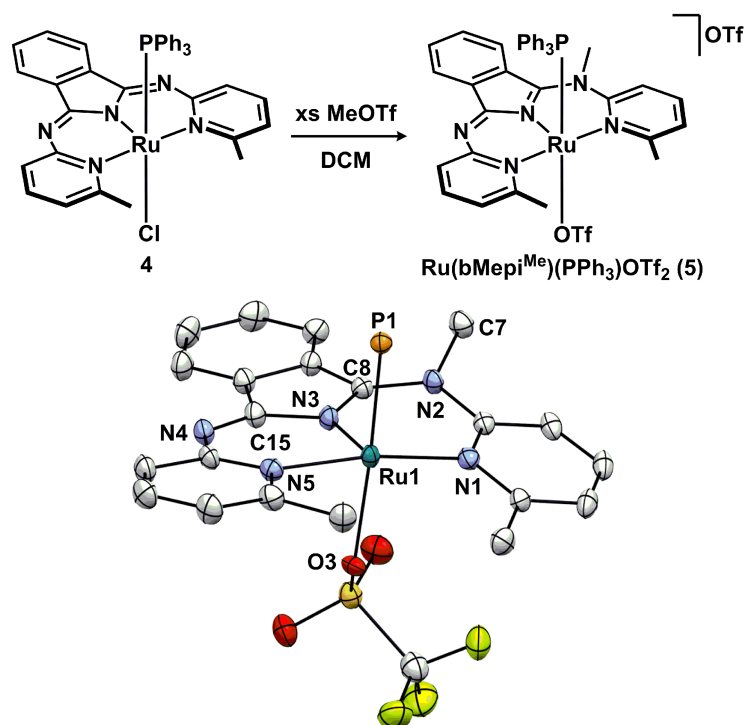


Figure 3-12 Synthesis and crystal structure (thermal ellipsoids depicted at 50% probability) of Ru(bMepi^{Me})(PPh₃)OTf₂.

In addition to the covalent methylated imine bond in **5**, noncovalent interactions of the *ortho*-methyl groups were found. Agostic M–H–C interactions are characterized by relatively short M–H distances (1.8 to 2.3 Å), small M–H–C bond angles (90 to 140°), and upfield chemical shifts of the agostic hydrogen atoms.²³ All three criteria for an agostic interaction are met in complex **5**. The crystal structure of **5** reveals a short M–H distance of 2.29 Å²⁴ and a small M–H–C bond angle of 119° from one hydrogen of the *ortho*-CH₃ groups. In addition, the two singlet resonances for the methyl groups are upfield of the free HbMepi ligand (the hydrogen atoms of the methyl groups on the free HbMepi ligand were observed in the ¹H NMR spectrum as a singlet at 2.50 ppm, $\Delta = 0.93, 0.72$ ppm). The analogous protonated complex (Ru(HbMepi)(PPh₃)Cl[PF₆]) was also synthesized by heating a THF solution containing HbMepi, RuCl₂(PPh₃)₃, and TlPF₆ (Figure 3-13). In contrast to sharp ligand resonances observed in the ¹H NMR spectrum of **5**, the analogous protonated complex, Ru(HbMepi)(PPh₃)Cl[PF₆], contains broad ligand resonances at room temperature, which are consistent with a dynamic protonation

equilibrium between the imine nitrogens. The solid-state structure shows square-based pyramidal geometry about the Ru center with a chloride ligand *trans* to PPh₃. For Ru(HbMepi)(PPh₃)Cl[PF₆], two out of the three criteria are met for an agostic interaction; the M–H distance is slightly longer (2.44 Å). However, the M–H–C bond angle of 107° and the upfield shift of the *ortho*-CH₃ groups (1.78 and 1.70 ppm, $\Delta = 0.72, 0.80$ ppm) are consistent with an agostic M–H–C interaction. Complex **4** exhibited similar structural and spectroscopic properties as the protonated complex, such as the M–H distance (2.41 Å), a M–H–C bond angle of 113°, and the upfield shift of the *ortho*-CH₃ groups (1.72 ppm, $\Delta = 0.78$ ppm).

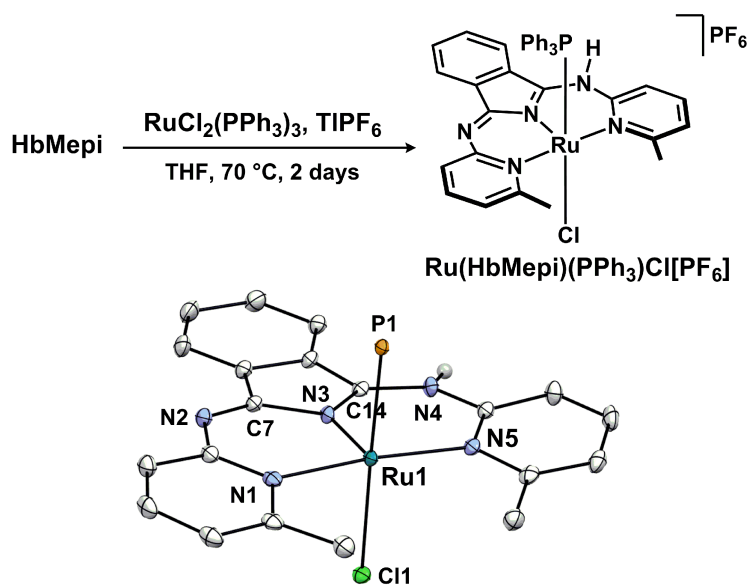


Figure 3-13 Synthesis and crystal structure (thermal ellipsoids depicted at 50% probability) of Ru(HbMepi)(PPh₃)Cl[PF₆].

Because the isotopic labeling studies were not consistent with a concerted dehydrogenation pathway (*vide supra*), a stepwise, hybrid metal–ligand cooperative pathway was evaluated. This bifunctional hybrid mechanism is a combination of the inner-sphere β -H elimination and the outer-sphere bifunctional pathway, in which proton transfer takes place at the backbone imine group on the bMepi ligand, affording a Ru-alkoxide intermediate (Figure 3-14, eq 7) that could undergo β -H elimination. Unless H₂ is eliminated, this pathway is not probable because the Ru-alkoxide intermediate is an 18 e⁻ species and could not undergo β -H elimination without losing another ligand (or dissociation of the alkoxide or a pyridine arm). Dissociation of the PPh₃ ligand would deviate from the observed zero-order [PPh₃] dependence.

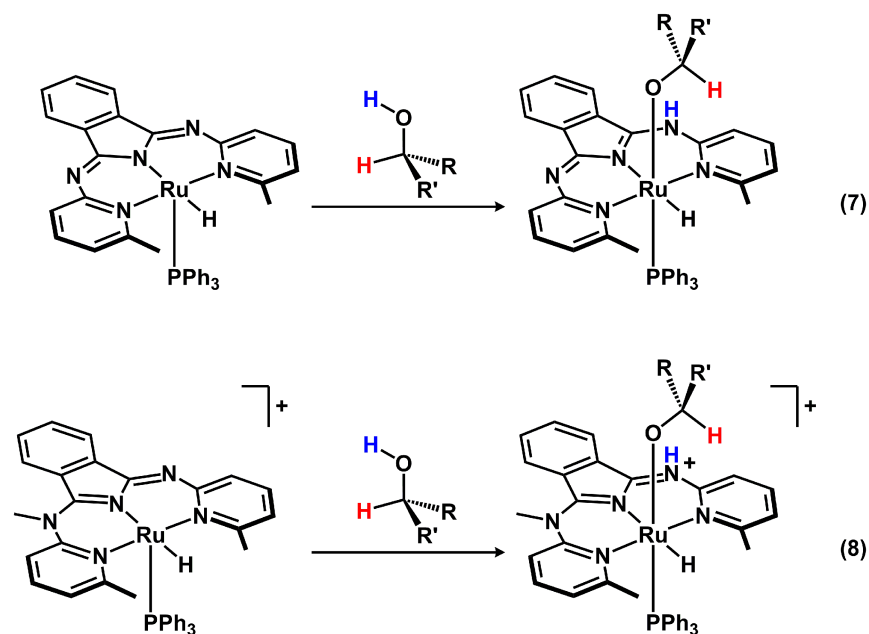


Figure 3-14 Proposed proton transfer *via* stepwise metal–ligand cooperativity.

To assess the potential participation of the backbone imine group on the bMepi ligand in the dehydrogenation of alcohols *via* bifunctional metal–ligand catalysis, the dehydrogenation of 1PhEtOH catalyzed by **5** was evaluated. Of key importance to a bifunctional metal–ligand pathway is proton transfer to the backbone imine nitrogen. This protonation event would seem energetically unfavorable for the alkylated complex (Figure 3-14, eq 8) given that heating **4** in excess MeOTf afforded only the monomethylated complex, which suggests that the remaining imine functionality is less basic in the bMepi^{Me} ligand than in the parent bMepi ligand.

The proposed hybrid metal–ligand cooperative pathway was evaluated by comparing the reaction rates of 1PhEtOH dehydrogenation catalyzed by **4** and **5** (Figure 3-15). Heating a 7.8 M 1PhEtOH solution containing 0.024 mol% of **4** and 0.048 mol% NaO^tBu to 120 °C for 4 h resulted in an averaged TON of 1441, which corresponds to a reaction rate of $7.7(3) \times 10^{-5} \text{ M}\cdot\text{s}^{-1}$. The alkylated Ru complex (**5**) was also a competent dehydrogenation precatalyst. For instance, under the same reaction conditions, complex **5** oxidized 1PhEtOH to acetophenone and H₂ with a reaction rate of $8.7(1) \times 10^{-5} \text{ M}\cdot\text{s}^{-1}$.²⁵ These results demonstrate that a cooperative interaction involving the imine functionality is not necessary to achieve efficient rates for catalytic AAD reaction.²⁶

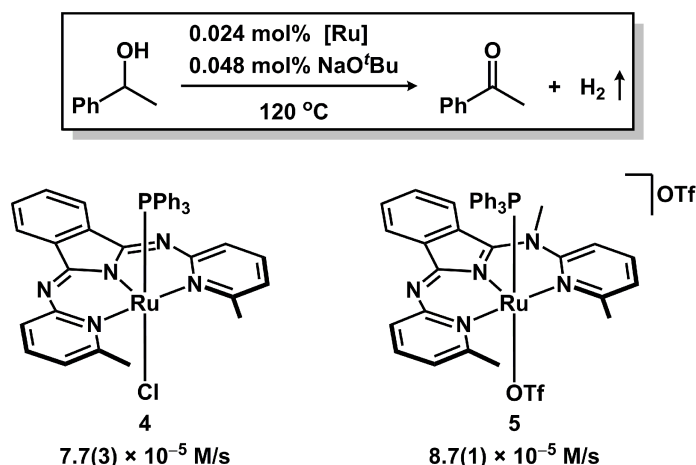


Figure 3-15 Reaction rate comparison between the bMepi and bMepi^{Me} ligated Ru complexes.

3.2.8 Hammett Studies

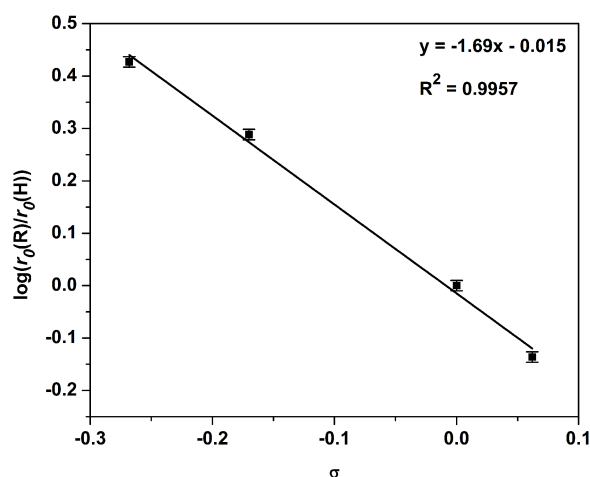
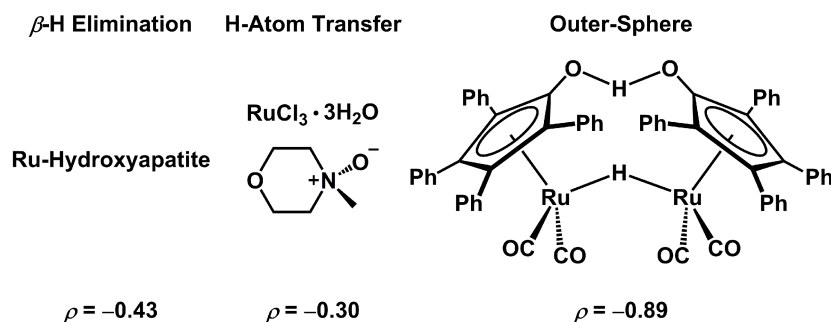
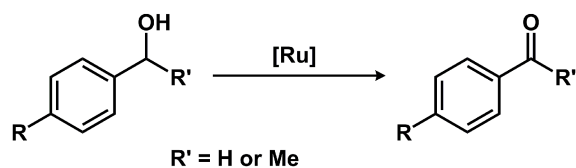


Figure 3-16 Hammett plot for 1PhEtOH dehydrogenation catalyzed by HRu(bMepi)(PPh₃)₂.

The electronic character of the turnover-limiting transition state in catalytic AAD promoted by **3** was investigated by conducting a linear free energy analysis using initial rates of dehydrogenation of *para*-substituted 1PhEtOH substrates (Figure 3-16). The ρ value has previously been used to differentiate between limiting mechanistic regimes of alcohol dehydrogenation (Figure 3-17). For instance, distinct ρ values were reported for Ru-catalyzed alcohol dehydrogenation reactions that operate through turnover-limiting β -H elimination ($\rho = -0.43$),²⁷ free-radical H atom transfer ($\rho = -0.30$),²⁸ or outer-sphere pathway ($\rho = -0.89$)²⁹. In contrast to these values, the Hammett analysis for **3** afforded a ρ value of $-1.69(5)$. The negative ρ value signifies a positive charge buildup in the transition state, supporting a β -H elimination

turnover-limiting step in the inner-sphere pathway. Although **3** and the heterogeneous Ru-hydroxyapatite system are proposed to undergo a β -H elimination turnover-limiting step, the difference in magnitude of the ρ values may be explained by the nature of the transition state. The smaller ρ value of -0.43 observed for Ru-hydroxyapatite indicates that electronic changes have a subtle effect on β -H elimination, which is consistent with a late transition state with almost complete C–H bond cleavage and Ru–H bond formation. For our system **3**, electron-donating groups increase the nucleophilicity of the benzylic hydrogen atom, which acquires hydridic character during β -H elimination. Stabilization of the positive charge buildup at the benzylic carbon as the hydride is transferred in the transition state suggests an early transition-state model.

Previous Work



This Work

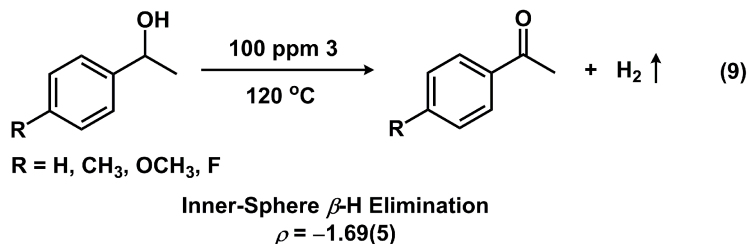


Figure 3-17 Comparison of Hammett parameters derived from Ru-catalyzed alcohol oxidation.

3.2.9 Isolation of a Ruthenium(II)-Alkoxide Complex

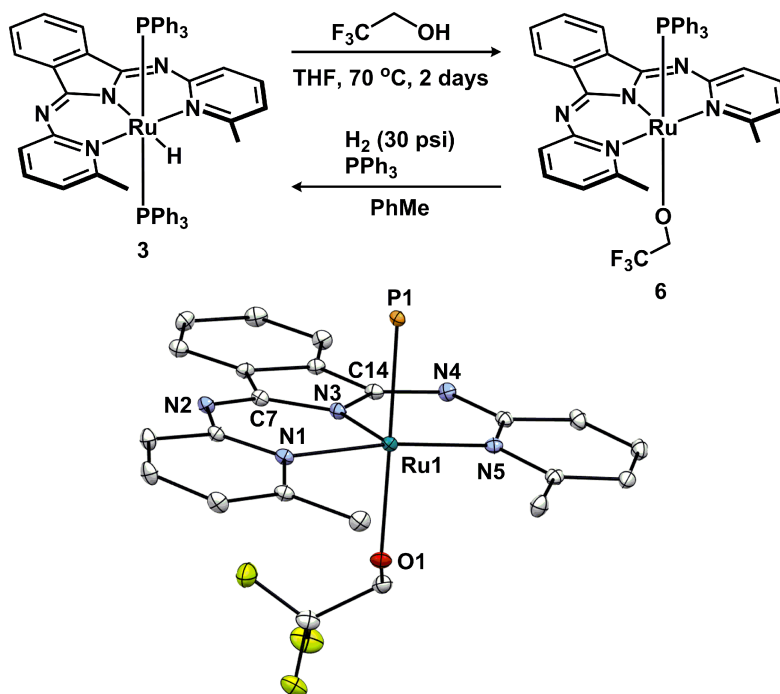


Figure 3-18 Synthesis and crystal structure (thermal ellipsoids depicted at 50% probability) of Ru(bMepi)(PPh₃)(OCH₂CF₃).

Following the kinetic experiments, which support an inner-sphere β -H elimination pathway, stoichiometric reactions were performed to examine the intermediate species during catalysis. In particular, a Ru-alkoxide species was implicated as the catalyst resting state that undergoes β -H elimination in an inner-sphere pathway. To trap such a species prior to β -H elimination, trifluoroethanol, whose conjugate base is resistant to β -H elimination,³⁰ was selected. The addition of 1.1 equiv of trifluoroethanol to a solution of **3** in THF resulted in the clean conversion to Ru(bMepi)(PPh₃)(OCH₂CF₃) (**6**), which was isolated as a dark blue solid in 76% yield after heating at 70 °C for 2 days (Figure 3-18). The ¹H NMR spectrum features a single set of bMepi resonances with the methyl resonances at 1.75 ppm and the ³¹P{¹H} NMR spectrum of **6** exhibits a singlet at 43.8 ppm, which is similar to the ³¹P spectrum observed for Ru(bMepi)(PPh₃)Cl (**4**, 43.5 ppm). Crystals suitable for single-crystal X-ray diffraction were obtained from vapor diffusion of pentane into a PhMe solution of **6**. The solid-state structure shows a square-based pyramid geometry about the Ru(II) center ($\tau = 0.01$)²² with the -OCH₂CF₃ ligand *trans* to PPh₃ (Figure 3-18). The shortest M-H distance is 2.69 Å with a M-H-C bond

angle of 99° and the chemical shift of the methyl groups is upfield of the free HbMpi ligand. The structural and spectroscopic properties satisfy two out of three criteria for determining an agostic interaction between the Ru center and the methyl C–H group.

Given that complex **6** is similar to the proposed Ru-alkoxide intermediate in the AAD catalytic cycle, intermediates species prior to H₂ liberation were investigated by allowing **6** to react with H₂. When a J. Young NMR tube containing a toluene-*d*₈ solution of **6** and PPh₃ was charged with 30 psig of H₂, the immediate formation of trifluoroethanol was detected as a triplet at –76.5 ppm in the proton-coupled ¹⁹F spectrum, and **6** and **3** were the *only* complexes observed by ¹H and ³¹P NMR spectroscopy. In addition, no reaction was observed when the same experiment was performed at –75 °C. Upon slowly warming the J. Young tube in the NMR spectrometer, the formation of trifluoroethanol and **3** resulted from the clean conversion of **6** and H₂. No Ru intermediate species were observed at low temperature and **3** was the only Ru species observed when **6** reacted with H₂. These observations suggest that both alcohol and η²-H₂ adducts are short-lived intermediates with respect to the alkoxide and/or **3**. Furthermore, no reaction (β-H elimination or decomposition) was observed when a solution of **6** with and without 100 equiv of trifluoroethanol in C₆D₆ was heated to operating temperatures for catalytic AAD reaction (120 °C for 3 h), which is consistent with an increase (~15 kcal/mol) in the activation barrier effected by the trifluoromethyl group.^{30a}

3.2.10 Catalyst Resting State and Mechanistic Discussion

With known spectroscopic features of a Ru–bMepi alkoxide species in hand, NMR experiments were performed to observe the catalyst resting state *in situ*. A solution of 8.3 M 1PhEtOH containing 0.1 mol% of **3** inside a J. Young tube was monitored by ¹H and ³¹P NMR spectroscopy at room temperature and 100 °C. After 10 min at room temperature 73% of **3** was converted to a new species with a ³¹P resonance at 41.7 ppm with concomitant formation of free PPh₃. The hydride region of the ¹H NMR spectrum showed no new species. This new species at 41.7 ppm is consistent with the chemical shift of the isolated Ru alkoxide (**6**) and thus is proposed as Ru(bMepi)(PPh₃)(OCHPhMe).³¹ Heating the J. Young tube inside the NMR spectrometer for 10 min at 100 °C resulted in the full conversion of **3** to the proposed Ru alkoxide. At 100 °C the ³¹P NMR spectrum exhibited only two resonances corresponding to the Ru alkoxide (40.6 ppm) and free PPh₃ with 1:1 integration values. Observation of the catalyst

resting state as Ru-alkoxide species at high [1PhEtOH] further supports a β -H elimination turnover-limiting step during catalysis.

The catalyst resting state was also examined at low [1PhEtOH]. A C_6D_6 solution containing 0.83 M 1PhEtOH and 0.1 mol% of **3** was monitored by 1H and ^{31}P NMR spectroscopy at room temperature and 100 °C. After 10 min at room temperature, 13% of a species consistent with formulation of the proposed alkoxide ($^{31}P = 41.7$ ppm) was observed by ^{31}P NMR spectroscopy. The hydride region of the 1H NMR spectrum showed only the hydride resonance of **3** as a triplet, which was broadened and suggestive of a dynamic process associated with ligand substitution and/or proton transfer. The equilibrium constant between **3** and the proposed Ru-alkoxide species is invariant from 0.83 to 6.0 M 1PhEtOH, which is consistent with a pre-equilibrium process. After the NMR tube was heated for 10 min at 100 °C, a 1:1 ratio of the Ru alkoxide to **3** was observed. Continued monitoring of the reaction mixture at 100 °C for 1 h (corresponding to *ca.* 0.3% acetophenone) resulted in no change in the ratio of the alkoxide species to **3**. This suggests that at low alcohol concentrations proton transfer is much slower and becomes competitive with β -H elimination. Thus, as reactant alcohol is consumed during catalysis, the turnover-limiting step is proposed to change from β -H elimination to proton transfer.

With the results of catalyst resting state at low and high [1PhEtOH] in hand, an in-depth analysis of $[PPh_3]$ dependence, [1PhEtOH] dependence, and activation parameters was pursued. The reaction rate dependence on [1PhEtOH] fits a pre-equilibrium model with an equilibrium proton-transfer step occurring before turnover-limiting β -H elimination. This is consistent with the zero-order dependence on $[PPh_3]$ and our previous analysis showing that phosphine binding is not in equilibrium with the turnover-limiting step. At high [1PhEtOH], the forward rate of proton transfer is fast and β -H elimination is the turnover-limiting step. As [1PhEtOH] decreases, proton transfer becomes slower and eventually becomes turnover-limiting. This implies that the Eyring data collected at low [1PhEtOH] contains contributions from both proton transfer and β -H elimination with β -H elimination as the major component. Hence, the activation parameters ($\Delta H^\ddagger = 15$ kcal/mol and $\Delta S^\ddagger = -41$ eu) determined at high [1PhEtOH] exclusively describe the transition state structure for a β -H elimination turnover-limiting step.

Although experimental evidence supports a β -H elimination turnover-limiting step, the large negative ΔS^\ddagger differs significantly from the previously reported values for β -H elimination from metal-alkoxide species.¹⁷ The classic β -H elimination process involves cleavage of a β -C–H of the coordinated alkoxide, with concomitant formation of hydride on an empty *cis* coordination site and coordinated ketone (or aldehyde) ligand. It follows that β -H elimination reactions are typically unimolecular and largely enthalpically controlled (considerable bond making and breaking character in the transition state). To account for the atypical activation parameters for **3**, alternative mechanisms, such as binuclear hydride abstraction³² and alcohol-assisted alkoxide dissociation,³³ for β -H elimination were considered. Our kinetic experiments discredit both processes as possible β -H elimination pathways for our catalyst. A binuclear mechanism is inconsistent with the observed first-order dependence on [**3**]. An alcohol-assisted alkoxide dissociative pathway is also unlikely because of the zero-order dependence on [1PhEtOH] at high [1PhEtOH]. Alternatively, we propose that **3** operates under a traditional β -H elimination process in which the highly negative activation entropy reflects contributions from solvent reorganization likely imparted by hydrogen bonding.³⁴ Such large entropic contributions are consistent with the reactions performed in neat alcohol solvent that allows the formation of a network of hydrogen bonds with a coordinated alkoxide ligand. Comparison of the activation parameters at low and high [1PhEtOH] revealed that entropy, not enthalpy, is the main contributor to the β -H elimination process. Thus, reorganization in the transition state, as reflected by the negative and large ΔS^\ddagger , must be due to rearrangement of the hydrogen bonds interacting with the Ru-alkoxide species in order for the β -C–H to migrate onto the Ru center.

3.2.11 Proposed Mechanism

Based on the series of kinetic and isotopic labeling experiments, an inner-sphere catalytic cycle for 1PhEtOH dehydrogenation mediated by **3** is implicated. We propose that a single PPh₃ dissociation from **3** generates a coordinatively unsaturated Ru–H species that can reversibly bind 1PhEtOH. This species likely undergoes a fast proton-transfer event in equilibrium with a β -H elimination turnover-limiting step to yield the ketone product and generate the coordinatively unsaturated Ru–H species to re-enter in the dehydrogenation cycle (Figure 3-19).

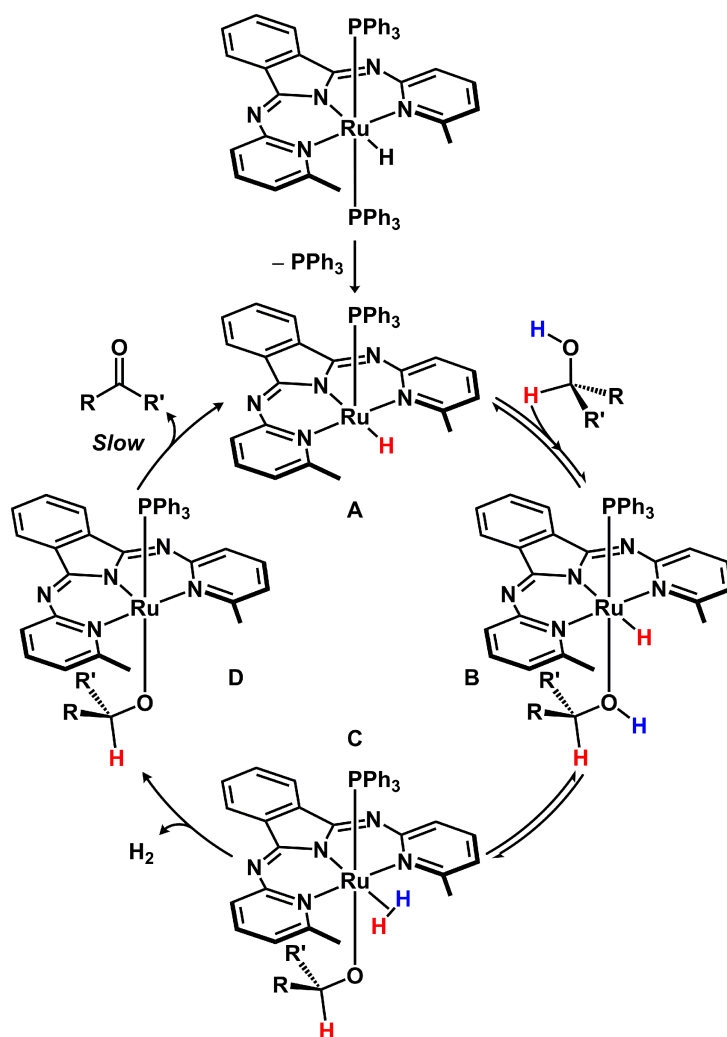


Figure 3-19 Proposed mechanism for AAD catalyzed by $\text{HRu}(\text{bMepi})(\text{PPh}_3)_2$.

3.2.12 Primary versus Secondary Alcohol Dehydrogenation

An unusual feature of precatalyst **3** is the high selectivity for secondary alcohol dehydrogenation in the presence of primary alcohols.³⁵ To a first approximation, thermodynamic arguments might be invoked to support the formation of the ketone over the aldehyde product.³⁶ However, this consideration assumes equilibrium conditions are met, which is not likely under the catalytic conditions. To gain further insight into the origin of the chemoselectivity bias, we evaluated competition experiments between benzyl alcohol (BnOH) and 1PhEtOH. Heating an equimolar (0.5 mmol) mixture of BnOH and 1PhEtOH containing 5 mol% **3** to 100 °C for 3 h resulted in the quantitative conversion of 1PhEtOH to acetophenone, while BnOH remained unreacted (Figure 3-20, eq 10). This result is consistent with our previously reported findings

that dehydrogenation of secondary alcohols is favored in the presence of primary alcohols when using temperatures lower than those required for acceptorless dehydrogenative coupling reactivity to afford esters.⁸ However, because these conditions do not afford coupling reactivity of primary alcohols, more forcing conditions were used to promote dehydrogenation activity of primary and secondary alcohols. Heating a PhMe solution containing BnOH and **3** (5 mol%) to 120 °C for 3 h afforded 65% benzyl benzoate and 5% benzaldehyde (Figure 3-20, eq 12).

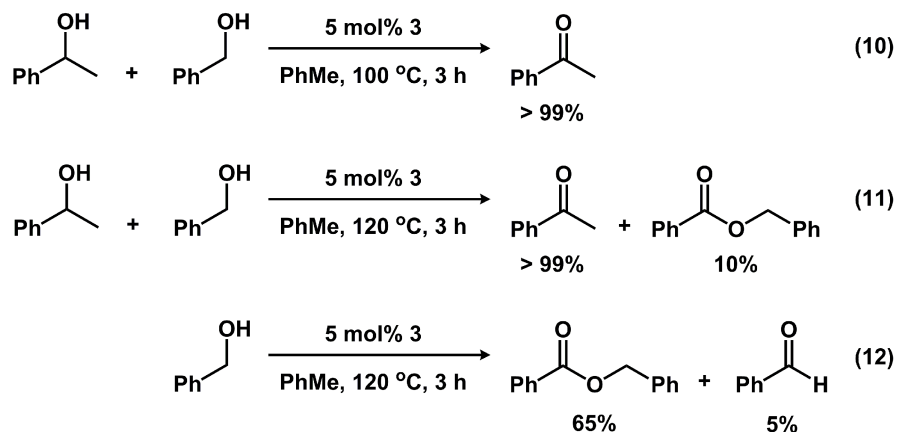


Figure 3-20 Competition experiments between BnOH and 1PhEtOH.

When a competition experiment using BnOH and 1PhEtOH was performed under identical reaction conditions, 10% benzyl benzoate and >99% acetophenone were observed (Figure 3-20, eq 11). These results demonstrate that **3** chemoselectively dehydrogenates secondary alcohols in the presence of primary alcohols under conditions which promote the dehydrogenation of both primary and secondary alcohols. The origin of this preference was considered to arise from differences in rates of either (a) proton transfer or (b) β -H elimination. In addition to implications of β -H elimination, rather than proton transfer, as the turnover-limiting step, the pK_a difference between primary ($pK_a(n\text{-PrOH}) = 16.0$) and secondary ($pK_a(i\text{-PrOH}) = 16.5$) alcohols also cannot account for the observed chemoselectivity because primary alcohols are more acidic and should be easily deprotonated.³⁷ To further support this hypothesis, *in situ* examination of the catalyst resting state by ^{31}P NMR spectroscopy revealed the quantitative formation of a primary Ru-alkoxide species ($^{31}\text{P} = 42.5$ ppm) when 0.2 mol% of **3** was dissolved in a 4.3 M BnOH C_6D_6 solution at room temperature. In a different experiment under identical conditions using 4.3 M 1PhEtOH, only 45% of **3** was converted to the secondary

Ru-alkoxide species as observed in the ^{31}P NMR spectrum. Thus, the origin of the observed chemoselectivity must occur *after* the formation of the Ru alkoxide intermediate.

To address chemoselectivity-inducing β -H elimination dependent reactions, we monitored the catalyst resting state and product(s) formation of an AAD reaction of a 1:1 mixture of BnOH (4.3 M) to 1PhEtOH (4.3 M) catalyzed by 0.2 mol% of **3**. Prior to heating the reaction to 120 °C, the ^{31}P NMR spectrum exhibited only two resonances: one for free PPh_3 and another at 42.5 ppm, which was previously identified as the primary Ru-alkoxide species ($\text{Ru}(\text{bMepi})(\text{PPh}_3)(\text{OCH}_2\text{Ph})$). Upon heating the reaction to 120 °C, a 9:1 ratio of the primary to secondary alkoxide species were observed. Continuous monitoring of the reaction showed no change in the ratio of the primary to secondary alkoxides species in the ^{31}P NMR spectrum and *only* the production of acetophenone (34 turnovers in 30 min) was observed in the ^1H NMR spectrum (Figure 3-21).

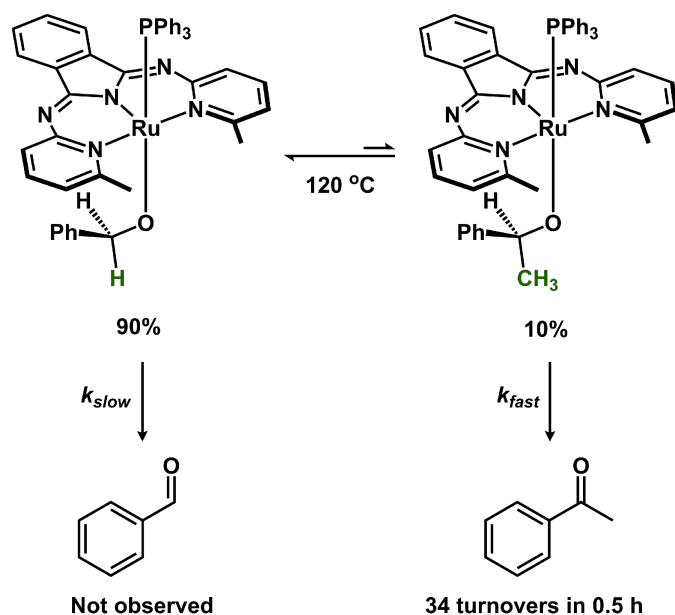


Figure 3-21 Catalyst resting state and activity for competitive experiment between BnOH and 1PhEtOH.

The competition experiments implicate slower β -H elimination from the primary alkoxide compared to the secondary alkoxide, which is consistent with the absence of BnOH dehydrogenation activity at lower (< 120 °C) temperatures, and the stronger BDE of the C–H bond cleaved.³⁸ In addition, the activation parameters at high alcohol concentration for β -H

elimination suggests that hydride transfer is dominated by entropic factors derived from hydrogen-bonding solvation effects. Hydrogen bonding with the alcohol solvent would be more favorable for the primary alkoxide species because of the decreased steric environment surrounding the oxygen atom ($-\text{OCPhH}_2$ versus $-\text{OCPhMeH}$). Therefore, a higher degree of reorganization in the transition state for β -H elimination would be anticipated for the primary alkoxide species, thus leading to a larger kinetic barrier.

3.2.13 Steric and Electronic Effects of the bMepi Ligand on Dehydrogenation Activity

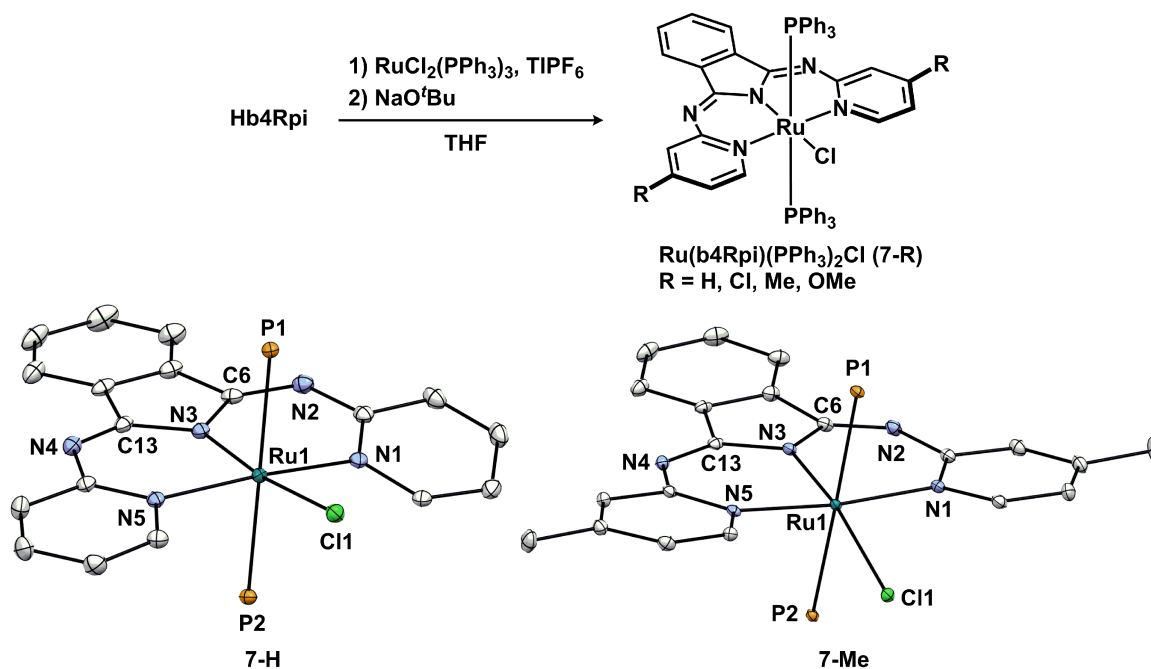


Figure 3-22 Synthesis and crystal structures (thermal ellipsoids depicted at 50% probability) of $\text{Ru}(\text{b4Rpi})(\text{PPh}_3)_2\text{Cl}$.

The requirement of the *ortho*-methyl units around the primary coordination sphere was interrogated with the ligands 1,3-bis(4',6'-methyl-2'-pyridylimino)isoindolate (b4,6-Mepi) and 1,3-bis(2'-pyridylimino)isoindolate (bpi). Complementary to evaluation of a steric effect, the effects of electronically rich and deficient ligands were also examined using para-substituted variants, b4Rpi ($\text{R} = \text{H}, \text{Cl}, \text{Me}, \text{OMe}, \text{OH}$). A series of $\text{Ru}(\text{b4Rpi})(\text{PPh}_3)_2\text{Cl}$ (7-R, $\text{R} = \text{H}, \text{Cl}, \text{Me}, \text{OMe}$) complexes were synthesized by heating a THF solution containing Hb4Rpi, $\text{RuCl}_2(\text{PPh}_3)_3$, and TIPF_6 to 60–70 °C for 16–24 h, followed by the addition of 1.05 equiv of NaO^tBu (Figure 3-22). After isolation of complexes 7-R, the composition and purity were confirmed by ^1H , ^{13}C ,

and ^{31}P NMR spectroscopy, infrared spectroscopy, and elemental analysis. The ^1H NMR spectra of **7-R** feature a single set of ligand-based resonances with the absence of the isoindole proton, and the $^{31}\text{P}\{^1\text{H}\}$ NMR spectra exhibit a singlet at 26.1, 25.1, 26.1, and 26.4 ppm (**7-R**, R = H, Cl, Me, OMe, respectively), consistent with *trans* disposed phosphorous atoms and meridional binding of the b4Rpi ligand. Single crystals of **7-H** and **7-CH₃** were subjected to X-ray diffraction experiments, and the solid-state structures confirm octahedral geometry around the Ru(II) center with a chloride ligands *trans* to the isoindolate nitrogen atom (Figure 3-22).

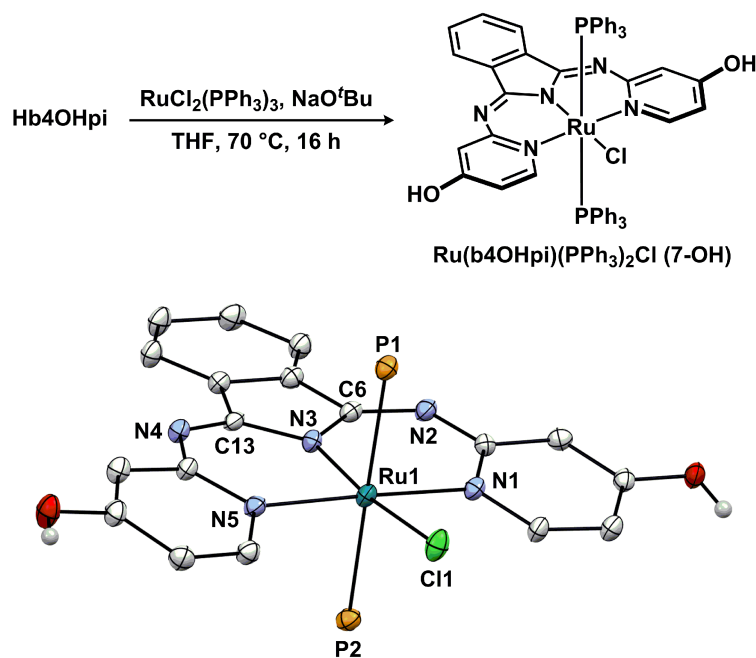


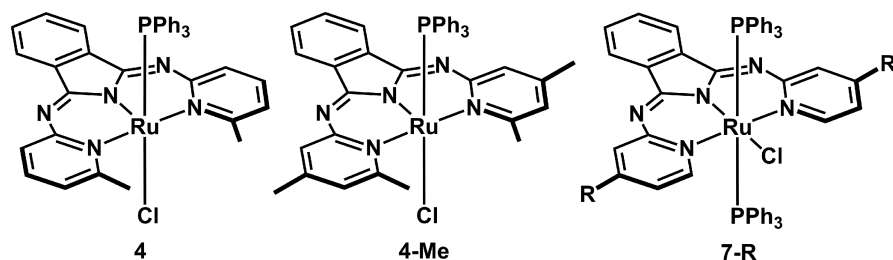
Figure 3-23 Synthesis and crystal structure (thermal ellipsoids depicted at 50% probability) of Ru(b4OHpi)(PPh₃)₂Cl.

To enhance the stability of a coordinatively unsaturated Ru species during AAD catalysis, we targeted an electron-rich metal environment by synthesizing a Ru compound with the ligand b4OHpi, in which strongly electron-donating hydroxyl groups are substituted *para* to the pyridyl nitrogens. Deprotonation of the hydroxyl groups to generate aryl-oxide groups *in situ* would further enhance the electron-richness of the metal environment. Ru(b4OHpi)(PPh₃)₂Cl (**7-OH**) was prepared by allowing a THF solution containing Hb4OHpi, RuCl₂(PPh₃)₃, and NaO^tBu to stir at 70 °C for 16 h. **7-OH** was isolated in 79% yield as a dark blue solid with only slight solubility in THF. The ^1H NMR spectrum reveals multiple broad resonances, and the $^{31}\text{P}\{^1\text{H}\}$ NMR spectrum in THF displays resonances at 68.38, 26.19, and -5.51 ppm (free PPh₃),

suggesting a dynamic process likely caused by the dissociation of one of the PPh₃ ligands in solution. This solution dissociation dynamics was suppressed with the addition of excess PPh₃. For example, in the presence of 1 equiv of PPh₃, the singlet at 68.38 ppm was absent in the ³¹P{¹H} NMR spectrum. Crystals suitable for single-crystal X-ray diffraction were obtained from vapor diffusion of pentane into a THF solution of **7-OH** at -35 °C. Analogous to the single-crystal structures for **7-H** and **7-Me**, the solid-structure reveals an octahedral geometry around the Ru(II) center with the b4OHpi ligand meridionally coordinated with two *trans* PPh₃ ligands and a chloride, thus confirming the identity of the product (Figure 3-23).

Table 3-1 Reaction Rates of 1PhEtOH Dehydrogenation

entry	catalyst	rate ($\times 10^{-5} \text{ M}\cdot\text{s}^{-1}$)
1	4	7.7(3)
2	4-Me	7.7(3)
3	7-H	10.9(2)
4	7-Me	10.9(2)
5	7-Cl	8.0(5)
6	7-OMe	11.8(2)
7	7-OH	12.0(2)
8	7-OH	13.3(2)
9	7-H	12.4(2)



In the proposed AAD mechanism shown in Figure 3-19, the steric profile of the methyl groups may play a blocking role to impede hydride transfer in the turnover-limiting step. This steric effect imposed by the methyl groups was examined by comparing the reaction rates of 1PhEtOH dehydrogenation catalyzed by **4**, **4-Me** (Ru(b4,6-Mepi)(PPh₃)Cl), **7-H**, and **7-Me** (Table 3-1). The reaction rates for **4** ($7.7(3) \times 10^{-5} \text{ M}\cdot\text{s}^{-1}$) and **4-Me** ($7.7(3) \times 10^{-5} \text{ M}\cdot\text{s}^{-1}$) were identical (Table 3-1, entries 1 and 2), which suggests that the weakly electron-donating methyl

groups have no electronic effect on the dehydrogenation activity. This observation allowed evaluation of the steric influence of the *ortho*-methyl substituents of the bMepi ligand by comparing the reaction rates of **4** and **7-H**. The reaction rate was increased by 42% when **7-H** ($10.9(2) \times 10^{-5} \text{ M}\cdot\text{s}^{-1}$, Table 3-1, entry 3) or **7-Me** ($10.9(2) \times 10^{-5} \text{ M}\cdot\text{s}^{-1}$, Table 3-1, entry 4) was used instead of **4**. The rate enhancement is consistent with a sterically blocking effect of the methyl groups, which hinders β -H elimination in the turnover-limiting step (Figure 3-19).

While the addition of a modestly donating methyl group in the *para*-position had no effect on the overall rate, we evaluated the effect of adding highly donating substituents to the flanking pyridine rings. Increased electron donor strength of the ligand is expected to concomitantly enhance the hydricity of any metal-based hydrides.³⁹ However, because the turnover-limiting step is β -H elimination, the ligand electronic effect on the turnover-limiting step may be less than dramatic.

The electronic variations at the Ru center imposed by electronically rich and deficient bpi ligands were evaluated by examining the dehydrogenation rates of 1PhEtOH. The reaction rate was increased when **7-OMe** ($11.8(2) \times 10^{-5} \text{ M}\cdot\text{s}^{-1}$; $\sigma_{\text{para}}(\text{OMe}) = -0.27$;⁴⁰ Table 3-1, entry 6) and **7-OH** ($12.0(2) \times 10^{-5} \text{ M}\cdot\text{s}^{-1}$; $\sigma_{\text{para}}(\text{OH}) = -0.37$;⁴⁰ Table 3-1, entry 7) were used instead of **7-Cl** ($8.0(5) \times 10^{-5} \text{ M}\cdot\text{s}^{-1}$; $\sigma_{\text{para}}(\text{Cl}) = 0.23$;⁴⁰ Table 3-1, entry 5). To further enhance the donor strength, the aryl-oxide (**7-O⁻**; $\sigma_{\text{para}}(\text{O}^-) = -0.81$)⁴⁰ was prepared. **7-OH** was allowed to react with 5 equiv of NaO^tBu, which resulted in a further 11% increase in rate ($13.3(2) \times 10^{-5} \text{ M}\cdot\text{s}^{-1}$, Table 3-1, entry 8) of 1PhEtOH dehydrogenation. Although, these results indicate that a more electron-rich Ru environment exhibits higher AAD activity, the changes to the reaction rate are small; thus, the electronic environment at the Ru center has a minimal effect on the turnover-limiting step in the AAD catalytic cycle.

3.2.14 Base-Promoted Acceptorless Alcohol Dehydrogenation Catalysis

Benchtop-stable reagents provide greater synthetic utility and accessibility and thus are more commonly and easily handled by most synthetic laboratories. The air-sensitive precatalyst **3** is capable of mediating promoterless AAD reactions, likely due in part to the Ru-H, an internal basic site. Alternatively, entry into the AAD catalytic cycle should also be possible using the air-stable complex **4** in the presence of an external base or using an *in situ* preparation of the Ru-

bMepi catalytic species. Indeed, when a toluene solution containing 0.5 mmol of 1PhEtOH, 1 mol% of **4**, and 2 mol% of NaO^tBu was heated to reflux for 4 h, acetophenone was observed in quantitative (>99%) yield (Figure 3-24, eq 13). This reactivity demonstrates the synthetic applicability of **4** as a dehydrogenation catalyst that can be prepared using air-stable reagents. Furthermore, AAD catalysis by *in situ* formation of the catalytically active Ru–bMepi species was evaluated. In the presence of 1 mol% RuCl₂(PPh₃)₃, 1 mol% HbMepi, and 3 mol% NaO^tBu, 1PhEtOH was converted to acetophenone in >99% yield after heating for 4 h in refluxing toluene (Figure 3-24, eq 14). Control experiments showed no reaction in the absence of HbMepi. Therefore, the broad applicability of our system to promote dehydrogenation by well-defined precatalysts as well as *in situ* generation from air-stable precursors highlights the robustness of the system.

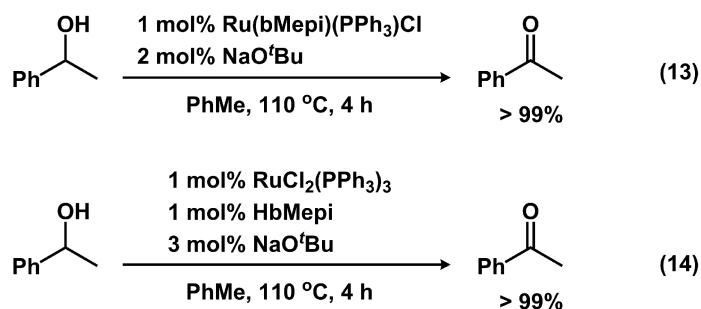


Figure 3-24 Base-promoted AAD catalysis.

In addition to the alcohol dehydrogenation activity of the *in situ* prepared catalyst, stoichiometric reactions were performed to uncover intermediates en route to the well-defined precatalyst **4**. Allowing HbMepi and RuCl₂(PPh₃)₃ to react in dichloroethane at 70 °C for 4 h generated Ru(HbMepi)(PPh₃)₂Cl₂ (**8**) in 70% yield as a green solid (Figure 3-25). The ³¹P{¹H} spectrum displays a singlet at 24.9 ppm, and the ¹H NMR spectrum reveals a solution structure consistent with asymmetric binding of the HbMepi ligand. For example, two resonances for the *ortho*-CH₃ substituents were observed at 0.99 and 2.31 ppm, and nine distinct resonances were observed for the HbMepi scaffold in the aromatic region of the ¹H NMR spectrum. Crystals suitable for a single X-ray diffraction experiment were obtained from slow evaporation of a DCM solution of **8** at 5 °C. The solid-state structure exposes an octahedral geometry around the Ru(II) center, supported by a κ²-HbMepi, two PPh₃ and two chloride ligands. Addition of 1.05

equiv of NaO^tBu to a THF solution containing **8** cleanly afforded complex **4**, which is a benchtop-stable precatalyst in the base-promoted AAD reaction.

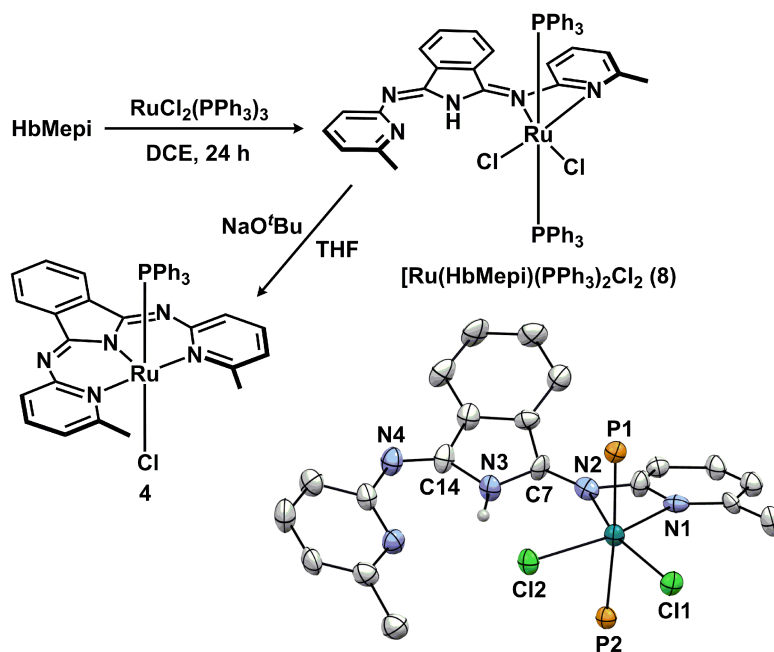


Figure 3-25 Synthesis and crystal structure (thermal ellipsoids depicted at 50% probability) of Ru(HbMepi)(PPh₃)₂Cl₂.

3.2.15 Isolation of an Alternative Promoterless Alcohol Dehydrogenation Catalyst

In (de)hydrogenation catalysis, active Ru complexes are often generated using exogenous base additives.⁴¹ We previously showed that **4** was activated in the presence of NaO^tBu to provide an active dehydrogenation catalyst; however, the mechanism of activation was unclear. Stoichiometric reactions between **4** and base were performed to examine the reaction pathway. Under basic conditions, deprotonation of the *ortho*-methyl group was achieved by ⁻O^tBu base, and the deprotonated intermediate was subsequently trapped by coordination with another Ru complex to afford a dimer (**9**), which was isolated in 78% yield (Figure 3-26). Crystals suitable for single-crystal X-ray diffraction were obtained from vapor diffusion of pentane into a benzene solution of **9**, and the solid-state structure reveals a square-based pyramidal geometry about the Ru center ($\tau = 0.02, 0.03$)²² with the pincer ligand meridionally coordinated and the pyridinylmethanide motif coordinated to another Ru(II) center (Figure 3-26). The asymmetry of the pincer ligand is confirmed in solution by >10 distinct resonances in the aromatic region of the ¹H NMR spectrum.

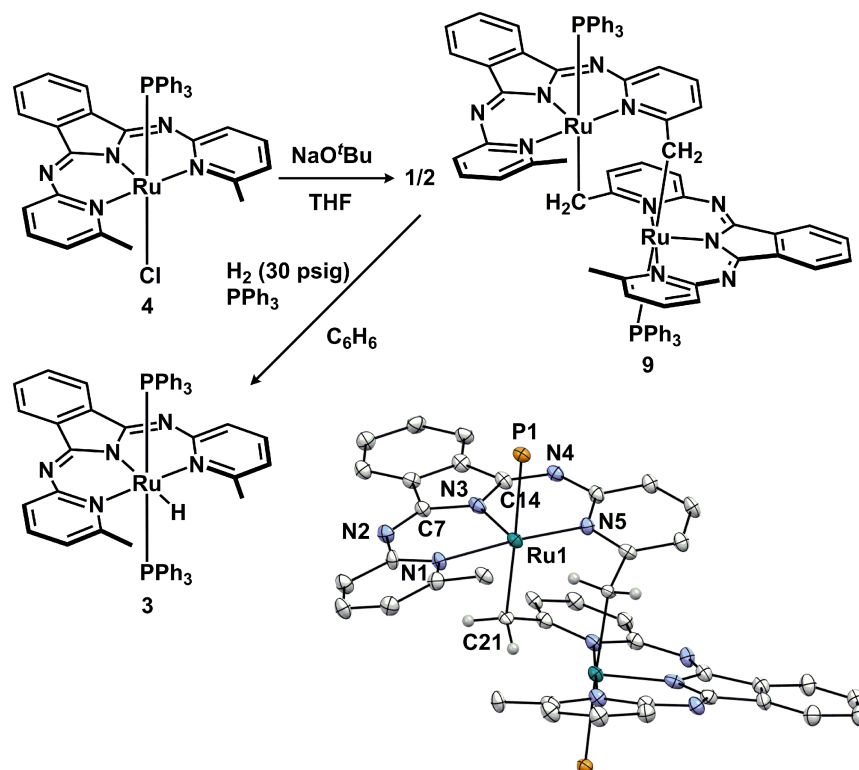


Figure 3-26 Synthesis and crystal structure (thermal ellipsoids depicted at 50% probability) of $[\text{Ru}(\text{CH}_2\text{Mepi})(\text{PPh}_3)]_2$.

To investigate complex **9** as a precursor en route to the catalytically-active $\text{HRu}(\text{bMepi})(\text{PPh}_3)$ species, a reaction with H_2 was examined. H_2 was heterolytically cleaved by the pyridinylmethanide group and the Ru center at low pressure (30 psig) and reacted with another PPh_3 molecule to afford **3** (Figure 3-26). This demonstrates that complex **9** is a precursor to the $\text{HRu}(\text{bMepi})(\text{PPh}_3)$ species and that the methanide motif is an internal basic site that may promote dehydrogenation reactions without requiring any additives. To illustrate the latter point, refluxing a 0.25 M 1PhEtOH toluene solution containing 0.5 mol% **9** for 4 h resulted in quantitative conversion (>99%) of 1PhEtOH to acetophenone (Figure 3-27). Hence, complex **9** is a precursor to generate a catalytically-active $\text{HRu}(\text{bMepi})(\text{PPh}_3)$ species that operates *via* the AAD catalytic cycle proposed in Figure 3-19

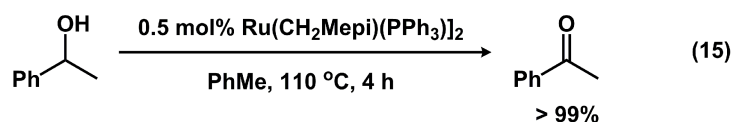


Figure 3-27 $[\text{Ru}(\text{CH}_2\text{Mepi})(\text{PPh}_3)]_2$ promoted AAD catalysis.

3.2.16 Reversible Catalytic Hydrogenation–Dehydrogenation Reactions

Catalytic hydrogenation and dehydrogenations reactions are attractive candidates to target for reversible energy storage.^{2,42} Although a myriad of catalysts can mediate the forward *or* reverse reaction, very few systems are capable of catalyzing reversible hydrogenation–dehydrogenation reactions.^{2a,7,43} The ability of **3** to effect a catalytic transfer hydrogenation reaction using *i*PrOH as the H₂ surrogate was previously demonstrated.⁸ Thus, we hypothesized that the hydrogenation reactions should be possible using H₂ given that entry to **3** was also gained by treating the Ru-alkoxide (**6**) with H₂. Indeed, acetophenone was completely consumed to afford 1PhEtOH within 1 h at 110 °C using 1 mol% **3** and 30 psig H₂ in PhMe-*d*₈ inside a J. Young NMR tube. Following the hydrogenation reaction, the solution was transferred from the J. Young NMR tube to a Schlenk flask to assess the ability to promote the dehydrogenation of 1PhEtOH. Refluxing the toluene solution under an inert atmosphere for 4 h restored acetophenone quantitatively (Figure 3-28). This demonstrates the complete and reversible transformations between acetophenone and 1PhEtOH *via* successive hydrogenation–dehydrogenation reactions using complex **3** as the *single* catalyst.

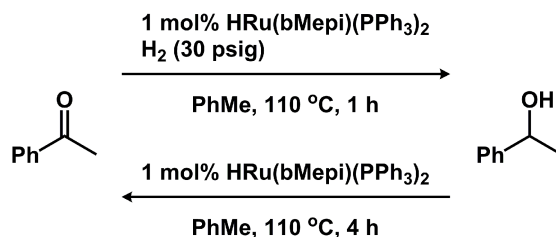


Figure 3-28 Reversible hydrogenation–dehydrogenation reactions catalyzed by HRu(bMepi)(PPh₃)₂.

3.2.17 Summary

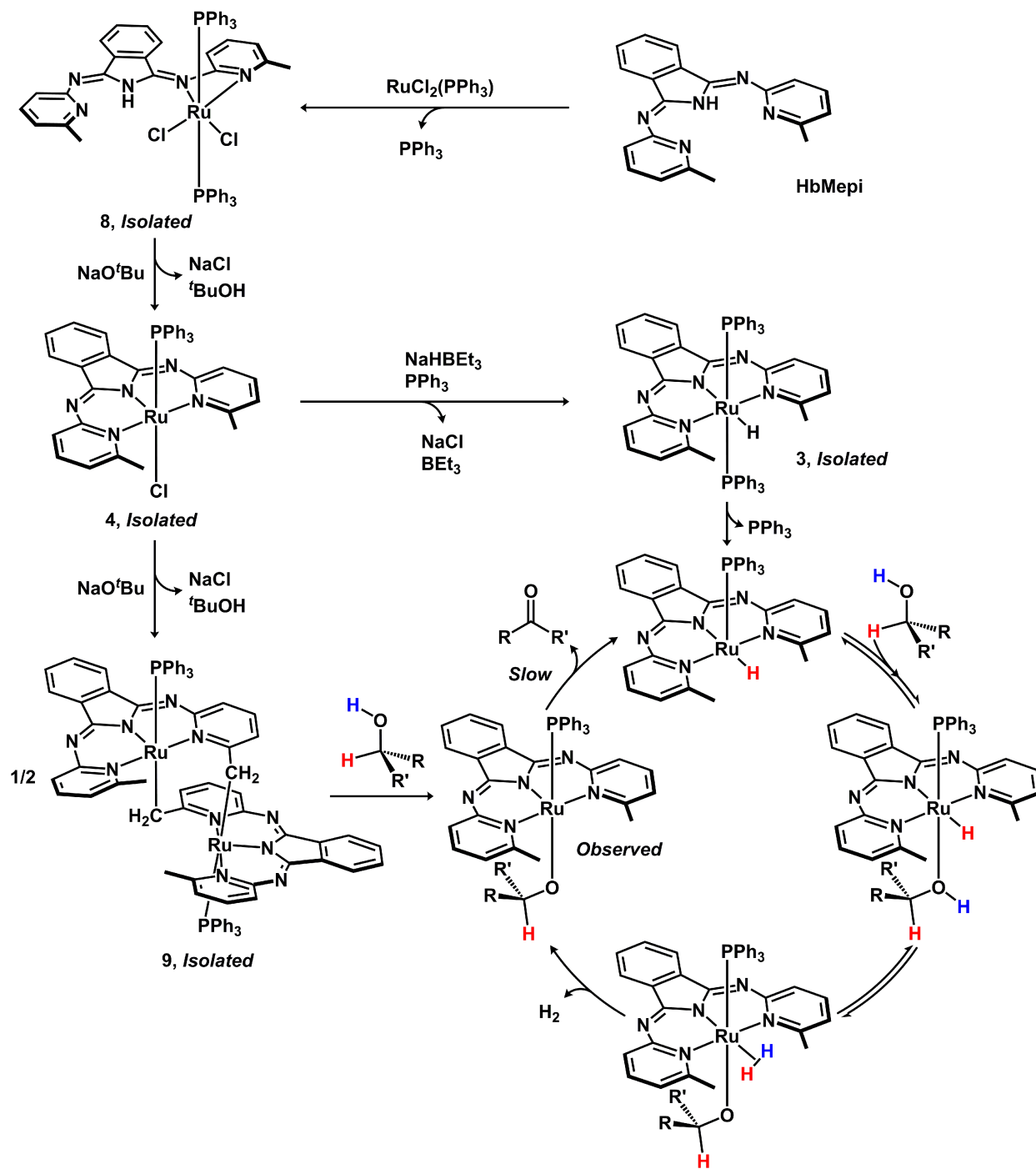


Figure 3-29 Proposed cycle for catalytic acceptorless alcohol dehydrogenation and isolation of precursors.

The mechanism of the AAD reaction catalyzed by complex **3** was studied by a series of kinetic and isotopic labeling experiments, isolation of intermediates, and catalyst modifications.

Experimental evidence supported an inner-sphere, stepwise pathway for proton and hydride transfers with a β -H elimination turnover-limiting step. Selective isotopic labeling experiments combined with catalyst modification (methylation of the pincer ligand backbone) demonstrated that a cooperative metal–ligand pathway involving the imine functionality is not necessary for efficient dehydrogenation. The activation parameters suggested an associative pathway involving a highly ordered transition-state structure. Thus, we propose that a single PPh₃ dissociation event from **3** generates a coordinatively unsaturated HRu(bMepi)(PPh₃) species, which undergoes a proton-transfer equilibrium to generate a transient Ru-H₂ alkoxide species. H₂ loss affords a Ru-alkoxide intermediate that can participate in a turnover-limiting β -H elimination reaction to complete the catalytic cycle (Figure 3-29). Moreover, modifications to the pincer ligand revealed that the steric profiles of the methyl groups on bMepi slightly impeded catalytic activity, while electronic modifications of the pincer ligand have a minimal effect on the rate of catalytic dehydrogenation.

In addition to delineating a detailed mechanistic understanding of dehydrogenative catalysis mediated by **3**, we also showed **3** as an efficient hydrogenation precatalyst. By coupling the hydrogenation and the dehydrogenation abilities of **3**, we have thus demonstrated that completely reversible transformations between ketones and alcohols are achieved and are dictated by hydrogen input or release. Overall, such reversible catalytic reactions are of broad interest to the field of hydrogen storage as well as chemical synthesis.

3.3 Experimental Section

3.3.1 General Considerations

All manipulations were conducted under a nitrogen atmosphere on a Schlenk manifold or in a glovebox using standard Schlenk techniques, unless otherwise stated. All reagents were purchased from commercial vendors. Anhydrous dichloroethane (DCE, Acros), NaO^tBu (Sigma-Aldrich), and MeOTf (Sigma-Aldrich) were used without further purification. 1-Phenylethanol, phenyltrimethylsilane, acetophenone, 1-(4-methylphenyl)ethanol, 1-(4-methoxyphenyl)ethanol, 1-(4-fluorophenyl)ethanol, 1PhEtOD, 1PhCH₃CDOH, 1PhCH₃CDOD, and 2,2,2-trifluoroethanol were distilled from CaH₂ under a nitrogen atmosphere, and then stored over 3Å molecular sieves for at least 24 h. The following compounds were synthesized according to literature methods:

HRu(bMepi)(PPh₃)₂ (**3**),⁸ Ru(bMepi)(PPh₃)Cl (**4**),⁸ 1PhEtOH isotopologues,¹⁹ and the Hb4Rpi ligands.⁴⁴ The 3Å Molecular sieves were dried at 250 °C under dynamic vacuum for 24 h. Dichloromethane (DCM), diethyl ether (Et₂O), pentane, benzene (C₆H₆), dimethoxyethane (DME), and tetrahydrofuran (THF) were purified using a Glass Contour solvent purification system consisting of a copper catalyst, neutral alumina, and activated molecular sieves, then passed through an in-line, 2 μm filter immediately before being dispensed. Toluene (PhMe) and hexanes (Hex) were sparged using nitrogen and then stored over 3Å molecular sieves for at least 24 h.

NMR spectra were recorded on Varian Inova 500, Varian MR400, Varian vnmrs 500, and Varian vnmrs 700 spectrometers at room temperature. ¹H and ¹³C shifts are reported in parts per million (ppm) relative to TMS, with the residual solvent peak used as an internal reference. ³¹P and ¹⁹F NMR spectra were referenced on a unified scale to their respective ¹H NMR spectra. At elevated temperatures, ³¹P spectra were referenced relative to an internal standard of PPh₃ at -5.6 ppm. The following abbreviations are reported as follows: broad (br), singlet (s), doublet (d), doublet of doublets (dd), triplet (t), quartet (q), multiplet (m), methyl (Me), methoxy (OMe), and triphenylphosphine (PPh₃). ¹³C NMR resonances were observed as singlets unless otherwise stated. For atom numbering of the bpi ligand in complexes **4–7**, see Figure 3-30.

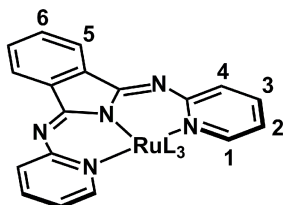


Figure 3-30 Atom numbering of the bpi ligand for NMR characterizations.

Solid-state IR spectra were collected using a Nicolet iS10 spectrometer equipped with a diamond attenuated total reflectance (ATR) accessory. Elemental analyses were performed by Midwest Microlab, LLC.

3.3.2 General Procedure for 1PhEtOH Dehydrogenation Catalyzed by HRu(bMepi)(PPh₃)₂

1PhEtOH (5 mL, 41.4 mmol) was added to a 20 mL vial charged with **3** (3.9 mg, 0.00409 mmol), PhTMS (0.5 mL, 2.9 mmol), and a stir bar. The vial was capped with a septum and

pierced with a 27-gauge needle. Then the vial was heated to the desired temperature (90, 100, 110, 120, or 130 °C) using an aluminum heating block inside an inert-atmosphere glovebox. The formation of acetophenone was monitored by sampling 0.5 mL aliquots and then analyzed by ¹H NMR spectroscopy against PhTMS as an internal standard. To confirm reproducibility, all kinetic experiments were performed in triplicate.

3.3.3 General Procedure for Base-Promoted 1PhEtOH Dehydrogenation

PhMe (2 mL) was added to a 10 mL Schlenk flask charged with [Ru] (0.005 mmol; **4**, 3.6 mg; **5**, 5.0 mg; RuCl₂(PPh₃)₃, 4.8 mg; and HbMepi, 1.6 mg), NaO^tBu (2 mol%, 0.01 mmol, 1.0 mg; 3 mol%, 0.015 mmol, 1.4 mg), and a stir bar. 1PhEtOH (60 μL, 0.5 mmol) was added to the mixture. A reflux condenser was connected to the Schlenk flask, capped with a septum, and pierced with a 27-gauge needle in addition to a nitrogen inlet 16-gauge needle. The reaction solution was heated to 120 °C using an aluminum heating block. After 4 h, the reaction mixture was cooled to room temperature and exposed to air to quench the reaction. The solvent was evaporated under vacuum, and the residue was purified through a plug of silica gel eluting with Et₂O (5 mL). Evaporation of the Et₂O solution afforded acetophenone as a colorless oil. The purity and identity were confirmed by comparison to previously reported NMR data.

3.3.4 Preparation and Characterization of Ruthenium HbMepi, bMepi, bpi, b4Rpi, and bMepi^{Me} Complexes.

Ru(HbMepi)(PPh₃)Cl[PF₆]. THF (3 mL) was added to a vial charged with HbMepi (51.6 mg, 0.158 mmol), RuCl₂(PPh₃)₃ (137.4 mg, 0.143 mmol), TlPF₆ (50.1 mg, 0.143 mmol), and a stir bar. The reaction solution was allowed to stir at 70 °C for 2 days. After the solution cooled to room temperature, TlCl was filtered using a fine frit and the THF solvent was removed under vacuum. The crude product was washed with C₆H₆ (4 × 10 mL) and Et₂O (4 × 10 mL). The crude product was dissolved in minimum DCM and layered with Et₂O. After 24 h at room temperature, the precipitates were collected and washed with Et₂O (4 × 10 mL). Evaporation of the volatiles under vacuum afforded the product as a dark blue solid. Crystals were obtained from vapor diffusion of Et₂O into a DCM solution at room temperature. Yield: 94 mg (75%). ¹H NMR (700 MHz, CD₂Cl₂): δ 10.85 (s, 1H, NH), 8.17 (t, *J*_{HH} = 7.0 Hz, 1H), 7.94 (d, *J*_{HH} = 7.7 Hz, 1H), 7.69 (d, *J*_{HH} = 5.6 Hz, 1H) 7.62 (br s, 1H), 7.51 (br s, 1H), 7.45-7.44 (m, 2H), 7.34 (d, *J*_{HH} =

7.0 Hz, 1H), 7.27 (br s, 1H), 7.17 (t, $J_{\text{HH}} = 7.0$ Hz, 3H, PPh₃), 6.92 (t, $J_{\text{HH}} = 7.0$ Hz, 6H, PPh₃), 6.52 (t, $J_{\text{HH}} = 9.1$ Hz, 6H, PPh₃), 1.78 (s, 3H, Me), 1.70 (s, 3H, Me). ¹³C{¹H} (176 MHz, CD₂Cl₂): δ 160.99, 160.90, 156.363, 153.37, 147.34, 146.49, 139.11, 138.98, 138.57, 132.71, 132.58, 132.53, 131.93, 131.04, 130.86, 129.65, 129.13, 129.08, 124.43, 123.46, 122.55, 121.30, 115.64, 23.56, 22.76. ³¹P{¹H} NMR (162 MHz, CD₂Cl₂): δ 39.17 (s, PPh₃), -144.30 (septet, $J_{\text{PF}} = 710$ Hz, PF₆). ¹⁹F NMR (376 MHz, CD₂Cl₂): δ -72.77 (d, $J_{\text{FP}} = 710$ Hz, PF₆). IR (ATR, cm⁻¹): 3331, 3059, 1631, 1600, 1552, 1532, 1463, 1449, 1433, 1372, 1292, 1210, 1163, 1104, 1088, 998, 833, 795, 740, 692. Anal. Calculated (found): C, 52.39 (52.51); H, 3.70 (3.80); N, 8.04 (7.85).

Preparation of Ru(bMepi)(PPh₃)Cl from Ru(HbMepi)(PPh₃)Cl[PF₆]. THF (5 mL) was added to a 20 mL vial charged with Ru(HbMepi)(PPh₃)Cl[PF₆] (10 mg, 0.0115 mmol), NaO^tBu (1.1 mg, 0.0115 mmol), and a stir bar. The reaction solution was allowed to stir at room temperature for 30 min. Solvent was removed under vacuum and the crude product was extracted with DCM (10 mL). The DCM solvent was removed under vacuum and the product was washed with Et₂O (4 × 10 mL). Evaporation of the volatiles under vacuum afforded the product as a dark purple powder. The purity and identity were confirmed by comparison to previously reported NMR data. Yield: 7.5 mg (90%).

Ru(b4,6-Mepi)(PPh₃)Cl. THF (10 mL) was added to a 20 mL vial charged with Kb4,6-Mepi (103.7 mg, 0.264 mmol), RuCl₂(PPh₃)₃ (240.6 mg, 0.251 mmol), and a stir bar. The resulting solution was stirred at room temperature for 17 h. Solvent was removed under vacuum. The crude product was washed with Et₂O (4 × 5 mL) and extracted with DCM (4 × 5 mL). The DCM solvent was removed under vacuum, and the product was washed with pentane (4 × 10 mL), affording the product as a dark blue powder. The product was recrystallized from layering pentane on top of a DCM solution at -35 °C. Yield: 126 mg (68%). ¹H NMR (400 MHz, C₆D₆): δ 7.98 (dd, $J_{\text{HH}} = 5.6, 3.2$ Hz, 2H, H⁵), 7.51 (s, 2H, H⁴), 7.05 (dd, $J_{\text{HH}} = 5.2, 2.8$ Hz, 2H, H⁶), 6.86 (t, $J_{\text{HH}} = 8.4$ Hz, 6H, PPh₃), 6.77 (t, $J_{\text{HH}} = 7.2$ Hz, 3H, PPh₃), 6.67 (t, $J_{\text{HH}} = 6.8$ Hz, 6H, PPh₃), 6.24 (s, 2H, H²), 1.98 (s, 6H, *p*-Me), 1.78 (s, 6H, *o*-Me). ¹³C{¹H} (176 MHz, CD₂Cl₂): δ 158.69, 154.87, 153.30, 147.36, 141.48, 134.26, 134.03, 133.01, 129.53, 128.92, 128.20, 125.82, 121.44, 119.96. ³¹P{¹H} NMR (162 MHz, C₆D₆): δ 45.34 (s, PPh₃). IR (ATR, cm⁻¹): 3052, 1622, 1566, 1498, 1447, 1430, 1372, 1327, 1289, 1251, 1229, 1204, 1182, 1109, 1087, 1030, 1001, 969, 900,

843, 773, 745, 726, 694. Anal. Calculated (found): C, 63.78 (63.59); H, 4.68 (4.48); N, 9.30 (9.17).

Ru(bMepi^{Me})(PPh₃)(OTf)₂. MeOTf (150 μ L, 1.39 mmol) was added to a 20 mL vial containing DCM solution of Ru(bMepi)(PPh₃)Cl (101 mg, 0.139 mmol) and a stir bar. The reaction solution was allowed to stir at room temperature for 16 h. The DCM solvent was removed under vacuum, and the crude product was washed with Et₂O (4 \times 10 mL). The crude product was dissolved in minimum DCM and layered with Et₂O. After 24 h at room temperature, the precipitates were collected and washed with Et₂O (4 \times 10 mL). Evaporation of the volatiles under vacuum afforded the product as a dark purple crystalline solid. Crystals were obtained from vapor diffusion of pentane into a DCM/C₆H₆ solution at room temperature. Yield: 111 mg (79%). ¹H NMR (500 MHz, CD₂Cl₂): δ 8.30-8.27 (m, 2H), 8.13 (t, $J_{\text{HH}} = 7.5$ Hz, 1H), 7.95 (d, $J_{\text{HH}} = 8.0$ Hz, 1H), 7.83-7.80 (m, 2H), 7.72-7.65 (m, 2H), 7.39-7.35 (m, 5H), 7.14 (t, $J_{\text{HH}} = 8.0$ Hz, 6H, PPh₃), 6.81 (t, $J_{\text{HH}} = 10.5$ Hz, 6H, PPh₃), 3.73 (s, 3H, N-Me), 1.78 (s, 3H, Me), 1.57 (s, 3H, Me). ¹³C{¹H} (176 MHz, CD₂Cl₂): δ 165.67, 160.83, 160.25, 153.97, 152.62, 148.97, 141.13, 140.89, 139.70, 134.86, 132.81, 132.76, 132.39, 131.55, 131.05, 130.77, 129.55, 129.49, 124.94, 124.59, 124.44, 123.76, 116.42, 44.46, 22.97, 21.76. ³¹P{¹H} NMR (202 MHz, CD₂Cl₂): δ 47.84 (s, PPh₃). IR (ATR, cm⁻¹): 3062, 1609, 1565, 1519, 1459, 1435, 1400, 1308, 1266, 1230, 1206, 1187, 1156, 1117, 1090, 1015, 909, 811, 797, 779, 742, 696. Anal. Calculated (found): C, 49.10 (48.97); H, 3.42 (3.51); N, 6.98 (6.88).

Ru(bMepi)(PPh₃)(OCH₂CF₃). CF₃CH₂OH (4.3 μ L, 0.0563 mmol) was added to a 20 mL vial containing THF solution of HRu(bMepi)(PPh₃)₂ (48.8 mg, 0.051 mmol) and a stir bar. The reaction solution was allowed to stir at 70 $^{\circ}$ C for 2 days. After the solution cooled to room temperature, the THF solvent was removed under vacuum and the crude product was washed with Et₂O (4 \times 10 mL) and pentane (4 \times 10 mL). The product was extracted with C₆H₆ (15 mL). The C₆H₆ solution was lyophilized, affording the product as a purple powder. Crystals were obtained from vapor diffusion of pentane into a PhMe solution at 5 $^{\circ}$ C. Yield: 22 mg (55%). ¹H NMR (700 MHz, C₆D₆): δ 8.09 (dd, $J_{\text{HH}} = 5.6, 3.5$ Hz, 2H, H⁵), 7.69 (d, $J_{\text{HH}} = 7.7$ Hz, 2H, H⁴), 7.19 (t, $J_{\text{HH}} = 7.7$ Hz, 2H, H³), 7.06 (dd, $J_{\text{HH}} = 5.6, 2.8$ Hz, 2H, H⁶), 6.77-6.72 (m, 9H, PPh₃), 6.65 (t, $J_{\text{HH}} = 7.0$ Hz, 6H), 6.35 (d, $J_{\text{HH}} = 7.0$ Hz, 2H, H²), 3.28 (q, $J_{\text{HF}} = 7.7, J_{\text{HH}} = 2.1$ Hz, 2H, OCH₂CF₃), 1.75 (s, 6H, Me). ¹³C{¹H} (176 MHz, C₆D₆): δ 159.69, 155.41, 152.68, 142.22,

136.03, 135.83, 134.59, 132.92, 132.86, 125.59, 120.31, 118.69, 67.59, 23.48. $^{31}\text{P}\{^1\text{H}\}$ NMR (283 MHz, PhMe- d_8): δ 43.88 (s, PPh_3). $^{19}\text{F}\{^1\text{H}\}$ NMR (376 MHz, PhMe- d_8) δ -76.52 (s, OCH_2CF_3). IR (ATR, cm^{-1}): 3041, 2814, 2714, 1568, 1538, 1512, 1460, 1433, 1388, 1264, 1184, 1153, 1121, 1107, 1009, 949, 905, 794, 769, 742, 693. Anal. Calculated (found): C, 60.91 (60.88); H, 4.22 (4.29); N, 8.88 (8.63).

Ru(bpi)(PPh₃)₂Cl. THF (15 mL) was added to a 20 mL vial charged with Hbpi (319.4 mg, 1.07 mmol), $\text{RuCl}_2(\text{PPh}_3)_3$ (974.4 mg, 1.02 mmol), TIPF_6 (355 mg, 1.02 mmol), and a stir bar. The reaction solution was allowed to stir at 70 °C for 21 h. After the solution cooled to room temperature, TiCl_4 was filtered using a fine frit and the THF solvent was removed under vacuum. The crude product was washed with Et_2O (4×20 mL), affording $\text{Ru}(\text{Hbpi})(\text{PPh}_3)_2\text{Cl}[\text{PF}_6]$ in 83% yield (932 mg). THF (15 mL) was added to a 20 mL vial charged with $\text{Ru}(\text{Hbpi})(\text{PPh}_3)_2\text{Cl}[\text{PF}_6]$ (925.5 mg, 0.837 mmol), NaO^tBu (84.5 mg, 0.879 mmol), and a stir bar. The reaction solution was allowed to stir at room temperature for 30 min. The THF solvent was removed under vacuum, and the crude product was extracted with C_6H_6 (50 mL). The C_6H_6 solution was lyophilized, and the product was washed with pentane (4×20 mL). Evaporation of the volatiles under vacuum afforded the product as a green powder. Crystals were obtained from slow evaporation of a DCM solution at room temperature (DCM/Hex). Yield: 562 mg (70%). ^1H NMR (400 MHz, C_6D_6): δ 10.60 (d, $J_{\text{HH}} = 6.4$ Hz, 2H, H^1), 7.95 (dd, $J_{\text{HH}} = 4.8, 2.4$ Hz, 2H, H^5), 7.37-7.33 (m, 14H), 6.88 (t, $J_{\text{HH}} = 8.4$ Hz, 2H, H^3), 6.81-6.71 (m, 18H), 6.00 (t, $J_{\text{HH}} = 8.8$ Hz, 2H, H^2). $^{13}\text{C}\{^1\text{H}\}$ (176 MHz, CD_2Cl_2): δ 158.47, 157.43, 152.63, 141.83, 134.43, 133.89, 132.69 (t, $J_{\text{CP}} = 17.2$ Hz, *ipso*-CP), 128.86, 128.56, 127.59, 127.21, 119.93, 116.59. $^{31}\text{P}\{^1\text{H}\}$ NMR (162 MHz, C_6D_6): δ 26.09 (s, PPh_3). IR (ATR, cm^{-1}): 3053, 1568, 1552, 1513, 1454, 1434, 1378, 1305, 1290, 1210, 1186, 1105, 1087, 1007, 909, 843, 770, 744, 696. Anal. Calculated (found): C, 67.60 (67.25); H, 4.41 (4.40); N, 7.30 (7.20).

Ru(b4Mepi)(PPh₃)₂Cl. THF (10 mL) was added to a 20 mL vial charged with Hb4Mepi (103.7 mg, 0.317 mmol), $\text{RuCl}_2(\text{PPh}_3)_3$ (303.7 mg, 0.317 mmol), TIPF_6 (110.7 mg, 0.317 mmol), and a stir bar. The reaction solution was allowed to stir at 60 °C for 24 h. After the solution cooled to room temperature, TiCl_4 was filtered using a fine frit and the THF solvent was removed under vacuum. The crude product was washed with Et_2O (4×10 mL), affording $\text{Ru}(\text{Hb4Mepi})(\text{PPh}_3)_2\text{Cl}[\text{PF}_6]$ in 87% yield (312 mg). THF (15 mL) was added to a 20 mL vial

charged with Ru(Hb4Mepi)(PPh₃)₂Cl[PF₆] (122 mg, 0.108 mmol), NaO^tBu (10.9 mg, 0.113 mmol), and a stir bar. The reaction solution was allowed to stir at room temperature for 30 min. The THF solvent was removed under vacuum, and the crude product was extracted with C₆H₆. The C₆H₆ solution was lyophilized, and the product was washed with pentane (4 × 10 mL). Evaporation of the volatiles under vacuum afforded the product as a green powder. Crystals were obtained from layering pentane on top of a DCM solution at -35 °C. Yield: 90 mg (85%). ¹H NMR (400 MHz, C₆D₆): δ 10.44 (d, *J*_{HH} = 6.4 Hz, 2H, H¹), 7.98 (dd, *J*_{HH} = 5.2, 2.8 Hz, 2H, H⁵), 7.44-7.39 (m, 12H, PPh₃), 7.26 (s, 2H, H⁴), 6.81-6.73 (m, 18H, PPh₃), 5.92 (d, *J*_{HH} = 6.8 Hz, 2H, H²), 1.76 (s, 6H, Me). ¹³C{¹H} (176 MHz, CD₂Cl₂): δ 157.44, 156.94, 152.95, 145.93, 141.85, 133.96, 133.08 (t, *J*_{CP} = 17.0 Hz, *ipso*-CP), 128.72, 128.45, 127.49, 119.75, 118.50. ³¹P{¹H} NMR (162 MHz, C₆D₆): δ 26.14 (s, PPh₃). IR (ATR, cm⁻¹): 3053, 1552, 1501, 1481, 1462, 1431, 1403, 1375, 1293, 1189, 1102, 1088, 1007, 941, 840, 817, 746, 693. Anal. Calculated (found): C, 68.11 (68.38); H, 4.70 (4.79); N, 7.09 (6.99).

Ru(b4Clpi)(PPh₃)₂Cl. THF (10 mL) was added to a 20 mL vial charged with Hb4Clpi (88 mg, 0.239 mmol), RuCl₂(PPh₃)₃ (218.2 mg, 0.228 mmol), TlPF₆ (79.5 mg, 0.228 mmol), and a stir bar. The reaction solution was allowed to stir at 60 °C for 18 h. After the solution cooled to room temperature, TlCl was filtered using a fine frit and the THF solvent was removed under vacuum. The crude product was washed with Et₂O (4 × 10 mL), affording Ru(Hb4Clpi)(PPh₃)₂Cl[PF₆] in 91% yield (242 mg). THF (10 mL) was added to a 20 mL vial charged with Ru(Hb4Clpi)(PPh₃)₂Cl[PF₆] (242 mg, 0.206 mmol), NaO^tBu (20.8 mg, 0.216 mmol), and a stir bar. The reaction solution was allowed to stir at room temperature for 30 min. The THF solvent was removed under vacuum, and the crude product was extracted with C₆H₆. The C₆H₆ solution was lyophilized, and the product was washed with pentane (4 × 10 mL). Evaporation of the volatiles under vacuum afforded the product as a green powder. Yield: 131 mg (62%). ¹H NMR (700 MHz, CD₂Cl₂): δ 9.87 (d, *J*_{HH} = 7.0 Hz, 2H, H¹), 7.60 (dd, *J*_{HH} = 5.6, 2.8 Hz, 2H, H⁵), 7.39 (dd, *J*_{HH} = 5.6, 2.8 Hz, 2H, H⁶), 7.17 (d, *J*_{HH} = 2.1 Hz, H⁴), 7.07 (t, *J*_{HH} = 7.0 Hz, 6H, PPh₃), 6.94-6.88 (m, 24H, PPh₃), 6.27 (dd, *J*_{HH} = 7.0, 2.8 Hz, 2H, H²). ¹³C{¹H} (176 MHz, CD₂Cl₂): δ 158.61, 157.72, 153.38, 141.84, 141.55, 133.84, 132.46 (t, *J*_{CP} = 17.5 Hz, *ipso*-CP), 129.11, 129.02, 127.72, 126.49, 120.25, 116.92. ³¹P{¹H} NMR (162 MHz, C₆D₆): δ 25.13 (s, PPh₃). IR (ATR, cm⁻¹): 3056, 1544, 1514, 1492, 1446, 1372, 1318, 1299, 1210, 1186, 1121,

1089, 1001, 914, 887, 868, 808, 776, 737, 694. Anal. Calculated (found): C, 63.07 (62.64); H, 3.92 (4.02); N, 6.81 (6.63).

Ru(b4OMepi)(PPh₃)₂Cl. THF (10 mL) was added to a 20 mL vial charged with Hb4OMepi (99 mg, 0.276 mmol), RuCl₂(PPh₃)₃ (251.6 mg, 0.262 mmol), TlPF₆ (91.7 mg, 0.262 mmol), and a stir bar. The reaction solution was allowed to stir at 60 °C for 16 h. After the solution cooled to room temperature, TlCl was filtered using a fine frit and the THF solvent was removed under vacuum. The crude product was washed with Et₂O (4 × 10 mL), affording Ru(Hb4OMepi)(PPh₃)₂Cl[PF₆] in 87% yield (267 mg). THF (10 mL) was added to a 20 mL vial charged with Ru(Hb4OMepi)(PPh₃)₂Cl[PF₆] (264 mg, 0.227 mmol), NaO^tBu (22.9 mg, 0.238 mmol), and a stir bar. The reaction solution was allowed to stir at room temperature for 30 min. The THF solvent was removed under vacuum, and the crude product was extracted with C₆H₆. The C₆H₆ solution was lyophilized, and the product was washed with pentane (4 × 10 mL). Evaporation of the volatiles under vacuum afforded the product as a dark blue powder. Yield: 192 mg (83%). ¹H NMR (400 MHz, C₆D₆): δ 10.32 (d, *J*_{HH} = 7.2 Hz, 2H, H¹), 7.99 (dd, *J*_{HH} = 5.6, 3.2 Hz, 2H, H⁵), 7.50-7.46 (m, 12H, PPh₃), 6.99 (d, *J*_{HH} = 2.8 Hz, 2H, H⁴), 6.79-6.78 (m, 18H, PPh₃), 5.86 (dd, *J*_{HH} = 7.2, 3.2 Hz, 2H, H²), 3.10 (s, 6H). ¹³C{¹H} (176 MHz, CD₂Cl₂): δ 165.35, 158.46, 158.10, 153.57, 141.82, 133.99, 133.23 (t, *J*_{CP} = 16.6 Hz, *ipso*-CP), 128.76, 128.57, 127.55, 119.76, 109.69, 106.69, 55.76. ³¹P{¹H} NMR (162 MHz, C₆D₆): δ 26.40 (s, PPh₃). IR (ATR, cm⁻¹): 3050, 1619, 1558, 1509, 1467, 1436, 1378, 1328, 1178, 1091, 1039, 1002, 845, 744, 694. Anal. Calculated (found): C, 65.98 (65.45); H, 4.55 (4.44); N, 6.87 (6.86).

Ru(b4OHpi)(PPh₃)₂Cl. THF (10 mL) was added to a 20 mL vial charged with Hb4OHpi (63.6 mg, 0.192 mmol), RuCl₂(PPh₃)₃ (184.1 mg, 0.192 mmol), NaO^tBu (19.4 mg, 0.202 mmol), and a stir bar. The reaction solution was allowed to stir at 70 °C for 16 h. After the solution was cooled to room temperature, the THF solvent was removed under vacuum. The crude product was washed with DCM (4 × 10 mL), H₂O (4 × 10 mL), and Et₂O (4 × 10 mL). Evaporation of the volatiles under vacuum afforded the product as a dark blue powder. Crystals were obtained from vapor diffusion of pentane into a THF solution at -35 °C. Yield: 151 mg (79%). ³¹P{¹H} NMR (162 MHz, THF): δ 26.40 (s, PPh₃). IR (ATR, cm⁻¹): 3046, 1555, 1517, 1478, 1432, 1324, 1296, 1186, 1103, 1091, 1017, 972, 912, 862, 795, 744, 693. Anal. Calculated (found): C, 65.42 (65.45); H, 4.27 (4.13); N, 7.06 (7.12).

Ru(HbMepi)(PPh₃)₂Cl₂. DCE (5 mL) was added to a vial charged with HbMepi (51.2 mg, 0.156 mmol), RuCl₂(PPh₃)₃ (136.3 mg, 0.142 mmol), and a stir bar. The reaction solution was allowed to stir at room temperature for 24 h. The precipitates were collected on a frit and washed with Et₂O (4 × 10 mL), and the product was extracted with DCM. Evaporation of the volatiles under vacuum afforded the product as a green solid. Crystals were obtained from slow evaporation of a DCM solution at 5 °C (DCM/Hex). Yield: 113 mg (78%). ¹H NMR (400 MHz, CD₂Cl₂): δ 10.78 (s, 1H), 7.79 (d, *J*_{HH} = 7.6 Hz, 1H), 7.73-7.69 (m, 12H), 7.57 (t, *J*_{HH} = 7.6 Hz, 1H), 7.51 (t, *J*_{HH} = 7.6 Hz, 2H), 7.30 (t, *J*_{HH} = 7.8 Hz, 1H), 7.22 (t, *J*_{HH} = 7.8 Hz, 1H), 7.13-7.04 (m, 19H), 6.89 (d, *J*_{HH} = 7.6 Hz, 1H), 6.30 (d, *J*_{HH} = 8.0 Hz, 1H), 6.21 (d, *J*_{HH} = 8.0 Hz, 1H), 2.31 (s, 3H, Me), 0.99 (s, 3H, Me). ¹³C{¹H} (176 MHz, CD₂Cl₂): δ 159.83, 159.34, 148.76, 138.27, 136.19, 135.56, 135.02, 134.19, 131.71, 131.10, 130.14, 129.86, 129.17, 128.76, 127.65, 127.09, 124.64, 123.27, 120.49, 118.49, 108.24, 24.23, 20.54. ³¹P{¹H} NMR (162 MHz, CD₂Cl₂): δ 24.94 (s, PPh₃). IR (ATR, cm⁻¹): 3170, 3056, 1640, 1609, 1581, 1548, 1482, 1467, 1432, 1305, 1270, 1214, 1150, 1107, 1089, 1030, 1007, 805, 760, 748, 685, 655. Anal. Calculated (found): C, 65.69 (65.46); H, 4.63 (4.65); N, 6.84 (6.65).

[Ru(CH₂Mepi)(PPh₃)₂]. THF (5 mL) was added to a 20 mL vial charged with **4** (110 mg, 0.152 mmol), NaO^tBu (18.9 mg, 0.197 mmol), and a stir bar. The reaction solution was allowed to stir at room temperature for 18 h. The THF solvent was removed under vacuum, and the crude product was washed with pentane (4 × 20 mL) then extracted with C₆H₆. The C₆H₆ solution was lyophilized, and the product was washed with Et₂O (5 mL) and pentane (4 × 10 mL). Evaporation of the volatiles under vacuum afforded the product as a green powder. Crystals were obtained from vapor diffusion of pentane into a C₆H₆ solution at room temperature. Yield: 64 mg (62%). ¹H NMR (700 MHz, C₆D₆): δ 8.46 (t, *J*_{HH} = 7.0 Hz), 7.23-7.18 (m), 6.09-6.86 (m, PPh₃), 6.75-6.71 (m, PPh₃), 6.62-6.57 (m, PPh₃); Major species: 7.99 (d, *J*_{HH} = 7.7 Hz, 1H), 7.94 (d, *J*_{HH} = 7.0 Hz, 1H), 7.14 (t, *J*_{HH} = 7.0 Hz, 1H), 6.81 (d, *J*_{HH} = 7.7 Hz, 1H), 6.68 (t, *J*_{HH} = 7.7 Hz, 1H), 6.10 (d, *J*_{HH} = 7.0 Hz, 1H), 5.41 (d, *J*_{HH} = 7.7 Hz, 1H), 2.37 (t, *J* = 9.1 Hz, 1H), 1.78 (s, 3H, Me), -2.62 (t, *J* = 9.1 Hz, 1H); Minor species: 7.98 (d, *J*_{HH} = 7.0 Hz, 1H), 7.92 (d, *J*_{HH} = 7.7 Hz, 1H), 7.09-7.06 (m, 2H), 7.00 (d, *J*_{HH} = 7.7 Hz, 1H), 6.65 (t, *J*_{HH} = 7.7 Hz, 1H), 5.83 (d, *J*_{HH} = 7.0 Hz, 1H), 5.69 (d, *J*_{HH} = 7.7 Hz, 1H), 3.10 (t, *J* = 9.1 Hz, 1H), 0.70 (s, 3H, Me), -2.77 (t, *J* = 9.1 Hz, 1H). ¹³C{¹H} (176 MHz, CD₂Cl₂): δ 174.34, 159.04, 157.10, 151.97, 150.29, 149.06, 142.89, 141.59, 134.77, 134.62, 133.51, 133.45, 133.13, 132.49, 126.08, 120.14, 119.67, 118.20, 116.30,

112.59, 27.60, 24.78, 20.37, 19.95. $^{31}\text{P}\{^1\text{H}\}$ NMR (283 MHz, C_6D_6): δ 33.05 (s, minor), 31.34 (s, major). IR (ATR, cm^{-1}): 3046, 2968, 2900, 2613, 1533, 1560, 1504, 1461, 1431, 1387, 1324, 1286, 1239, 1188, 1159, 1112, 1090, 1030, 998, 976, 903, 792, 764, 739, 693. Anal. Calculated (found): C, 66.27 (66.06); H, 4.39 (4.35); N, 10.17 (10.16).

3.4 References

- (1) (a) Gunanathan, C.; Milstein, D. *Science* **2013**, *341*, 249. (b) Dobereiner, G. E.; Crabtree, R. H. *Chem. Rev.* **2010**, *110*, 681. (c) Friedrich, A.; Schneider, S. *ChemCatChem* **2009**, *1*, 72.
- (2) (a) Bonitatibus, P. J.; Chakraborty, S.; Doherty, M. D.; Siclovan, O.; Jones, W. D.; Soloveichik, G. L. *Proc. Natl. Acad. Sci.* **2015**, *112*, 1687. (b) Marr, A. C. *Catal. Sci. Technol.* **2012**, *2*, 279. (c) Johnson, T. C.; Morris, D. J.; Wills, M. *Chem. Soc. Rev.* **2010**, *39*, 81.
- (3) Clapham, S. E.; Hadzovic, A.; Morris, R. H. *Coord. Chem. Rev.* **2004**, *248*, 2201.
- (4) Gunanathan, C.; Milstein, D. *Acc. Chem. Res.* **2011**, *44*, 588.
- (5) (a) Li, H.; Wang, X.; Huang, F.; Lu, G.; Jiang, J.; Wang, Z.-X. *Organometallics* **2011**, *30*, 5233. (b) Li, H.; Zheng, B.; Huang, K.-W. *Coord. Chem. Rev.* **2015**, *293-294*, 116.
- (6) Zeng, G.; Sakaki, S.; Fujita, K.-i.; Sano, H.; Yamaguchi, R. *ACS Catal.* **2014**, *4*, 1010.
- (7) Zhang, G.; Vasudevan, K. V.; Scott, B. L.; Hanson, S. K. *J. Am. Chem. Soc.* **2013**, *135*, 8668.
- (8) Tseng, K.-N. T.; Kampf, J. W.; Szymczak, N. K. *Organometallics* **2013**, *32*, 2046.
- (9) Complex HRu(bMepi)(PPh₃)₂ (**3**) and Ru(bMepi)(PPh₃)Cl (**4**) are now commercially available.
- (10) The effect of catalyst dependence on the catalytic rate was examined by changing the [**3**] while holding the initial concentration of 1PhEtOH constant.
- (11) Mikhailine, A. A.; Maishan, M. I.; Lough, A. J.; Morris, R. H. *J. Am. Chem. Soc.* **2012**, *134*, 12266.
- (12) Concentrations higher than 20-fold excess of PPh₃ with respect to **3** are likely to have an effect on the dehydrogenation rate; however, those scenarios deviate greatly from the standard conditions (Figure 3-5) and thus are not meaningful to obtaining relevant analysis on the AAD mechanism.
- (13) The neat concentration of 1PhEtOH is 8.3 M. Low 1PhEtOH concentrations are operationally challenging because replacing 1PhEtOH impacts other factors, such as dielectric constant, solvation, and polarizability, which influence the kinetic studies and the AAD mechanism.

- (14) Morse, P. M.; Spencer, M. D.; Wilson, S. R.; Girolami, G. S. *Organometallics* **1994**, *13*, 1646.
- (15) Wilkins, R. G. *Kinetics and Mechanism of Reactions of Transition Metal Complexes*; Wiley-VCH: Weinheim, Germany, 2003; pp199.
- (16) Casey, C. P.; Singer, S. W.; Powell, D. R.; Hayashi, R. K.; Kavana, M. *J. Am. Chem. Soc.* **2001**, *123*, 1090.
- (17) (a) Mueller, J. A.; Goller, C. P.; Sigman, M. S. *J. Am. Chem. Soc.* **2004**, *126*, 9724. (b) Blum, O.; Milstein, D. *J. Am. Chem. Soc.* **1995**, *117*, 4582. (c) Martínez-Prieto, L. M.; Ávila, E.; Palma, P.; Álvarez, E.; Cámpora, J. *Chem. - Eur. J.* **2015**, *21*, 9833.
- (18) For further discussions of equilibrium isotope effects at transition-metal centers see: (a) Slaughter, L. M.; Wolczanski, P. T.; Klinckman, T. R.; Cundari, T. R. *J. Am. Chem. Soc.* **2000**, *122*, 7953. (b) Janak, K. E.; Parkin, G. *J. Am. Chem. Soc.* **2003**, *125*, 6889. (c) Gómez-Gallego, M.; Sierra, M. A. *Chem. Rev.* **2011**, *111*, 4857.
- (19) Johnson, J. B.; Bäckvall, J.-E. *J. Org. Chem.* **2003**, *68*, 7681.
- (20) Tseng, K.-N. T.; Kampf, J. W.; Szymczak, N. K. *ACS Catal.* **2015**, *5*, 411.
- (21) Csonka, R.; Speier, G.; Kaizer, J. *RSC Adv.* **2015**, *5*, 18401.
- (22) Addison, A. W.; Rao, T. N.; Reedijk, J.; van Rijn, J.; Verschoor, G. C. *J. Chem. Soc., Dalton Trans.* **1984**, 1349.
- (23) Brookhart, M.; Green, M. L. H.; Parkin, G. *Proc. Natl. Acad. Sci.* **2007**, *104*, 6908.
- (24) The hydrogen atoms were refined assuming an idealized geometry for the sp³ carbon; thus the M–H distances are approximate values.
- (25) An identical rate ($7.7(3) \times 10^{-5} \text{ M}\cdot\text{s}^{-1}$) was obtained for **4** when 2 equiv of NaOTf was added, which suggests that the NaOTf generated when **5** was used had no effect on the catalytic rate of 1PhEtOH dehydrogenation.
- (26) It should be noted that although the metal–ligand cooperative pathway was effectively turned off for **5**, this hybrid hydrogen-transfer mechanism may still be a plausible competing pathway for **3**.
- (27) Kaneda, K.; Mori, K.; Hara, T.; Mizugaki, T.; Ebitani, K. *Catal. Surv. Asia* **2004**, *8*, 231.
- (28) Vijayasri, K.; Rajaram, J.; Kuriacose, J. C. *J. Mol. Catal.* **1987**, *39*, 203.
- (29) Thorson, M. K.; Klinkel, K. L.; Wang, J.; Williams, T. J. *Eur. J. Inorg. Chem.* **2009**, 2009, 295.
- (30) Fluorination has a destabilizing effect (15 kcal/mol) on the transition state for β -H elimination. See references: (a) Gellman, A. J.; Dai, Q. *J. Am. Chem. Soc.* **1993**, *115*, 714. (b) Johnson, T. J.; Huffman, J. C.; Caulton, K. G. *J. Am. Chem. Soc.* **1992**, *114*, 2725.

- (31) Further confirmation of the Ru-alkoxide complex was not possible by 2D NMR correlation experiments, such as HMBC. For a discussion, see: *Phosphorous-31 NMR Spectroscopy*; Kuhl, O., Ed.; Springer: New York, 2008; p7.
- (32) Ritter, J. C. M.; Bergman, R. G. *J. Am. Chem. Soc.* **1998**, *120*, 6826.
- (33) Blum, O.; Milstein, D. *J. Organomet. Chem.* **2000**, *593-594*, 479.
- (34) For a recent example of large entropic factors in a unimolecular reaction performed in a protic solvent, see: Byers, J. A.; Jamison, T. F. *Proc. Natl. Acad. Sci.* **2013**, *110*, 16724.
- (35) For other examples demonstrating similar chemoselectivity see: (a) Chakraborty, S.; Lagaditis, P. O.; Förster, M.; Bielinski, E. A.; Hazari, N.; Holthausen, M. C.; Jones, W. D.; Schneider, S. *ACS Catal.* **2014**, *4*, 3994. (b) Manzini, S.; Urbina-Blanco, C. A.; Nolan, S. P. *Organometallics*, **2013**, *32*, 660.
- (36) The standard enthalpy of formation in the gas phase for acetophenone and benzaldehyde are -87 and -37 kJ/mol, respectively. See <http://webbook.nist.gov/chemistry/name-ser.html>.
- (37) Olmstead, W. N.; Margolin, Z.; Bordwell, F. G. *J. Org. Chem.* **1980**, *45*, 3295.
- (38) Golden, D. M.; Benson, S. W. *Chem. Rev.* **1969**, *69*, 125.
- (39) Ellis, W. W.; Ciancanelli, R.; Miller, S. M.; Raebiger, J. W.; Rakowski DuBois, M.; DuBois, D. L. *J. Am. Chem. Soc.* **2003**, *125*, 12230.
- (40) Hansch, C.; Leo, A.; Taft, R. W. *Chem. Rev.* **1991**, *91*, 165.
- (41) (a) Spasyuk, D.; Smith, S.; Gusev, D. G. *Angew. Chem., Int. Ed.* **2012**, *51*, 2772, (b) He, L.-P.; Chen, T.; Gong, D.; Lai, Z.; Huang, K.-W. *Organometallics* **2012**, *31*, 5208. (c) Wang, Z.; Belli, J.; Jensen, C. M. *Faraday Discuss.* **2011**, *151*, 297. (d) Nielsen, M.; Kammer, A.; Cozzula, D.; Junge, H.; Gladiali, S.; Beller, M. *Angew. Chem., Int. Ed.* **2011**, *50*, 9593.
- (42) (a) Grellier, M.; Sabo-Etienne, S. *Dalton Trans.* **2014**, *43*, 6283. (b) Crabtree, R. H. *Energy Environ. Sci.* **2008**, *1*, 134.
- (43) (a) Chakraborty, S.; Brennessel, W. W.; Jones, W. D. *J. Am. Chem. Soc.* **2014**, *136*, 8564. (b) Fujita, K.-i.; Tanaka, Y.; Kobayashi, M.; Yamaguchi, R. *J. Am. Chem. Soc.* **2014**, *136*, 4829. (c) Kawahara, R.; Fujita, K.-i.; Yamaguchi, R. *Angew. Chem., Int. Ed.* **2012**, *51*, 12790. (d) Yamaguchi, R.; Ikeda, C.; Takahashi, Y.; Fujita, K.-i. *J. Am. Chem. Soc.* **2009**, *131*, 8410.
- (44) Siegl, W. O. *J. Org. Chem.* **1977**, *42*, 1872.

CHAPTER 4

Oxidant-Free Conversion of Primary Amines to Nitriles

Portions of this chapter have been published:

Tseng, K.-N. T.; Rizzi, A. R.; Szymczak, N. K. *J. Am. Chem. Soc.* **2013**, *135*, 16352. Reprinted with permission; Copyright (2013) American Chemical Society.

4.1 Introduction

Nitriles are a prominent class of organic molecules included in a wide variety of natural products,¹ biologically active compounds,² industrial processes (polymers, agrochemicals, and dyes/pigments),³ and used as synthons for further synthetic elaboration.⁴ Typical routes to prepare nitriles proceed with low atom economy, require toxic reagents, and/or have limited selectivity. Common laboratory-scale syntheses include Sandmeyer-type reactivity,⁵ cyanation of alkyl or aryl halides,⁶ dehydration of amides/aldoximes,⁷ and metal-catalyzed cyanation/cyanomethylation,⁸ among others.⁹ In contrast, industrial syntheses typically rely on ammoxidation protocols that operate at high temperatures (300–550 °C).^{3, 10} All of the above synthetic methodologies require either the use of hazardous/energy-intensive reagents, harsh reaction conditions, and/or produce stoichiometric waste. Moreover, reagents and conditions required for these transformations often show limited compatibility with other functional groups. Another methodology for nitrile synthesis that does not introduce a carbon unit is the oxidation of primary amines,¹¹ which can be mediated using stoichiometric inorganic¹² or iodine-based oxidants,¹³ or a transition metal catalyst and O₂.¹⁴ Unfortunately, many transition-metal catalyzed oxidation protocols require excess quantities of oxidant and/or basic reagent for efficient catalysis, which decreases atom economy by contributing to unwanted waste products.^{11b,13b,13c,14a,14b} Furthermore, the use of an external oxidant limits selectivity and

functional group tolerance, because oxidant-incompatible functionality must then be protected prior to the nitrile formation step.¹⁴

An alternative procedure for amine oxidation is to use transition-metal catalyzed dehydrogenation, which has been widely exploited for alcohol oxidation.¹⁵ However, reports detailing oxidant-free amine dehydrogenation are limited and either proceed with low conversion,¹⁶ or require exogenous additives and harsh reaction conditions (160–200 °C).¹⁷ Our laboratory recently reported base-free, acceptorless, and chemoselective dehydrogenation and dehydrogenative coupling reactions of secondary and primary alcohols/diols, respectively, catalyzed by an amide-derived *N,N,N*-Ru(II) hydride complex (**1**, HRu(bMepi)(PPh₃)₂; bMepi = 1,3-bis(6'-methyl-2'-pyridylimino)isoindolate).¹⁸ Because of the ability of **1** to promote rapid H₂ release from alcohol groups without product inhibition, we surmised that **1** might also dehydrogenate other polar substrates by a similar mechanistic pathway. Herein, we report the application of **1** as a catalyst that efficiently promotes dehydrogenation of primary and secondary amines to nitriles and imines, respectively, without the requirement of exogenous oxidant or hydrogen acceptor.

4.2 Results and Discussion

4.2.1 Dehydrogenation of *n*-Octylamine to *n*-Octanenitrile

In contrast to the growing number of reports detailing catalytic dehydrogenation of alcohols, analogous dehydrogenative reactivity of amines is sparse,^{15f,19} and even less reported for the double dehydrogenation to afford the corresponding nitrile.^{16,17} Moreover, one of the only well-defined examples of direct amine dehydrogenation employed an olefin as a hydrogen acceptor^{17a} or excess base^{17b} to drive the reaction at high temperatures (160–200 °C).¹⁷ In light of this precedent, we initiated investigations by examining *transfer* dehydrogenation of *n*-octylamine with cyclohexene catalyzed by **1**. When a toluene solution containing 0.5 mmol *n*-octylamine, 5 mmol (10 equiv) of cyclohexene and 1 mol% of **1** was heated to 110 °C for 24 h in a sealed vessel, *n*-octanenitrile was observed (40%) with concomitant formation of cyclohexane, as determined by GC-MS analysis (Figure 4-1, eq 1).

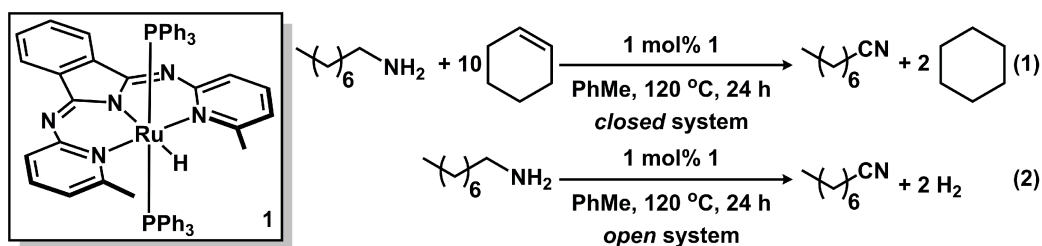


Figure 4-1. Transfer and acceptorless dehydrogenation of *n*-octylamine.

Under these conditions, the added hydrogen acceptor (cyclohexene) was critical to promote the reaction, and in the absence of a hydrogen acceptor (3.5 mL headspace), less than 4% conversion to *n*-octanenitrile was observed. The conversion efficiency was found to be sensitive to the overall reaction volume (liquid plus headspace), consistent with a reaction in which a gas is generated. In the limiting regime of an infinitely large headspace (i.e. an open system), the efficiency of **1** was further improved. For example, in the presence of **1** (1 mol%),²⁰ *n*-octylamine was converted to *n*-octanenitrile in 76% yield after heating for 24 h in refluxing toluene open to a N₂ atmosphere (Figure 4-1, eq 2). H₂ and *n*-octanenitrile were confirmed as the sole reaction products by *in situ* examination of the reaction mixture in a sealed NMR tube and control experiments showed no reaction in the absence of **1**.

4.2.2 Dependence of *n*-Octylamine Dehydrogenation on H₂ pressure

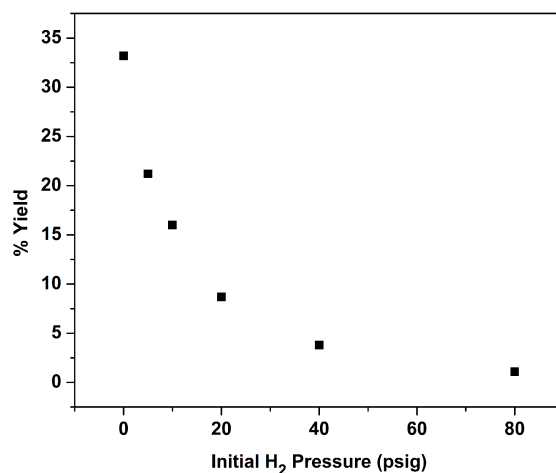


Figure 4-2 Dependence of *n*-octylamine dehydrogenation catalyzed by HRu(bMepi)(PPh₃)₂.

In order to evaluate the extent to which the release of H₂ mediates the dehydrogenation reaction, we assessed the product profile under elevated H₂ pressures (Figure 4-2). Consistent

with prior dehydrogenative alcohol oxidation studies,¹⁸ the conversion efficiency of the reaction was found to be highly sensitive to pressure and the dehydrogenation reaction was significantly suppressed (33% yield) when performed in a sealed Fischer–Porter tube (84.5 mL headspace). The conversion decreased with increased H₂ pressure: halving at 10, 20, 40, and 80 psig.

4.2.2 Scope of Amine Dehydrogenation

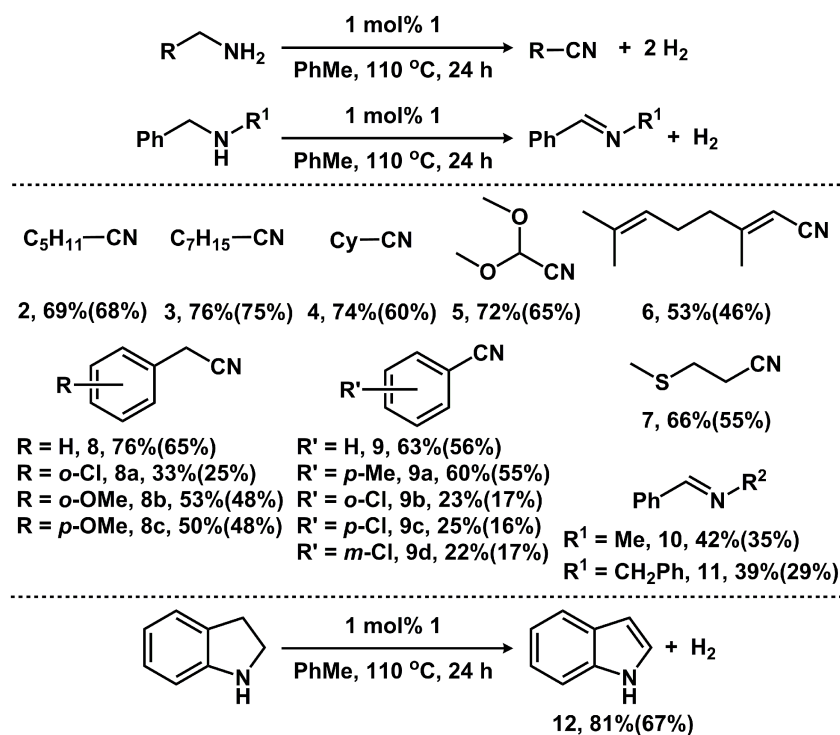


Figure 4-3 Dehydrogenation of amines catalyzed by HRu(bMepi)(PPh₃)₂.

Dehydrogenation of aliphatic amines was general to afford the corresponding nitriles as the *exclusive* product (2–7). For instance, when 1-cyclohexylmethanamine was used as a substrate, cyclohexanecarbonitrile (4) was generated in 74% yield. Furthermore, the dehydrogenation of 2-phenethylamine to 2-phenylacetonitrile (8), an important precursor to several pharmaceutical drugs,³ proceeded with 76% yield. When *ortho*- and *para*- substituted phenethylamines were used as substrates, conversions to the corresponding phenylacetonitriles depended on the electron-donating and -withdrawing groups on the benzene ring (8a–c). A modest (33%) yield was observed for the *ortho*-substituted chlorophenethylamine, however, replacing the chloro group for an electron-donating methoxy substituent increased the yield to 53%. The proximity of the methoxy substituent to the –CH₂NH₂ group had little effect on the

conversion efficiency, since both the *ortho*- and *para*- substituted methoxyphenethylamines gave similar yields.

Dehydrogenation reactions of activated amines were investigated with benzylic substrates, which were converted cleanly to the corresponding benzonitriles. Substituent effects were examined using a series of functionalized benzylamines. While electron-donating groups were tolerated (**9a**), electron-withdrawing groups decreased the yields, regardless of the substitution pattern on the aromatic ring. For instance, deactivating chloro groups at either the *ortho*-, *meta*-, or *para*- positions led to decreased conversions (**9b–d**).

Because we observed high selectivity for primary amines, we investigated whether **1** could also catalyze the selective dehydrogenation of secondary amines. Oxidative protocols for primary and secondary amines have been reported using O₂; however, selectivity is generally low with this methodology.¹⁴ For example, oxidation of secondary amines affords mixtures of products that include aldehydes and alcohols in addition to nitrogen-containing species.^{14e-h} In contrast, a *single* product was obtained from the dehydrogenation of secondary and heterocyclic amines with –CH₂NRH functionalities catalyzed by **1**. In the case of secondary amines, secondary aldimines (**10** and **11**) were obtained in moderate yields, and indoline was cleanly converted to indole (**12**) in high (81%) yield. Thus, in addition to primary amine oxidation, **1** exhibits high selectivity for the catalytic dehydrogenation of secondary and select heterocyclic amines.

The oxidation of amines to nitriles without any required additives allows our system to tolerate potentially oxidizable functional groups; a limitation of traditional amine to nitrile conversions. To highlight the utility of the amine oxidation under the reducing conditions used by **1**, we examined primary amine dehydrogenation in the presence of a thioether functionality, a motif typically susceptible to oxidation.²⁹ Indeed, when 3-(methylthio)propylamine was subjected to **1**, only the amino moiety was oxidized under the standard reaction conditions and 3-(methylthio)propanenitrile (**7**) was obtained as the single product, produced in 66% yield. This reactivity demonstrates the utility of **1** as an amine oxidation catalyst that is compatible with an oxidant intolerant functionality.

4.2.3 Comparison of Common Transfer Hydrogenation Catalysts for *n*-Octylamine Dehydrogenation

In contrast to (transfer) dehydrogenation reactivity of alcohols,^{15h,21} reports of analogous reactivity with amines are limited.^{16,17} Consistent with the lack of literature precedent, we observed only trace (1–3%) nitrile formation from *n*-octylamine using several common transfer hydrogenation catalysts (Noyori's HRuCl(PPh₃)₂(en) catalyst,²² Ru(H)₂(PPh₃)₄,²³ HRuCl(PPh₃)₃,²⁴ and HRuCl(PPh₃)₃CO²⁵). Similar results (<1% *n*-octanenitrile) were obtained when HRh(P^{*i*}Pr)₃ and *n*-octylamine were subjected to identical condition as for the dehydrogenation by **1**.²⁶ Shvo's catalyst²⁷ exhibited a reaction profile consistent with amine coupling, affording dioctylamine in 22% yield after 24 h with no conversion to *n*-octanenitrile.²⁸ Based on known reports as well as our own comparative experiments, the double dehydrogenation reactivity mediated by **1** is atypical in terms of conversion and product selectivity.

4.2.4 Chemoselective Oxidation of Primary Amines

The preparation of aryl nitriles is typically achieved using Sandmeyer-type⁵ or Rosenmund-von Braun⁶ methodologies, but conditions necessary to promote these transformations also limit chemoselectivity. Because α -CH hydrogens are required to eliminate H₂, an amine double dehydrogenative methodology allows the differentiation of a substrate containing two chemically distinct amino functional groups (–CH₂NH₂ versus –CR₂NH₂). To highlight this difference, complex **1** selectively oxidized the benzyl amine moiety of 3-aminobenzylamine in the presence of the aromatic amino group, which afforded 3-aminobenzonitrile (**13**) as the *sole product* in 58% yield (54% isolated yield), demonstrating the high chemoselectivity of **1** (Figure 4-4). Furthermore, this illustrates the utility of *dehydrogenative* oxidation reactions mediated by **1**; instead of requiring an oxidant, amine oxidation is achieved by H₂ elimination.

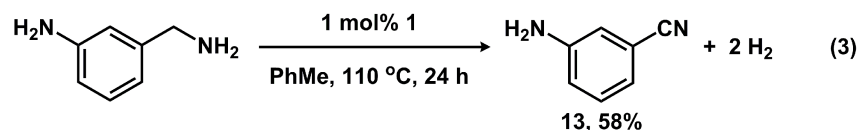


Figure 4-4 Chemoselective oxidation of 3-aminobenzylamine.

4.2.5 Preliminary Results for the Mechanism of Amine Dehydrogenation

Catalytic dehydrogenation reactions can be mediated by either heterogeneous or homogenous pathways, and the catalytically-active form of **1** was initially probed using catalyst poisoning studies.³⁰ Consistent with an operative homogeneous system, the catalytic activity of *n*-octanenitrile formation was unaffected by the addition of Hg(0) (~800 equiv) when added *during catalysis*. A substoichiometric ligand poisoning experiment was conducted to further interrogate the active catalytic species.³¹ In the presence of 0.25 equiv of 1,10-phenanthroline, no change in the product distribution was noted, however, complete poisoning was achieved using 1 equiv of 1,10-phenanthroline, inconsistent with a heterogeneous system, where low surface area aggregates are typically poisoned by $\ll 1$ equiv of added ligand poison.³²

Further investigations into the identity of catalytically-active species are currently underway, and preliminary analyses suggest a catalytic cycle similar to alcohol dehydrogenation.^{15h} *In situ* analysis of the amine dehydrogenation reaction revealed the release of PPh₃ from **1** during catalysis, as visualized by ³¹P NMR spectroscopy and GC-MS analysis. Furthermore, catalytic reactions using Ru(bMepi)(PPh₃)Cl (**14**) exhibited a similar dehydrogenation profile to **1** in the presence of KO^tBu (Figure 4-5), and free PPh₃ was not observed. This is consistent with a single PPh₃ dissociation event from **1** to generate a catalytically-active 16 e⁻ Ru(II) species, able to participate in an inner-sphere type dehydrogenation pathway.³³

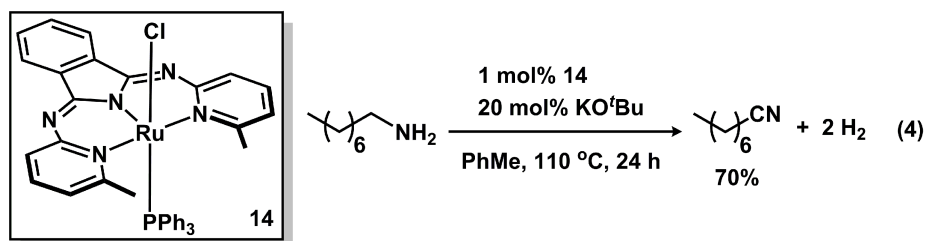


Figure 4-5 Ru(bMepi)(PPh₃)Cl mediated *n*-octylamine dehydrogenation in the presence of base.

When the dehydrogenation of *n*-octylamine was monitored *in situ* by GC-MS and ¹H NMR spectroscopy over 24 h in an open system (Figure 4-6),³⁴ unreacted *n*-octylamine and *n*-octanenitrile were the *only* species observed. Because an imine or imine-derived products were not detected, a fast secondary dehydrogenation event is proposed to yield the nitrile product.³⁵

Since nitriles are competent ligands for transition metals, nitrile coordination might be an operative inhibition pathway at high nitrile concentrations. To probe this possibility, the dehydrogenation of *n*-octylamine was performed in the presence of *n*-octanenitrile (50 equiv).³⁶ Under the standard reaction conditions, 54% conversion was noted, consistent with competitive binding of nitrile to the catalytically-active Ru species. This trend continued at 75 equiv of *n*-octanenitrile, where only 12% conversion was noted. These results are consistent with catalyst inhibition at high concentrations of nitrile, where an irreversible nitrile-coordination event likely occurs, diverting the catalyst from a productive dehydrogenation pathway. Hence, we propose that following amine coordination, H₂ loss affords an imine intermediate that remains coordinated to Ru. This species likely undergoes a further fast dehydrogenation reaction to afford a Ru-nitrile adduct that is substitutionally labile at low nitrile concentrations, but inert at high nitrile concentrations.

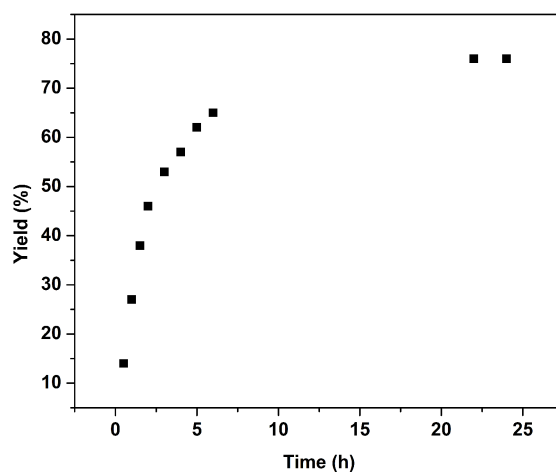


Figure 4-6 Reaction profile of *n*-octylamine dehydrogenation catalyzed by HRu(bMepi)(PPh₃)₂.

4.2.5 Summary

In conclusion, we have developed a selective dehydrogenative amine oxidation protocol that requires no oxidant or hydrogen acceptor additives, tolerates oxidizable functionality, and liberates H₂ as a product. Although, prior reports demonstrated oxidative reactivity of primary amines to nitriles, our system is the only reported homogeneous catalyst to accomplish this without *any* additives and in good yields. Additionally, the amine dehydrogenation methodology is notable because **1** mediates the chemoselective oxidation of primary amines with –CH₂NH₂ functionality in the presence of primary amines without α-CH hydrogens.

4.3 Experimental Section

4.3.1 General Considerations

All reagents were purchased from commercial vendors. The 3Å Molecular sieves were dried at 250 °C under dynamic vacuum for 24 h. All liquid amines were distilled from CaH₂ under a nitrogen atmosphere, and then stored over 3Å molecular sieves for 4 days. 3-aminobenzylamine was sublimed under vacuum at room temperature for 12 h. All manipulations were conducted under a nitrogen atmosphere unless otherwise stated. Dichloromethane (DCM) was purified using a Glass Contour solvent purification system consisting of a Cu(II) catalyst, neutral alumina, and activated molecular sieves, then passed through an in-line, 2 μm filter immediately before being dispensed. Toluene was sparged with N₂ for 2 h, and then stored over 3Å molecular sieves for 48 h. HRu(bMepi)(PPh₃)₂ (**1**),¹⁸ Ru(bMepi)(PPh₃)Cl (**14**),¹⁸ Ru(H)₂(PPh₃)₄,³⁸ HRuCl(PPh₃)₃,³⁹ HRuCl(PPh₃)₂(en),³⁹ HRuCl(PPh₃)₃CO,⁴⁰ Ru₂(η⁵-C₅Ph₄O)₂(H)₂(CO)₄,⁴¹ HRh(P^{*i*}Pr)₃,⁴² were prepared according to previously reported methods.

NMR spectra were obtained on Varian Inova 500 or Varian MR400 spectrometer. GC-MS analyses were performed using a Shimadzu QP-2010 GC/MS; the GC contains a 30 m long DB-5 column with a 0.25 mm I.D. GC measurements were conducted using the following method: 30 °C hold for the first 5 min, ramp to 270 °C at 20 °C/min and hold for 2 min and the solvent cutoff was set for 2.5 min. The respective response factor was obtained by the GC analysis of a series of samples of known concentration, plotting the ratio of the areas, A_{sample}/A_{standard} of each versus the ratio of the concentrations, [Sample]/[Standard].

4.3.2 General Procedure for Amine Dehydrogenation Catalyzed by HRu(bMepi)(PPh₃)₂

The amine (0.5 mmol) was added to a NMR tube containing a solution of **1** (1 mol%, 0.005 mmol) in PhMe (0.5 mL). The NMR tube was capped with a septum and pierced with a 27 gauge needle, and then heated to 110 °C inside an inert-atmosphere glovebox. After 24 h, a 0.005 mL aliquot was diluted with 1 mL DCM, and the product(s) and yield were determined by GC-MS analysis. After cooling to room temperature, the solvent was evaporated under reduced pressure. Purification by silica gel chromatography (5 cm × 0.5 cm) using 4-5 mL hexanes:ethyl acetate (3:1) afforded the corresponding nitrile as the isolated product in 16-75% yield. The

identity of the nitrile product was confirmed by comparison to the reported NMR spectra of known compounds.

4.3.3 Procedure for *n*-Octylamine Dehydrogenation Catalyzed by Ru(bMepi)(PPh₃)Cl

n-Octylamine (0.5 mmol) was added to a NMR tube containing a solution of **14** (1 mol%, 0.005 mmol) and KO^tBu (20 mol%, 0.1 mmol) in PhMe (0.5 mL). The NMR tube was capped with a septum and pierced with a 27 gauge needle, and then heated to 110 °C inside an inert-atmosphere glovebox. After 24 h, a 0.005 mL aliquot was diluted with 1 mL DCM, and the product(s) and yield were determined by GC-MS analysis.

4.3.4 General Procedure for the H₂ Pressure Dependence Experiments

A Fischer–Porter tube was rinsed with PhMe (3 × 1 mL). *n*-Octylamine (0.5 mmol) was added to the tube containing a solution of **1** (1 mol%, 0.005 mmol) in PhMe (0.5 mL) and a stir bar. The tube was subjected to three charge/vent cycles with H₂ at a given pressure (5, 10, 20, 40, or 80 psig), and then heated to 110 °C in an oil bath, while stirring at 1500 RPM. After 24 h, the tube was vented and a sample was prepared by diluting a 0.005 mL aliquot with 1 mL DCM, and the product(s) and yield were determined by GC-MS analysis.

4.3.5 General Procedure for Poisoning Experiments

Following the general procedure for the dehydrogenation of amines, the poisoning experiments were conducted by allowing the reaction to proceed for 1 h, and then the additives were added to the reaction solution at 110 °C. For the H₂O and *n*-octanenitrile poisoning experiments, H₂O and *n*-octanenitrile were introduced concomitant with *n*-octylamine.

4.3.6 Procedure for Mercury Poisoning Experiment

n-Octylamine (0.5 mmol) was added to a 10 mL Schlenk flask containing a solution of **1** (1 mol%, 0.005 mmol) in PhMe (2 mL). The Schlenk flask was fitted with a reflux condenser capped with an adapter connected to the Schlenk line. The reaction solution was heated to 110 °C using an aluminum heating block and stirred at 1500 RPM. After the reaction had progressed for 1 h, one drop of mercury was added to the reaction solution at 110 °C. After 24 h,

a 0.005 mL aliquot was diluted with 1 mL DCM, and the product(s) and yield were determined by GC-MS analysis.

4.4 References

- (1) Fleming, F. F. *Nat. Prod. Rep.* **1999**, *16*, 597.
- (2) Fleming, F. F.; Yao, L.; Ravikumar, P. C.; Funk, L.; Shook, B. C. *J. Med. Chem.* **2010**, *53*, 7902.
- (3) Pollak, P., Romeder, G., Hagedorn, F., Gelbke, H.-P. Nitriles. In *Ullmann's Encyclopedia of Industrial Chemistry*; Wiley-VCH: Weinheim, Germany, 2012.
- (4) (a) Srimani, D.; Feller, M.; Ben-David, Y.; Milstein, D. *Chem. Commun.* **2012**, *48*, 11853. (b) Gunanathan, C.; Hoelscher, M.; Leitner, W. *Eur. J. Inorg. Chem.* **2011**, *2011*, 3381. (c) Herr, R. *J. Bioorg. Med. Chem.* **2002**, *10*, 3379.
- (5) (a) Sandmeyer, T. *Ber. Dtsch. Chem. Ges.* **1885**, *18*, 1496. (b) Sandmeyer, T. *Ber. Dtsch. Chem. Ges.* **1885**, *18*, 1492.
- (6) Rosenmund, K. W.; Struck, E. *Ber. Dtsch. Chem. Ges.* **1919**, *52*, 1749.
- (7) (a) Yamaguchi, K.; Fujiwara, H.; Ogasawara, Y.; Kotani, M.; Mizuno, N. *Angew. Chem., Int. Ed.* **2007**, *46*, 3922. (b) Ishihara, K.; Furuya, Y.; Yamamoto, H. *Angew. Chem., Int. Ed.* **2002**, *41*, 2983.
- (8) (a) Chakraborty, S.; Patel, Y. J.; Krause, J. A.; Guan, H. *Angew. Chem., Int. Ed.* **2013**, *52*, 1. (b) Falk, A.; Goederz, A.-L.; Schmalz, H.-G. *Angew. Chem., Int. Ed.* **2013**, *52*, 1576. (c) Velcicky, J.; Soicke, A.; Steiner, R.; Schmalz, H.-G. *J. Am. Chem. Soc.* **2011**, *133*, 6948.
- (9) (a) Lualhe, S.; Gori, S. S.; Nantz, M. H. *J. Org. Chem.* **2012**, *77*, 9334. (b) Kamijo, S.; Hoshikawa, T.; Inoue, M. *Org. Lett.* **2011**, *13*, 5928. (c) Lamani, M.; Prabhu, K. R. *Angew. Chem., Int. Ed.* **2010**, *49*, 6622. (d) Oishi, T.; Yamaguchi, K.; Mizuno, N. *Angew. Chem., Int. Ed.* **2009**, *48*, 6286. (e) Rajender Reddy, K.; Uma Maheswari, C.; Venkateshwar, M.; Prashanthi, S.; Lakshmi Kantam, M. *Tetrahedron Lett.* **2009**, *50*, 2050. (f) Zhou, S.; Junge, K.; Addis, D.; Das, S.; Beller, M. *Org. Lett.* **2009**, *11*, 2461.
- (10) Grasselli, R. K. *Catal. Today* **1999**, *49*, 141.
- (11) (a) Murahashi, S.-I., Imada, Y. Amine Oxidation. In *Transition Metals for Organic Synthesis*; Beller, M., Bolm, C., Eds.; Wiley-VCH: Weinheim, Germany, 2008; pp 497. (b) Porta, F.; Crotti, C.; Cenini, S.; Palmisano, G. *J. Mol. Catal.* **1989**, *50*, 333.
- (12) (a) Green, G.; Griffith, W. P.; Hollinshead, D. M.; Ley, S. V.; Schroder, M. *J. Chem. Soc. Perkin Trans. 1* **1984**, 681. (b) Lee, J. B.; Parkin, C.; Shaw, M. J.; Hampson, N. A.; Macdonald, K. I. *Tetrahedron* **1973**, *29*, 751. (c) Clarke, T. G.; Hampson, N. A.; Lee, J. B.; Morley, J. R.; Scanlon, B. *Tetrahedron Lett.* **1968**, *9*, 5685. (d) Stojiljković, A.; Andrejević, V.; Mihailović, M. L. *Tetrahedron* **1967**, *23*, 721.

(13) (a) Nicolaou, K. C.; Mathison, C. J. N. *Angew. Chem., Int. Ed.* **2005**, *44*, 5992. (b) P. Griffith, W.; Reddy, B.; G. F. Shoair, A.; Suriaatmaja, M.; J. P. White, A.; J. Williams, D. *J Chem. Soc. Dalton Trans.* **1998**, 2819. (c) Yamazaki, S.; Yamazaki, Y. *Bull. Chem. Soc. Jpn.* **1990**, *63*, 301.

(14) (a) Kim, J.; Stahl, S. S. *ACS Catal.* **2013**, *3*, 1652. (b) Aiki, S.; Taketoshi, A.; Kuwabara, J.; Koizumi, T.-a.; Kanbara, T. *J. Organomet. Chem.* **2011**, *696*, 1301. (c) Zhang, Y.; Xu, K.; Chen, X.; Hu, T.; Yu, Y.; Zhang, J.; Huang, J. *J. Catal. Commun.* **2010**, *11*, 951. (d) Maeda, Y.; Nishimura, T.; Uemura, S. *Bull. Chem. Soc. Jpn.* **2003**, *76*, 2399. (e) Yamaguchi, K.; Mizuno, N. *Angew. Chem., Int. Ed.* **2003**, *42*, 1480. (f) Mori, K.; Yamaguchi, K.; Mizugaki, T.; Ebitani, K.; Kaneda, K. *Chem. Commun.* **2001**, 461. (g) Bailey, A. J.; James, B. R. *Chem. Commun.* **1996**, 2343. (h) Tang, R.; Diamond, S. E.; Neary, N.; Mares, F. *J. Chem. Soc. Chem. Commun.* **1978**, 562.

(15) (a) Nielsen, M.; Alberico, E.; Baumann, W.; Drexler, H.-J.; Junge, H.; Gladiali, S.; Beller, M. *Nature* **2013**, *495*, 85. (b) Rodriguez-Lugo, R. E.; Trincado, M.; Vogt, M.; Tewes, F.; Santiso-Quinones, G.; Grutzmacher, H. *Nature Chem.* **2013**, *5*, 342. (c) Spasyuk, D.; Smith, S.; Gusev, D. G. *Angew. Chem., Int. Ed.* **2012**, *51*, 2772. (d) Nielsen, M.; Junge, H.; Kammer, A.; Beller, M. *Angew. Chem., Int. Ed.* **2012**, *51*, 5711. (e) Marr, A. C. *Catal. Sci. Technol.* **2012**, *2*, 279. (f) Prades, A.; Peris, E.; Albrecht, M. *Organometallics* **2011**, *30*, 1162. (g) Johnson, T. C.; Morris, D. J.; Wills, M. *Chem. Soc. Rev.* **2010**, *39*, 81. (h) Dobereiner, G. E.; Crabtree, R. H. *Chem. Rev.* **2010**, *110*, 681.

(16) Yoshida, T.; Okano, T.; Otsuka, S. *J. Chem. Soc. Chem. Commun.* **1979**, 870.

(17) (a) Bernskoetter, W. H.; Brookhart, M. *Organometallics* **2008**, *27*, 2036. (b) Wang, Z.; Belli, J.; Jensen, C. M. *Faraday Discuss.* **2011**, *151*, 297. (c) Gu, X.-Q.; Chen, W.; Morales-Morales, D.; Jensen, C. M. *J. Mol. Catal. A: Chem* **2002**, *189*, 119.

(18) Tseng, K.-N. T.; Kampf, J. W.; Szymczak, N. K. *Organometallics* **2013**, *32*, 2046.

(19) (a) Wu, J.; Talwar, D.; Johnston, S.; Yan, M.; Xiao, J. *Angew. Chem., Int. Ed.* **2013**, *52*, 6983. (b) Schumperli, M. T.; Hammond, C.; Hermans, I. *ACS Catal.* **2012**, *2*, 1108. (c) Luca, O. R.; Wang, T.; Konezny, S. J.; Batista, V. S.; Crabtree, R. H. *New J. Chem.* **2011**, *35*, 998. (d) Yi, C. S.; Lee, D. W. *Organometallics* **2009**, *28*, 947.

(20) When 5 mol% of **1** was used, *n*-octylamine was converted to *n*-octanenitrile in 80% yield. While this small increase in conversion was noted with higher catalyst loadings, our standard reaction conditions employed 1 mol%.

(21) Kitamura, M., Noyori, R. Hydrogenation and Transfer Hydrogenation. In *Ruthenium in Organic Synthesis*; Murahashi, S.-I., Eds.; Wiley-VCH: Weinheim, Germany, 2005; pp 3.

(22) Doucet, H.; Ohkuma, T.; Murata, K.; Yokozawa, T.; Kozawa, M.; Katayama, E.; England, A. F.; Ikariya, T.; Noyori, R. *Angew. Chem., Int. Ed* **1998**, *37*, 1703.

(23) Murahashi, S.; Naota, T.; Ito, K.; Maeda, Y.; Taki, H. *J. Org. Chem.* **1987**, *52*, 4319.

(24) Hallman, P. S.; McGarvey, B. R.; Wilkinson, G. *J. Chem. Soc. A* **1968**, 3143.

- (25) Muthaiah, S.; Hong, S. H. *Adv. Synth. Catal.* **2012**, *354*, 3045.
- (26) We note that amine double dehydrogenation catalysis was reported (see ref 16) with a single amine substrate (benzylamine) in low yield with no experimental provided.
- (27) Blum, Y.; Shvo, Y. *J. Organomet. Chem.* **1985**, *282*, C7.
- (28) Note that this complex was previously reported to promote amine coupling to generate secondary amines. The proposed pathway operates *via* a hydrogen borrowing mechanism where imine dissociation occurs after amine dehydrogenation. The free imine is susceptible to nucleophilic attack by an amine, followed by ammonia elimination. See (a) B. L. Conley, M. K. Pennington-Boggio, E. Boz, T. J. Williams, *Chem. Rev.* **2010**, *110*, 2294 (b) Hollmann, D.; Haijun, J.; Spannerberg, A.; Bahn, S.; Tillack, A.; Parton, R.; Altink, R.; Beller, M. *Organometallics* **2009**, *28*, 473. (c) Jung, C. W.; Fellmann, J. D.; Garrou, P. E. *Organometallics* **1983**, *2*, 1042.
- (29) Oae, S. *Organic Sulfur Chemistry: Structure and Mechanism*; CRC Press; Boca Raton, Florida, 1991; pp 203.
- (30) (a) Crabtree, R. H. *Chem. Rev.* **2012**, *112*, 1536. (b) Widegren, J. A.; Finke, R. G. *J. Mol. Catal. A: Chem.* **2003**, *198*, 317.
- (31) Bayram, E.; Finke, R. G. *ACS Catal.* **2012**, *2*, 1967.
- (32) Water also acts as a catalyst poison. For instance, in the presence of 0.25 equiv of H₂O, 42% yield of *n*-octanenitrile was noted. Accordingly, the reproducibility of catalysis was highly susceptible to water content. All amines were subjected to an identical protocol for drying, and highly reproducible yields were obtained.
- (33) Attempts to elucidate the catalytic species under stoichiometric amine or nitrile conditions were complicated by the presence of paramagnetic species that were generated during the reaction.
- (34) Although 65% conversion was noted within 6 h for *n*-octylamine, 24 h was used for all amine substrates to ensure maximum conversion.
- (35) Note that primary aldimines are unstable under our reaction conditions, see reference: Lee, J. H.; Gupta, S.; Jeong, W.; Rhee, Y. H.; Park, J. *Angew. Chem., Int. Ed.* **2012**, *51*, 10851.
- (36) Large excess equiv of *n*-octanenitrile was used to attempt to duplicate the nitrile concentration under standard reaction conditions. Note that using 1 or 2 equiv of *n*-octanenitrile did not affect the overall yield.
- (37) Crabtree, R. H. *Energy Environ. Sci.* **2008**, *1*, 134.
- (38) Harris, R. O.; Hota, N. K.; Sadavoy, L.; Yuen, J. M. C. *J. Organomet. Chem.* **1973**, *54*, 259.
- (39) Abbel, R.; Kamaluddin, A.; Faatz, M.; Hadzovic, A.; Lough, A. J.; Morris, R. H. *J. Am. Chem. Soc.* **2005**, *127*, 1870.
- (40) Ahmad, N.; Levison, J. J.; Robinson, S. D.; Uttley, M. F. *Inorg. Synth.* **1974**, *15*, 45.

(41) Conley, B. L.; Pennington-Boggio, M. K.; Boz, E.; Williams T. J. *Chem. Rev.* **2010**, *110*, 2294.

(42) Yoshida, T.; Okano, T.; Otsuka, T. *J. Chem. Soc. Chem. Commun.* **1979**, 870.

CHAPTER 5

Iron-Catalyzed Hydrofunctionalization Reactions

Portions of this chapter have been published:

Tseng, K.-N. T.; Kampf, J. W.; Szymczak, N. K. *ACS Catal.* **2015**, *5*, 411. Reprinted with permission; Copyright (2015) American Chemical Society.

5.1 Introduction

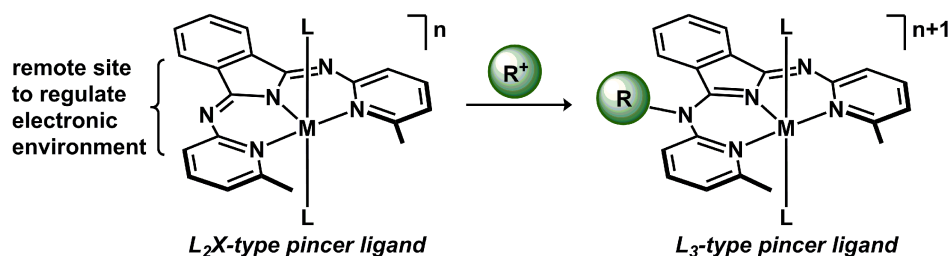


Figure 5-1 Electronic tunability of a pincer ligand *via* backbone alkylation.

Regulation of catalysis by an applied chemical, electrochemical, or photochemical response is broadly used in biology,¹ yet these principles are not widely adapted in synthetic systems.^{2,3} In some cases, modifications at a site far removed from a metal's active site can have dramatic effects on reactivity, substrate turnover, and importantly, can turn reactions on or off.⁴ To mimic such functions, metal complexes containing redox active and/or proton responsive ligands have been shown to work synergistically for selective bond activation and cooperative catalysis.^{5,6} Many multifunctional complexes direct reactivity by presenting groups at a site proximal to a metal's primary coordination sphere.⁷ Alternatively, a remote site removed from the primary coordination sphere environment can also serve to modify the electronic properties of a metal center without perturbing the primary coordination environment.^{6a,8} Our group is working to evaluate how the precise structural, electronic, and cooperative modes of a metal's secondary

coordination sphere can be used to regulate reactivity,^{6f,9} and herein, we report a system where the ligand's donor properties can be tuned by modifying a remote site (Figure 5-1).

We recently reported a series of Ru complexes containing an *N,N,N*-bMepi pincer ligand (bMepi = 1,3-bis(6'-methyl-2'-pyridylimino)isoindolate), which are precatalysts for the dehydrogenation of alcohols and amines.¹⁰ The backbone of the isoindoline framework contains imine linkers whose lone pair can be engaged upon protonation.¹¹ Alternatively, alkylation or binding a Lewis acid to the imine may also be used to confer a more electrophilic metal environment to bias catalytic reactivity.

One class of reactions to test these reactivity concepts are hydrogenation¹² and/or hydrofunctionalization¹³ reactions because the rate-limiting steps are largely influenced by electronics at the metal. In particular, transition-metal catalyzed olefin hydroboration is an atom-economical and selective methodology to generate alkyl boronate esters,¹⁴ which are widely used as intermediates in organic synthesis.¹⁵ Although this reaction has classically required expensive Rh or Ir catalysts,^{14b,16} a few recent reports have shown that a select few low-valent Fe complexes can also catalyze olefin hydroboration.¹⁷ In this communication, we report the synthesis and characterization of Fe–bMepi complexes and showcase the ligand's electronic tunability by modifying a remote site within the secondary coordination sphere in order to control activity and selectivity in olefin hydroboration reactions.

5.2 Results and Discussion

5.2.1 Syntheses and Characterization of Iron–bMepi Complexes

The Fe(bMepi)Br complex¹⁸ was synthesized using a similar methodology to that reported for bMepi-ligated Ru complexes recently reported by our laboratory.^{10a} Addition of 1.05 equiv of the K(bMepi) to FeBr₂ over 17 h in THF solvent afforded the desired complex, Fe(bMepi)Br, as an orange solid in 83% yield (Figure 5-2). The ¹H NMR spectrum features six paramagnetically shifted resonances, which is consistent with symmetric binding of the ligand. Crystals suitable for single-crystal X-ray diffraction were obtained from vapor diffusion of pentane into a THF solution of Fe(bMepi)Br, and the solid-state structure reveals a distorted trigonal monopyramidal geometry around the Fe(II) center ($\tau' = 1.10$).¹⁹ The solution magnetic

moment of Fe(bMepi)Br is $5.1 \mu_B$, as assessed using the Evans method in CD_2Cl_2 , which is consistent with a high spin, $S = 2$ molecule. The analogous triflate (OTf = $-CF_3SO_3$) complex, Fe(bMepi)(THF)OTf, was isolated as a brown solid in 84% yield by allowing equimolar amounts of Fe(bMepi)Br and TlOTf to react in THF solvent for 2 h (Figure 5-2). 1H NMR spectroscopy revealed six paramagnetically shifted resonances ($\mu_{eff} = 5.1 \mu_B$), distinct from those observed for Fe(bMepi)Br. A brown crystal of Fe(bMepi)(THF)OTf was subjected to an X-ray diffraction experiment, and the solid-state structure exposed a square-based pyramid geometry around the Fe(II) center ($\tau = 0.06$)²⁰ with a THF ligand *trans* to the triflate anion (Figure 5-2).

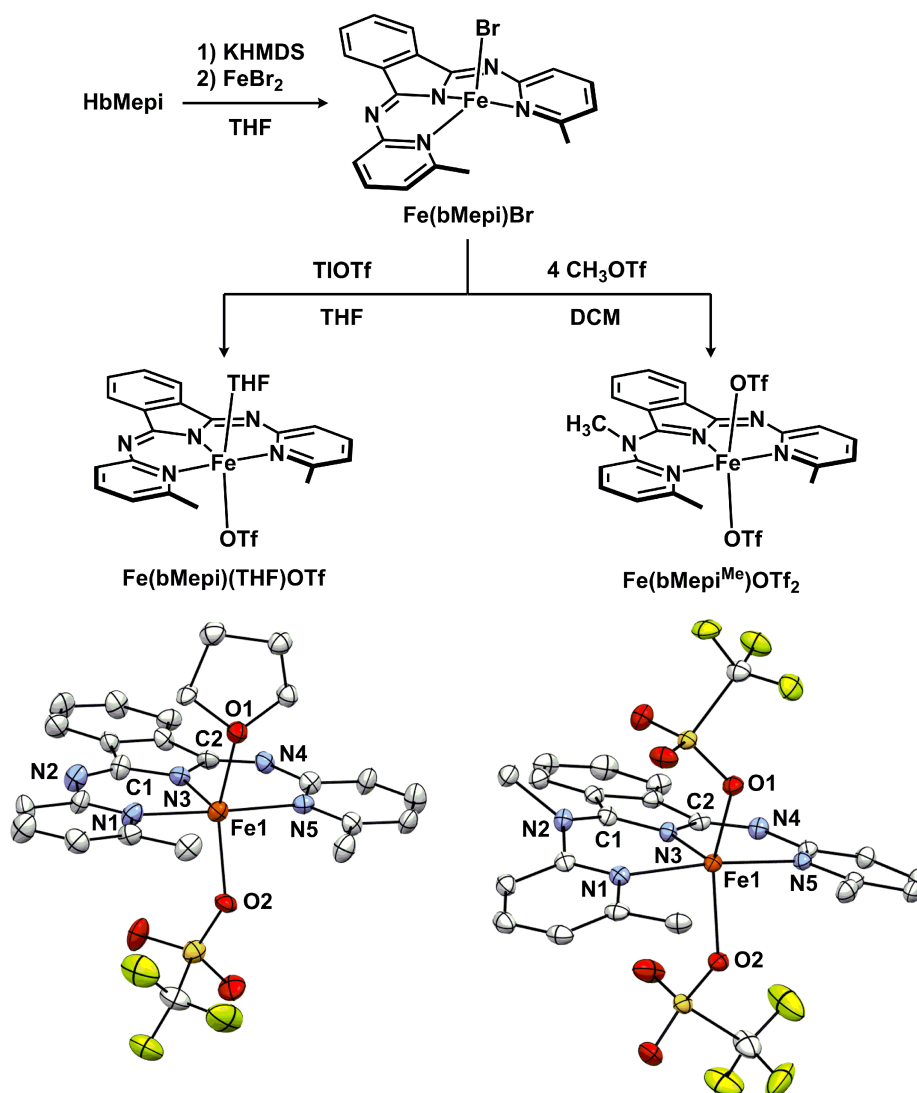


Figure 5-2 Synthesis of Fe(bMepi)(THF)OTf (left) and Fe(bMepi^{Me})OTf₂ (right) with thermal ellipsoids depicted at 50% probability.

We next examined the viability of modifying the bMepi pincer scaffold by treatment with an electrophile, which we predicted would induce a change from an L_2X -type to an L_3 -type ligand. When $\text{Fe}(\text{bMepi})\text{Br}$ was subjected to a Brønsted acid such as HOTf, a mixture of products was obtained, which is likely due to multiple reversible protonation events. In contrast, the addition of 4 equiv of MeOTf to a suspension of $\text{Fe}(\text{bMepi})\text{Br}$ in CH_2Cl_2 resulted in the clean conversion to $\text{Fe}(\text{bMepi}^{\text{Me}})\text{OTf}_2$ after 21 h, isolated in 86% yield as brown crystalline plates (Figure 5-2). The solid-state structure reveals a distorted square-based pyramid geometry about Fe ($\tau = 0.21$)²⁰ with an asymmetric neutral bMepi^{Me} ligand meridionally coordinated with two *trans* triflate ligands. The asymmetry of the bMepi^{Me} ligand is retained in solution, confirmed by 13 distinct paramagnetically shifted resonances in the ^1H NMR spectrum, and the solution magnetic moment of $5.1 \mu_{\text{B}}$ is consistent with a high spin $S = 2$ Fe(II) complex.

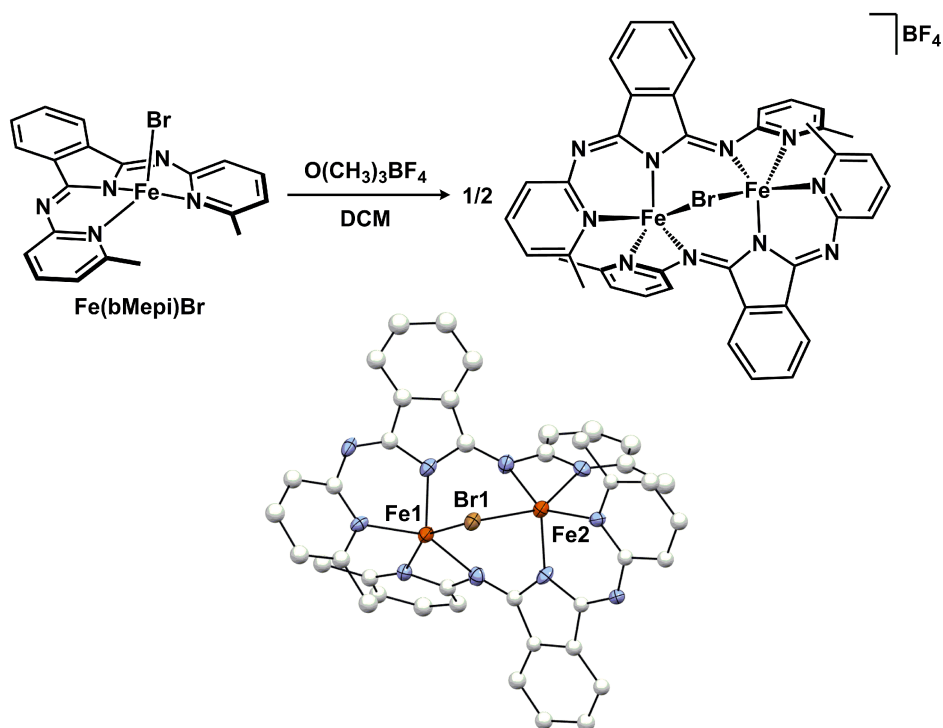


Figure 5-3 Synthesis and crystal structure (thermal ellipsoids depicted at 30% probability) of $\text{Fe}_2(\text{bMepi})_2\text{Br}[\text{BF}_4]$.

Prior to the formation of $\text{Fe}(\text{bMepi}^{\text{Me}})\text{OTf}_2$, CH_3Br loss afforded an intermediate dimer ($\text{Fe}_2(\text{bMepi})_2[\text{BF}_4]$). The addition of 1.05 equiv $\text{O}(\text{CH}_3)_3\text{BF}_4$ to a DCM solution of $\text{Fe}(\text{bMepi})\text{Br}$ resulted in the conversion to $\text{Fe}_2(\text{bMepi})_2[\text{BF}_4]$ after 3 h. The ^1H NMR spectrum features 12 distinct paramagnetically shifted resonances, which is consistent with asymmetric binding of the

ligand. Crystals suitable for single-crystal X-ray diffraction were obtained from layering pentane on top of a DCM solution of $\text{Fe}_2(\text{bMepi})_2[\text{BF}_4]$ at 5 °C. The solid-state structure shows distorted square-based pyramid geometries about the Fe centers (Fe1 , $\tau = 0.09$; Fe2 , $\tau = 0.05$)²⁰ with 2 bMepi ligands coordinated across the Fe centers and a bridging Br ligand (Figure 5-3).

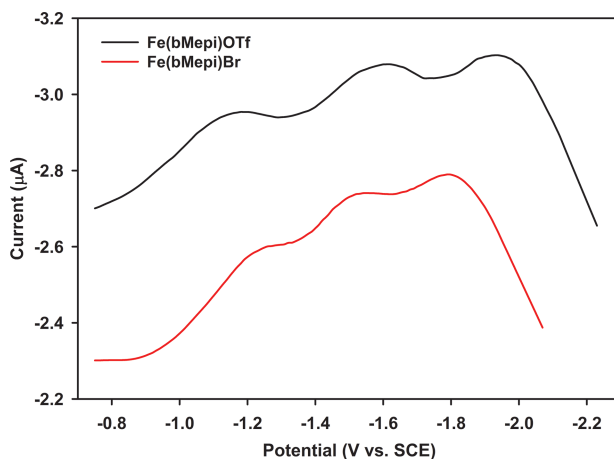


Figure 5-4 DPV of $\text{Fe}(\text{bMepi})\text{Br}$ and $\text{Fe}(\text{bMepi})(\text{THF})\text{OTf}$.

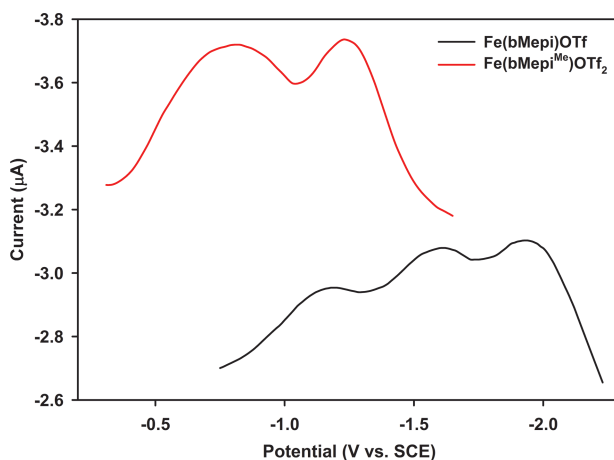


Figure 5-5 DPV of $\text{Fe}(\text{bMepi})(\text{THF})\text{OTf}$ and $\text{Fe}(\text{bMepi}^{\text{Me}})\text{OTf}_2$.

The electronic differences at the Fe center imposed by bMepi and bMepi^{Me} were assessed by electrochemical studies. Differential pulse voltammetry (DPV) was used to evaluate the reduction potentials cathodic of the open-circuit potential for the three Fe complexes at a Pt electrode in 0.1 M $[\text{nBu}_4\text{N}]\text{PF}_6$ in THF. The potentials for the first reduction event of $\text{Fe}(\text{bMepi})\text{Br}$ and $\text{Fe}(\text{bMepi})(\text{THF})\text{OTf}$ are within 60 mV (-1.26 and -1.20 V versus SCE,

respectively; Figure 5-4), which is consistent with similar ligand donor strength of Br^- and OTf^- ligands.²¹ In contrast, $\text{Fe}(\text{bMepi}^{\text{Me}})\text{OTf}_2$ exhibits a reductive wave anodically shifted by 390 mV (-0.81 V versus SCE; Figure 5-5) from $\text{Fe}(\text{bMepi})(\text{THF})\text{OTf}$, suggesting that the bMepi^{Me} ligand furnishes a more stable reduced species.²²

5.2.2 Hydroboration of 1-Octene Catalyzed by $\text{Fe}(\text{bMepi})\text{Br}$

As quantified by electrochemical experiments, $\text{Fe}(\text{bMepi}^{\text{Me}})\text{OTf}_2$ features a metal center that is more electrophilic than $\text{Fe}(\text{bMepi})(\text{THF})\text{OTf}$ and thus easier to reduce. The difference in electrophilicity might be exploited by a catalytic hydrofunctionalization reaction whose rate-determining steps are perturbed by electronics at a metal site.^{8a} We initiated studies by examining the hydroboration of 1-octene, a transformation most commonly performed with Rh or Ir complexes.^{14b,16,23} When a vial containing $\text{Fe}(\text{bMepi})\text{Br}$ (2.5 mol%) in neat 1-octene (1.0 mmol) was charged with 2.0 mmol of catecholborane (HBCat) or pinacolborane (HBPin), NaHBET_3 (7.5 mol%) and stirred at 23 °C for 20 h, the anti-Markovnikov hydroboration product (**1** and **2**) was isolated in 99% and 90% yield, respectively (Figure 5-6).²⁴ *In situ* examination of the reaction mixture revealed no branched or dehydrogenative borylation products, determined by GC-MS, and control experiments showed that $\text{Fe}(\text{bMepi})\text{Br}$ and NaHBET_3 were both required for catalysis.

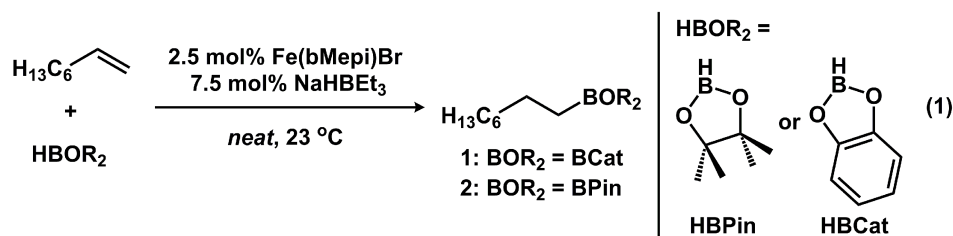


Figure 5-6 Hydroboration of 1-octene catalyzed by $\text{Fe}(\text{bMepi})\text{Br}$.

5.2.3 Olefin and Alkyne Hydroboration Catalyzed by Electronically Distinct Iron Complexes

In order to evaluate the catalytic competence of the electronically distinct Fe complexes, as well as the generality of the hydroboration reaction, the reaction products of hydroboration mediated by both $\text{Fe}(\text{bMepi})(\text{THF})\text{OTf}$ and $\text{Fe}(\text{bMepi}^{\text{Me}})\text{OTf}_2$ systems were assessed. Hydroboration reactivity with acyclic and cyclic olefins was investigated, and both were

converted to the boronate ester as the sole product (Figure 5-7). For instance, when either Fe(bMepi)(THF)OTf or Fe(bMepi^{Me})OTf₂ was used, the hydroboration of 1-octene afforded the corresponding anti-Markovnikov product **2** in high yields (88% and 91%, respectively). Furthermore, cyclooctyl boronate ester (**3**) was formed from cyclooctene (COE) in high isolated yields, 84% and 90% for Fe(bMepi)(THF)OTf and Fe(bMepi^{Me})OTf₂, respectively.²⁵

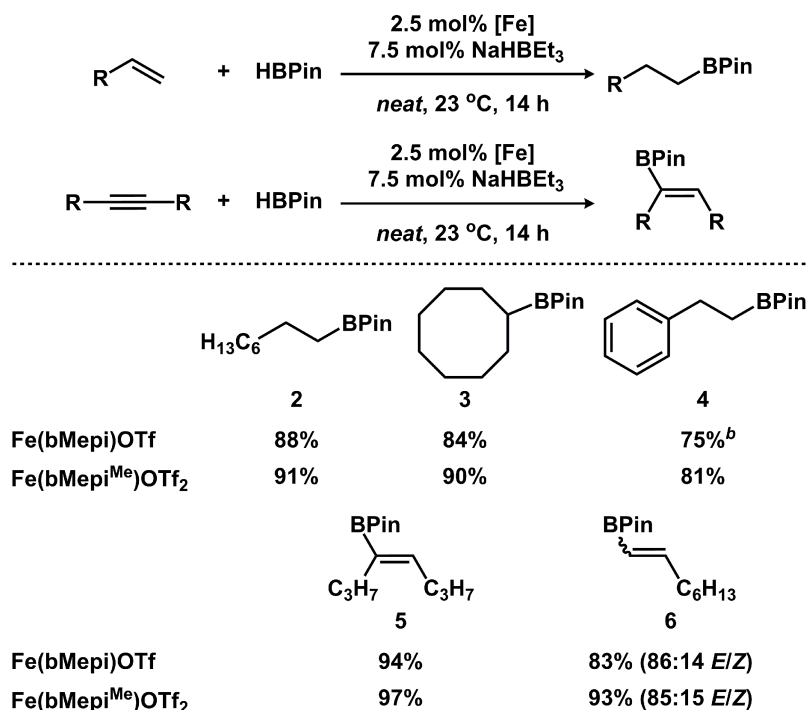


Figure 5-7 Hydroboration of unsaturated hydrocarbons catalyzed by Fe(bMepi)(THF)OTf or Fe(bMepi^{Me})OTf₂.

Guided by the high selectivity for anti-Markovnikov hydroboration of aliphatic olefins, we examined whether regioselective hydroboration was possible with styrene (Figure 5-7), an activated alkene that has proven challenging for Rh and Fe catalysts.^{14b,17b} When the hydroboration of styrene was performed with Fe(bMepi)(THF)OTf, the anti-Markovnikov hydroboration product was generated in 75% yield, however dehydrogenative borylation and hydrogenation products were also detected by ¹H NMR spectroscopy.²⁶ In contrast, **4** was obtained in 81% isolated yield as the *exclusive* product when using Fe(bMepi^{Me})OTf₂ under the same reaction conditions. The hydroboration of internal and terminal alkynes also afforded high conversions of the corresponding vinyl boronate esters with stereoselectivity dependent on the substrate (Figure 5-7). For example, the conversion of 1-octyne to **6** proceeded with a

regioselectivity of 86:14 and 85:15 *E/Z* for Fe(bMepi)(THF)OTf and Fe(bMepi^{Me})OTf₂ precatalysts, respectively. In contrast, when 4-octyne was used as the substrate, a single regioisomer (**5**) was formed in high yields (94% and 97%) when using either precatalyst.

5.2.4 The Effect of the Metal Environment on Rate of Hydroboration

In addition to the reaction regioselectivity, we evaluated the effect of the metal–ligand electronic environment on reaction rate. The rates of 1-octene hydroboration catalyzed by Fe(bMepi)Br, Fe(bMepi)(THF)OTf, and Fe(bMepi^{Me})OTf₂ were obtained by using the method of initial rates. The reaction rates for Fe(bMepi)Br ($5.2(3) \times 10^{-4}$ M/s, Figure 5-8) and Fe(bMepi)(THF)OTf ($5.2(4) \times 10^{-4}$ M/s, Figure 5-9) were identical, which is consistent with the similar reduction potentials, *vide supra*. Electron-deficient metal complexes can accelerate certain organometallic transformations including reductive elimination,^{8a} which is a key step in catalytic hydroboration reactions. The reaction rate was significantly increased (>4×) when Fe(bMepi^{Me})OTf₂ ($2.2(3) \times 10^{-3}$ M/s, Figure 5-10) was used instead of Fe(bMepi)X (X = Br, OTf). Furthermore, an identical reaction rate ($5.4(4) \times 10^{-4}$ M/s) was obtained for Fe(bMepi)(THF)OTf when sodium naphthalenide was used as the reductant, which suggests that the alkylation state affects an elementary step within the catalytic cycle, rather than reduction to a low valent state. The enhancement of catalytic rates demonstrates the dramatic impact that may be realized through simple electronic modifications of a ligand's secondary coordination environment.

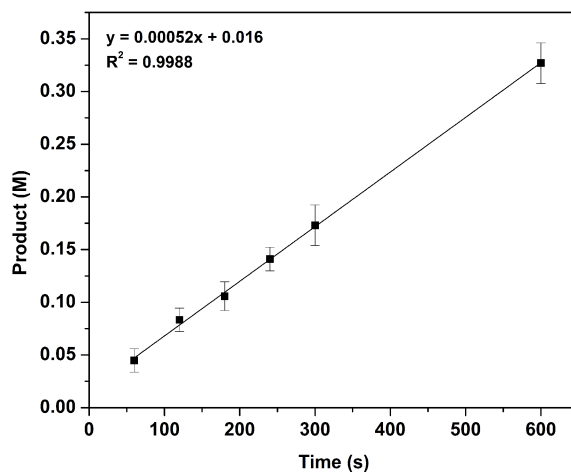


Figure 5-8 Initial rate of 1-octene hydroboration for Fe(bMepi)Br.

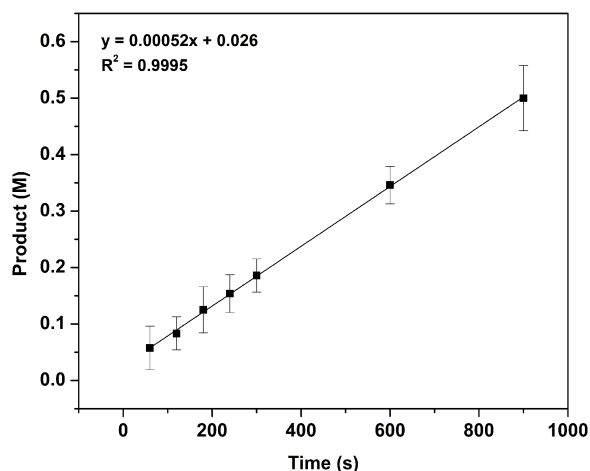


Figure 5-9 Initial rate of 1-octene hydroboration for Fe(bMepi)(THF)OTf.

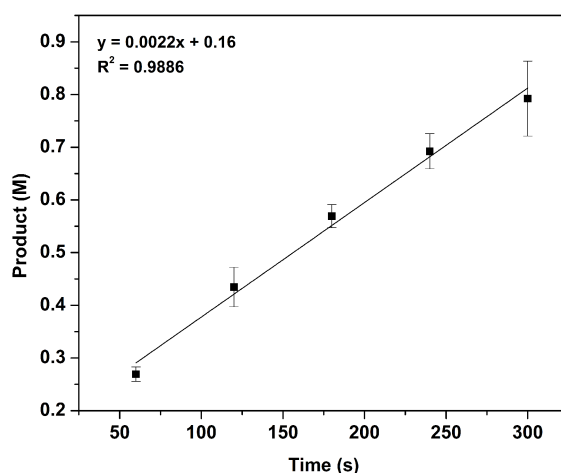


Figure 5-10 Initial rate of 1-octene hydroboration for Fe(bMepi^{Me})OTf₂.

5.2.5 Distinct Selectivity for Internal Alkene Hydroboration

The synthesis of branched alkyl boronate esters using HBPin from acyclic internal olefins remains a limitation of metal-catalyzed hydroboration reactions,^{14b,27} and only one Fe catalyst has been reported for this transformation.^{17c} During catalysis, chain walking is often fast and reversible, relative to C–B bond formation at the terminal position of an aliphatic acyclic substrate, which affords linear boronate esters.^{17c,28} Based on the reaction rate enhancement observed for the hydroboration of 1-octene, we hypothesized that the hydroboration of an acyclic internal olefin catalyzed by Fe(bMepi^{Me})OTf₂ should yield branched hydroboration products due to acceleration of the rate-limiting reductive elimination step (Figure 5-11). Indeed, when *cis*-4-octene was subjected to Fe(bMepi^{Me})OTf₂, a mixture of **7**, **8**, **9**, and **10** was isolated in a 4:1 ratio

of branched to linear hydroboration products. In contrast, only the linear product (**7**) was obtained in when using Fe(bMepi)(THF)OTf. Hence, in addition to enhanced reaction rates, the regioselectivity of olefin hydroboration was also affected by tuning the electrophilicity of Fe complexes from a remote site in the secondary coordination sphere.

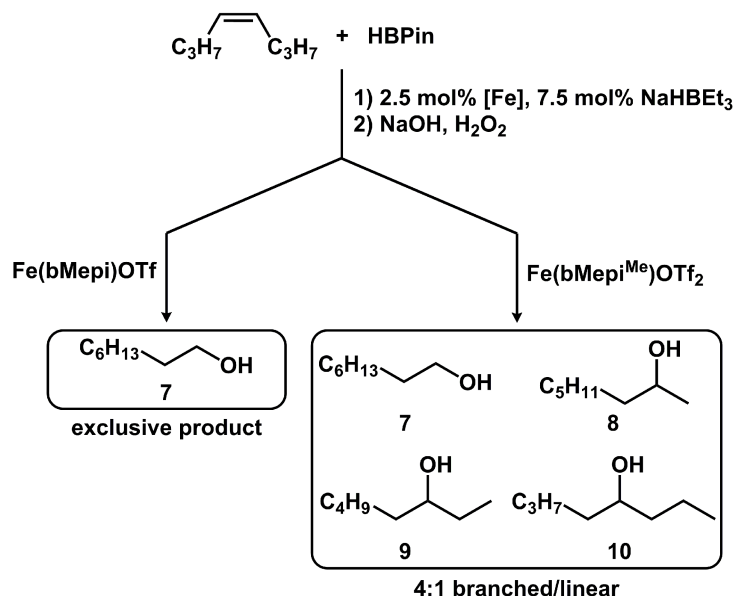


Figure 5-11 Selectivity of internal alkene hydroboration.

5.2.6 Poisoning Experiments for Iron-Catalyzed Alkene Hydroboration

Fe nanoparticles, formed from molecular Fe(II) precatalysts, have been implicated as the catalytically-active species in several Fe-mediated reductive reactions.²⁹ Because catalyst structure/function re-optimization is predicated on the knowledge (or assumption) of active catalyst structure, the elucidation of catalyst nuclearity is critical. In contrast to irreproducible kinetic data often associated with heterogeneous catalysts, reproducible kinetic data has been observed from reactions catalyzed by homogeneous catalysts as well as nanoparticles.³⁰ We probed the active catalyst identity of Fe(bMepi^{Me})OTf₂ promoted 1-octene hydroboration to interrogate the nature of the observed catalysis. Although classic mercury poisoning experiments are an ineffective method of catalyst identification with Fe catalysis,^{29,31} substoichiometric ligand poisoning experiments are a simple and effective means of assessing whether a given precatalyst forms a catalyst of higher nuclearity.³² Complete poisoning of catalysis was observed with 2 equiv of PMe₃ (Figure 5-12). In contrast, in the presence of 0.1 and 0.5 equiv of PMe₃, the

product distribution remained unchanged. These results are inconsistent with a heterogeneous or nanoparticle system where low surface area aggregates are typically poisoned by $\ll 1$ equiv of ligand poison. Finally, in the absence of any poisoning reagent, nonsigmoidal reaction profiles and a lack of induction period are consistent with a homogeneous iron complex as the active catalytic species.

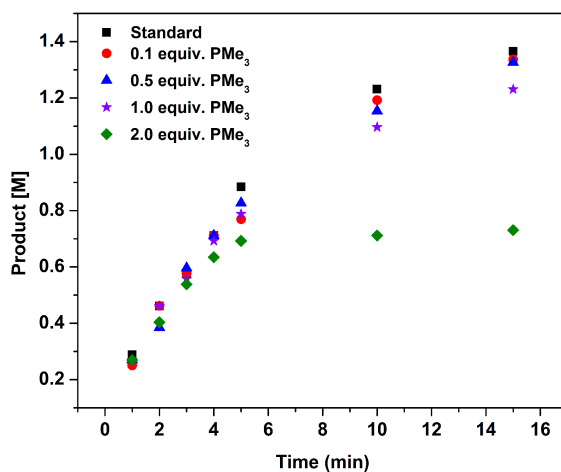


Figure 5-12 Reaction profiles of 1-octene hydroboration with and without added PMe_3 .

5.2.7 Iron-Catalyzed Hydrosilylation of Ketones

Given the same principles of hydroboration reactions can be applied to hydrosilylation reactions, we initiated studies by examining the hydrosilylation of 1-octene. Unfortunately no hydrosilylation was observed when a vial containing 5 mol% $\text{Fe}(\text{bMepi})\text{X}$ ($\text{X} = \text{Br}, \text{I}, \text{OTf},$ or CH_2SiMe_3) and 15 mol% NaHBEt_3 in neat 1-octene and silane ($\text{PhSiH}_3, \text{HSiEt}_3, \text{HSi}(\text{OEt})_3,$ or H_2SiMePh) was stirred at 100°C for 24 h. However, we hypothesized that hydrosilylation of ketones should be possible because prior literature report demonstrated asymmetric hydrosilylation of ketones catalyzed by Co with chiral ligands based on the bMepi framework.³³ Indeed, when a benzene solution containing acetophenone, 5 mol% $\text{Fe}(\text{bMepi})(\text{CH}_2\text{SiMe}_3)$, and silane ($\text{HSi}(\text{OEt})_3$ or H_2SiMePh) was heated to 50°C for 17 h, the corresponding hydrosilylation product, determined by ^1H NMR spectroscopy, was observed in quantitative (>99%) yield (Figure 5-13). Control experiments showed no reaction in the absence of $\text{Fe}(\text{bMepi})(\text{CH}_2\text{SiMe}_3)$. Furthermore, no reaction took place in the absence of an internal basic site. For instance, under the reaction conditions listed above, no hydrosilylation product was detected when $\text{Fe}(\text{bMepi})\text{Br}$ or $\text{Fe}(\text{bMepi})(\text{THF})\text{OTf}$ was employed.

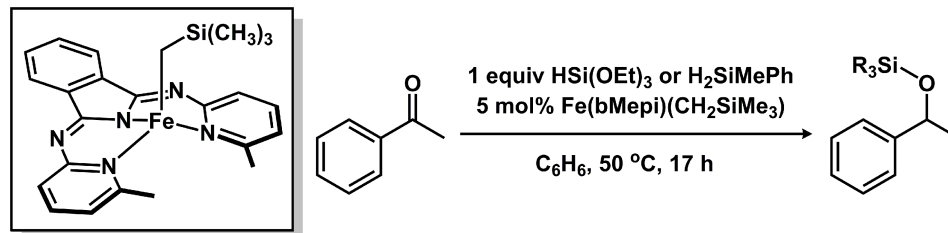


Figure 5-13 Hydrosilylation of acetophenone catalyzed by Fe(bMepi)(CH₂SiMe₃).

5.2.8 Summary

In conclusion, this work demonstrates the application of using a catalyst's secondary coordination environment to facilitate facile electronic modifications that can change reaction activity and selectivity. We have developed Fe–bMepi complexes capable of catalyzing the hydroboration of olefins and alkynes at room temperature and hydrosilylation of ketones. Although prior reports demonstrated Fe-catalyzed olefin hydroboration, our systems are unique because they feature control over activity and regioselectivity by modifications at a remote site on the ligand backbone, which serve to tune the ligand's electronic environment. Of particular note, higher reaction rate and distinct regioselectivity were observed for olefin hydroboration when using the more electrophilic Fe(bMepi^{Me})OTf₂ complex.

5.3 Experimental Section

5.3.1 General Considerations

All manipulations were conducted under a nitrogen atmosphere on a Schlenk manifold or in a glovebox using standard Schlenk techniques, unless otherwise stated. All reagents were purchased from commercial vendors. HBPIn (Aldrich), HBCat (Aldrich), NaHBET₃ (1.0 M in toluene, Aldrich), KHMDS (Aldrich), FeBr₂ (Alfa Aesar), TlOTf (Aldrich), TfOH (Aldrich) and MeOTf (Aldrich) were used without further purification. All hydroboration substrates (1-octene, Aldrich; COE, Aldrich; styrene, Aldrich; 4-octyne, Aldrich; 1-octyne, Aldrich; cis-4-octene, Alfa Aesar) were distilled from CaH₂ under a nitrogen atmosphere, and then stored over 3Å molecular sieves for 24 h. The 3Å Molecular sieves were dried at 250 °C under dynamic vacuum for 24 h. Dichloromethane (DCM), diethyl ether (Et₂O), pentane, and tetrahydrofuran (THF) was purified using a Glass Contour solvent purification system consisting of a copper catalyst, neutral

alumina, and activated molecular sieves, then passed through an in-line, 2 μm filter immediately before being dispensed.

NMR spectra were recorded on Varian Inova 500, Varian MR400, and Varian vnmrs 500 spectrometers. To collect the ^1H NMR spectra of the Fe complexes, the relaxation delay was set to 0.05 s and the acquisition time was set to 0.2 s. Elemental Analyses were performed by Midwest Microlab, LLC. Solution magnetic moments were measured using Evans method;³⁴ for these measurements, concentrations were typically around 10 mM. GC-MS analyses were performed using a Shimadzu QP-2010 GC/MS; the GC contains a 30 m long DB-5 column with a 0.25 mm I.D. GC measurements were conducted using the following method: 30 $^\circ\text{C}$ hold for the first 8 min, ramp to 270 $^\circ\text{C}$ at 10 $^\circ\text{C}/\text{min}$, and the solvent cutoff was set for 3 min. The respective response factor was obtained by the GC analysis of a series of samples of known concentration, plotting the ratio of the areas, $A_{\text{sample}}/A_{\text{standard}}$ of each versus the ratio of the concentrations, $[\text{Sample}]/[\text{Standard}]$.

For electrochemical measurements, the electrochemical cell consisted of a modified three electrode set-up with a glassy carbon working electrode, a Pt counter electrode, and an Ag wire pseudo-reference electrode. Differential pulse voltammetry (DPV) was measured in THF with 0.1 M NBu_4PF_6 as the supporting electrolyte. Ferrocene was used as an internal reference and introduced at the end of the experiment, and then the voltammograms were referenced to SCE (ferrocene/ferrocenium = 0.56 V versus SCE in THF).³⁵

5.3.2 Preparation of Iron–bMepi Complexes

Fe(bMepi)Br. THF (10 mL) was added to a 20 mL vial charged with K(bMepi) (521 mg, 1.429 mmol), FeBr_2 (294 mg, 1.361 mmol), and a stir bar. The resulting solution was stirred at room temperature for 17 h and the THF solvent was removed under vacuum. The crude product was washed with Et_2O (4×20 mL) and extracted with DCM (4×25 mL) to afford an orange solution. The DCM extractions were combined and concentrated under vacuum to 10 mL and then layered with Et_2O (90 mL). After 24 h at room temperature, the precipitates were collected and washed with Et_2O (4×20 mL) to afford the product as an orange powder. Yield: 522 mg (83%). Crystals were obtained from vapor diffusion of pentane into a THF solution at room temperature. ^1H NMR (500 MHz, THF): δ 51.37 (s, 2H), 26.86 (br s, 8H), 10.86 (s, 2H), 10.11 (s,

2H), -2.42 (s, 2H). IR (ATR, cm^{-1}): 3053, 2971, 1660, 1592, 1538, 1444, 1363, 1288, 1239, 1191, 1160, 1077, 996, 818, 784, 709. Anal. Calculated for $\text{C}_{20}\text{H}_{16}\text{BrFeN}_5$ (found): C, 51.98 (51.77); H, 3.49 (3.59); N, 15.15 (14.97). Solution effective magnetic moment (CD_2Cl_2) = $5.1 \mu_{\text{B}}$.

Fe(bMepi)(THF)OTf. THF (10 mL) was added to a 20 mL vial charged with Fe(bMepi)Br (114 mg, 0.246 mmol), TiOTf (87 mg, 0.246 mmol), and a stir bar. The reaction solution was stirred at room temperature for 2 h and then filtered to remove TiBr. The filtered solution was concentrated to 2 mL and then layered with pentane and placed at $-35 \text{ }^\circ\text{C}$ to precipitate out the product. After 24 h, the precipitates were collected and washed with pentane ($4 \times 10 \text{ mL}$) to afford the product as a brown powder. Yield: 125 mg (84%). Crystals were obtained from vapor diffusion of pentane into a THF solution at $5 \text{ }^\circ\text{C}$. ^1H NMR (500 MHz, THF): δ 60.56 (s, 2H), 32.92 (s, 2H), 23.42 (br s, 6 H), 7.21 (s 2H), 6.85 (s, 2H), 4.87 (s, 2H). IR (ATR, cm^{-1}): 3288, 3072, 1635, 1581, 1530, 1438, 1312, 1290, 1207, 1185, 1100, 1028, 897, 801, 780, 713. Anal. Calculated for $\text{C}_{25}\text{H}_{24}\text{F}_3\text{FeN}_5\text{O}_4\text{S}$ (found): C, 49.76 (49.78); H, 4.01 (4.00); N, 11.61 (11.53). Solution effective magnetic moment (THF) = $5.1 \mu_{\text{B}}$.

Fe(bMepi^{Me})OTf₂. MeOTf (100 μL , 0.926 mmol) was added to Fe(bMepi)Br (107 mg, 0.232 mmol) suspended in DCM (10 mL) charged with a stir bar. The reaction solution was allowed to stir at room temperature for 21 h and the DCM solvent was removed under vacuum. The crude product was washed with Et_2O ($4 \times 10 \text{ mL}$) and extracted with DCM (5 mL). The DCM solution was layered with Et_2O (45 mL). After 24 h at $-35 \text{ }^\circ\text{C}$, brown crystalline plates were collected and washed with Et_2O ($4 \times 10 \text{ mL}$) to afford crystals suitable for X-Ray diffraction experiment. Yield: 138 mg (86%). ^1H NMR (400 MHz, CD_2Cl_2): δ 60.17 (s, 1H), 55.19 (br s, 3H), 50.74 (s, 1H), 44.91 (s, 1H), 40.62 (s, 1H), 26.92 (s, 3H), 18.89 (br s, 3H), 10.56 (s, 1H), 6.00 (s, 1H), 2.45 (s, 1H), -0.93 (s, 1H), -6.73 (s, 1H), -7.38 (s, 1H). IR (ATR, cm^{-1}): 3094, 1660, 1606, 1520, 1456, 1406, 1311, 1233, 1204, 1165, 1114, 1007, 903, 809, 775, 710. Anal. Calculated for $\text{C}_{23}\text{H}_{19}\text{F}_6\text{FeN}_5\text{O}_6\text{S}_2$ (found): C, 39.73 (39.54); H, 2.75 (2.85); N, 10.07 (10.12). Solution effective magnetic moment (CD_2Cl_2) = $5.1 \mu_{\text{B}}$.

Fe(bMepi)I. THF (10 mL) was added to a 20 mL vial charged with K(bMepi) (214 mg, 0.586 mmol), $\text{FeI}_2(\text{CO})_4$ (235 mg, 0.558 mmol), and a stir bar. The resulting solution was allowed to stir at room temperature for 21 h and the THF solvent was removed under vacuum. The crude product was washed with Et_2O ($4 \times 20 \text{ mL}$), and then extracted with DCM (4×25

mL) to afford an orange solution. The DCM extractions were combined and concentrated under vacuum to 10 mL and then layered with Et₂O (90 mL). After 24 h at room temperature, the precipitates were collected and washed with Et₂O (4 × 20 mL) to afford the product as an orange powder. Yield: 256 mg (90%). Crystals were obtained from vapor diffusion of pentane into a THF solution at 5 °C. ¹H NMR (500 MHz, THF): δ 58.07 (s, 2H), 37.78 (br s, 8H), 29.34 (s, 2H), 12.15 (s, 2H), 10.88 (s, 2H), -0.42 (s, 2H). IR (ATR, cm⁻¹): 3050, 2974, 2844, 1663, 1591, 1539, 1444, 1356, 1287, 1236, 1190, 1157, 1077, 995, 812, 777, 709. Anal. Calculated for C₂₀H₁₆FeIN₅ (found): C, 47.18 (47.16); H, 3.17 (3.30); N, 13.76 (13.65). Solution effective magnetic moment (CD₂Cl₂) = 4.7 μ_B.

Fe₂(bMepi)₂Br[BF₄]. DCM (5 mL) was added to a 20 mL vial charged with Fe(bMepi)Br (50.5 mg, 0.109 mmol), O(CH₃)₃BF₄ (17.0 mg, 0.115 mmol), and a stir bar. The resulting solution was allowed to stir at room temperature for 3 h. The volatiles were removed under vacuum, and the crude product was washed with C₆H₆ (4 × 10 mL), DME (4 × 10 mL), and pentane (4 × 10 mL). Evaporation of the volatiles under vacuum afforded the product as a brown powder. Crystals were obtained from layering pentane on top of a DCM solution at 5 °C. Yield: 27 mg (42%). ¹H NMR (400 MHz, CD₂Cl₂): δ 81.94 (s, 4H), 68.87 (s, 4H), 54.56 (s, 4H), 53.68 (s, 4H), 40.04 (s, 4H), 35.20 (s, 4H), 34.92 (s, 4H), 23.44 (s, 4H), 9.73 (s, 4H), -6.06 (s, 4H), -40.94 (s, 6H), -56.37 (br s, 6H).

5.3.3 General Procedure for Catalytic Hydroboration

An 8 mL vial was charged with 0.025 mmol of the Fe precatalysts (Fe(bMepi)Br, 11.6 mg; Fe(bMepi)(THF)OTf, 15.1 mg; Fe(bMepi^{Me})OTf₂, 17.4 mg), 2 mmol of borane (HBCat, 215 μL; HBPin 290 μL), and NaHBEt₃ (75 μL, 0.075 mmol). The mixture was stirred for 3 min then 1 mmol of substrate (1-octene, 155 μL; COE, 130 μL; styrene 115 μL; 4-octyne 145 μL; 1-octyne 145 μL; *cis*-4-octene, 155 μL) was added. The vial was then capped and stirred for 14 h. The reaction was quenched by exposing the mixture to air. The solvent was evaporated under vacuum, and the residue was purified through a plug of silica gel eluting with pentane (5 mL). In the case of 1-octyne, *E*-**6** was purified by flash column chromatography using hexanes:ethyl acetate (9:1). A colorless oil was obtained after evaporation of pentane under vacuum. The identity of the hydroboration product was confirmed by comparison to previously reported ¹H NMR data of known compounds.

5.3.4 General Procedure for Hydroboration–Oxidation

The reaction of *cis*-4-octene with HBPIn using Fe(bMepi^{Me})OTf₂ yielded multiple products. To confirm the identity of the hydroboration products, oxidation with hydrogen peroxide was performed according to a previously reported procedure.³⁶ The oxidized mixture contained 1-octanol (**7**), 2-octanol (**8**), 3-octanol (**9**), and 4-octanol (**10**) as determined by GC-MS analysis.

5.3.5 General Procedure for Kinetic Experiments

Following the general procedure for catalytic olefin hydroboration, the kinetic experiments were conducted by sampling 5 μL aliquots into a GC-MS vial containing 5 μL 1-phenylethanol, which immediately quenched the reaction. The aliquots were diluted with 1 mL DCM and the yields were determined by GC-MS analysis. To confirm reproducibility and determine the initial rate, all kinetic experiments were performed in triplicate.

5.3.6 General Procedure for Poisoning Experiments

Following the general procedure for the kinetic experiments, the poisoning experiments were conducted by allowing the reaction to proceed for 4 min, and then PMe₃ was added to the reaction solution.

5.4 References

- (1) Lehninger, A. L.; Nelson, D. L.; Cox, M. M. *Principles of Biochemistry*; W. H. Freeman: New York, 2008.
- (2) (a) Raynal, M.; Ballester, P.; Vidal-Ferran, A.; van Leeuwen, P. W. N. M. *Chem. Soc. Rev.* **2014**, *43*, 1734. (b) Allgeier, A. M.; Mirkin, C. A. *Angew. Chem., Int. Ed.* **1998**, *37*, 894.
- (3) Traut, T. *Allosteric Regulatory Enzymes*; Springer: New York, 2008.
- (4) Feringa, B. L. *Molecular Switches*; Wiley-VCH: Weinheim, Germany, 2001.
- (5) For switchable catalysis, see: (a) Lüning, U. *Angew. Chem., Int. Ed.* **2012**, *51*, 8163. (b) Blanco, V.; Leigh, D. A.; Marcos, V.; Morales-Serna, J. A.; Nussbaumer, A. L. *J. Am. Chem. Soc.* **2014**, *136*, 4905. (c) Schmittl, M.; De, S.; Pramanik, S. *Angew. Chem., Int. Ed.* **2012**, *51*, 3832. (d) Mortezaei, S.; Catarineu, N. R.; Canary, J. W. *J. Am. Chem. Soc.* **2012**, *134*, 8054. (e) Wilson, D.; Branda, N. R. *Angew. Chem., Int. Ed.* **2012**, *51*, 5431. (f) Berryman, O. B.; Sather, A. C.; Lledó, A.; Rebek, J. *Angew. Chem., Int. Ed.* **2011**, *50*, 9400. (g) Wang, J.; Feringa, B. L.

Science **2011**, *331*, 1429. (h) Yoon, H. J.; Kuwabara, J.; Kim, J.-H.; Mirkin, C. A. *Science* **2010**, *330*, 66. (i) Sohtome, Y.; Tanaka, S.; Takada, K.; Yamaguchi, T.; Nagasawa, K. *Angew. Chem., Int. Ed.* **2010**, *49*, 9254. (j) Broderick, E. M.; Guo, N.; Vogel, C. S.; Xu, C.; Sutter, J.; Miller, J. T.; Meyer, K.; Mehrkhodavandi, P.; Diaconescu, P. L. *J. Am. Chem. Soc.* **2011**, *133*, 9278.

(6) For bifunctional catalysis, see: (a) Crabtree, R. H. *New J. Chem.* **2011**, *35*, 18. (b) Gunanathan, C.; Milstein, D. *Acc. Chem. Res.* **2011**, *44*, 588. (c) DuBois, M. R.; Dubois, D. L. *Chem. Soc. Rev.* **2009**, *38*, 62. (d) Paull, D. H.; Abraham, C. J.; Scerba, M. T.; Alden-Danforth, E.; Lectka, T. *Acc. Chem. Res.* **2008**, *41*, 655. (e) Ikariya, T.; Blacker, A. J. *Acc. Chem. Res.* **2007**, *40*, 1300. (f) Moore, C. M.; Szymczak, N. K. *Chem. Commun.* **2013**, *49*, 400. (g) Hull, J. F.; Himeda, Y.; Wang, W.-H.; Hashiguchi, B.; Periana, R.; Szalda, D. J.; Muckerman, J. T.; Fujita, E. *Nat. Chem.* **2012**, *4*, 383. (h) Askevold, B.; Nieto, J. T.; Tussupbayev, S.; Diefenbach, M.; Herdtweck, E.; Holthausen, M. C.; Schneider, S. *Nat. Chem.* **2011**, *3*, 532. (i) Ringenberg, M. R.; Kokatam, S. L.; Heiden, Z. M.; Rauchfuss, T. B. *J. Am. Chem. Soc.* **2007**, *130*, 788.

(7) Ikariya, T.; Shibasaki, M. *Bifunctional Molecular Catalysis*; Springer: New York, 2011.

(8) (a) Liberman-Martin, A. L.; Bergman, R. G.; Tilley, T. D. *J. Am. Chem. Soc.* **2013**, *135*, 9612. (b) Wang, W.-H.; Hull, J. F.; Muckerman, J. T.; Fujita, E.; Himeda, Y. *Energy Environ. Sci.* **2012**, *5*, 7923. (c) Dixon, N. A.; McQuarters, A. B.; Kraus, J. S.; Soffer, J. B.; Lehnert, N.; Schweitzer-Stenner, R.; Papish, E. T. *Chem. Commun.* **2013**, *49*, 5571. (d) Gary, J. B.; Cook, A. K.; Sanford, M. S. *ACS Catal.* **2013**, *3*, 700. (e) Stradiotto, M.; Hesp, K. D.; Lundgren, R. J. *Angew. Chem., Int. Ed.* **2010**, *49*, 494. (f) Betley, T. A.; Peters, J. C.; *Angew. Chem., Int. Ed.* **2003**, *42*, 2385.

(9) Tutusaus, O.; Ni, C.; Szymczak, N. K. *J. Am. Chem. Soc.* **2013**, *135*, 3403.

(10) (a) Tseng, K.-N. T.; Kampf, J. W.; Szymczak, N. K. *Organometallics* **2013**, *32*, 2046. (b) Tseng, K.-N. T.; Rizzi, A. M.; Szymczak, N. K. *J. Am. Chem. Soc.* **2013**, *135*, 16352.

(11) (a) Pap, J. S.; Cranswick, M. A.; Balogh-Hergovich, É.; Baráth, G.; Giorgi, M.; Rohde, G. T.; Kaizer, J.; Speier, G.; Que, L. *Eur. J. Inorg. Chem.* **2013**, *2013*, 3858. (b) Siggelkow, B.; Meder, M. B.; Galka, C. H.; Gade, L. H. *Eur. J. Inorg. Chem.* **2004**, *2004*, 3424. (c) Anderson, O. P.; la Cour, A.; Berg, A.; Garret, A. D.; Wicholas, M. *Inorg. Chem.* **2003**, *42*, 4513. (d) Balogh-Hergovich, É.; Kazier, J.; Speier, G.; Huttner, G.; Jacobi, A. *Inorg. Chem.* **2000**, *39*, 4224.

(12) Vries, J. G.; Elsevier, C. J. *Handbook of Homogeneous Hydrogenation*; Wiley-VCH: Weinheim, Germany, 2007.

(13) Ananikov, V. P.; Tanaka, M. *Hydrofunctionalization*; Springer: New York, 2013

(14) (a) Carroll, A.-M.; O'Sullivan, T. P.; Guiry, P. J. *Adv. Synth. Catal.* **2005**, *347*, 609. (b) Crudden, C. M.; Edwards, D. *Eur. J. Org. Chem.* **2003**, *2003*, 4695. (c) Hall, D. G. *Boronic Acids: Preparation and Applications in Organic Synthesis and Medicine*; Wiley-VCH: Weinheim, Germany, 2005.

(15) (a) Brown, H. C. *Organic Synthesis via Organoboranes*; Wiley Interscience: New York, 1975. (b) Suzuki, A. *Angew. Chem., Int. Ed.* **2011**, *50*, 6722.

- (16) (a) Burgess, K.; Van der Donk, W. A.; Westcott, S. A.; Marder, T. B.; Baker, R. T.; Calabrese, J. C. *J. Am. Chem. Soc.* **1992**, *114*, 9350. (b) Evans, D. A.; Fu, G. C.; Hoveyda, A. H. *J. Am. Chem. Soc.* **1992**, *114*, 6671. (c) Evans, D. A.; Fu, G. C.; Anderson, B. A. *J. Am. Chem. Soc.* **1992**, *114*, 6679. (d) Westcott, S. A.; Blom, H. P.; Marder, T. B.; Baker, R. T. *J. Am. Chem. Soc.* **1992**, *114*, 8863. (e) Burgess, K.; Ohlmeyer, M. J. *Chem. Rev.* **1991**, *91*, 1179. (f) Männig, D.; Nöth, H. *Angew. Chem., Int. Ed.* **1985**, *24*, 878.
- (17) (a) Zhang, L.; Huang, Z. *Synlett* **2013**, *24*, 1745. (b) Zhang, L.; Peng, D.; Leng, X.; Huang, Z. *Angew. Chem., Int. Ed.* **2013**, *52*, 3676. (c) Obligacion, J. V.; Chirik, P. J. *Org. Lett.* **2013**, *15*, 2680. (d) Greenhalgh, M. D.; Thomas, S. P. *Chem. Commun.* **2013**, *49*, 11230. (e) Zheng, J.; Sortais, J.-B.; Darcel, C. *ChemCatChem* **2014**, *6*, 763. (f) Wu, J. Y.; Moreau, B.; Ritter, T. *J. Am. Chem. Soc.* **2009**, *131*, 12915. (g) Cao, Y.; Zhang, Y.; Zhang, L.; Zhang, D.; Leng, X.; Huang, Z. *Org. Chem. Front.* **2014**, *1*, 1101.
- (18) Note that the synthesis of Fe(bMepi)(CH₂SiMe₃) was previously reported. See reference: Kruck, M.; Wadepohl, H.; Enders, M.; Gade, L. H. *Chem. Eur. J.* **2013**, *19*, 1599.
- (19) Das, U. K.; Bobak, J.; Fowler, C.; Hann, S. E.; Petten, C. F.; Dawe, L. N.; Decken, A.; Kerton, F. M.; Kozak, C. M. *Dalton Trans.* **2010**, *39*, 5462.
- (20) Addison, A. W.; Rao, T. N.; Reedijk, J.; van Rijn, J.; Verschoor, G. C. *J. Chem. Soc., Dalton Trans.* **1984**, 1349.
- (21) Pereira, C.; Ferreira, H. G.; Schultz, M. S.; Milanez, J.; Izidoro, M.; Leme, P. C.; Santos, R. H. A.; Gambardella, M. T. P.; Castellano, E. E.; Lima-Neto, B. S.; Carlos, R. M. *Inorg. Chim. Acta* **2005**, *358*, 3735.
- (22) The ΔE is consistent with a prior report that demonstrated a 380 mV difference after ligand alkylation. See reference: Creutz, C.; Taube, H. *J. Am. Chem. Soc.* **1973**, *95*, 1086.
- (23) Although uncommon, olefin hydroboration with select Fe precatalysts was recently demonstrated. See reference 17.
- (24) The chemical conversion was 75% after 2 h; however, the reaction was allowed to proceed for 20 h to provide maximal yield. Products derived from a competitive dehydrogenative borylation were not observed. For prior examples that feature this side reaction, see references: (a) Vogels, C. M.; Hayes, P. G.; Shaver, M. P.; Westcott, S. A. *Chem. Commun.* **2000**, 51. (b) Murata, M.; Kawakita, K.; Asana, T.; Watanabe, S.; Masuda, Y. *Bull. Chem. Soc. Jpn.* **2002**, *75*, 825.
- (25) Note that 1 equiv of THF did not affect the overall yield.
- (26) Side products (11%), including dehydrogenative borylation and hydrogenation products were also observed.
- (27) Pereira, S.; Srebnik, M. *J. Am. Chem. Soc.* **1996**, *118*, 909.
- (28) Obligacion, J. V.; Chirik, P. J. *J. Am. Chem. Soc.* **2013**, *135*, 19107.

- (29) Sonnenberg, J. F.; Coombs, N.; Dube, P. A.; Morris, R. H. *J. Am. Chem. Soc.* **2012**, *134*, 5893.
- (30) (a) Crabtree, R. H. *Chem. Rev.* **2012**, *112*, 1536. (b) Bayram, E.; Finke, R. G. *ACS Catal.* **2012**, *2*, 1967.
- (31) Sui-Seng, C.; Freutel, F.; Lough, A. J.; Morris, R. H. *Angew. Chem., Int. Ed.* **2008**, *47*, 940.
- (32) Widegren, J. A.; Finke, R. G. *J. Mol. Catal. A: Chem.* **2003**, *198*, 317.
- (33) Sauer, D. C.; Wadepohl, H.; Gade, L. H. *Inorg. Chem.* **2012**, *51*, 12948.
- (34) Schubert, E. M. *J. Chem. Educ.* **1992**, *69*, 62.
- (35) Connelly, N. G.; Geiger, W. E.; *Chem. Rev.* **1996**, *96*, 877.
- (36) Wu, J. Y.; Moreau, B.; Ritter, T. *J. Am. Chem. Soc.* **2009**, *131*, 12915.

CHAPTER 6

Modular Attachment of Appended Boron Lewis Acids to a Ruthenium Pincer Catalyst: Metal–Ligand Cooperativity Enables Selective Alkyne Hydrogenation

6.1 Introduction

For homogeneous catalysts, the selection and design of appropriate ancillary ligands serves an important role to control both the activity and the selectivity in subsequent catalytic reactions.¹ Although the steric and electronic properties of the primary coordination sphere are most often modified during catalyst optimization, secondary groups can also play a key role to promote substrate binding/activation.² Elaboration of an active catalyst's secondary structure often requires extensive synthetic redesign prior to metalation, which limits rapid evaluation of structure/function details. In contrast, late-stage modification of an already active catalyst can also be used to install appended groups and it offers several advantages: (1) functionalization of the ligand's secondary coordination sphere without perturbing the primary coordination environment, (2) methodical variation of the pendent group(s) for precise control over the steric and electronic properties, and (3) minimal need to re-optimize metalation conditions to ensure reaction compatibility (deleterious inter-ligand acid–base interactions).

Homogeneous hydrogenation/dehydrogenation reactions are an ideal platform to probe metal–ligand cooperative activation pathways because of their broad use in the manufacture of fine and commodity chemicals.³ Bifunctional transition-metal complexes have been shown to synergistically activate small molecules, such as H₂, *via* a metal–ligand cooperative pathway.⁴ Although such ligand-facilitated reactivity has emerged as a prominent reaction theme within catalysts for alkene, ketone, and imine hydrogenation reactions, highly selective and efficient

hydrogenation catalysts that employ Lewis acid–metal cooperativity remain underdeveloped.⁵ Complementary to the role that Brønsted acidic groups can serve in bifunctional activation/transfer,⁶ boron-based Lewis acids can also modulate substrate binding,⁷ in addition to promoting insertion-type reactions. Our group is working to evaluate how the precise structural, electronic, and cooperative modes in the secondary coordination sphere can be used to regulate reactivity,^{5e,8} and herein we report a multifunctional Ru catalyst where an appended borane group can be systematically varied as a means to tune subsequent reactivity (Figure 6-1).

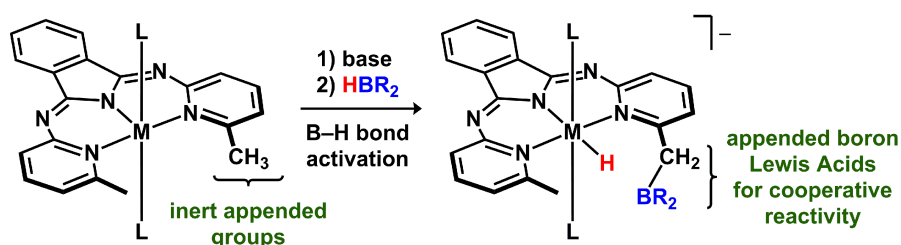


Figure 6-1 Conceptual development of late-stage catalyst redesign to introduce Lewis acidic sites for metal–ligand cooperativity.

We recently reported an N,N,N -bMepi (bMepi = 1,3-bis(6'-methyl-2'-pyridylimino)isoindolate) Ru–H complex (**1**, HRu(bMepi)(PPh₃)₂) capable of mediating promoterless dehydrogenation of alcohols,⁹ amines,¹⁰ and upgrading ethanol to 1-butanol.¹¹ In addition to the hydrogenation and dehydrogenation of polar bonds, **1** also is an active catalyst for alkene hydrogenation.¹² We recently found that a simple perturbation to this ligand framework (replacing *ortho* –CH₃ with –OH units prior to metalation) enabled distinct catalytic reactivity: rapid H–E (H₂ and HBPin) activation and catalytic nitrile hydroboration.^{8c} To further elucidate the changes in reactivity that can be imparted by appended groups, we have targeted a ligand variant that replaces the Brønsted acidic –OH group(s) with a boron-based Lewis acid that importantly can be readily installed post metalation.¹³ These appended groups may be used to bias selectivity for a given catalytic reaction when unselective catalysis is observed for an unmodified variant. In this Communication, we report the development of a new series of bifunctional Ru complexes with appended BR₂ groups *via* B–H bond activation and demonstrate that the Lewis acidity of the borane influences the reactivity of the Ru hydride and promotes *Z*-selective semi-hydrogenation of alkynes.

6.2 Results and Discussion

6.2.1 Synthesis and Characterization of Bifunctional Ruthenium Complexes with Appended Boron Lewis Acids

To evaluate the strategy of installing appended boron-based Lewis acids to provide borane-appended derivatives of **1**, we assessed the reaction with boranes following deprotonation. The addition of catecholborane (HBCat) to a C₆H₆ solution of [Ru(CH₂Mepi)PPh₃]₂ (**2**) resulted in the clean conversion to HRu(CH₂BCatMepi)PPh₃ (**3**), which was isolated as a brown powder in 71% yield (Figure 6-2). The ¹H NMR spectrum confirmed the asymmetry of the appended BCat group on the pincer ligand and featured a broad peak for the hydride ligand at -8.8 ppm.¹⁴ The ³¹P{¹H} NMR spectrum exhibited a singlet at 79.8 ppm, and the ¹¹B{¹H} NMR spectrum contained a broad signal at 14.6 ppm. The solid-state structure revealed a distorted octahedral geometry around the Ru center with the phosphorous and oxygen atoms in pseudo-axial positions [P1–Ru1–O2: 164.83(7)°] and the hydride ligand (located from the difference map) *trans* to the isoindolate nitrogen atom in the equatorial plane. The hydride–boron atom distance of ca. 1.37 Å is consistent with a B–H interaction, which is further supported by the high degree of pyramidalization at boron [$\sum B_{\alpha} = 339.3(3)^{\circ}$].¹⁵

The reaction between **2** and HBPIn afforded a distinct product that incorporated two BPIn units. Ru(CBPIn₂Mepi)PPh₃ (**4**) was isolated as a brown solid in 69% yield by allowing 4 equiv of pinacolborane (HBPIn) and **2** to react in C₆H₆ solvent at 80 °C for 20 h (Figure 6-2). The ³¹P{¹H} NMR spectrum displayed a singlet at 73.8 ppm, and the ¹H NMR spectrum supported the presence of two BPIn groups. In particular, three singlets for the BPIn methyl groups were located at 0.33, 1.29, and 1.33 ppm and a broad peak was detected at 0.44 ppm. The ¹¹B{¹H} NMR spectrum exhibited a broad signal at 28.1 ppm, consistent with minimal pyramidalization at both the boron centers. The X-ray crystal structure revealed the Ru atom in an octahedral environment with a bis(borylated) carbon atom cyclometalated *trans* to the isoindolate nitrogen atom. The appended BPIn units retain trigonal planar geometries at B3 and B4 [$\sum B3_{\alpha} = 359(1)^{\circ}$, $\sum B4_{\alpha} = 360(1)^{\circ}$], and overall, illustrate markedly different structures.

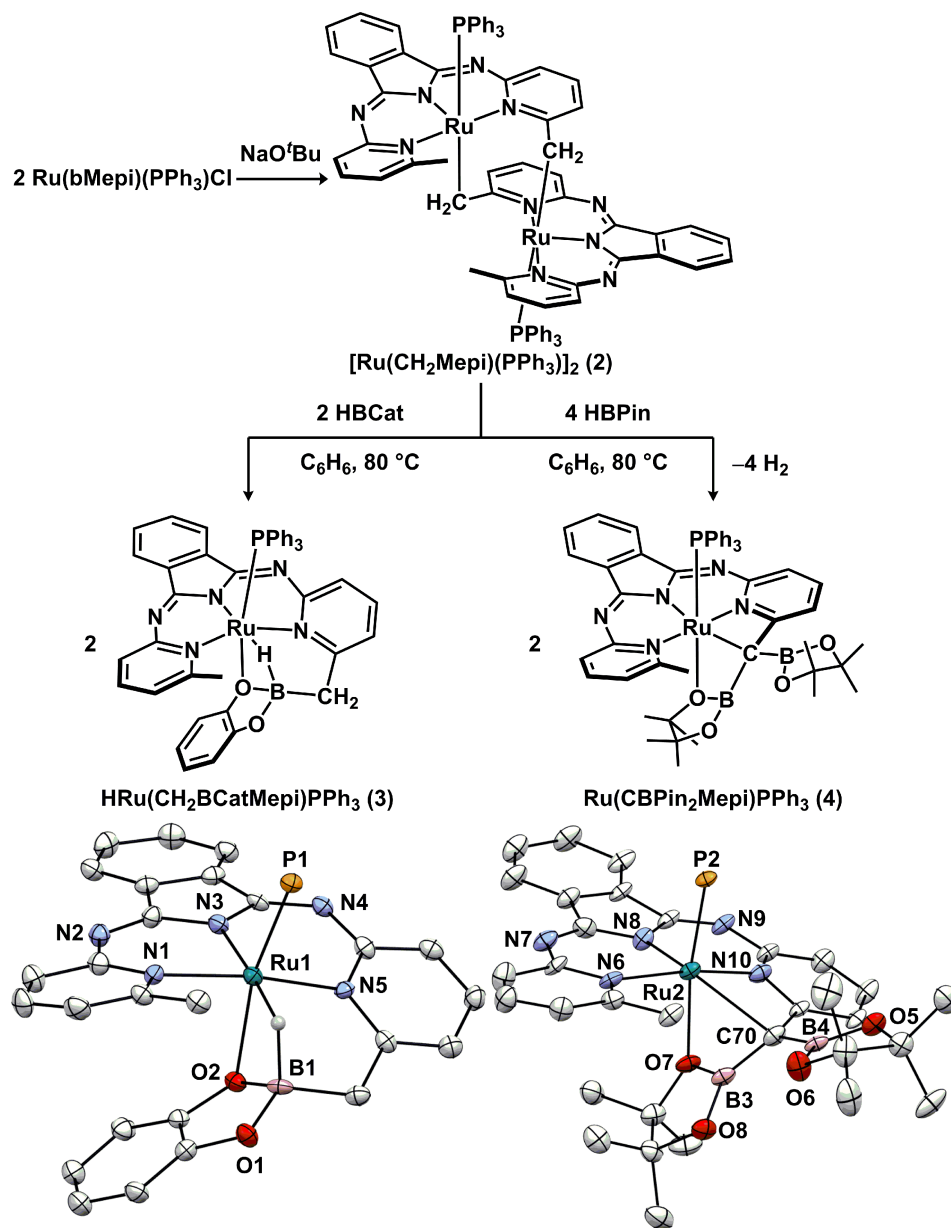


Figure 6-2 Synthesis and crystal structures (thermal ellipsoids depicted at 50% probability) of HRu(CH₂BCatMepi)PPh₃ and Ru(CBPIn₂Mepi)PPh₃. The hydrogen atoms, except the hydride, and PPh₃ phenyl groups are omitted for clarity.

The stronger boron-based Lewis acid 9-borabicyclo[3.3.1]nonane (9-BBN)¹⁶ afforded a distinct product, complex **5** (Ru(CH₉BBN Mepi)PPh₃) in 78% yield, when using analogous reaction conditions as those to prepare **3** (Figure 6-3). The X-ray crystal structure revealed a distorted octahedral environment about the Ru center with a rare Ru-(η^2 -B-C) interaction that may be viewed in one of two limiting resonance form of a borata-alkene, analogous to the Dewar-Chat-Duncanson description of alkene coordination (Figure 6-4).¹⁷ This unit results

from loss of H₂ from the ligand CH₂ (C20) and the B–H unit and represents a form of ligand-enabled H₂ elimination that is reminiscent of bifunctional complexes developed by Milstein's group.¹⁸ In those cases, bifunctional activation is achieved *via* aromatization–dearomatization of the pyridine group concomitant with protonation–deprotonation of the methylene arm. However, in contrast to aromatization–dearomatization observed in prior cases, we note retention of aromaticity in the pyridine ring, based on the normal C=C and C=N bonds as well as the distance between C19–C20 (1.490(3) Å), which is consistent with a single bond. Thus, by tuning the Lewis acidity of a pendent borane (BPin < BCat < 9-BBN), a cooperative bifunctional H₂ release step is enabled, which also serves to provide a Lewis acid in close proximity to a metal-coordinated substrate. Although the degree of pyramidalization at boron is considerably high [$\sum B_{\alpha} = 339.2(2)^{\circ}$], the Ru1–B1 distance of 2.592(3) Å is longer than the Ru–B distances (2.093–2.176 Å)¹⁹ found in reported Ru–BR₃ complexes, which suggest a weak Ru→B interaction.

Complementary to the solid-state characterization, the solution dynamic exchange process of **5** was investigated using variable temperature NMR spectroscopy. At 25 °C, the ¹H NMR spectrum exhibited broad signals in the alkyl region and a broad signal at –3.5 ppm, the ³¹P{¹H}NMR spectrum displayed a broad signal at 44.6 ppm, and the ¹¹B{¹H} NMR spectrum was featureless. However, upon cooling a CD₂Cl₂ solution of **5** to –80 °C, the ¹H and ³¹P signals sharpened and the ¹¹B{¹H} NMR spectrum showed a broad signal at –8.5 ppm, indicative of a fluxional structure at room temperature. Moreover, in the ¹H NMR spectrum at –80 °C, the signal at –3.87 ppm appeared as a well-resolved doublet with a coupling constant of 16.5 Hz that appeared concomitantly with a doublet at 2.06 ppm with the same coupling constant and a T₁(min) of 211 ms (–40 °C, 500 MHz) (Figure 6-4). This observation is consistent with an agostic interaction of a geminal –CH₂ group with Ru.^{7e} Thus, we propose two reversible coordination modes of the 9-BBN motif to the Ru center (Ru–(η²-B–C) and Ru–(η²-C–H)) at room temperature (Figure 6-4).

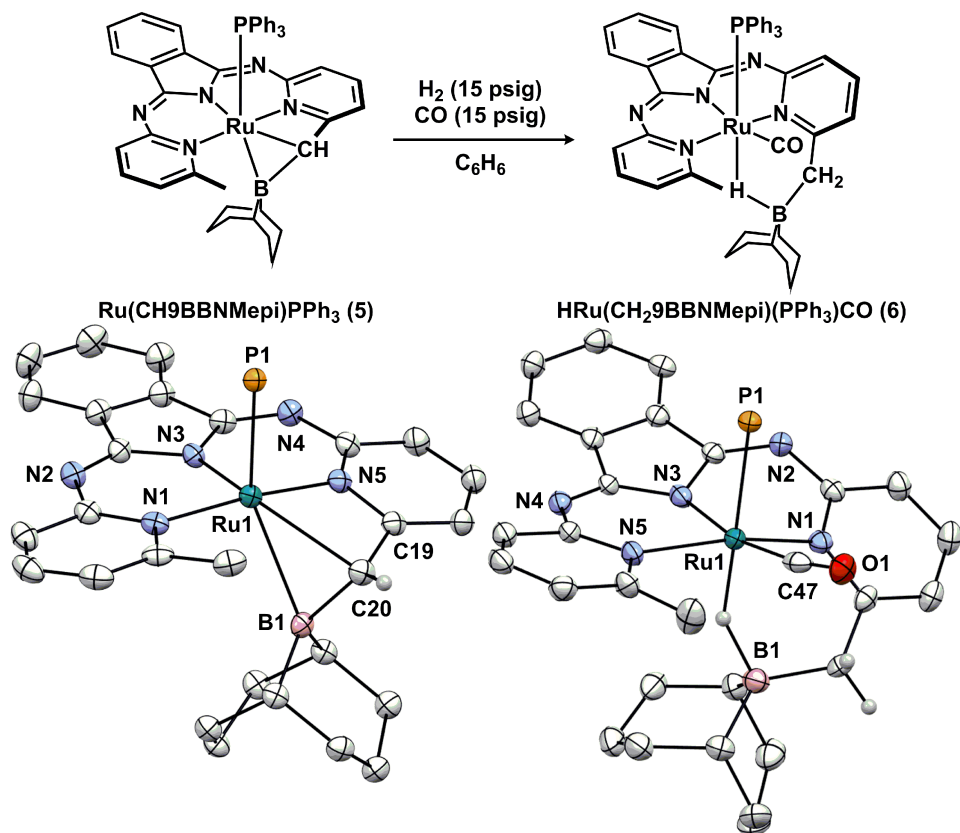


Figure 6-3 Synthesis and crystal structures (thermal ellipsoids depicted at 50% probability) of $\text{Ru}(\text{CH}_9\text{BBNMepi})\text{PPh}_3$ and $\text{HRu}(\text{CH}_2\text{9BBNMepi})(\text{PPh}_3)\text{CO}$. The hydrogen atoms, except the hydride, and PPh_3 phenyl groups are omitted for clarity.

To interrogate the capabilities of the pendent 9-BBN Lewis acid and Ru in **5** to cooperatively promote H–H activation, we evaluated the H_2 reactivity in the presence of a π -acidic ligand. The addition of H_2 (15 psig) and CO (15 psig) to a C_6H_6 solution of **5** yielded a new orange product, $\text{HRu}(\text{CH}_2\text{9BBNMepi})(\text{PPh}_3)\text{CO}$ (**6**; Figure 6-3). The $^{31}\text{P}\{^1\text{H}\}$ NMR spectrum displayed a singlet at 38.6 ppm, and the IR spectrum exhibited a ν_{CO} band at 1935 cm^{-1} and a broad Ru–H–B peak at 1820 cm^{-1} , which falls within the $1864\text{--}1780 \text{ cm}^{-1}$ range of previously reported complexes.²⁰ In the ^1H NMR spectrum, the hydride ligand was visualized as a broad doublet at -9.83 ppm with a J_{HP} of 97.5 Hz, consistent with a hydride ligand *trans* to a phosphine ligand. The X-ray crystal structure revealed the products of H_2 heterolysis: a Ru–H (located from the difference map), and a sp^3 carbon adjacent to the boron. Similar to **3**, the Ru–H unit is capped by the appended borane, forming a Ru–H–B bridge. Furthermore, the boron atom (B1) in **6** is pyramidalized at boron [$\sum \text{B}_\alpha = 339.2(3)^\circ$], consistent with the ^{11}B NMR resonance at -6.5 ppm. The structural characterization of **6** is consistent with H_2 heterolysis across the metal–

ligand framework promoted either by the basic methanide moiety, which is similar to Milstein's bifunctional complexes,^{4a} or with assistance from the pendent boron Lewis acid in concert with the metal.²¹

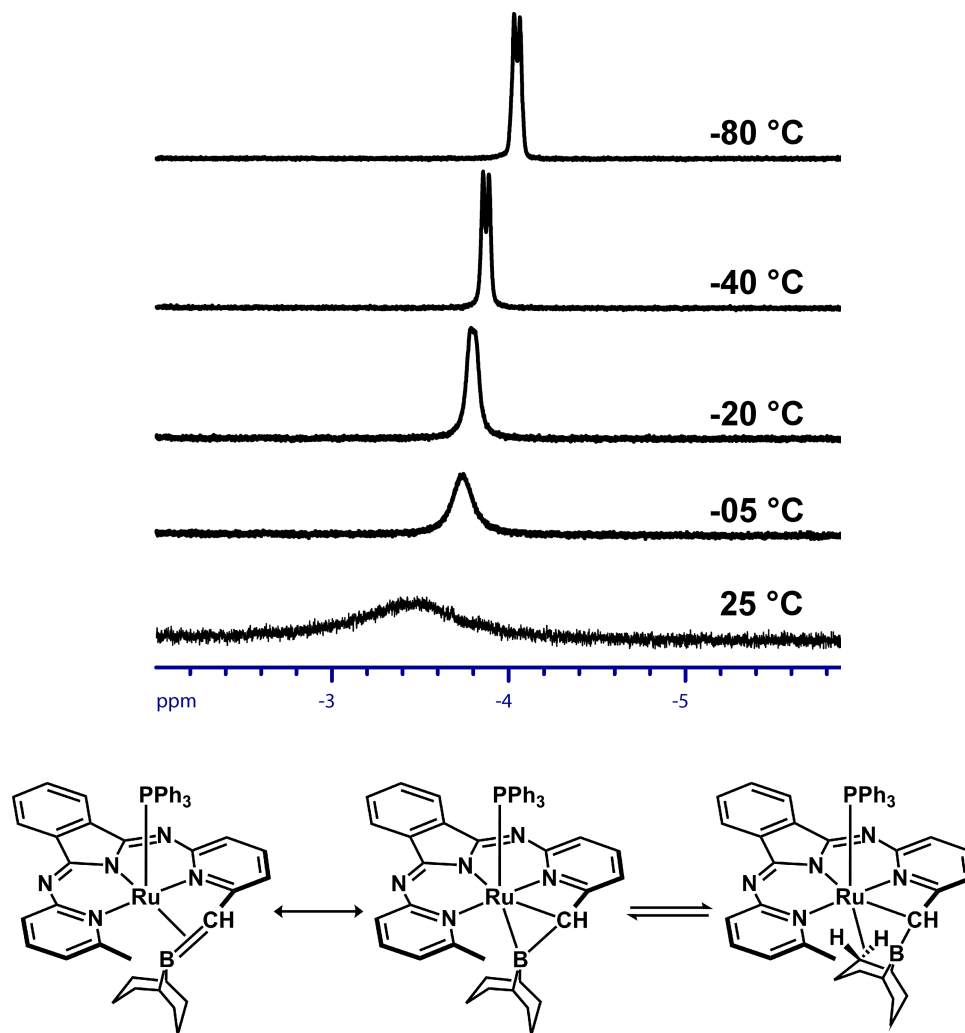


Figure 6-4 Limiting resonance description and solution equilibrium process for $\text{Ru}(\text{CH9BBNMepi})\text{PPh}_3$.

6.2.2 Reactivity of Bifunctional Ruthenium Complexes Toward H_2 and Chlorinated Hydrocarbons

The effect of the varied appended borane groups were evaluated by examining the reactivity of **3–5** toward H_2 (Figure 6-5). When a J. Young tube containing a C_6D_6 solution of **4** and PPh_3 was charged with 30 psig of H_2 , the immediate formation of **1** (the only Ru-containing product) was detected by ^1H and ^{31}P NMR spectroscopy. In contrast to the reactivity observed

with **4**, **1** was not observed when allowing **3** or **5** to react with H₂ under identical conditions even after 48 h, consistent with equilibrium of formation strongly favoring **3** or **5**. Moreover, these results suggest that both Ru–H and η^2 -H₂ adducts with appended BPin groups are unstable intermediates and the weak Lewis acidic BPin group cannot stabilize the Ru–H species analogous to **3** (Figure 6-6).

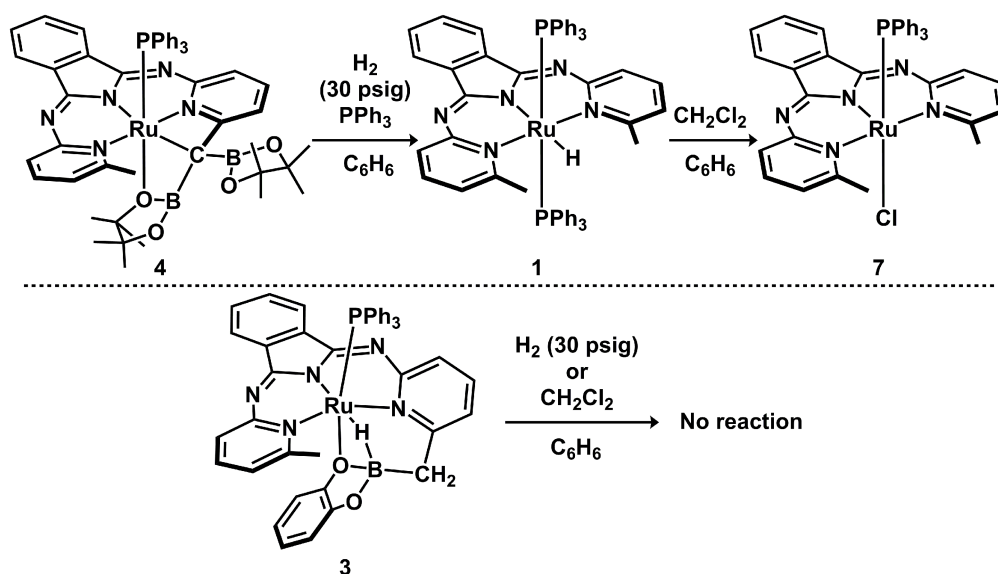


Figure 6-5 Influence of appended Lewis acids on the reactivity of Ruthenium hydride toward dihydrogen and dichloromethane.

The reactivity of the Ru–H unit was significantly suppressed when intramolecularly coordinated to a borane (Figure 6-5). H/Cl exchange has been used to evaluate the nucleophilicity of a given metal hydride, where facile exchange corresponds to a strong H[−] donor.^{7g} When **1** and 1 equiv of CH₂Cl₂ or CHCl₃ were allowed to react in C₆D₆, Ru(bMepi)(PPh₃)Cl (**7**) was immediately formed in quantitative yield. In contrast, no H/Cl exchange was observed when **3** was used under the same conditions, or in the presence of excess PPh₃. **7** was also generated quantitatively when performing a control experiment using **1**, 1 equiv of (9-BBN)CH₂CH₂Ph,²² and either CH₂Cl₂ or CHCl₃, which illustrates that the proximity of the intramolecular pendent BCat unit plays a critical role in regulating reactivity. Thus, the Lewis acidic properties of the borane moiety, when appropriately placed in the secondary coordination sphere has a significant effect on the reactivity of the hydride; the BCat–hydride (Lewis acid–base) interaction likely reduces the hydricity of the Ru–H and thus prevents the substitution reaction.

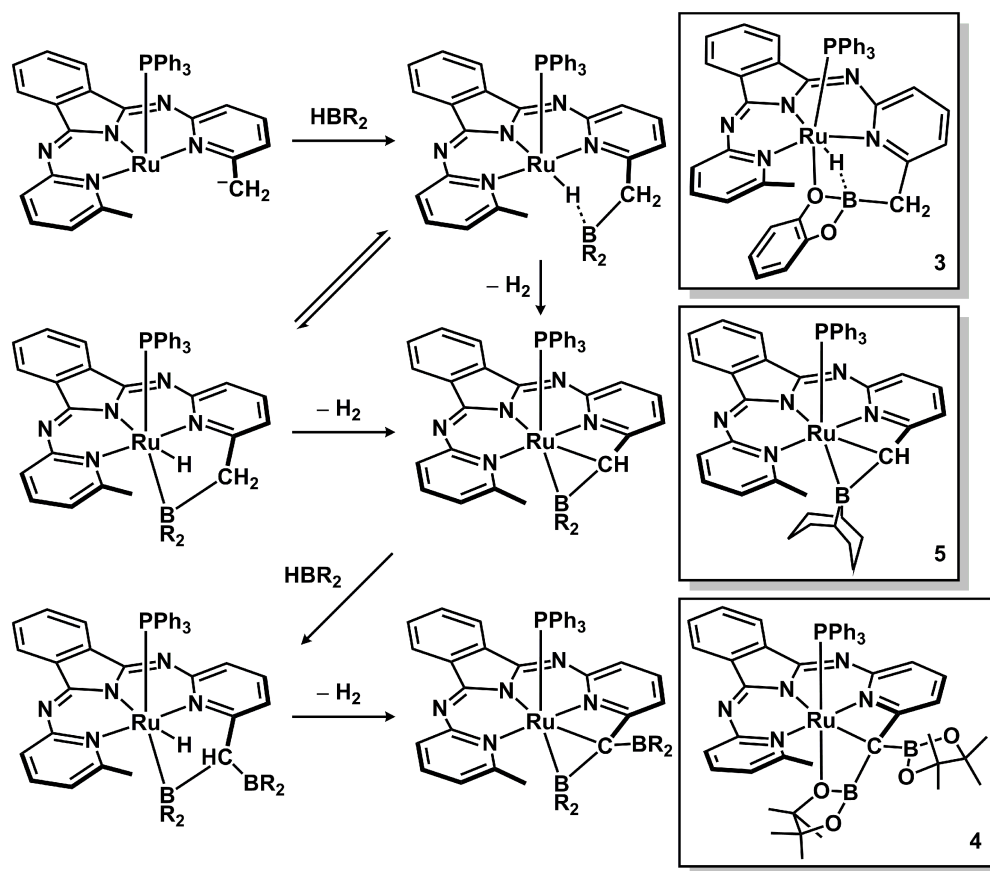
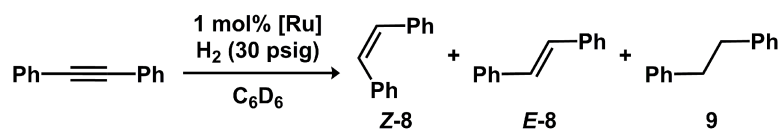


Figure 6-6 Proposed pathway for B–H bond activation *via* H₂ elimination .

6.2.3 Hydrogenation Catalysis Mediated by Bifunctional Ruthenium Complexes

In addition to the stoichiometric H₂ reactivity, we evaluated the catalytic activity of **3** and **5** for hydrogen-transfer. When a J. Young tube containing a C₆D₆ solution of 0.1 mmol of diphenylacetylene and 1 mol% of **3** or **5** was charged with H₂ (30 psig) at room temperature for 24 h, *cis*-stilbene (**Z-8**), was formed in 12% and 14% yields respectively, as assessed by ¹H NMR spectroscopy (Table 1, entries 1 and 2). In contrast to the catalysis observed with **3** and **5**, no reaction was observed when using **1** under identical conditions, even after a week (Table 6-1, entry 3) and in the presence of 1 equiv of (9-BBN)CH₂CH₂Ph. These results suggest that bifunctional metal–ligand catalysis might be accessed when the bMepi ligand is functionalized with a Lewis acidic borane center in close contacts with the metal center.

Table 6-1 Alkyne Semi-Hydrogenation Catalyzed by Bifunctional Ruthenium Complexes

entry	[Ru]	T (°C)	conversion (%) ^a	Z-8:E-8:9	selectivity (%) ^b
1	3	23	12	12:0:0	100
2	5	23	14	14:0:0	100
3 ^c	1	23	0	0:0:0	0
4	1	80	65	31:18:16	48
5	3	80	56	48:7:1	86
6 ^d	5	80	100	98:2:0	98
7	8^e	80	65	34:21:10	52

^aConversion determined by ¹H NMR integration versus phenyltrimethylsilane as an internal standard. ^bSelectivity determined by conversion of **Z-8** per total conversion. ^cNo change after 1 week. ^dNo change in the presence of Hg. ^eHRu(*b*ⁱPrpi)(PPh₃)₂.

Table 6-2 Catalytic Hydrogenations Promoted by Ru(CH₉BBNMepi)PPh₃ with H₂

entry	substrate	product	yield (%) ^a
1	4-octyne	Z-4-octene ^b	100
2	1-octyne	1-octene	100
3	phenylacetylene	styrene	100
4	Z-4-octene	octane	100
5	1-octene	octane	100
6	cyclooctene	cyclooctane	100
7	styrene	ethylbenzene	100

^aReactions performed on 0.1 mmol scale with 1 mol% **5** and 30 psig of H₂ in C₆D₆ at 80 °C for 2 h. Yields determined from ¹H NMR integration versus phenyltrimethylsilane as an internal standard. ^b100% selectivity.

To examine the extent to which the appended borane groups influence alkyne hydrogenation, we investigated the selectivity and reaction rate of diphenylacetylene hydrogenation at 80 °C. When the hydrogenation reaction was performed with **1**, diphenylacetylene was converted to a mixture of **Z-8** (31%), **E-8** (18%), and **9** (16%) with low selectivity (48%) for **Z-8** (Table 6-1, entry 4). In contrast, high selectivity for the semi-hydrogenation of diphenylacetylene to **Z-8** was achieved using either **3** or **5**. Selectivities of 86% and 98% were obtained when **3** and **5**, respectively, were used instead of **1** (Table 6-1, entries 5

and 6).²³ Furthermore, significantly higher conversion (100%) and faster reaction rate (4×) were found when **5** ($2.6(3) \times 10^{-3}$ M/s) was used instead of **3** ($5.6(5) \times 10^{-4}$ M/s) and **1** ($6.5(5) \times 10^{-4}$ M/s). Catalytic hydrogenation of alkynes and alkenes with **5** was general to afford the corresponding (*cis*-) alkenes and alkanes as the exclusive products in quantitative yields (Table 6-2). For instance, **5** mediated hydrogenation of internal and terminal alkynes as well as aliphatic (linear and cyclic) and aromatic alkenes. Thus, we found that incorporation of a sufficiently strong appended Lewis acidic site, such as 9-BBN, introduces a dramatic bias for three aspects related to alkyne hydrogenation: (1) selectivity for a single olefin stereoisomer, (2) selectivity for the reduction of alkynes over alkenes, and (3) enhanced reaction rate.

6.2.4 Origin of Selective Alkyne Reduction

To gain further insight into the origin of the preference for the alkyne over alkene, we evaluated stoichiometric competition experiments between 1-octyne and 1-octene. The addition of a C₆D₆ solution containing a mixture 1 equiv of 1-octyne and 1-octene to **3** resulted in the clean conversion to new species with ³¹P resonances at 21.5 and 41.8 ppm. In the ¹H NMR spectrum, the hydride region showed no resonances and the alkene region displayed two new peaks at 4.64 and 4.70 ppm in a 1:1 ratio. Identical ³¹P and ¹H NMR spectra were obtained when **3** was allowed to react with 2 equiv of 1-octyne. These two new products are proposed as isomeric species of Ru hydride insertion into 1-octyne. Furthermore, insertion reaction of alkyne was also maintained even when using 1000:1 mixtures of 1-octene to 1-octyne. In contrast, when the competition experiments were performed using **1** in the presence of 1000:1 of 1-octene to 1-octyne, the ³¹P NMR spectrum featured a broad peak at -5.4 ppm (free PPh₃) and the ¹H NMR spectrum showed broad peaks that were not resolved at low temperatures. This is consistent with a very fast dynamic equilibrium process between hydride insertion into the alkene and alkyne. In addition to Lewis acidic character of the appended borane units, they also impose increased steric profiles, compared to a CH₃ unit, and the distinct steric environments may determine selectivity. To evaluate whether a similar steric effect influences the preference for a single stereoisomer, alkyne hydrogenation was examined using HRu(*b*ⁱPrpi)(PPh₃)₂ (**8**), which contains isopropyl groups that are more sterically encumbering around the Ru center than the *ortho*-substituents in **1**–**7**. For diphenylacetylene hydrogenation, the product distribution and conversion were strikingly similar to **1** (52% selectivity, 65% conversion; Table 1, entry 7). Thus,

the origin of the selective semi-hydrogenation of alkynes most likely arises from the acidic character of the pendent boranes to direct cooperative substrate binding of alkynes over alkenes. This preference for alkynes is consistent with prior hydroboration studies which similarly demonstrated enhanced rates for alkyne substrates, which likely engages in a stronger interaction with the boron atom.²⁴

6.2.5 Proposed Mechanism for Alkyne Hydrogenation Mediated by Bifunctional Ruthenium Complexes

Overall, the appended boron Lewis acid was demonstrated to play a multifunctional role to promote stereoselective hydrogenation of alkynes. We propose that H₂ heterolysis across the metal–ligand scaffold generates a hydride intermediate stabilized by the borane unit *via* the formation of a Ru–H–B bridge. The breaking of the B–H interaction allows the Lewis acidic boron to direct alkyne binding, which is thermodynamically driven by the strengths of B–C (107 kcal/mol) versus B–H (81 kcal/mol) bond, for hydride insertion. Finally, addition of H₂ affords the *cis*-alkene product and the Ru–H–B species, which re-enters the hydrogenation cycle (Figure 6-7).

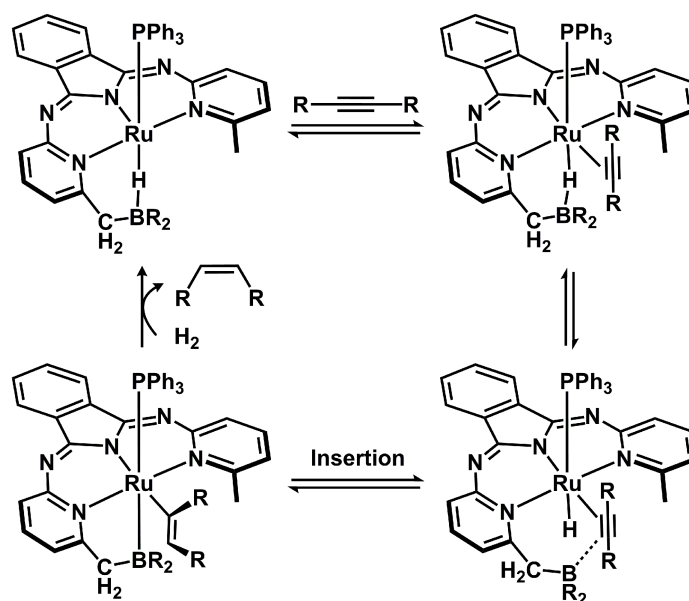


Figure 6-7 Proposed mechanism for stereoselective alkyne hydrogenation catalyzed by bifunctional complexes.

6.2.6 Summary

In conclusion, we have developed a new class of bifunctional Ru complexes with appended Lewis acidic BR₂ groups. This work demonstrates the use of the Lewis acidic properties of the boranes in the secondary coordination environment to modulate the reactivity of the Ru hydride group and turn on a metal–ligand cooperative pathway for hydrogenation catalysis. Of particular note, higher reaction rate, conversion, and selectivity were noted for the Z-selective semi-hydrogenation of alkynes when using the bifunctional complex **3** appended with the most Lewis acidic site. Comparison with the unfunctionalized complexes containing only inert groups illustrates the critical role of the Lewis acids in the secondary coordination sphere to synergistically mediate and regulate alkyne hydrogenation by (1) facilitating H–H heterolysis, (2) stabilizing the hydride intermediate *via* the formation of a Ru–H–B bridge, and (3) selectively reducing alkynes over alkenes.

6.3 Experimental Section

6.3.1 General Considerations

All manipulations were conducted under a nitrogen atmosphere on a Schlenk manifold or in a glovebox using standard Schlenk techniques, unless otherwise stated. All reagents were purchased from commercial vendors. Pinacolborane (HBPin; Aldrich), borabicyclo[3.3.1]nonane (9-BBN; Aldrich), and catecholborane (HBCat; Aldrich) were used without further purification. Substrates (1-octene, Aldrich; cyclooctene, Aldrich; styrene, Aldrich; 4-octyne, Aldrich; 1-octyne, Aldrich; cis-4-octene, Alfa Aesar) were distilled from CaH₂ under a nitrogen atmosphere, and then stored over 3Å molecular sieves for 24 h. The following compounds were synthesized according to literature methods: HRu(bMepi)(PPh₃)₂ (**1**)⁹ and [Ru(CH₂Mepi)PPh₃]₂ (**2**)¹³. The 3Å Molecular sieves were dried at 250 °C under dynamic vacuum for 24 h. Dichloromethane (DCM), diethyl ether (Et₂O), pentane, and benzene (C₆H₆) were purified using a Glass Contour solvent purification system consisting of a copper catalyst, neutral alumina, and activated molecular sieves, then passed through an in-line, 2 μm filter immediately before being dispensed. Toluene (PhMe) was sparged using nitrogen and then stored over 3Å molecular sieves for at least 24 h.

NMR spectra were recorded on Varian Inova 500, Varian MR400, Varian vnmrs 500, and Varian vnmrs 700 spectrometers at room temperature. ^1H and ^{13}C shifts are reported in parts per million (ppm) relative to TMS, with the residual solvent peak used as an internal reference. ^{31}P NMR spectra were referenced on a unified scale to their respective ^1H NMR spectra. The following abbreviations are reported as follows: broad (br), singlet (s), doublet (d), doublet of doublets (dd), triplet (t), quartet (q), multiplet (m), methyl (Me), and triphenylphosphine (PPh_3). ^{13}C NMR resonances were observed as singlets unless otherwise stated. Solid-state IR spectra were collected using a Nicolet iS10 spectrometer equipped with a diamond attenuated total reflectance (ATR) accessory. Elemental analyses were performed by Midwest Microlab, LLC.

6.3.2 General Procedure for Hydrogenation Reactions Catalyzed by $\text{Ru}(\text{CH}_9\text{BBNMe})\text{PPh}_3$

Alkynes or alkenes (0.1 mmol) were added to a J. Young NMR tube containing a C_6D_6 solution of **3** (1 mol%, 0.001 mmol, 0.8 mg). The J. Young NMR tube was capped with a Teflon key and charged with 30 psig of H_2 . After 2 h at 80 °C, the products and yields were determined by ^1H NMR spectroscopy against phenyltrimethylsilane as an internal standard. The identity of the product was confirmed by comparison to the reported NMR spectra of known compounds.

6.3.3 Preparation of Bifunctional Ruthenium Complexes with Appended Boron Lewis Acids

$\text{Ru}(\text{CH}_9\text{BBNMe})\text{PPh}_3$. C_6H_6 (10 mL) was added to a 20 mL vial containing $[\text{Ru}(\text{CH}_2\text{Me})\text{PPh}_3]_2$ (98 mg, 0.0571 mmol), 9-BBN (34.7 mg, 0.142 mmol), and a stir bar. The reaction solution was allowed to stir at 80 °C for 20 h. After the solution cooled to room temperature, the C_6H_6 solvent was removed under vacuum and the crude product was washed with pentane (4×20 mL). Evaporation of the volatiles under vacuum afforded the product as a dark green powder. Crystals were obtained from vapor diffusion of pentane into a C_6H_6 solution at room temperature. Yield: 90 mg (78%). ^1H NMR (500 MHz, CD_2Cl_2): δ 7.95 (d, $J_{\text{HH}} = 7.5$ Hz, 1H), 7.60–7.52 (m, 4H), 7.46 (t, $J_{\text{HH}} = 7.5$ Hz, 1H), 7.37 (t, $J_{\text{HH}} = 7.5$ Hz, 1H), 7.17 (t, $J_{\text{HH}} = 7.5$ Hz, 3H, PPh_3), 7.02–6.96 (m, 7H), 6.85 (t, $J_{\text{HH}} = 8.5$ Hz, 6H, PPh_3), 6.69 (d, $J_{\text{HH}} = 7.5$ Hz, 1H), 6.60 (d, $J_{\text{HH}} = 5.5$ Hz, 1H), 2.14 (br d, $J_{\text{HH}} = 15$ Hz, 1H), 2.00 (s, 3H, Me), 1.80–1.67 (m, 2H), 1.59–1.52 (m, 2H), 1.42–1.17 (m, 6H), 0.99 (br t, $J_{\text{HH}} = 6.8$ Hz, 1H) 0.52–0.41 (br m, 2 H),

-1.16 (s, 1H), -3.5 (br s). $^{13}\text{C}\{\text{}^1\text{H}\}$ (176 MHz, CD_2Cl_2): δ 172.37, 153.03, 141.63, 140.45, 134.94, 134.59, 133.64 (d, $J_{\text{CP}} = 9.5$ Hz), 133.44, 129.69, 128.97, 128.70, 128.33 (d, $J_{\text{CP}} = 8.4$ Hz), 125.86, 120.35, 119.05, 35.67 (br), 34.29, 34.07, 33.83, 33.64, 27.17 (br), 25.55. $^{31}\text{P}\{\text{}^1\text{H}\}$ NMR (202 MHz, CD_2Cl_2): δ 44.6 (br s, PPh_3). $^{31}\text{P}\{\text{}^1\text{H}\}$ NMR (202 MHz, CD_2Cl_2 , -80 °C): δ 44.6 (s, PPh_3). $^{11}\text{B}\{\text{}^1\text{H}\}$ NMR (160 MHz, CD_2Cl_2 , -80 °C) δ -8.5 (br s, 9-BBN). Anal. Calculated (found): C, 68.32 (68.63); H, 5.36 (5.55); N, 8.66 (8.70).

HRu(CH₂BCatMepi)PPh₃. C₆H₆ (10 mL) was added to a 20 mL vial containing [Ru(CH₂Mepi)PPh₃]₂ (94.2 mg, 0.0684 mmol), HBCat (32.8 mg, 0.274 mmol), and a stir bar. The reaction solution was allowed to stir at 80 °C for 4 h. After the solution cooled to room temperature, the C₆H₆ solvent was removed under vacuum and the crude product was washed with Et₂O (5 mL) and pentane (4 × 20 mL). Evaporation of the volatiles under vacuum afforded the product as a brown powder. Crystals were obtained from vapor diffusion of pentane into a C₆H₆ solution at room temperature. Yield: 79 mg (71%). ^1H NMR (500 MHz, CD_2Cl_2): δ 8.15 (br d, $J_{\text{HH}} = 6.5$ Hz, 1H), 7.72 (br d, $J_{\text{HH}} = 6.5$ Hz, 1H), 7.63 (t, $J_{\text{HH}} = 7.0$ Hz, 1H), 7.54 (t, $J_{\text{HH}} = 7.3$ Hz, 1H), 7.42 (t, $J_{\text{HH}} = 7.5$ Hz, 1H), 7.18 (t, $J_{\text{HH}} = 7.5$ Hz, 3H, PPh_3), 7.12 (br d, $J_{\text{HH}} = 7.5$ Hz, 1H), 7.03–6.94 (m, 14H), 6.56 (d, $J_{\text{HH}} = 7.5$ Hz, 2H), 6.49 (t, $J_{\text{HH}} = 7.5$ Hz, 1H), 6.23 (t, $J_{\text{HH}} = 7.5$ Hz, 1H), 6.10 (d, $J_{\text{HH}} = 7.5$ Hz, 1H), 5.98 (d, $J_{\text{HH}} = 6.5$ Hz, 1H), 3.51 (d, $J_{\text{HH}} = 18.5$ Hz, 1H), 2.66 (dd, $J_{\text{HH}} = 18.5, 4.8$ Hz, 1H), 2.22 (s, 3H, Me), -8.83 (br s, 1H, hydride). $^{13}\text{C}\{\text{}^1\text{H}\}$ (176 MHz, CD_2Cl_2): δ 167.38, 164.38, 152.53, 151.55, 148.37, 135.35, 134.88, 133.81 (d, $J_{\text{CP}} = 9.3$ Hz), 132.92, 129.74, 127.81 (d, $J_{\text{CP}} = 8.3$ Hz), 125.93 (br), 121.78 (br), 120.14, 119.43 (br), 118.59 (br), 112.81, 110.71, 108.99, 33.17, 31.02. $^{31}\text{P}\{\text{}^1\text{H}\}$ NMR (202 MHz, CD_2Cl_2): δ 79.9 (s, PPh_3). $^{11}\text{B}\{\text{}^1\text{H}\}$ NMR (160 MHz, CD_2Cl_2) δ 14.6 (br s, BCat). Anal. Calculated (found): C, 65.35 (65.16); H, 4.36 (4.13); N, 8.66 (8.46).

Ru(CBPin₂Mepi)PPh₃. HBPin (14.2 μL , 0.0981 mmol) was added to a 20 mL vial containing a C₆H₆ (10 mL) solution of [Ru(CH₂Mepi)PPh₃]₂ (30.7 mg, 0.0223 mmol) and a stir bar. The reaction solution was allowed to stir at 80 °C for 20 h. After the solution cooled to room temperature, the C₆H₆ solvent was removed under vacuum and the crude product was washed with pentane (4 × 10 mL). The crude product was dissolved in minimum DCM and layered with pentane. After 24 h at -35 °C, the precipitates were collected and washed with cold pentane. Evaporation of the volatiles under vacuum afforded the product as a brown solid. Crystals were

obtained from evaporation of a C₆H₆ solution at room temperature. Yield: 29 mg (69%). ¹H NMR (500 MHz, C₆D₆): δ 8.30 (d, *J*_{HH} = 7.5 Hz, 1H), 8.15 (d, *J*_{HH} = 7.0 Hz, 1H), 7.87 (d, *J*_{HH} = 8.0 Hz, 1H), 7.37 (t, *J*_{HH} = 7.8 Hz, 1H), 7.30–7.27 (m, 2 H), 6.86–6.84 (m, 9H), 6.45 (d, *J*_{HH} = 7.5 Hz, 1H), 2.60 (s, 3H, Me), 1.33 (s, 6H, BPin), 1.29 (s, 6H, BPin), 1.33 (s, 6H, BPin), 0.44 (br s, 6H, BPin), 0.33 (s, 6H, BPin). ¹³C{¹H} (176 MHz, CD₂Cl₂): δ 175.26, 165.80, 158.26, 153.17, 152.29, 150.76, 142.62, 141.25, 134.89, 134.57, 134.33, 133.68 (d, *J*_{CP} = 8.4 Hz), 128.90, 128.75, 127.63 (d, *J*_{CP} = 8.4 Hz), 126.21, 120.25, 119.47, 116.62, 116.45, 81.68, 31.69, 26.19 (br), 24.25. ³¹P{¹H} NMR (162 MHz, C₆D₆): δ 73.8 (s, PPh₃). ¹¹B{¹H} NMR (160 MHz, C₆D₆) δ 28.1 (br s, BPin). Anal. Calculated (found): C, 63.84 (63.70); H, 5.57 (5.76); N, 7.45 (7.54).

HRu(CH₂9BBNMe_{pi})(PPh₃)CO. A J. Young tube containing a C₆H₆ solution of **3** (8.8 mg, 0.0109 mmol) was charged with H₂ (15 psig) and CO (30 psig). After 1 h at room temperature, the C₆H₆ solvent was removed under vacuum and the crude product was extracted with pentane. After 48 h at –35 °C, the precipitates were collected and dried under vacuum to afford the product as orange needles. Yield: 5 mg (55%). ¹H NMR (700 MHz C₆D₆): δ 7.70 (d, *J*_{HH} = 7.0 Hz, 1H), 7.61 (t, *J*_{HH} = 7.4 Hz, 1H), 7.56 (t, *J*_{HH} = 7.4 Hz, 1H), 7.47 (d, *J*_{HH} = 7.7 Hz, 2H), 7.41 (t, *J*_{HH} = 7.0 Hz, 1H), 7.34 (t, *J*_{HH} = 7.0 Hz, 1H), 7.14–7.09 (m, 4H), 6.97 (t, *J*_{HH} = 7.0 Hz, 6H, PPh₃), 6.91–6.85 (m, 8H), 3.64 (d, *J*_{HH} = 16.1 Hz, 1H), 2.64 (d, *J*_{HH} = 19.6 Hz, 1H), 2.23 (s, 3H, Me), 1.81 (br s, 1H), 1.57 (br s, 2H), 1.45 (br s, 1H), 1.34–1.23 (br m, 3H), 1.09 (br s, 3H), 1.01 (br s, 1H), 0.93 (br s, 1H), 0.23 (br s, 1H), –0.37 (br s, 1H), –10.38 (br d, *J*_{HP} = 91.7 Hz, 1H, hydride). ¹³C{¹H} (176 MHz, CD₂Cl₂): δ 160.89, 160.74, 156.20, 140.53, 137.17, 136.91, 133.83 (d, *J*_{CP} = 9.2 Hz), 133.05, 130.12, 130.02, 129.58, 129.15, 128.70, 128.15 (d, *J*_{CP} = 8.1 Hz), 127.43, 126.47, 121.70, 121.58, 121.48, 120.41, 120.13, 34.04, 33.83, 32.61, 31.97, 26.22, 25.64. ³¹P{¹H} NMR (202 MHz, C₆D₆): δ 38.6 (s, PPh₃). ¹¹B{¹H} NMR (160 MHz, C₆D₆) δ –6.5 (br s, 9-BBN). Anal. Calculated (found): C, 67.30 (66.88); H, 5.41 (5.33); N, 8.35 (7.85).

6.4 References

- (1) P. W. N. M. van Leeuwen, P. W. N. M., Chadwick, J. C. *Homogeneous Catalysts*; Wiley-VCH: Weinheim, Germany, 2011.
- (2) Cook, S. A.; Borovik, A. S. *Acc. Chem. Res.* **2015**, *48*, 2407. (b) Crabtree, R. H. *New J. Chem.* **2011**, *35*, 18. (c) Grotjahn, D. B. *Dalton Trans.* **2008**, 6497.

- (3) (a) Kitamura, M.; Noyori, R. In *Ruthenium in Organic Synthesis*; Wiley-VCH: Weinheim, Germany, 2005. (b) Zell, T.; Milstein, D. *Acc. Chem. Res.* **2015**, *48*, 1979. (c) Gunanathan, C.; Milstein, D. *Science* **2013**, *341*. (d) Verendel, J. J.; Pamies, O.; Dieguez, M.; Andersson, P. G. *Chem. Rev.* **2014**, *114*, 2130. (e) de Vries, J. G.; Elsevier, C. J. *Handbook of Homogeneous Hydrogenation*; Wiley-VCH: Weinheim, Germany, 2007.
- (4) (a) Khusnutdinova, J. R.; Milstein, D. *Angew. Chem., Int. Ed.* **2015**, *54*, 12236. (b) Ikariya, T.; Shibasaki, M. *Bifunctional Molecular Catalysis*; Springer: New York, 2011. (c) Muniz, K. *Angew. Chem., Int. Ed.* **2005**, *44*, 6622. (d) Kuzu, I.; Krummenacher, I.; Meyer, J.; Armbruster, F.; Breher, F. *Dalton Trans.* **2008**, 5836. (e) Li, Y.; Hou, C.; Jiang, J.; Zhang, Z.; Zhao, C.; Page, A. J.; Ke, Z. *ACS Catal.* **2016**, *6*, 1655.
- (5) (a) Lin, T.-P.; Peters, J. C. *J. Am. Chem. Soc.* **2013**, *135*, 15310. (b) Fong, H.; Moret, M.-E.; Lee, Y.; Peters, J. C. *Organometallics* **2013**, *32*, 3053. (c) Boone, M. P.; Stephan, D. W. *J. Am. Chem. Soc.* **2013**, *135*, 8508. (d) Harman, W. H.; Peters, J. C. *J. Am. Chem. Soc.* **2012**, *134*, 5080. (e) Moore, C. M.; Bark, B.; Szymczak, N. K. *ACS Catal.* **2016**, *6*, 1981.
- (6) Zhao, M.; Wang, H.-B.; Ji, L.-N.; Mao, Z.-W. *Chem. Soc. Rev.* **2013**, *42*, 8360.
- (7) (a) Braunschweig, H.; Dewhurst, R. D. *Dalton Trans.* **2011**, *40*, 549. (b) Amgoune, A.; Bourissou, D. *Chem. Commun.* **2011**, *47*, 859. (c) Alcaraz, G.; Grellier, M.; Sabo-Etienne, S. *Acc. Chem. Res.* **2009**, *42*, 1640. (d) Drover, M. W.; Schafer, L. L.; Love, J. A. *Angew. Chem., Int. Ed.* **2016**, *55*, 3181. (e) Cassen, A.; Gloaguen, Y.; Vendier, L.; Duhayon, C.; Poblador-Bahamonde, A.; Raynaud, C.; Clot, E.; Alcaraz, G.; Sabo-Etienne, S. *Angew. Chem., Int. Ed.* **2014**, *53*, 7569. (f) Barnett, B. R.; Moore, C. E.; Rheingold, A. L.; Figueroa, J. S. *J. Am. Chem. Soc.* **2014**, *136*, 10262. (g) Ostapowicz, T. G.; Merckens, C.; Hoelscher, M.; Klankermayer, J.; Leitner, W. *J. Am. Chem. Soc.* **2013**, *135*, 2104. (h) Podiyanachari, S. K.; Froehlich, R.; Daniliuc, C. G.; Petersen, J. L.; Mueck-Lichtenfeld, C.; Kehr, G.; Erker, G. *Angew. Chem., Int. Ed.* **2012**, *51*, 8830. (i) Koren-Selfridge, L.; Query, I. P.; Hanson, J. A.; Isley, N. A.; Guzei, I. A.; Clark, T. B. *Organometallics* **2010**, *29*, 3896. (j) Herrmann, C.; Kehr, G.; Froehlich, R.; Erker, G. *Organometallics* **2008**, *27*, 2328. (k) Miller, A. J. M.; Labinger, J. A.; Bercaw, J. E. *J. Am. Chem. Soc.* **2008**, *130*, 11874.
- (8) (a) Moore, C. M.; Szymczak, N. K. *Chemical Science* **2015**, *6*, 3373. (b) Tseng, K.-N. T.; Kampf, J. W.; Szymczak, N. K. *ACS Catal.* **2015**, *5*, 411. (c) Geri, J. B.; Szymczak, N. K. *J. Am. Chem. Soc.* **2015**, *137*, 12808. (d) Tutusaus, O.; Ni, C.; Szymczak, N. K. *J. Am. Chem. Soc.* **2013**, *135*, 3403.
- (9) Tseng, K.-N. T.; Kampf, J. W.; Szymczak, N. K. *Organometallics* **2013**, *32*, 2046.
- (10) Tseng, K.-N. T.; Rizzi, A. M.; Szymczak, N. K. *J. Am. Chem. Soc.* **2013**, *135*, 16352.
- (11) Tseng, K.-N. T.; Lin, S.; Kampf, J. W.; Szymczak, N. K. *Chem. Commun.* **2016**, *52*, 2901.
- (12) Complex **1** catalyzes alkene hydrogenation under 30 psig of H₂ at 80 °C.
- (13) Tseng, K.-N. T.; Kampf, J. W.; Szymczak, N. K. *ACS Catal.* **2015**, *5*, 5468.

- (14) Note that the broadness of the hydride signal reflects interaction with the quadrupole ^{11}B nucleus. In some cases, the H–B coupling was not be observed by NMR spectroscopy even at low temperatures, for an example see reference 7g.
- (15) (a) Crevier, T. J.; Mayer, J. M. *Angew. Chem., Int. Ed.* **1998**, *37*, 1891. (b) Bontemps, S.; Bouhadir, G.; Miqueu, K.; Bourissou, D. *J. Am. Chem. Soc.* **2006**, *128*, 12056.
- (16) Sivaev, I. B.; Bregadze, V. I. *Coord. Chem. Rev.* **2014**, *270-271*, 75.
- (17) (a) Kolpin, K. B.; Emslie, D. J. H. *Angew. Chem., Int. Ed.* **2010**, *49*, 2716. (b) Cook, K. S.; Piers, W. E.; Hayes, P. G.; Parvez, M. *Organometallics* **2002**, *21*, 2422. (c) Emslie, D. J. H.; Cowie, B. E.; Kolpin, K. B. *Dalton Trans.* **2012**, *41*, 1101. (d) Chiu, C.-W.; Gabbai, F. P. *Angew. Chem., Int. Ed.* **2007**, *46*, 6878.
- (18) Gunanathan, C.; Milstein, D. *Acc. Chem. Res.* **2011**, *44*, 588.
- (19) (a) Crossley, I. R.; Foreman, M. R. S. J.; Hill, A. F.; Owen, G. R.; White, A. J. P.; Williams, D. J.; Willis, A. C. *Organometallics* **2008**, *27*, 381. (b) Hill, A. F.; Owen, G. R.; White, A. J. P.; Williams, D. J. *Angew. Chem., Int. Ed.* **1999**, *38*, 2759. (c) Owen, G. R.; Hugh Gould, P.; Charmant, J. P. H.; Hamilton, A.; Saithong, S. *Dalton Trans.* **2010**, *39*, 392.
- (20) Gloaguen, Y.; Benac-Lestrille, G.; Vendier, L.; Helmstedt, U.; Clot, E.; Alcaraz, G.; Sabo-Étienne, S. *Organometallics* **2013**, *32*, 4868.
- (21) Note that previous computational studies demonstrated that H_2 activated by a bifunctional Lewis acid–metal complex likely operates through a synergetic heterolytic pathway.
- (22) Ohmiya, H.; Shido, Y.; Yoshida, M.; Sawamura, M. *Chem. Lett.* **2011**, *40*, 928.
- (23) (a) Chernichenko, K.; Madarasz, A.; Papai, I.; Nieger, M.; Leskelae, M.; Repo, T. *Nat. Chem.* **2013**, *5*, 718. (b) Richmond, E.; Moran, J. *J. Org. Chem.* **2015**, *80*, 6922.
- (24) Brown, H. C. *Hydroboration*; W. A. Benjaminem: New York, 1962.

CHAPTER 7

Outlook

7.1 Publications from This Doctoral Research

The following contributions have been published as a result of this thesis research:

- (1) Tseng, K.-N. T.; Kampf, J. W.; Szymczak, N. K. Base-Free, Acceptorless, and Chemoselective Alcohol Dehydrogenation Catalyzed by an Amide-Derived *N,N,N*-Ruthenium(II) Hydride Complex. *Organometallics* **2013**, *32*, 2046.
- (2) Tseng, K.-N. T.; Rizzi, A. R.; Szymczak, N. K. Oxidant-Free Conversion of Primary Amines to Nitriles. *J. Am. Chem. Soc.* **2013**, *135*, 16352.
- (3) Tseng, K.-N. T.; Szymczak, N. K. Dehydrogenative Oxidation of Primary Amines to Nitriles. *Synlett* **2014**, *25*, 2385.
- (4) Tseng, K.-N. T.; Kampf, J. W.; Szymczak, N. K. Regulation of Iron-Catalyzed Olefin Hydroboration by Ligand Modifications at a Remote Site. *ACS Catal.* **2015**, *5*, 411
- (5) Tseng, K.-N. T.; Kampf, J. W.; Szymczak, N. K. Mechanism of *N,N,N*-Amide Ruthenium(II) Hydride Mediated Acceptorless Alcohol Dehydrogenation: Inner-Sphere β -H Elimination versus Outer-Sphere Bifunctional Metal–Ligand Cooperativity. *ACS Catal.* **2015**, *5*, 5468.
- (6) Tseng, K.-N. T.; Lin, S.; Kampf, J. W.; Szymczak, N. K. Upgrading Ethanol to 1-Butanol with a Homogeneous Air-Stable Ruthenium Catalyst. *Chem. Commun.* **2016**, *52*, 2901.
- (7) Tseng, K.-N. T.; Kampf, J. W.; Szymczak, N. K. Modular Attachment of Appended Boron Lewis Acids to a Ruthenium Pincer Catalyst: Metal–Ligand Cooperativity Enables Selective Alkyne Hydrogenation. *manuscript submitted*.
- (8) Hale, L. V. A.; Malakar, T.; Tseng, K.-N. T.; Zimmerman, P. M.; Paul, A.; Szymczak, N. K. The Mechanism of Acceptorless Amine Double Dehydrogenation by *N,N,N*-Amide Ruthenium Hydrides: A Combined Experimental and Computation Study. *manuscript to be submitted*.
- (9) Kehl, J. A.; Tseng, K.-N. T.; Szymczak, N. K.; Byers, J. A. Formation of High-Molecular Weight Polyethylene from a Sterically Unencumbered Iron-Based Catalyst. *manuscript to be submitted*.

7.2 Outlook

7.2.1 Development of Next Generation Catalysts for Sustainable Energy Applications Derived from Biomass Feedstocks

Acceptorless dehydrogenation is a rapidly expanding field in homogeneous catalysis due to broad interest across several areas including sustainable energy applications and chemical synthesis. Chapter 1 highlights the importance of metal–ligand cooperation in the development of bifunctional systems capable of catalyzing promoterless dehydrogenation and dehydrogenative coupling reactions. However, in systems that contain bifunctional groups, it may be ambiguous whether a cooperative pathway is actually required for efficient dehydrogenation. In studying the mechanism of acceptorless alcohol dehydrogenation reactions using Ru 1,3-bis(2'-pyridylimino)isoindolate (bpi) complexes, experimental evidence support an inner-sphere, stepwise pathway for proton and hydride transfer with a β -H elimination turnover limiting step, which was presented in Chapter 3. A metal–ligand cooperative pathway is not necessary for alcohol dehydrogenation catalysis as demonstrated by the high efficiency of these systems in dehydrogenation of secondary alcohols to ketones, dehydrogenative coupling of primary alcohols to esters, and upgrading ethanol to 1-butanol (Chapter 2).

To our knowledge, Ru(bpi)(PPh₃)₂Cl exhibits state-of-the-art activity for ethanol upgrading by a homogeneous catalyst. This improvement in catalyst performance represents a substantial step forward toward processes that use bio-derived feedstocks for one-step fuel-forming reactions with minimal intervention required to the existing transportation infrastructure. Ongoing efforts are focused on obtaining a mechanistic understanding in Guerbet-type reactions to guide the development of next generation catalysts with improved stability and activity. Preliminary analysis of the deactivated Ru species from Guerbet reactions reveals the presence of a carbonyl ligand as observed by IR spectroscopy. This observation and the comprehensive mechanistic study of acceptorless alcohol dehydrogenation will be used as an entry point to evaluate the Guerbet mechanism by a series of stoichiometric reactions to probe catalytic intermediates, examining competition experiments and product distribution to identify contributors to aldol condensation, and analyzing the impact of low and high hydrogen pressure on catalyst activity and selectivity. These experimental studies will aim to answer the following mechanistic questions: (1) What are the details of the intermediates? (2) What key parameters

govern selectivity for the aldol condensation? (3) Is hydrogenation or dehydrogenation involved in the rate-determining step? (4) How will catalyst decarbonylation be prevented? The mechanistic findings will be used to guide catalyst redesign efforts to optimize catalytic biomass-relevant reactions using hydrogen transfer.

7.2.2 Hydrogen Storage Based on Primary Amine–Nitrile Couples

In addition to the impressive alcohol dehydrogenation capabilities, the HRu(bMepi)(PPh₃)₂ (bMepi = 1,3-bis(6'-methyl-2'-pyridylimino)isoindolate) complex, to our knowledge, is the best homogenous catalyst for double dehydrogenation of amines to nitriles that requires no oxidant or any promoter, such as hydrogen acceptor or base, additives (Chapter 4). Prior to this study, there were no well-defined examples of catalysts that effect this transformation with such selectivity and efficiency. While catalytic amine dehydrogenation presents a selective, atom-efficient methodology for organic synthesis, this reaction may also find application in alternative energy solutions. For example, amines can act as potential hydrogen carriers within the context of a “hydrogen energy economy” cycle. Liquid chemical hydrogen carriers might be more readily implemented within the current transportation/storage infrastructure than solid or gaseous systems. A major challenge for any future hydrogen storage/delivery system is an appropriate energy density (gravimetric and/or volumetric) contained within the fuel and storage components. High hydrogen gravimetric densities (mass of H₂ that can be removed divided by the overall mass of molecule) are possible with low molecular weight amines or polyamines. As a tutorial example using 1,4-diaminobutane, the elimination of 4 equiv of H₂ would provide a 9.1 wt% material, which surpasses the gravimetric density target (5.5 wt%) set by the United States Department of Energy for 2017. Although prior efforts have examined liquid amines as hydrogen carriers, selective dehydrogenation was identified as the major roadblock. Given that nitrile hydrogenation catalysis can now be mediated under relatively mild conditions, using RCH₂NH₂–RCN couples for hydrogen storage may be achievable. Efforts to understand the mechanism of our current system will provide a foundation for improving the design, activity, and stability that might be translated to both arenas of synthetic methodology and hydrogen storage.

7.2.3 Late-State Functionalization Strategy Opens up New Possibilities in Small Molecule Transformations

A part of my doctoral research is to evaluate how the precise structural, electronic, and cooperative modes in the secondary coordination sphere can be used to regulate metal-based catalysis. Specifically in Chapter 5, the secondary coordination environment of a Fe–bMepi system was chemically modified to facilitate facile electronic modifications to bias activity and selectivity of hydroboration reactions. Although prior reports demonstrated Fe-catalyzed olefin hydroboration, our systems are unique because they feature control over activity and regioselectivity by modifications at a remote site on the bMepi ligand backbone. Methylating the imine moiety on the pincer ligand was used as a late-stage modification to provide a more electrophilic complex as determined by electrochemical studies. The alkylated variant, compared to the parent complex, catalyzes alkene hydroboration with an increased reaction rate and exhibits distinct regioselectivity for internal alkene hydroboration.

In a separate study described in Chapter 6, the development of a new class of bifunctional Ru complexes with appended Lewis acidic borane centers demonstrated the use of the Lewis acidic properties of the boranes in the secondary coordination environment to tune the reactivity of the Ru hydride motif and turn on a metal–ligand cooperative pathway for hydrogenation catalysis. Comparison with the unfunctionalized complexes containing only inert alkyl groups illustrates the critical role of the Lewis acids in the secondary coordination sphere to synergistically mediate and regulate alkyne hydrogenation by (1) facilitating H–H heterolysis, (2) stabilizing the hydride intermediate *via* the formation of a Ru–H–B bridge, and (3) selectively reducing alkynes over alkenes. Given that the principles of hydrogenation can be applied to hydrofunctionalization reactions, a potential application would be to use these bifunctional complexes to achieve *cis*-selectivity in hydrosilylation and hydroboration of alkenes, which is a rare stereoselectivity mode in these types of catalysis. Furthermore, this late-stage approach of installing appended boron-based Lewis acids might be extended to the analogous Fe–bMepi systems to develop new bifunctional catalysts that are non-toxic, abundant, and inexpensive.

In general, both of these projects use a late-stage functionalization strategy to modify an already active catalyst to bias activity and selectivity. This highly modular approach offers

several advantages over the more traditional synthesis of specialized ligands: (1) functionalization in the secondary coordination sphere without perturbing the primary coordination environment, (2) methodical variation of the pendent group(s) for precise control over the steric and electronic properties, (3) the simplicity of changing functional (directing) group(s) to achieve the desired transformation, and (4) minimal need to re-optimize metalation conditions to limit unwanted coordination modes or multinuclear metal–ligand ensembles. In addition, because installation of the pendent groups occurred at the last step, this synthetic strategy may be exploited as a versatile protocol to access a large variety of appended functional groups with a wide range of steric and electronic properties. For instance, incorporation of pendent Lewis acidic and basic groups in the secondary coordination environment would construct multifunctional ligand architectures to work in concert with a metal site for synergistic activation of small molecules. Such frameworks have potential applications in biomimetic studies, catalysis, and organic synthesis. Future efforts can also explore this late-stage method to install chiral information on the ligand for asymmetric catalysis. Finally, the long-term goal of this research is to discover fundamental principles and develop a knowledge base that can be used to predict structure–reactivity properties to design catalysts for a targeted application.

APPENDIX

Preparation of Related Bis(pyridylimino)isoindoline Compounds

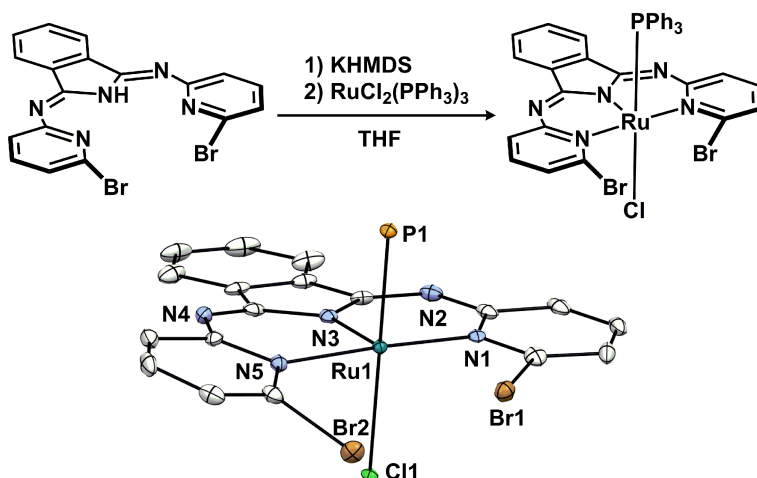
Ru(HbMepi)(PPh₃)(Cl)CO[PF₆]. DCM (5 mL) was added to a Fischer–Porter tube containing Ru(HbMepi)(PPh₃)Cl[PF₆] (23.4 mg, 0.0269 mmol) and a stir bar. The reaction vessel was charged with CO (30 psig) and allowed to stir at room temperature for 18 h. The DCM solution was layered with Et₂O (15 mL) in a 20 mL vial. After 24 h at room temperature, the precipitates were collected on a fine frit and washed with Et₂O (4 × 10 mL). Evaporation of the volatiles under vacuum afforded the product as an orange solid. Crystals were obtained from vapor diffusion of Et₂O into a DCM solution at room temperature. Yield: 20 mg (83%). ¹H NMR (700 MHz, CD₂Cl₂): δ 9.72 (s, 1H, NH), 8.09 (br m, 1H), 7.82-7.78 (br m, 3H), 7.68-7.60 (br m, 2H), 7.42-7.37 (br m, 4H), 7.23 (t, *J*_{HH} = 7.7 Hz, 3H, PPh₃), 6.98 (m, 6H, PPh₃), 6.55 (t, *J*_{HH} = 9.8 Hz, 6H, PPh₃), 3.71 (s, 3H), 3.65 (s, 3H). ³¹P {¹H} (283 MHz, CD₂Cl₂): δ 40.22 (s).

Ru(bMepi)(PPh₃)₂[BAr^F]. THF (5 mL) was added to a 20 mL vial charged with HRu(bMepi)(PPh₃)₂ (21.2 mg, 0.0222 mmol), HB(C₆H₃(CF₃)₂)₄·(Et₂O)₂ (24.8 mg, 0.0245), and a stir bar. The reaction solution was allowed to stir at room temperature for 24 h. The THF solvent was removed under vacuum and the crude product was extracted with Et₂O. Evaporation of the volatiles under vacuum overnight afforded the product as a bright purple solid. ¹H NMR (400 MHz, CD₂Cl₂): δ 7.75-7.71 (m, 11H), 7.64 (dd, *J*_{HH} = 5.2, 3.2 Hz, 2H), 7.56 (s, 3H), 7.47 (d, *J*_{HH} = 7.6 Hz, 2H), 7.41 (dd, *J*_{HH} = 5.6, 3.2 Hz, 2H), 7.20 (t, *J*_{HH} = 7.4 Hz, 6H, PPh₃), 6.97 (t, *J*_{HH} = 7.8 Hz, 12H, PPh₃), 6.64-6.59 (m, 14 H), 1.21 (s, 6H). ³¹P {¹H} (162 MHz, CD₂Cl₂): δ 20.78 (s). ¹⁹F {¹H} (377 MHz, CD₂Cl₂): δ 62.93 (s).

Purification of Ru(bOMepi)(PPh₃)Cl. The crude product was washed with Et₂O (4 × 10 mL), C₆H₆ (4 × 10 mL), and THF (1 mL). Evaporation of the volatiles under vacuum afforded the product as a dark blue powder. ¹H NMR (400 MHz, CD₂Cl₂): δ 7.82 (dd, *J*_{HH} = 5.6, 3.2 Hz,

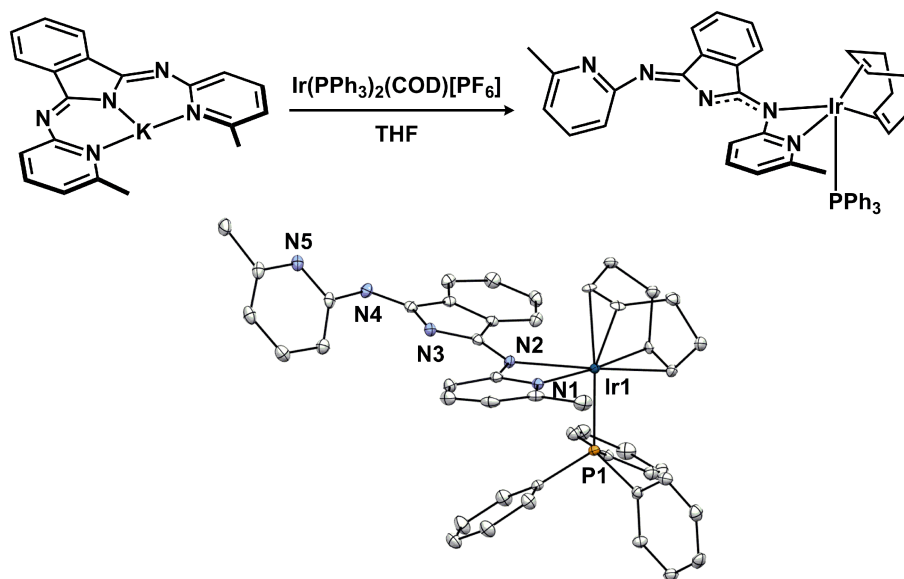
2H), 7.77 (t, $J_{\text{HH}} = 8.0$ Hz, 2H), 7.40 (dd, $J_{\text{HH}} = 5.6, 3.2$ Hz, 2H), 7.28 (d, $J_{\text{HH}} = 7.6$ Hz, 2H), 7.19 (t, $J_{\text{HH}} = 7.6$ Hz, 3H, PPh₃), 7.02 (t, $J_{\text{HH}} = 7.8$ Hz, 6H, PPh₃), 6.72 (t, $J_{\text{HH}} = 8.4$ Hz, 6H, PPh₃), 6.41 (d, $J_{\text{HH}} = 7.6$ Hz, 2H), 3.94 (s, 6H). $^{31}\text{P}\{^1\text{H}\}$ (162 MHz, CD₂Cl₂): δ 53.82 (s).

KbBrpi. THF (10 mL) was added to a 20 mL vial charged with HbBrpi (243 mg, 0.532 mmol), KHMDS (101 mg, 0.507 mmol), and a stir bar. The reaction solution was allowed to stir at room temperature for 18 h. The precipitates were collected on a medium frit and washed with Et₂O (4 × 20 mL). Evaporation of the volatiles under vacuum afforded the product as a yellow powder. Yield: 221 mg (88%). ^1H NMR (400 MHz, THF): δ 7.53 (br s, 2H), 7.44-7.35 (m, 4H), 7.19-7.18 (br m, 2H), 6.91 (d, $J_{\text{HH}} = 7.2$ Hz, 2H).



Ru(bBrpi)(PPh₃)Cl. THF (10 mL) was added to a 20 mL vial charged with KbBrpi (221 mg, 0.446 mmol), RuCl₂(PPh₃)₃ (408 mg, 0.425 mmol), and a stir bar. The reaction solution was allowed to stir at room temperature for 24 h. The precipitates were collected on a fine frit and washed with C₆H₆ (4 × 20 mL) and Et₂O (4 × 20 mL). The crude product was extracted with DCM. The DCM solvent was removed under vacuum, and the crude product was washed with C₆H₆ (4 × 10 mL) and Et₂O (4 × 10 mL). Evaporation of the volatiles under vacuum afforded the product as a violet powder. Crystals were obtained from slow evaporation of a DCM solution at 5 °C. Yield: 260 mg (73%). ^1H NMR (400 MHz, CD₂Cl₂): δ 7.82 (m, 2H), 7.61 (t, $J_{\text{HH}} = 7.6$ Hz, 2H), 7.52 (d, $J_{\text{HH}} = 7.6$ Hz, 2H), 7.44 (m, 2H), 7.17 (t, $J_{\text{HH}} = 7.2$ Hz, 3H, PPh₃), 7.09 (d, $J_{\text{HH}} = 7.2$ Hz, 2H), 6.99 (t, $J_{\text{HH}} = 6.8$ Hz, 6H, PPh₃), 6.88 (t, $J_{\text{HH}} = 8.6$ Hz, 6H, PPh₃). $^{31}\text{P}\{^1\text{H}\}$ (162 MHz, CD₂Cl₂): δ 47.22 (s).

Ir(bMepi)(PPh₃)COD. THF (5 mL) was added to a 20 mL vial charged with KbMepi (26.3 mg, 0.0722 mmol), Ir(COD)(PPh₃)₂[PF₆] (66.7 mg, 0.0687 mmol), and a stir bar. The reaction solution was allowed to stir at room temperature for 20 h. The THF solvent was removed under vacuum, and the crude product was washed with pentane (4 × 10 mL) and extracted with Et₂O (20 mL). Evaporation of the volatiles under vacuum afforded the product as a red solid. Crystals were obtained from slow evaporation of a DCM solution at 5 °C. ¹H NMR (400 MHz, C₆D₆): δ 7.40 (br s), 7.03 (br s), 6.93 (br s), 2.47-2.17 (br m).



[Ir₂(H)₄(bMepi)(PPh₃)₄]⁺. Method A: DCM (10 mL) was added to a 20 mL vial charged with HbMepi (29.3 mg, 0.0895 mmol), Ir(H)₅(PPh₃)₂ (71.8 mg, 0.0994 mmol), and a stir bar. The reaction solution was allowed to stir at room temperature for 24 h. The DCM solution was filtered and removed under vacuum. The crude product was washed with Et₂O (4 × 10 mL). Evaporation of the volatiles under vacuum afforded the product as a red solid. Crystals were obtained vapor diffusion of Et₂O into a DCM solution at 5 °C. **Method B:** PhMe (5 mL) was added to a 20 mL vial charged with HbMepi (19.5 mg, 0.0595 mmol), Ir(H)₂(THF)₂(PPh₃)₂[PF₆] (60 mg, 0.0595 mmol), and a stir bar. The reaction solution was allowed to stir at 90 °C for 30 min. After the solution cooled to room temperature, the precipitates were collected on a fine and washed with Et₂O (4 × 10 mL). Evaporation of the volatiles under vacuum afforded the product as a red solid. Yield: 50 mg (84%). ¹H NMR (400 MHz, CD₂Cl₂): δ 8.25 (dd, *J*_{HH} = 5.2, 3.2 Hz, 2H), 7.52 (d, *J*_{HH} = 8.0 Hz, 2H), 7.45-7.40 (m, 24H, PPh₃), 7.35 (t, *J*_{HH} = 7.8 Hz, 2H, PPh₃), 7.20

(t, $J_{\text{HH}} = 7.4$ Hz, 12H, PPh₃), 7.09 (t, $J_{\text{HH}} = 7.4$ Hz, 24H, PPh₃), 6.91 (dd, $J_{\text{HH}} = 5.6, 2.8$ Hz, 2H), 6.41 (d, $J_{\text{HH}} = 7.6$ Hz, 2H), 1.53 (s, 6H), -21.68 (dt, $J_{\text{HP}} = 16.0$ Hz, $J_{\text{HH}} = 8.0$ Hz, 2H), -24.20 (dt, $J_{\text{HP}} = 16.0$ Hz, $J_{\text{HH}} = 8.4$ Hz, 2H). $^{31}\text{P}\{^1\text{H}\}$ (162 MHz, CD₂Cl₂): δ 21.36 (s).

